



# Experimental investigation of laminar flame speeds of kerosene fuel and second generation biofuels in elevated conditions of pressure and preheat temperature

Yi Wu

## ► To cite this version:

Yi Wu. Experimental investigation of laminar flame speeds of kerosene fuel and second generation biofuels in elevated conditions of pressure and preheat temperature. Chemical Physics [physics.chem-ph]. INSA de Rouen, 2016. English. NNT : 2016ISAM0011 . tel-01430861

**HAL Id: tel-01430861**

**<https://theses.hal.science/tel-01430861>**

Submitted on 10 Jan 2017

**HAL** is a multi-disciplinary open access archive for the deposit and dissemination of scientific research documents, whether they are published or not. The documents may come from teaching and research institutions in France or abroad, or from public or private research centers.

L'archive ouverte pluridisciplinaire **HAL**, est destinée au dépôt et à la diffusion de documents scientifiques de niveau recherche, publiés ou non, émanant des établissements d'enseignement et de recherche français ou étrangers, des laboratoires publics ou privés.

## THÈSE

**Pour obtenir le diplôme de doctorat**

**Spécialité (Physique & Energétique)**

**Préparée au sein de l'INSA de Rouen et de laboratoire CORIA UMR-6614, Rouen**

**Experimental investigation of laminar flame speeds of kerosene fuel and second generation biofuels in elevated conditions of pressure and preheat temperature**

**Présentée et soutenue par  
Yi WU**

Thèse soutenue publiquement le 21-07-2016 devant le jury composé de		
Mme CHAUMEIX Nabiha	Directrice de recherche CNRS, ICARE	Rapporteur
M. Fabrice FOUCHER	Professeur Université d'Orléans, PRISME	Rapporteur
M. Julien SOTTON	Professeur ENSMA, PPRIME	Examineur
M. Stéphane RICHARD	Docteur Ingénieur, SAFRAN	Examineur
M. Mourad BOUKHALFA	Professeur, INSA de ROUEN, CORIA	Examineur
M. Frédéric GRISCH	Professeur, INSA de ROUEN, CORIA	Directeur
M. Vincent MODICA	Maitre de conférences, Université de Rouen, CORIA	Co-encadrant

**Thèse dirigée par Frédéric GRISCH, laboratoire CORIA**



# Thèse

Présentée par :

**Yi WU**

En vue de l'obtention du grade de :

**Docteur de la Normandie Université,**

délivré par l'**Institut National des Sciences Appliquées de Rouen**

Discipline	:	Physique
Spécialité	:	Energétique
Laboratoire d'accueil	:	CORIA UMR-6614, ROUEN
Ecole doctorale	:	SPMII

**Experimental investigation of laminar flame speeds of kerosene fuel  
and second generation biofuels in elevated conditions of pressure  
and preheat temperature**

*Devant le jury composé de :*

N. CHAUMEIX	Directrice de recherche CNRS, ICARE	<b>Rapporteur</b>
F. FOUCHER	Professeur Université d'Orléans, PRISME	<b>Rapporteur</b>
J. SOTTON	Professeur ENSMA, PPRIME	<b>Examineur</b>
S. RICHARD	Docteur Ingénieur, SAFRAN	<b>Examineur</b>
M. BOUKHALFA	Professeur, INSA de ROUEN, CORIA	<b>Examineur</b>
F. GRISCH	Professeur, INSA de ROUEN, CORIA	<b>Directeur</b>
V. MODICA	Maitre de conférences, Université de Rouen, CORIA	<b>Co-encadrant</b>



## Résumé:

La vitesse de flamme laminaire représente une grandeur physique clé à mesurer car elle permet d'obtenir des données fondamentales sur la réactivité, la diffusivité et l'exothermicité du carburant. Elle est également un des paramètres utilisés pour le développement et la validation des mécanismes réactionnels détaillés ainsi que pour la modélisation de la combustion turbulente. Bien que cette grandeur physique ait fait l'objet de nombreuses études expérimentales depuis plusieurs décennies, sa méconnaissance sur des carburants multi-composant dans des conditions haute-pression et haute-température similaires à celles existantes dans les chambres de combustion reste un sujet d'actualité pour les industriels des secteurs automobile et aéronautique. Au cours de cette thèse, un brûleur de configuration bec Bunsen fonctionnant avec un prémélange gazeux combustible/air a été conçu pour produire une flamme laminaire à pression élevée tout en permettant la mesure par voie optique de la vitesse de flamme laminaire de carburants multi-composant (kérosène, biocarburants de seconde génération...). La mesure est basée sur la détection du contour de flamme par diverses diagnostics optiques comme la chimiluminescence OH\*, la PLIF-OH et la PLIF-acétone/aromatique. En premier lieu, les mélanges de carburants purs gazeux (CH<sub>4</sub>) ou liquide (acétone) avec de l'air ont été étudiés pour valider le brûleur expérimental et la méthodologie de mesure de la vitesse de flamme laminaire par voie optique. Les évolutions de la vitesse de flamme laminaire pour des carburants de type kérosène (composants purs, surrogate LUCHE et Jet A-1) en fonction de la pression, température de préchauffage et richesse ont été ensuite étudiées et comparées avec des simulations numériques utilisant un mécanisme réactionnel détaillé. La dernière partie de la thèse est consacrée à l'étude de l'influence des composés oxygénés présents dans un biocarburant de seconde génération de type d'essence sur la vitesse de flamme laminaire. Après avoir mesuré la vitesse de flamme laminaire de différentes molécules oxygénées, les effets d'addition de ces composés oxygénés dans le carburant ont été quantifiés.

## **Abstract:**

Laminar flame speed is one of the key parameters for understanding reactivity, diffusivity and exothermicity of fuels. It is also useful to validate both the kinetic chemical mechanisms as well as turbulent models. Although laminar flame speeds of many types of fuels have been investigated over many decades using various combustion methodologies, accurate measurements of laminar flame speeds of multicomponent liquid fuels in high-pressure and high-temperature conditions similar to the operating conditions encountered in aircraft/automobile combustion engines are still required. In this current study, a high-pressure combustion chamber was specifically developed to measure the laminar flame speed of multicomponent liquid fuels such as kerosene and second generation of biofuels. The architecture of the burner is based on a preheated premixed Bunsen flame burner operated in elevated pressure and temperature conditions. The optical diagnostics used to measure the laminar flame speed are based on the detection of the flame contour by using OH\* chemiluminescence, OH- and acetone/aromatic- Planar laser induced fluorescence (PLIF). The laminar flame speed of gaseous CH<sub>4</sub>/air and acetone/air premixed laminar flames were first measured for validating the experimental setup and the measurement methodologies. Then, the laminar flame speeds of kerosene or surrogate fuels (neat kerosene compounds, LUCHE surrogate kerosene and Jet A-1) were investigated and compared with simulation results using detailed kinetic mechanisms over a large range of conditions including pressure, temperature and equivalence ratio. The last part of the thesis was devoted to study the effect of oxygenated compounds contained in the second generation of biofuels on the laminar flame speeds. After measuring the laminar flame speeds of various oxygenated components present in partially hydro-processed lignocellulosic biomass pyrolysis oils, the effect of these oxygenates on the flame speeds of these fuels were quantitatively investigated.

# Contents

Nomenclature.....	i
Chapter 1 Introduction.....	1
1.1    Background and general aspects of laminar flame speeds .....	1
1.2    Purpose of this study .....	4
1.3    Thesis structure.....	5
Chapter 2 Background on laminar premixed combustion.....	8
2.1    Laminar premixed flames.....	9
2.1.1    Premixed flame structure.....	9
2.1.2    Laminar flame speed definition.....	14
2.1.3    Flame stretch .....	16
2.1.4    Experimental determination of laminar flame speed.....	17
2.1.5    Choice of the experimental flame method.....	20
2.2    Literature review on measurements of laminar flame speeds .....	22
2.2.1    Methane /air mixtures.....	22
2.2.2    Acetone/air mixtures .....	24
2.2.3    Kerosene fuel.....	26
2.2.4    Oxygenated fuels .....	32
2.3    Numerical tools for one-dimensional flames.....	34
2.3.1    Laminar, one-dimensional, premixed, and freely propagating flames .....	34
2.3.2    Chemical kinetic mechanisms .....	35
2.4    Conclusions .....	37
Chapter 3 Experimental Setup.....	38
3.1    High-pressure burner.....	39
3.2    Liquid fuel vaporization and gas feeding .....	40
3.3    Monitoring of the high-pressure burner .....	41
3.3.1    Temperature monitoring.....	41
3.3.2    Pressure monitoring.....	42
3.4    Reliability of physical parameter control .....	44
3.4.1    Reliability of temperature and pressure control .....	44



3.4.2	Reliability of fluid flow control.....	44
3.4.3	Reliability of the velocity profile at the burner outlet .....	47
3.5	Optical diagnostics .....	48
3.5.1	OH* chemiluminescence.....	48
3.5.2	OH-PLIF.....	48
3.5.3	Ketone-PLIF .....	50
3.5.4	Aromatics-PLIF .....	51
<b>Chapter 4 Laminar flame speed determination .....</b>		<b>52</b>
4.1	Laminar flame speed measurement approaches .....	53
4.1.1	Flame angle method .....	53
4.1.2	Flame area method .....	54
4.2	Optical diagnostics .....	56
4.2.1	OH* Chemiluminescence .....	57
4.2.2	Planar Laser-induced fluorescence.....	58
4.3	Sources of interferences on laminar premixed flame structure .....	64
4.3.1	Heat losses .....	65
4.3.2	Buoyancy effects .....	65
4.3.3	Stretch effects .....	65
4.3.4	Flame thickness effects.....	66
4.4	Data processing of OH*-chemiluminescence and PLIF images .....	68
4.4.1	OH* chemiluminescence.....	68
4.4.2	PLIF diagnostic .....	72
4.5	Measurement Uncertainties .....	73
<b>Chapter 5 Measurements on CH<sub>4</sub>/air and Acetone/N<sub>2</sub>/O<sub>2</sub> mixtures.....</b>		<b>74</b>
5.1	Validation of the measurement methodologies .....	75
5.1.1	OH* chemiluminescence imaging.....	75
5.1.2	OH-PLIF and acetone-PLIF imaging .....	81
5.2	Laminar flame speeds of CH <sub>4</sub> /Air mixtures .....	83
5.2.1	Comparison with literature data .....	83
5.2.2	Preheating temperature.....	84
5.2.3	Pressure .....	85

5.3	Laminar flame speeds of acetone/N <sub>2</sub> /O <sub>2</sub> mixtures.....	87
5.3.1	Correlation formulation .....	87
5.3.2	Preheating temperature dependence .....	89
5.3.3	Pressure dependence.....	91
5.3.4	Validation of the empirical correlation expression.....	94
5.4	Conclusions .....	95

## Chapter 6 Laminar flame speed of kerosene fuel..... 96

6.1	Introduction and objectives .....	97
6.2	Operating conditions .....	97
6.3	Limitations of the optical techniques for laminar flame speeds determination .....	99
6.3.1	OH* Chemiluminescence versus OH-PLIF .....	99
6.3.2	Comparison between OH-PLIF, chemiluminescence and aromatics-PLIF .....	101
6.3.3	Flame tip opening phenomenon .....	103
6.3.4	Concluding remarks.....	106
6.4	Laminar Flame Speeds of neat kerosene compound .....	106
6.4.1	n-Decane.....	107
6.4.2	n-Propylbenzene .....	108
6.4.3	Propylcyclohexane .....	109
6.4.4	Comparison between the pure compounds .....	111
6.5	Laminar flame speeds of fuel surrogate and Jet A-1 kerosene.....	112
6.5.1	LUCHE surrogate.....	112
6.5.2	Jet A-1 .....	115
6.5.3	Comparison between LUCHE surrogate and Jet A-1 fuels .....	119
6.7	Conclusions .....	120

## Chapter 7 Laminar flame speed of biofuels containing oxygenated compounds ..... 122

7.1	Introduction and objectives .....	123
7.2	Commercial and surrogate gasoline fuels.....	125
7.3	Oxygenated fuels .....	128
7.3.1	Selection of oxygenates .....	129
7.3.2	Laminar flame speeds of pure oxygenates .....	131
7.4	Effect of the addition of oxygenates on the laminar flame speeds of surrogate gasoline....	133

7.5	Conclusions .....	138
Chapter 8 Conclusions and future work .....		139
8.1	Summary and conclusions .....	139
8.2	Recommendations for further study .....	142
Appendix I: Schematic drawing of the high-pressure burner .....		145
List of Tables .....		146
List of Figures .....		147
References.....		152

# Nomenclature

---

## Greek alphabet

$\alpha$	Temperature dependence coefficient Half cone angle of Bunsen flame
$\beta$	Pressure dependence coefficient
$\delta_r$	Flame reaction thickness
$\delta_p$	Flame preheat zone thickness
$\omega$	Reaction rate
$\lambda$	Thermal conductivity
$\varphi$	Equivalence ratio
$\rho$	Density
$\eta_{opt}$	Solid angle of light collection and transmission efficiency

## Latin alphabet

$\dot{m}$	Mass flux
$K$	Strain rate
$Le$	Lewis number
$P$	Pressure
$T$	Temperature
$S_L$	Laminar flame speed
$Y$	Specie concentration
$f^0$	Laminar flame burning flux
$Ze$	Zeldovich number
$C_p$	Constant pressure specific heat
$n$	Overall reaction order
$D_{th}$	Thermal diffusivity
$S_d$	Displacement speed
$S_c$	Consumption speed
$\vec{s_f}$	Local flame velocity vector
$\vec{n}$	Normal vector to flame surface
$u$	Local flow velocity
$A$	Flame surface element Flame surface of Bunsen flame

$\mathcal{L}$	Markstein length
$S$	Emission signal
$I$	Signal intensity
$B$	Matrix of geometrical factor
$U_{Qm}$	uncertainty on the total flow rate
$U_A$	Uncertainty of flame area calculation

### **Subscript and Superscript**

0	Related to unstretched condition
$b$	Related to the burned gas
$c$	Related to the critical condition
$u$	Related to the unburned gas

# Chapter 1 Introduction

---

## 1.1 Background and general aspects of laminar flame speeds

Even though considerable progress of the renewable energy development has been recently achieved, for the coming decades, hydrocarbons will continue to be the primary energy source of the modern society. In particular, it is expected that liquid hydrocarbon fuels will continue to dominate the transportation sector due to their high energy efficiency and their facility to be transported and stocked. Nevertheless the necessity to drastically reduce pollutant emissions from ground and aero transportation engines becomes a relevant aspect in designing combustion systems such as helicopter turbines, aircraft or automotive engines. Since the combustion behavior of liquid hydrocarbons has a strong influence on engine performances, a better understanding of liquid fuel combustion is still a key point in developing high efficiency and clean-burning engines of next generation. This is crucial for certain applications, such as aviation in which there are a limited number of possible energy sources that are available today. For commercial aviation applications, the choice of kerosene has remained much the same during the last decades, yet many fundamental combustion characteristics remain largely unknown. In addition, these kerosene-derived fuels, such as Jet-A1, are produced from non-renewable sources, which result in a significant net production of greenhouse gases. The increasing demand for these limited fossil fuels motivates the development of new alternative fuels and technologies which mitigate the environmental, supply and social issues that surround conventional fuels. A major recent example is the emergence of new synthetic jet fuels used in the aviation sector and produced via the Fischer-Tropsch process from synthesis gas derived from natural gas or with the development of biofuels derived from renewable sources, such as biomass.

In recent years, biomass derived fuels have gained much attention as potential alternatives to petroleum based fuels. Apart from the advantage of renewability, biofuels have shown to be sustainable and less harmful to the environment; especially those derived from 2nd generation biofuels where lignocellulosic biomass is used as feedstock. One of the common features of biofuels is that they are all oxygenated hydrocarbons, containing oxygen as an additional element in their molecular composition. This feature distinguishes them from hydrocarbons in conventional petroleum based fuels whose the combustion chemistry has for a long time been studied. The existence of oxygen atoms in the oxygenated fuel molecules changes the electronic structure, and almost all the C-H bond strengths for the oxygenated fuels are different from their values for hydrocarbon fuels. Their use in combustion offers significant potential for reduction in particulates and NO<sub>x</sub> emission as compared to hydrocarbons. On the other hand, the incomplete combustion of oxygenated hydrocarbons may contribute to the emission of small amount of oxygenated hydrocarbons themselves or their intermediates or even harmful chemical components for

environmental safety and human health. For instance, aldehydes play a significant role in the decomposition and oxidation of alcohols as key stable intermediated species. In the same way, ketones are another important reaction intermediate species in flames of hydrocarbons and oxygenated compounds.

The combustion of these practical fuels, whether conventional or alternative, is further complicated by their variable and complex chemical composition. For instance, kerosene-based aviation fuels commonly used in modern turbofan engines are composed of a wide range of hydrocarbons including n-paraffin, iso-paraffin and aromatics that makes the elucidation of each component's chemistry in the fuels very difficult. To understand the associated combustion characteristics for such fuels, it is imperative to obtain accurate detailed kinetic models not only for these multi-component fuels but also for different classes of molecules playing a key role on their formation and consumption in flames. A useful approach in developing detailed kinetic mechanisms for complex fuels is to use surrogate mixtures of pure hydrocarbons compounds to replicate the physical and chemical characteristics of a practical fuels. The fidelity of the surrogate depends directly not only on the accuracy of the pure compounds models, but also the ability to reproduce the global flame characteristics of practical fuels. The corresponding kinetic schemes need then to be developed and validated for large ranges of operating conditions, expressed in terms of equivalence ratio, pressure and temperature. Kinetic schemes are generally validated based on ignition delays time, species profiles and flame speed measurements.

In particular, the laminar flame speed,  $S_L^0$ , represents the rate at which the fresh gases are consumed through the flame front considering a 1D unstretched propagating planar premixed flame. It is a fundamental flame property which depends only on the fuel/air mixture and its initial thermodynamic conditions: pressure, temperature and equivalence ratio. Flame speed is a global indicator for the reactivity of a specific mixture of fuel and air. This parameter has been extensively studied for more 70 years and at the beginning of the flame speed experimentations, the measurements were mostly concentrated to simple gaseous mixtures like for example, methane/air, hydrogen/air or small molecular weight fuels at standard conditions of temperature and pressure [1] [2] [3] [4] [5]. During this early period of combustion research, flame speed measurements were inaccurate and very scattered (up to 20 cm/s between results). Data scattering began to significantly reduce from 1980s when the aerodynamic stretch effects were well quantified. Nowadays the discrepancy between flame speed measurements are expected to be around 5 cm/s [3] and it has to be still more reduced in a next future.

In the last several years, the interest in measuring the laminar flame speed continues to increase due to the relevance of  $S_L^0$  to kinetic model development and to high-pressure combustion. Many experimental approaches have been developed within this context: the steady burner-stabilized flames, the steady

stagnation-type flames and the unsteady spherically expanding flames. Some major and current issues concerning the experimental determination of the flame speed are presented below:

- **Accuracy of laminar flame speeds:**

Even though various experimental methodologies have been developed and numerous previous measurements of laminar flame speed have been accomplished for many different fuels, small but nevertheless still important differences exist. For example, differences of the order of 3-5 cm/s persist for low molecular weight fuels such as C<sub>1</sub>-C<sub>4</sub> hydrocarbons [3], which is not desirable for the validation of kinetic schemes because it is very difficult to constrain the uncertainty of chemical models using low quality (with large uncertainty) experimental data of laminar flame speed [6]. For larger molecular weight fuels, the scattering in reported values of flame speeds is notably greater [7] [8], especially under fuel rich mixtures. Different possible sources of uncertainty/inaccuracy resulting to large discrepancies in laminar flame speed measurements can be cited: mixture preparation, ignition, buoyancy, instability, confinement, radiation, nonlinear stretch behavior, and extrapolation. All these sources are illustrated for instance in the work reported in [6].

- **Experimental measurements in engine operating conditions:**

Most of the previous studies of experimental laminar flame speed measurements are still limited to atmospheric or moderate pressure ( $P < 1$  MPa) conditions [9] [10] [11] [12] [13]. Few experimental data of flame speed approaching practical thermodynamic conditions such as those encountered in automotive or aircraft engines are available in literature. High-pressure measurements for practical fuels or large molecular weight fuels such as diesel, gasoline and kerosene are even limited. For instance, the kerosene used in modern aircraft engines is preheated up to 900 K and combustion occurs at pressure approaching to 4 MPa. These operating conditions are difficult to experimentally reproduce in the laboratory. Moreover, because of fuel pyrolysis risks at elevated temperature, few laminar flame speed measurements of large molecular weight fuel are performed at temperature higher than 473 K. Experimental data are still lacking at extreme conditions such as sub-atmospheric pressure and at extreme conditions of lean mixtures [14] [15].

- **Large molecular weight fuels and biofuels:**

In the recent years, considerable progresses are achieved in the laminar flame speed measurements of large molecular weight fuels such as kerosene, diesel and single or multi-component surrogate fuels [16] [17] [18] [19] [20] [21] [22] [23] [24] [25]. For example, n-decane and n-dodecane which are the most representative components in diesel and kerosene fuels, has been extensively studied in recent years [17] [23] [26] [27]. Moreover, pure components of gasoline such as n-heptane, n-isooctane or their blends have been extensively studied [9] [11] [28] [29] [30]. Comparative studies between surrogate fuels and



commercial fuels have been also performed. With these progressive experimental investigations, detailed or skeletal surrogate fuel mechanisms have been successively developed and validated allowing simulating the combustion characteristics of commercial gasoline, diesel, kerosene and biofuels [28] [16] [17] [31] [32]. However, large experimental data scattering can be found among them: for example up to 10 cm/s in case of n-decane. More experimental and accurate measurements for large molecular weight fuels are still desirable.

Apart from the laminar flame speed measurements for conventional fossil fuels, the emergence of new biofuels (first and second generation), implies some new issues. For example, in the case of biofuels that contains a large amount of oxygenated compounds, the question now being asked is what are the effects of these components on laminar flame speed? Many studies try to respond to this question. For instance, in recent years laminar flame speed of ethanol or butanol and their addition effects to commercial gasoline and diesel fuels have been widely studied [10] [28] [29] [33] [34] [35]. However, with the advent of second generation biofuels, effects of some specific oxygenated compounds found after hydro-processing of bio-oil crude such as furan families (2, 5-dimethylfuran, methyltetrahydrofuran and 2-methylfuran etc.), phenolics (phenol, 2, 4-xyleneol etc.), and oxygenated aromatics (anisole, 4-methylanisole etc. ) still need to be studied.

## **1.2 Purpose of this study**

In considering the aforementioned issues, the objectives of this thesis are the followings:

- The primary objective of this thesis is to set-up a newly high-pressure laminar flame Bunsen burner designed as a basis for monitoring laminar flames of gaseous or liquid fuels over a wide range of operating conditions including preheating temperature, pressure and equivalence ratio. Critical analysis of the Bunsen flame methodology accuracy in high-pressure conditions is performed. The error sources associated to this methodology are discussed and new image processing methods are proposed. The modified Bunsen flame methodology is validated by measuring laminar flame speeds of gaseous fuel ( $\text{CH}_4$ ) and small molecular weight liquid fuel (acetone) over a large range of working conditions including equivalence ratio, pressure and temperature.
- A large part of the current work is devoted to establish a new experimental database of laminar flame speeds of kerosene fuels including pure components of kerosene, their blend as surrogate fuel and the commercial kerosene (Jet A-1), in a wide range of pressure, temperature and equivalence ratios conditions. Data embodies information of the diffusive and reactive aspects of these fuels and provides useful information to chemical mechanism enhancements. The laminar

flame structure of kerosene fuels is observed by using different optical diagnostic techniques (OH\* chemiluminescence, OH-PLIF and aromatics-PLIF), whose the measurement accuracy is discussed.

- With the development of second generation biofuels derived from biomass, new open issues related to laminar flame speed measurements of biofuels arise in recent years. One of these issues is that the biofuels derived from fast pyrolysis contains considerable oxygenated compounds. Different from the oxygenated fuels such as ethanol or butanol whose laminar flame speed and addition effects to gasoline have been previously investigated, oxygenated components resulting from fast pyrolysis have a higher molecular weight with a carbon number from C<sub>5</sub> to C<sub>12</sub> such as anisole, 4-methylanisole etc.. The effect of the presence of these oxygenated compounds to the performance of biofuels should be evaluated carefully to make sure that the new developed biofuels are compatible with traditional hydrocarbons. The present work aims to investigate the laminar flame speeds of these oxygenated components coming from fast pyrolysis production process. Then their effects to gasoline fuels in terms of laminar flame speeds at high-pressure and elevated temperature conditions will be addressed.

### 1.3 Thesis structure

The dissertation consists of four parts organized as follows:

After the presentation of the context and the objectives of this study and before getting into the experimental investigations, a theoretical background is presented in the *chapter 2* of the **first part**:

- *Chapter 2*: The concept of the idealistic one dimensional flame is presented. The different definitions of the laminar flame speed used in the literature are detailed and a presentation of a literature review of the experimental methodologies used to measure the laminar flame speed follows. The choice of the Bunsen burner is explained and this chapter is concluded by a concise presentation of the detailed kinetic schemes selected in this work.

The **second part** details in the *chapter 3* the experimental facility and then the measurement methodology of the laminar flame speed for the Bunsen flame in the *chapter 4*:

- *Chapter 3*: The experimental setup is described here: combustion chamber for Bunsen flames under high-pressure conditions, regulation process of equivalence ratio, temperature and pressure, vaporization system of liquid fuels, optical technique set-ups and corresponding experimental uncertainties.

- *Chapter 4:* The methodology to measure the laminar flame speed is described for the case of Bunsen flames. Advantages and drawbacks of the method are detailed. The factors influencing the methodology accuracy are experimentally investigated including piloted flame effects, flame stretch effects and flame thickness corrections. The image processing algorithms associated to the optical techniques selected in the current are presented.

The **third part** presents the experimental results of the fuels tested: simple gases ( $\text{CH}_4$ ), small molecular weight liquid fuel (acetone), pure heavy hydrocarbons (n-decane, n-propylbenzene, n-propylcyclohexane) kerosene fuel (Jet A-1), surrogate kerosene (LUCHE), surrogate bio-gasoline and oxygenated molecules (anisole, 4-methylanisole, ethyl valerate).

- *Chapter 5:* This chapter is dedicated to validate the experimental setup and the image post-processing by measuring laminar flame speeds of  $\text{CH}_4$ /air and acetone/air mixtures. Preliminary measurements of the laminar flame speed of gaseous  $\text{CH}_4$ /air mixtures are firstly performed with  $\text{OH}^*$  chemiluminescence and OH-PLIF and compared with literature data in order to validate the experimental setup. Laminar flame speed of acetone/air are then measured by  $\text{OH}^*$  chemiluminescence, OH-PLIF and acetone-PLIF methodologies. The effects of the preheating temperature (373 K - 523 K), pressure (0.1 - 1.0 MPa) and equivalence ratio (0.6 - 1.3) on the laminar flame speed of acetone/air mixtures are then examined. The experiments are complemented and compared with numerical simulations conducted with Cosilab software using chemical kinetic mechanisms in order to finally propose a correlation relationship of the acetone/air laminar flame speed with pressure, temperature and equivalence ratio.
- *Chapter 6:* Influences of temperature (400 – 523 K) and pressure (0.1 – 1.0 MPa) on the laminar flame speed of kerosene fuels are detailed in this chapter. Different fuels are concerned: pure kerosene components (n-decane, n-propylbenzene, n-propylcyclohexane), surrogate kerosene (blends of three components previously mentioned) and commercial jet fuel (Jet A-1). Several key issues concerning the laminar flame structure (flame opening phenomenon and flame thickness) are discussed. A comparison is made between numerical and experimental results of laminar flame speed for LUCHE surrogate kerosene. Finally, comparisons of laminar flame speeds between pure kerosene components, surrogate fuel and practical Jet A-1 fuel are performed. Temperature and pressure dependence correlation for commercial kerosene Jet A-1 is proposed.
- *Chapter 7:* This chapter is focused on the laminar flame speeds of oxygenated components present in partially hydro-processed lignocellulosic biomass pyrolysis oil. This investigation is targeted to study the impact of these compounds found in the second generation biofuels on

flame speed of gasoline. In order to address possible modifications to combustion properties, preliminary investigations are started by comparing laminar flame speeds of pure oxygenates (anisole, 4-methylanisole, ethyl valerate). Then surrogate fuels (blends of hexane, 2,3 dimethyl-2-butene, cyclohexane, isooctane and toluene) to emulate combustion properties of commercial gasoline are proposed. Finally, laminar flames speeds of surrogate gasoline mixed with various percentages of selected oxygenated compounds are investigated. Oxygenated compounds effects to laminar flame speed of gasoline are analyzed in varying temperature, pressure and equivalence ratios.

Finally, the **fourth part** concludes this study: the results of laminar flame speed of previous mentioned fuels are resumed and a future prospective work is presented.

## Chapter 2 Background on laminar premixed combustion

---

The present chapter intends to provide basic definitions related to laminar premixed combustion. In a first part, the simplest, idealized mode of wave propagation, namely the steady propagation of a planar, one-dimensional, adiabatic wave relative to a stationary, combustible mixture in the doubly infinite domain is briefly described and flame properties such as laminar flame speed, flame thicknesses and flame stretch are introduced. We will also examine experimental data that illustrate how equivalence ratio, temperature, pressure, and fuel type affect the laminar flame speed and flame thickness. In addition, a detailed description of the experimental configurations suitable for the determination of laminar burning velocities and including advantages and drawbacks of each of them will illustrate the choice of the appropriate experimental method to determine the laminar flame speed of various liquid multi-component fuels considered in this study. After reviewing the literature on the experimental studies on laminar flame speeds of the various fuels related in the current study, this chapter concludes with the presentation of the numerical tools and the detailed kinetic mechanisms employed in this study.

## 2.1 Laminar premixed flames

Hereby the present study is dedicated to the structure and propagation of the standard laminar premixed flame. Laminar premixed flame structure is governed by aerodynamics through the following elements: convection, transport (heat and mass diffusion) and chemistry. Laminar flame being a very complex phenomenon, many studies has simplified the problem for practical combustion analysis. An ideal conception and representation is the model of one-dimensional steady flame which is nowadays currently used. The flame is represented as an interface (infinitely thin or not) and separates the fresh gas or unburned gas (reactant side) – *subscript u* – at the temperature  $T = T_u$  from burned gases (product side) – *subscript b* – at  $T = T_b$ . The species mass fraction goes from the initial state  $Y = Y_u$  to  $Y_b = 0$  in the burned gas. Associated with these definitions, laminar flame speed is generally considered as the velocity at which the flame front moves towards the fresh gases, or, in the case of a steady flame, as the velocity at which the inlet gases make the flame sheet steady in the laboratory flame:  $S_L^0$ . Superscript <sup>0</sup> is for planar flame.

### 2.1.1 Premixed flame structure

As shown in the following figures, which are inspired from the work of Law [36], the structure and the propagation of a standard premixed flame can be described using three levels of complexity.

- The simplest model (Figure 2.1) corresponds to the hydrodynamic, flame-sheet level. In this case, the flame is considered as an interface (discontinuity) separating two fluid states of unburned and fresh gases considered at the thermodynamic equilibrium states. Transport and chemistry are not taken into account. At the interface, the temperature and reactant fractions change discontinuously from  $T_u$  (temperature of unburned gases) to  $T_b$  (temperature of burned gases) and from  $Y_u$  (mass fraction of the fresh mixture) to  $Y_b = 0$  respectively.
- A more detailed level of the flame description is completed by transport properties (Figure 2.2): the flame sheet is expanded to reveal a preheat zone which has a characteristic thickness  $\delta_p$  and is governed by heat and mass diffusion processes. When the fresh mixture approaches the flame, it is gradually heated by heat conductivity produced in the heat-release region. The reaction is only activated when temperature is close to the burned gas temperature. Once the reaction is initiated, it is completed rapidly as the deficient reactant is depleted. Thus at the transport level, the reaction zone can be considered to be concentrated at an interface – a reaction sheet, which serves as a source of heat and a sink for the reactant.

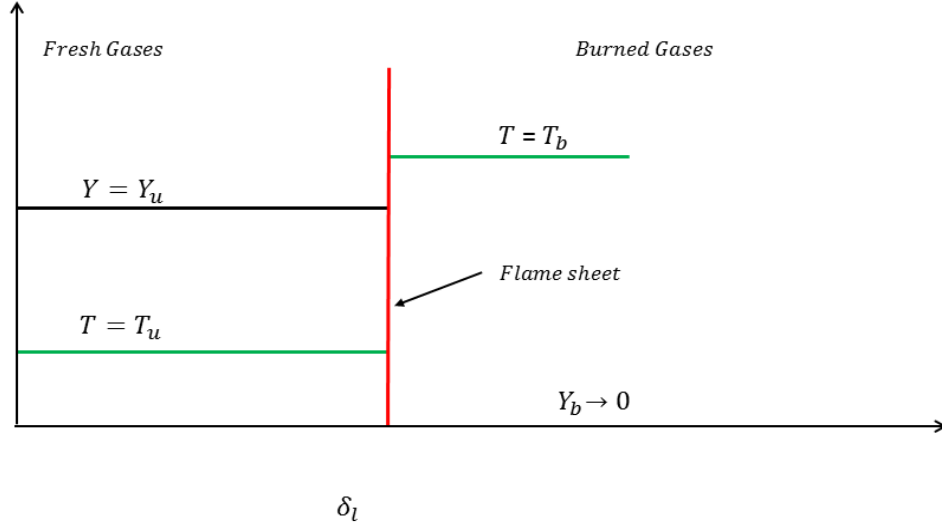


Figure 2.1: Schematic structure of a one-dimensional, planar, steady flame. Simplest model

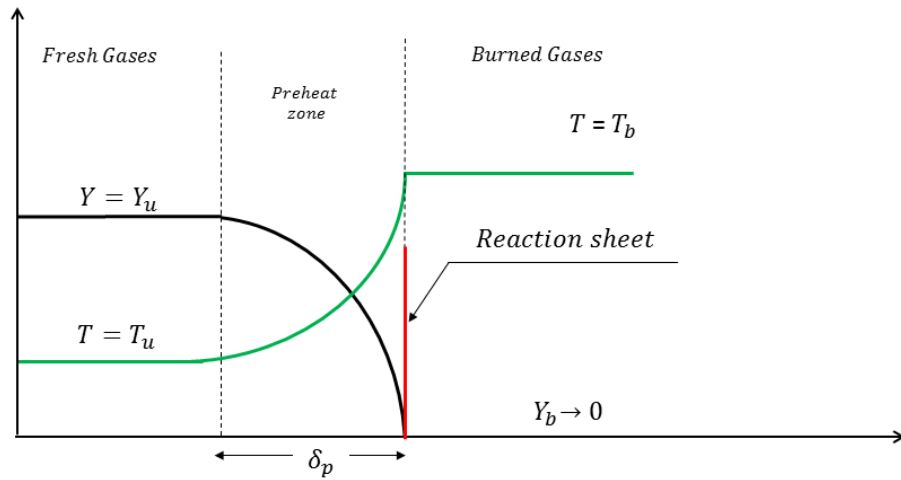


Figure 2.2: schematic structure of a one dimensional, planar, steady flame. Transport dominated model.

- The third level of flame description (theory of Zeldovich, Frank-Kamenetsky, and Semenov based on the one of Mallard and Le Chatelier [37]) takes into account thermal and molecular diffusions. As illustrated in Figure 2.3, the structure of the flame is then divided into two distinct zones: a thin reaction zone (thickness  $\delta_r$ ) in which reaction and diffusion balance and a preheat zone (thickness  $\delta_p$ ) in which convection and diffusion dominate and balance. It is assumed that  $\delta_r \ll \delta_p$ . In the reaction zone, the reaction rate profile results from the combined effect of the activation of the reaction and the depletion of reactants.

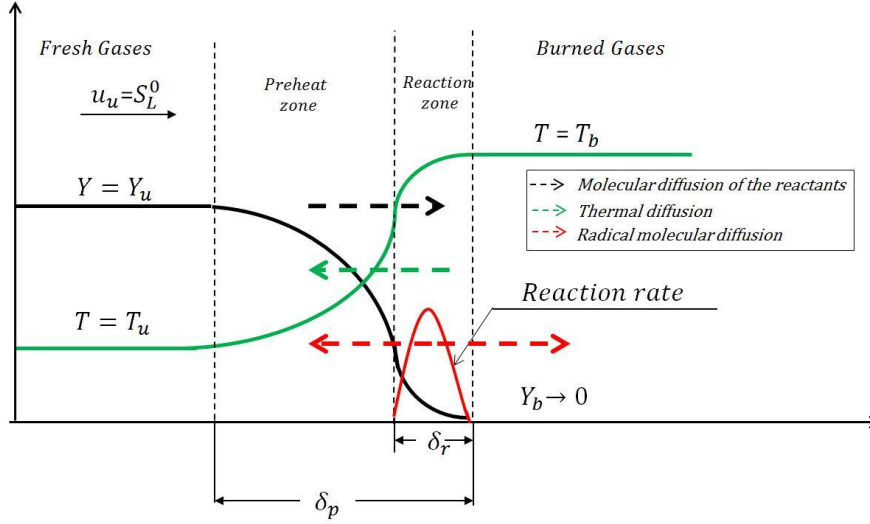


Figure 2.3: Schematic structure of a one dimensional, planar, steady flame. Full description model.

The diffusive and reactive nature of the premixed flame can be illustrated with the phenomenological analysis based on the flame structure previously described. This analysis has been conducted by Law [36] leading to a simple expression related to laminar flame burning flux:

$$(f^0)^2 \sim \left(\frac{\lambda}{c_p}\right) \frac{\omega_b^0}{Ze} \quad (2.1)$$

where  $f^0$  is the laminar flame burning flux defined from the conservation of the masse  $f^0 = \rho_u S_L^0 = \rho_b u_b^0$  (for a stationary flame, the unburned mixture approaches the flame with velocity  $u_u = S_L^0$ , where  $S_L^0$  is the laminar flame speed) and  $\lambda$  is the thermal conductivity of the mixture and  $\omega_b^0 = \omega(T_b)$  is the reaction rate evaluated at the temperature of the thin reaction zone.  $Ze$  is the Zeldovich number, defined by  $Ze = (T_b - T_u)T_a/(T_b)^2$ , where  $T_a = E_a/R$  is the activation temperature.

As reported by Law, by introducing the law  $\omega \sim p^n \exp(-T_a/T_b)$ , where  $n$  is the overall reaction order, Eq. 2.1 can be derived to:

$$S_L^0 \sim p^{\frac{n}{2}-1} \left[ \frac{\lambda}{c_p} e^{-T_a/T_b} \right]^{1/2} \quad (2.2)$$

The above expression shows that the flame speed is related to temperature, pressure and reactive mixtures composition properties as  $\lambda$  and  $C_p$  intergraded in the equation. According to literature, extensive investigations have been conducted on the dependence of the flame speed on the various physicochemical parameters of the mixtures. Laminar flame speed is then an intrinsic property of a fuel. For a given fuel/air mixture, the laminar flame speed is only depending on temperature, pressure and equivalence



ratio. As one of the key objectives of the thesis is to investigate temperature and pressure effects to various hydrocarbon/air mixtures, here a brief introduction of laminar flame speed dependences with temperature and pressure is given.

- Temperature dependence:** The upstream temperature affects the flames in three ways. The first factor is through the adiabatic flame temperature which influences the reaction rate. For low and small changes in the upstream temperature, the influence is not expected to be strong because the chemical heat release, represented by  $q_c$ , is much larger than the thermal energy contained in the upstream flow. For larger values of  $T_u$  the dependence is more sensitive because of the Arrhenius factor. The second factor is due to the change in the transport properties. From the constant property derivation  $\rho_u S_L^0 \sim (\lambda / C_p)^{1/2}$ , since  $\lambda / C_p \sim T^\gamma$ , with  $\gamma < 1$ , the temperature dependence through transport property variation is only moderately sensitive. The last factor is through the sensitivity to the density. For a given mass flow rate with increasing preheat temperature will lead to faster flame speed.
- Pressure dependence:** Equation 2.2 permits one to understand how the flame speed changes with pressure. For a first-order dependence such as that observed for a hydrazine decomposition flame, the flame speed variation trend will be  $S_L^0 \sim P^{-1/2}$  that a higher pressure leads to a decrease of flame speed. Specifically, for a second-order reaction, where  $n = 2$ ,  $S_L^0$  appears to be independent of pressure. However, although for most of the other hydrocarbon air oxidation kinetics is roughly of the second-order, many hydrocarbon/air flame speeds decrease as the pressure rises. This trend is due to the increasing role of the third order reaction  $H+O_2+M \rightarrow HO_2+M$  inducing the chain branching and slowing the rate of energy release.

To describe one dimensional laminar flame, two flame thickness are often referred: the flame thickness  $\delta_r$  characteristics of the reaction zone and the flame thickness  $\delta_p$  taken into account the convective preheat-diffusing zone ( $\delta_r \ll \delta_p$ ). It is important to note that the estimation of the flame thickness is not trivial.  $\delta_p$  estimation was firstly referred by Zeldovich [38] as:

$$\delta_p = \frac{\lambda_u}{\rho_u C_p S_L^0} = \frac{D_{th}}{S_L^0} \quad (2.3)$$

where  $D_{th}$  is the thermal diffusivity of the fresh gases,  $\lambda_u$  is the thermal conductivity of the fresh gases,  $\rho_u$  is the fresh gases density,  $C_p$  is the constant pressure heat capacity and  $S_L^0$  is the laminar flame speed. This expression results from the equilibrium between mass and heat diffusions.  $\delta_p$  represents the diffusive thickness. Since the flame thickness  $\delta_p$  varies inversely with  $\rho_u S_L^0$ , then it should also vary

inversely with pressure which is usually the case. This is physically reasonable because with increasing pressure, the rates of molecular collisions and thereby reactions are facilitated, resulting in faster completion of the reaction as the mixtures flows downstream. At the same time, the tendency for heat and mass diffusion is minimally influenced by changes in pressure because  $\lambda/C_p$  is insensitive to pressure variation. According the numerical work of Law et al. [36], the flame thickness decreases with pressure and the decrease is rather small or even insensitive to pressure for higher pressure. The net effect is that pressure affects the flame thickness primarily through its influence on the reaction rate. In the present work, considering the need of flame thickness values in correcting laminar flame speed, the variation of flame thickness versus pressure, temperature and fuel/air mixtures properties will be further assessed below.

In practice, this thickness calculated by equation 2.3 is not in a good agreement with experimental measurements. Indeed, the calculated values of  $\delta_p$  are usually too small by a factor of order 5 than those experimentally measured [39]. A more useful thickness is obtained from the temperature profile developing into the reaction zone:

$$\delta_{th} = \frac{T_b - T_u}{\max \left( \left| \frac{\partial T}{\partial x} \right| \right)} \quad (2.4)$$

where  $T_b$  and  $T_u$  are the temperatures of burned and unburned gases respectively.

To estimate this thickness, the temperature gradient must be determined. A numerical simulation is needed and the associated grid point number must be large enough to accurately define the reaction zone. These flame simulations make it possible to access different macroscopic flame information such as flame thickness and flame velocity. In order to obtain a better understand of the inner flame structure and reactivity, it is necessary to firstly give basic definition such as flame speed and flame stretch before exploring the governing equations in one-dimension directions.

### 2.1.2 Laminar flame speed definition

In combustion theory, the notion of “the speed of a flame” is the source of many complications because there are several definitions for flame speeds and multiple ways to measure them. First, the fundamental flame speed is the laminar flame speed  $S_L^0$  also called laminar burning velocity; it is the velocity at which a laminar, steady, plane, unstretched, adiabatic flame freely propagates relative to the unburned premixed gas in the direction normal to the flame surface [36]. It is an intrinsic parameter of the flame which only depends on pressure, temperature and species composition of fresh gases. But this theoretical velocity of a “perfect” and undisturbed flame cannot be directly and accurately measured in the case of experimental configurations.

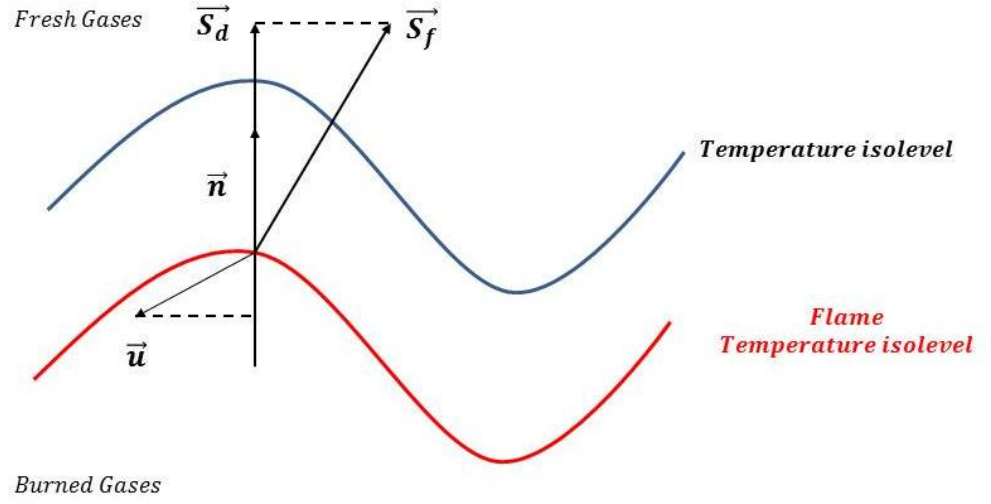


Figure 2.4: Illustration of the displacement speed determination with  $\vec{n}$ , normal to the flame front oriented towards fresh gases,  $\vec{S}_f$ , local flame velocity vector evaluated on the flame temperature isolevel,  $\vec{u}$ , local flow velocity vector evaluated at a chosen fresh gas temperature isolevel,  $\vec{S}_d$ , resulting displacement speed.

Two other definitions of laminar flame speed are then used in the combustion community: the displacement speed and the consumption speed [39]. As described in Figure 2.4 the displacement speed  $S_d$  measures the speed of the flame front relative to the flow, i.e. the difference between the front speed  $S_f$  and the flow speed  $u$  as:

$$S_d = (\vec{S}_f - \vec{u}) \cdot \vec{n} = S_f - u \quad (2.5)$$

with  $\vec{n}$  is the normal direction to the flame front oriented towards the fresh gases,  $\vec{S}_f$  is the local flame velocity vector evaluated on the flame temperature isolevel and  $\vec{u}$  is the local flow velocity vector evaluated at a chosen fresh gas temperature isolevel.

$S_f$ , often referred as the ‘flame propagation speed’ is the absolute speed at which the flame front is moving with respect to the laboratory frame and  $u$  is the fresh gas inlet speed with respect to the laboratory frame.

As for the absolute speed  $S_f$ , the displacement speed  $S_d$  is a local quantity depending on the flame temperature isolevel where it is measured. The displacement speed measured on the fresh reactant side is the speed used intuitively by experimentalists [39].

A third speed is the consumption speed  $S_c$  based only on reaction rates and defined by:

$$S_c = \frac{1}{\rho_u(Y_k^b - Y_k^u)} \int_{-\infty}^{+\infty} \dot{\omega}_k dx \quad (2.6)$$

With  $\rho_u$  the density of unburned gases,  $Y_k^u$  and  $Y_k^b$  the mass fractions of species  $k$  at  $-\infty$  and  $+\infty$  respectively and  $\dot{\omega}_k$  the reaction rate of species  $k$ .

The consumption speed  $S_c$  measures the speed at which the flame burns the reactants. It is a global quantity resulting from an integral over all the temperature isolevels across the flame front. In the case of a laminar, premixed, one-dimensional, steady, plane, unstretched and adiabatic flame, these three definitions give an identical value of the flame speed:  $S_d = S_c = S_L^0$ . Indeed, the steady plane flame moves towards fresh gases at the velocity  $S_L^0$  (so  $S_d = S_L^0$ ) and burns them at the velocity  $S_L^0$  (so  $S_c = S_L^0$ ). For unsteady flames, differences exist between velocities because the effects of stretch and curvature of the flame front modify the flame speed.

In the case of a Bunsen flame (present thesis), it is the averaged consumption speed all along the flame which is measured. The results reported by Selle et al. [40], Dhué [41] and Albin et al. [42] revealed that the averaged value of  $S_c$  is close to  $S_L^0$  in the unstretched region of the flame but these velocities differ in the quenched zone (at the flame base) and in the curved zone (at the flame tip).

### 2.1.3 Flame stretch

A flame front propagating in a non-uniform flow is subject to strain and curvature effects which modify the flame area [43]. These effects are quantified by the flame stretch. The flame stretch is defined by the fractional rate of change of a flame surface element  $A$ .

$$K = \frac{1}{A} \frac{dA}{dt} \quad (2.7)$$

From this expression, various derivations of the flame stretch can be found in the literature [44] [45] [46]. The definition referred in the present work is the formulation proposed by Candel and Poinso [46]:

$$K = \nabla_t \cdot \vec{u} + s_d \nabla_t \cdot \vec{n} \quad (2.8)$$

where  $\vec{u}$  is the local flow velocity,  $\vec{n}$  is the unit vector normal to the flame surface pointing towards the fresh gases and  $s_d$  is the displacement speed. The term  $\nabla_t \cdot \vec{u}$  represents the tangential velocity component of the flow velocity at the flame. It is a strain term which is related to the flow non-uniformity. The term  $s_d \nabla_t \cdot \vec{n}$  is relative to the curvature of the reaction front.

Thus, it is conventionally admitted that the flame is subject to three types of stretch effects, individually referred to aerodynamic straining, flame curvature and flame motion. For stretched flames, the asymptotic theories developed by [47] [48] [49] [50] suggest that in the limit of weakly stretched flames (small strain and curvature terms) and for a Lewis number close to unity, the stretch  $K$  is the only parameter controlling the flame structure and therefore the laminar flame speed through the following linear relationship:

$$S_L = S_L^0 - \mathcal{L}K \quad (2.9)$$

With  $\mathcal{L}$  the Markstein length [51] characterizing the flame sensibility to stretch.

In the case of high stretch rates and/or mixtures with strong thermo-diffusive instabilities, recent studies [52] [53] [54] pointed out that linear extrapolation to zero stretch rate can result in an over-prediction of the unstretched laminar burning velocity  $S_L^0$  and they recommended the use of the following non-linear relationship:

$$\left(\frac{S_L}{S_L^0}\right)^2 \ln \left(\frac{S_L}{S_L^0}\right)^2 = -2 \frac{\mathcal{L}K}{S_L^0} \quad (2.10)$$

Relations (2.7) and (2.8) can be used with the three preceding definitions of the velocity: the flame propagation speed  $S_f$ , the displacement speed  $S_d$ , the consumption speed  $S_c$  and with their associated Markstein lengths  $\mathcal{L}_f$ ,  $\mathcal{L}_d$ ,  $\mathcal{L}_c$ .

#### 2.1.4 Experimental determination of laminar flame speed

As indicated before, the laminar flame speed is defined as the velocity at which unburned gases move through the combustion wave in the direction normal to the wave surface. In situation of an ideal system like an infinite plane flame, the theoretical conditions presented above can be unambiguously applied to determine the laminar flame speed. However, performing measurements of burning velocities in “real” laminar flames are often subject to distortions of the flame surface related to the effects of stretch, as well as the adiabaticity of the process. Since it is impossible to get a planar, adiabatic flame in a uniform velocity field, several experimental methodologies were specifically developed and used in the past to reduce the influence of these perturbations on the flame or to subtract their effect on the measured flame speeds. Several experimental configurations are commonly mentioned in the scientific literature for fundamental laminar flame speed measurements. They include spherically expanding flames, counter-flow and jet-wall stagnation flames, flat and one-dimensional flames (heat flux method) and conical flames. All of these configurations, presenting distinct advantages and drawbacks which have to be taken when performing the measurements of laminar flame speeds are now briefly described in the remaining part of this section.

##### (a) *The spherically expanding flame method*

In this configuration, a spherical bomb is filled with the quiescent gaseous air/fuel mixture to be studied. The mixture ignited at the center of the chamber with thin electrodes, then produces the propagation of a spherical expanding flame in the outward direction. From the pressure records, burning velocity could be deduced using an approach developed and described by Lewis and Von Elbe (1961). Nowadays, most of the bombs provide optical accesses to visualize flame propagation. The temporal evolution of the flame front is then tracked with Schlieren and shadow visualizing techniques or PIV laser diagnostic and the temporal evolution of the flame radius is recorded, leading to the determination of the burned gases propagation velocity as a function of the stretch. The unstretched laminar flame speed is then inferred from this velocity, which is obtained with linear or non-linear extrapolation to zero stretch rates [55] [52] and rescaled by the burned-to-unburned gas density ratio. This configuration is quasi-adiabatic, well adapted to rich flames produced in a large range of inlet temperatures and elevated pressure environments (up to 5 MPa [3]). Its disadvantages arise from possible distortion of the flame surface due to buoyancy effects (especially for burning flames developed at low speed), the influence of the ignition process (electrodes, heat losses, and energy deposition), the need to use linear or nonlinear extrapolation to zero

stretch and the existence of possible intrinsic flame instabilities at elevated pressures (especially for large flame radius). Another issue, which was often overlooked in the derivation of the flame velocity, is the normalization of the velocity using densities before and after the flame front. Usually, the ratio of these densities is calculated on the assumption of ideal adiabatic flame propagation; however, the validity of this assumption has never been checked. Further analysis is therefore needed to reconcile inconsistent results obtained using spherical flames. Another limitation is the difficulty in measuring flame speed in relatively high preheating temperatures. At elevated temperatures, the residence time necessary to ensure no motion of the reactants inside the bomb vessel could yield to auto oxidation of reactants inside the vessel which will significantly influence the measurement accuracy [56] [57] [58] [59]. The last major issue concerns the difficulty to ensure that the reactants do not re-condense inside the spherical bomb when heavy fuels with high boiling points are studied.

*(b) The counter-flow and jet-wall stagnation methods*

The counter flow and jet wall stagnation methods consist in the stabilization in a well-defined stagnation flow fields of a steady one-dimensional laminar flame [60]. The stagnation flow field is generated either by impinging two identical premixed flows onto each other or by impinging a premixed flow on a solid wall. Depending on the configuration, one or two symmetrical stretched flat flames are stabilized on each side of the stagnation plane. Using LDV or PIV laser diagnostics, the flow velocities are measured and the corresponding stretch is deduced. Then choosing the velocity just before the flame front, a correlation between this velocity and stretch can be evaluated. As for the spherically expanding flame method, the unstretched flame speed has to be extrapolated from correlations using linear or non-linear methods [55] [61] [62] [63]. Advantages of these methods come mainly from the fact that the aerodynamically stabilized flames are nearly adiabatic and stable and so facilitate the implementation of laser diagnostics. The curvature effects are also eliminated and the aerodynamic strain can be well-controlled. Furthermore, fresh gases can be preheated before feeding the burner and the burner can be placed in high-pressure facility to measure the laminar flame speed [64]. Major disadvantages are related to the extrapolation to zero stretch. Flow uniformity is also a key parameter to approach 1D conditions of stretch. The use of laser velocimetry diagnostics requires a steady source of seeding particles. Furthermore, these methods are not adapted for reactive mixtures featuring high burning velocities (typically more than  $1 \text{ m.s}^{-1}$ ) [65].

*(c) The flat flame and heat flux methods*

This original method is based on the procedure initially introduced by Botha and Spalding (1954) [66]. In doing so, a premixed planar flame is stabilized through heat loss to the surface of the burner from which the fresh mixture is injected. Then the flame becomes adiabatic only in the limited range of zero heat loss to the burner when the burner turns unstable. Heat loss rate variations are then used to determine the

laminar flame speed without heat losses by extrapolating the cooling rate to zero. This method has been recently improved by De Goey and co-workers. In this method, the planar flame is stabilized on a heated perforated brass plate. The heat loss required for the flame stabilization can be then balanced by the convective heat flux from the burner surface to the flame front [67] [68]. One of the major advantages of the heat flux method is nearly zero stretch of the flames, and thus no extrapolation of the stretch is required. Another advantage is that the flame is planar and adiabatic with respect to the burner, thus the determination of the laminar flame speed without any corrections for stretch is facilitating. Furthermore, this method was also recently extended for measurements at pressures up to 0.5 MPa [69]. However, this method also presents some drawbacks. A major disadvantage is that the flame can be too close to the burner surface at atmospheric pressure (but mostly at larger pressures) and possible depletion of radicals at the burner surface could impact on the flame chemistry. Another issue is the limited range of laminar flame speed to be investigated. Only flames with laminar burning velocities up to 40 - 60 cm.s<sup>-1</sup> can be analyzed. Above that, the flame surface presents some distortion induced by the presence of the perforated burner plate preventing a good accuracy on laminar burning velocities [65] [70]. Difficulties in flame stabilization at elevated pressures due to cellularity could also occur. Finally, the last major drawback of this method is that the laminar flame speed is determined by extrapolation.

*(d) The conical flame method (Bunsen flame configuration)*

The Bunsen approach uses a 2D or axisymmetric conical premixed flame stabilized on the lip of a contoured nozzle or a slot burner, respectively. A nearly straight flame cone can then be produced over the shoulder region of the flame. The Bunsen flame method is recognized to be robust and reliable. Only a stable flow of a combustible mixture is required. The burner could be preheated to study temperature dependence and set in a high-pressure chamber to measure laminar burning velocities in conditions relevant of real combustion engines. Unlike other methods, the Bunsen burner method is well adapted for measuring burning velocities over a wide range of velocities. As with other methods, The Bunsen burner method presents some limitations. The conical flame can be influenced by aerodynamic straining (tangential velocity gradient along the flow axis) and curvature (at the flame lip and azimuthal curvature for 3D conical flame) and their combined impact on local flame speed depends on the Markstein length of the reactive mixture [55]. Furthermore, the laminar flame speed can be varied over the whole flame surface area [71], especially at the flame tip in which non-equidiffusion effects can be observed [72] [73]. Finally, thermal heat losses can occur at the burner rim while this effect could be reduced significantly in case of a confinement of the heat loss to the base of the flame [73]. Despite these restrictions, the Bunsen burner method can be used when all other methods fails for some reasons. For instance, several recent studies [74] [75] suggested that a modified Bunsen flame area method that relies on the reaction-zone area of the flame for determining the flame speed, provides a good estimate of the unstretched and unburned flame speed. Various imaging techniques such as Schlieren, shadowgraph, chemiluminescence,



PIV and PLIF can be used to visualize and record the cone boundaries from which the laminar flame speed is deduced. They are two conventional methods to deduce the laminar burning velocity from this conical flame: flame area method and flame angle method. These methods will be further addressed in chapter 4.

### **2.1.5 Choice of the experimental flame method**

A suitable experimental burner for laminar flame speed measurements mainly depends on the range of burning velocities and experimental operating conditions (pressure, temperature, equivalence ratio and fuel composition) to be explored. In the current work, a modified Bunsen flame burner has been selected and developed to measure the laminar flame speeds of various gaseous and pre-vaporized fuels, namely methane, acetone, kerosene and its LUCHE surrogate fuel, gasoline and oxygenated fuels. The reasons that explain the choice of the Bunsen flame method in the present work are now presented:

- All the measurements must be performed in a large range of preheating temperatures (up to 650 K), pressures (up to 2.0 MPa) and equivalence ratios (0.6 to 1.3). It is also established that the range of the expected burning velocities obtained for such conditions could be extend on a large domain. On the basis of the performances of the flame methods previously described, it appears that the methods suitable for these “hard” operating conditions are only limiting to the spherically expanding flame and the conical flame methods for which measurements of laminar flame speeds at elevated pressure are quite easy to perform. As tempting as the performances of the other methods may exist, their uses are not retained in our study in regards to the complexity to perform measurements of flame burning velocities in an extended domain and to control the stabilization of laminar flames in elevated pressures.
- As the burner should be able to generate laminar flames of a large range of fuel/air mixtures, the diversity of the chemical characteristics of the fuels presently investigated is also a key parameter to be considered. One parameter to take into account is the boiling point of the liquid fuels that can be elevated ( $> 200^{\circ}\text{C}$ ), thus complicating the evaporation process and the propensity to keep the fuels in vapor before they are burning. To achieve this, the burner used to produce laminar flames must be equipped with an evaporation module, thus forming an experimental setup capable of burning either gaseous or vaporized liquid fuels at elevated preheating temperature and pressure conditions. This system must ensure a complete evaporation of the liquid fuel as well a perfect mixing of the vapor fuel with air. The resultant vapor fuel/air must then be heated at a temperature sufficient to avoid any condensation of the fuel on the walls of the elements guiding the vapor mixture in the combustion chamber. On the basis of the performances of the spherically expanding flame and Bunsen flame methods, the precise control of a uniform gas temperature distribution within the bomb during the

delay time required to establish a quiescent flow before ignition seems remains a hard task while the steady state flow conditions established within the Bunsen flame method makes easy the monitoring of the gas temperature at the entrance of the combustion chamber.

- Another parameter to be taken into account is the propensity of these fuels to pyrolyze easily in the operating conditions investigated in the current study. Indeed, measurements in elevated preheating temperatures imposes a reduction of the resident time of the preheating vapor fuel/air mixture inside the inlet pipes in order to avoid any change of the chemical structure of the fuel before its burns into the combustion chamber. In case of the spherically expanding flame method, this phenomenon cannot be well controlled because the reactants need time to be injected into the combustion chamber and to ensure a quiescent flow before ignition. During this delay, the removal of the fuel by pyrolysis can occur especially when the preheating temperature is comparable to the temperature of pyrolysis of the fuels investigated [22]. Furthermore, this phenomenon is exacerbated at elevated pressure. It makes the spherical flame method then unsuitable for our study. On the contrary, an efficient design of the Bunsen burner enables the reduction of the residence time of the preheating mixture, preventing then the pyrolysis of the fuel when measurements are performed at the maximum preheating temperatures investigated in the current study.
- The last issue of the selection of Bunsen flame method is related to the robustness and the simplicity of this method for experiments intended to measure laminar flame speeds over a wide range of experimental conditions and fuel mixtures [76] [75].

## **2.2 Literature review on measurements of laminar flame speeds**

The first measurement of laminar flame speeds was performed in 1934 by Lewis and Von Elbe [77] for ozone/oxygen mixtures inside a spherically expanding flame. From then on, numerous measurements have been accomplished with various experimental techniques as previously mentioned for both gaseous and liquid fuels. Most of the studies were initially focused to the study of mixtures of pure gaseous fuels with air such as methane, ethane or propane. At the same time, the accuracy on the measurements of laminar flame speeds has been continuously improved while the operating conditions were progressively extended to higher pressures and preheating temperatures. From some years now, an increasing number of experimental investigations of laminar flame speed measurements of liquid fuels representing higher hydrocarbons as well as real multi-component fuels such as gasoline, diesel or kerosene have emerged. In the current study, the prime purpose of the studies is focused on measurements of the laminar flame speeds of several fuels belonging to the preceding chemical families: methane for pure gaseous fuels, acetone for single-component liquid fuels, kerosene fuels (n-decane, n-propylbenzene, propylcyclohexane, surrogate kerosene and Jet A-1) and biomass oxygenated fuels (anisole, 4-methylanisole, ethyl valerate and surrogate biofuel of the second generation). A state-of-the-art about the knowledge of the evolution of the laminar flame speeds of these fuels with pressure, inlet temperature and equivalence ratio is now briefly examined in the remaining part of this section.

### **2.2.1 Methane /air mixtures**

Methane ( $\text{CH}_4$ ) is the simplest of the hydrocarbons and is the major constituent of natural gas, typically comprising 93 – 96 % by volume. Laminar burning velocities of methane-air mixtures as a function of temperature, pressure and stoichiometric ratio have been measured by many investigators using several experimental techniques. A large summary of the laminar flame speeds measurements published in the scientific literature on methane/air mixtures is presented in Table 2.1. This table lists the operating conditions for which measurements of laminar burning velocities were performed as well as the associated flame methods. As observed in Table 2.1, these experiments were conducted most often at moderate pressures (between 0.1 and 1.0 MPa) and room temperature conditions.

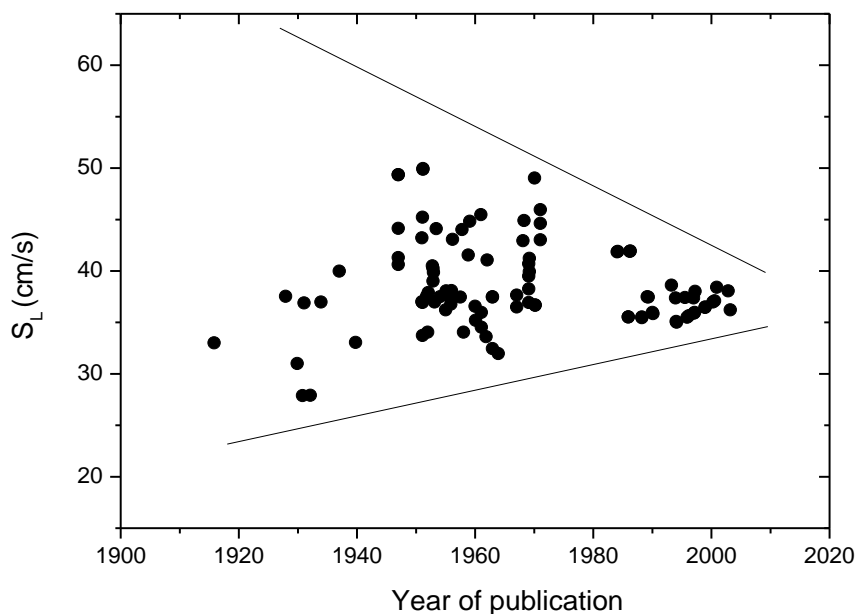


Figure 2.5: Evolution of the laminar flame speed of  $\text{CH}_4/\text{air}$  mixtures at 298 K, atmospheric pressure and  $\phi = 1.0$  as a function of the years [78].

As shown in Figure 2.5, the experimental laminar burning velocity data for this molecule were inconsistent for a long time. The laminar burning velocity for a stoichiometric mixture at ambient conditions varied typically between 35 and 45 cm/s. With the progresses of the flame methods, a major breakthrough came when Van Maaren and de Goeij [79] demonstrated numerically that flame stretch due to flame front curvature and/or flow divergence must be taken into account. For this reason, the methodology of the determination of laminar burning velocity with the counter flow twin-flame technique by extrapolation to zero stretch rates has been further improved [80]. The same author yields for the spherically expanding flame method where the experimentalist has to use essentially the same approach to determine the unstretched burning velocities. More recently, the heat flux burner has improved the accuracy of measurements of the laminar flame speed of methane. Nowadays experimental data of laminar burning velocities of methane/air mixtures, with the applied new insights, lead to a better consensus that is for stoichiometric methane-air flames  $\approx 36.5$  cm/s within  $\pm 1$  cm/s. It also comes from progresses in the measurements methodologies used to take into account the effect of flame stretch (linear or non-linear) and to use more accurate and reliable experimental devices (digital flow meters, pressure and temperature sensors). Undoubtedly, this molecule can be now commonly used as a reference fuel for validating measurements of laminar flame speeds with various flame methods. However, extensive research remains to be done in this field, particularly in high-pressure (more than 1.0 MPa) and high temperature operating conditions for which measurements of laminar flame speeds are still incomplete [56]. In the current study, methane was used 1) for validating the experimental setup specifically developed in the current study and 2) for improving our understanding on the evolution of the laminar flame speeds with pressure and preheating temperatures.

Year	Author	Flame	P (MPa)	T (K)	$\Phi$
1984	Gulder [81]	Spherical	0.1	300	0.8-1.3
1985	Wu and Law [82]	Stagnation/Bunsen	0.1	298	0.8-1.3
1989	Egolfopoulos et al. [83]	Counter flow	0.025-0.3	298	0.55-1.5
1989	Haniff et al. [84]	Bunsen	0.1	298	0.85-1.2
1994	Van Maaren et al. [67]	Heat flux	0.1	298	0.65-1.5
1995	Lauer et al. [85]	Bunsen	0.1	298-673	0.65-1.5
1998	Hassan et al. [86]	Spherical	0.05-0.4	298	0.6-1.35
1998	Egolfopoulos [87]	Counter flow	0.1	298	0.7-1.4
2000	Gu et al. [12]	Spherical	0.1-1.0	300-400	0.6-1.35
2004	Bosschaart et de Goey [68]	Heat flux	0.1	293-353	0.6-1.6
2005	Halter et al. [10]	Spherical	0.1	298	0.7-1.2
2005	Takizawa et al. [88]	Spherical	0.1	280-330	0.7-1.3
2006	Huang et al. [89]	Spherical	0.1	300	0.6-1.4
2009	Hu et al. [90]	Spherical	0.1	303	0.6-1.3
2010	Hermanns et al. [91]	Heat flux	0.1	298-418	0.8-1.2
2011	Mazas et al. [92]	Bunsen	0.1	298, 373	0.8-1.5
2013	Goswami et al. [69]	Heat flux	0.1-0.5	298	0.8-1.4
2013	Hu et al. [93]	Spherical	0.099-0.69	298	0.6-1.4
2013	Troshin et al. [94]	Spherical	0.-1.0	295-573	0.6-1.0

*Table 2.1: Literature review of laminar flame speed methane/air mixtures.*

### 2.2.2 Acetone/air mixtures

Ketones are present as reaction intermediates in flames of oxygenates and it is therefore necessary to understand their combustion characteristics for development of accurate detailed mechanisms. Among the few ketones which have been studied under flame conditions, acetone has drawn increasing interest in recent years because it is an oxygenated hydrocarbon representing the smallest hydrocarbon regrouping alcohol isomers, aldehyde and acetones structures. An analysis of its performances in combustion shows that this molecule represents a good candidate to build a first combustion mechanism block required for the development of more accurate kinetic models for larger oxygenated hydrocarbons that concerns to renewable biofuels issues. Another reason for the interest in acetone is that this molecule is commonly used as a fuel tracer for the Planar Laser-induced Fluorescence (PLIF) diagnostic used to measure the

spatial distribution of fuel inside reactive flow fields. In the current study, acetone was used for two main reasons: 1) the validation of the experimental laminar premixed burner when this one is operated with liquid fuels as well as the associated experimental methodology for measuring laminar flame speeds and 2) the measurement of laminar flame speeds over a wide range of conditions including temperature, pressure and equivalence ratios for improving the accuracy of the measurements published in literature.

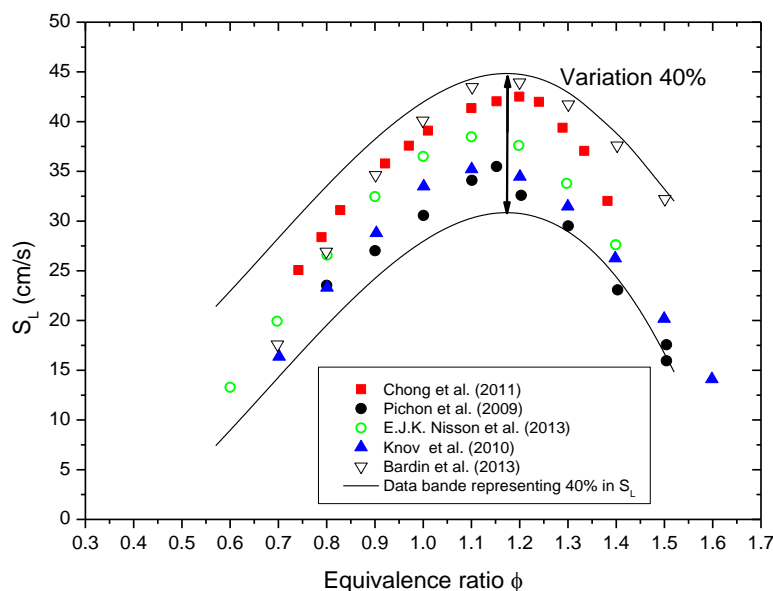


Figure 2.6: Laminar flame speed acetone/air mixture; literature data at atmospheric pressure and room temperature.

An analysis of the data published in literature reveals that the laminar flame speed of acetone/air mixtures has been already visited by several research groups [95] [96] [97] [31] [98] [99]. Chong and Hochgreb [31] performed laminar flame speed measurements using the particle imaging velocimetry (PIV) laser diagnostic in a jet-wall stagnation flame at atmospheric pressure and for a preheating temperature of 300 K. The laminar flame speeds were also measured by Nilsson et al. [98] using a perforated plated burner at atmospheric pressure and initial temperatures ranging from 298 to 358 K. Information concerning fundamental scalar parameters such as ignition delays were also issued from studies reported by Pichon et al. [99]. Shown in Figure 2.6 are the evolution of the laminar flame speeds published in literature with the equivalence ratio for experiments performed at 298 K and atmospheric pressure [96] [97] [31] [98] [99]. As with the case of methane, large variations between laminar flame speeds are observed. The gap between measurements could be up to 40%, making difficult from these results to accurately validate detailed kinetic mechanisms. Furthermore, few experimental investigations at elevated pressures and preheating temperatures greater than 400 K are reported in literature. As a consequence, efforts have to be done to perform measurements in a wide range of preheating temperature, pressure and equivalence ratio to establish a good relationship between the laminar burning velocities and the operating conditions and then to validate or not the actual detailed kinetic mechanism published in literature.

### 2.2.3 Kerosene fuel

Kerosene (or Jet A1) fuel is a practical transportation liquid hydrocarbon multicomponent fuel mainly used for aeronautic propulsion systems. Its composition is complex and consists of a mixing of several hundred molecules. Typically, this one involves approximately 50 – 65 % paraffins, 10 – 20 % aromatics and 20 - 30 % naphthenics that make the elucidation of each component's chemistry in the fuel very difficult. A useful approach in developing detailed chemical-kinetic mechanism for such complex fuels is then to use surrogate mixtures of a limited pure hydrocarbon components to replicate the physical and chemical properties of kerosene. In that case, the surrogate fuel simplifies the complex composition of kerosene but maintains the main characteristic of the practical fuel. The fidelity of the surrogate fuel depends directly not only on the accuracy of the pure components models, but also the ability to reproduce the flame characteristics of the practical fuel. Hence, fundamental combustion properties such as the laminar flame speed of pure hydrocarbons and the practical fuel can be very useful as target validation of the detailed kinetic mechanism. In the following, this section provides an initial source of references and guidance regarding the present status of laminar flame speeds measurements on kerosene and associated surrogate fuels as well as the main pure components contained in the surrogate fuel investigated in the current study.

#### (a) *Commercial kerosene fuel*

While the commercial kerosene (Jet A-1) fuel has been used for decades in aeronautics, the knowledge of the laminar flame speed and laminar flame structure characteristics were until very recently limited. It is only in recent years that the science of laminar flame speeds has matured dramatically thanks to the progress of the measuring devices used. Table 2.2 illustrates the results found in the literature. In the recent work of Kumar et al. [100], the evolution of the laminar flame speeds of Jet A-1 with the equivalence ratio was investigated with the counter-flow flame method at atmospheric pressure and preheating temperatures of 400 , 450 and 470 K. Hui et al. also measured the laminar flame speed of Jet A-1 using the same methodology [101] and efforts were focused on measurements in pressure ranged between 0.1 and 0.3 MPa, preheated temperature comprised between 350 and 470 K and equivalence ratio extending from 0.7 to 1.3. In this study, the unstretched laminar flame speed was deduced from linearly extrapolation of the stretched laminar flame speeds. While their measurements were both generated using the same counter-flow flame burner, the scattering of the experimental data are significant. Furthermore, their results for fuel rich mixtures were systematically overestimated compared to the results obtained in other studies. Considerable discrepancies with simulation results were also observed. For pressure higher than 0.5 MPa, the only investigation on laminar flame speed measurements of Jet A-1 was reported by V. Vukadinovic et al. [22]. In this study, the laminar flame speed was measured at pressure up to 0.8 MPa using the constant volume combustion-bomb method. The linear

correlation was used to derive the unstretched flame speed. Another laminar flame speed measurements are listed in the work of Chong et al. [31]. The application of the PIV optical technique on a jet wall stagnation flame method was used to measure not only the laminar flame speed of Jet A1, but also the practical Diesel fuel and fuel blends.

Authors	Fuel	P (bar)	T (K)	$\Phi$	Flame	Ref.
Singh et al. 2011	Jet A-1	1	400	0.75-1.4	Spherical	[26]
V.Vukadinovic et al. 2013	Jet A-1	1-8	373-473	0.7-1.3	Spherical	[22]
Chong et al. 2011	Jet A-1	1	470	0.7-1.4	Stagnation	[31]
Hui et al. 2013	Jet A-1	1-3	400	0.7-1.3	Counter flow	[23]
Kumar et al 2011	Jet A-1	1	400-470	0.7-1.4	Counter flow	[100]
Far et al. 2006	JP-10	1-6	450	0.8-1.0	Spherical	[102]
Kick et al.2012	Synthetic Paraffinic Kerosene	1	470	1.0-1.4	Bunsen	[103]

*Table 2.2: Summary of laminar flame speeds of commercial kerosene fuel.*

Generally, large discrepancies (up to 15 cm/s) are observed between the different results. The origins of these discrepancies are multifold: (a) for experiments inside the spherical bomb, the variation of the energy deposited by the spark plug during ignition can explain a variability of the laminar flame speeds; similarly, linear or non-linear correlation extrapolation to unstretched flame speed could yield differences [9]; (b) due to the high variability in composition of kerosene from the different batches, the chemical composition of kerosene respecting the ASTM standards can be different and then affect the laminar flame speed measurements [14]; (c) the measurement uncertainties relative to the experimental parameters that control the experimental devices (flowrate control for mixture preparation, temperature and pressure) can also be at the origin of some variations [6].

#### *(b) Surrogate kerosene fuels*

As previously noted, the study of neat hydrocarbon surrogate fuels to model the properties of conventional aviation fuel is common in the combustion research community. Surrogates can be classified as physical, chemical or comprehensive; the first simulates the physical properties of the conventional practical fuel such as viscosity, surface tension, and density, while the second is selected to replicate one or more combustion properties, and comprehensive surrogate blends match both physical and chemical properties. Table 2.3 summaries the surrogate fuels proposed by the research teams in the past to simulate the industrial kerosene fuel.



Composition	Emulating target fuel	Reference
m-Xylene, isooctane, Methyl cyclohexane, n-Dodecane, n-Tetradecane, Tetralin	JP-8	Holley et al. 2007 [24]
n-decane, n-butyl cyclohexane, n-butyl benzene	General jet fuel	Natelson 2008 [104]
n-decane and 1,2,4-trimethylbenzene (Aachen surrogate)	General jet fuel	Honnet et al. 2009 [25]
iso-octane ,methylcyclohexane ,m-xylene, dodecane, tetralin, tetradecane (Utah/Yale surrogate)	JP-8	Cooke et al. [105]
n-decane, n-butyl benzene and n-n-propylbenzene	General jet fuel	Comandini et al. 2015 [17]
n-decane, n-n-propylbenzene, n-propylcyclohexane	Jet A-1 (reduced mechanism)	Luche et al. 2004 [32]
n-decane, n-n-propylbenzene, n-propylcyclohexane	Jet A-1	Dagaut et al. 2006 [106]

*Table 2.3: Summary of the studies on the laminar flame speed of surrogate kerosene fuels in the last decade*

Apart of the aforementioned studies of the laminar flame speed measurements of the industrial kerosene fuel, several single-, and two- or multi-component surrogate fuels were proposed and experimentally studied. Generally, the composition of the surrogate fuels is consisted of three main compounds: paraffins, aromatics, and naphthenics [16]. The earliest proposal on the definition of a surrogate kerosene fuel started from the study performed in the late 1980s by Wood in which a 14 hydrocarbon component blend was proposed to simulate the JP-4 kerosene [107]. Similarly, Schulz et al. defined a 12-component surrogate for the JP-8 fuel in 1991 [108]. More recently, efforts were devoted to reduce the components to about 10 since it was common to model the surrogates based on the composition of the practical fuel, including low concentration components such as naphthalene and several hydrocarbons of the same type [109]. Then, the number of components has progressively decreased to culminate in one-, two- or three-component surrogate fuels [108] [110] [111] [112] [113]. Among the available surrogates, the UCSD (n-dodecane/methyl cyclohexane/o-xylene) surrogate [113] and the Aachen surrogate (n-decane/1, 2, 4-trimethylbenzene) [80] were able to show good agreements for auto-ignition and extinction strain rate of

commercial kerosene fuels. Laminar flame speeds of the Aachen surrogate fuel was measured using the spherically expanding flame method at atmospheric pressure and  $T = 473$  K. A. T. Holley et al measured the extinction strain rate and the ignition temperature of the surrogate fuels using a counter-flow burner at atmospheric pressure and elevated preheating temperature [24]. Comparisons between single component hydrocarbon and surrogate jet fuel for JP-8 was also conducted. A very recent investigation of the laminar flame speed the surrogate fuel consisted in n-decane, n-butyl benzene and n-n-propylbenzene was also conducted by Comandini et al. [17] with the spherically expanding flame method at  $T = 403$  K and  $P = 0.1$  MPa. In this study, the comparison between the laminar flame speeds of pure components and a surrogate mixture was discussed in detail. Besides the Aachen surrogate and the surrogate proposed by Comandini, few measurements of laminar flame speeds for other surrogate fuels were reported and compared to those obtained with commercial kerosene fuels. Other compositions of surrogate fuels involving only three components, n-decane, n-propylbenzene and propylcyclohexane, were also proposed by Dagaut et al. and Luche et al. to develop detailed kinetic mechanisms able to reproduce the combustion of industrial kerosene fuels [16]. However, until now no measurements of laminar flame speeds were performed to validate these kinetic models.

(c) *Pure components of kerosene fuel*

The elaboration of new surrogate fuels usually consists of two tasks: the development of a detailed kinetic mechanism and its validation from the comparison of the simulation results with experimental data. Generally, the detailed kinetic mechanism of the surrogate fuel consists in the integration of existing single component fuel and/or multi-component chemical mechanisms and extends to include new fuel components. The detailed kinetic reaction mechanisms for pure components of the surrogate fuel usually have first to be established before merging the sub-mechanism to yield a kerosene kinetic reaction mechanism. Hence, laminar flame speed measurements of single component fuel have practical importance. For the current work, the pure components that have been selected are n-decane, n-propylbenzene and n-propylcyclohexane.

- n-decane

Most of the complex fuel models use the linear n-alkane chemical family as part of the mechanism development. At such, the knowledge of the laminar flame speed of the Jet A1 fuel require a detailed understanding of the laminar flame speed of such molecules. In particular, n-decane has retained the attention of many researchers in the past because this is one species belonging to the three chemical families representative of an industrial kerosene composition (linear alkanes, aromatic and naphtenic). Furthermore, it has been also demonstrated that its kinetic mechanism reproduces well the main profiles of concentration of species issued from the oxidation of kerosene in a perfectly stirred reactor [114]. With

this in mind, considerable efforts were undertaken in the past for measuring the laminar flame speed of n-decane. To do this, many flame methods were used. For instance, the measurements of the laminar flame speeds of n-decane as well as a comparison with simulations performed using the Jet surf 2.0 detailed kinetic mechanism [82] are presented in Figure 2.7. The pioneer work carried out with the stagnation flame method was the one reported by Kumar et al. [7]. Then, X. Hui [23] used the same methodology to measure the laminar flame speeds in similar conditions. An observation of the results presented in Figure 2.7 reveals that except the work of Munzar et al. [115] most of the laminar flame speeds recorded using stagnation flame methods gives larger values compared to the simulation ones as well as to the results obtained with other measurement methods. This general tendency that stagnation flame method gives overestimated flame speeds has been also reported in the work of Singh et al. [26]. A plausible reason of these overestimated values related to stagnation flame method may be caused by the use of the linear extrapolation technique as noticed by Comandini et al. [17]. On the contrary, other studies conducted with a spherical bomb method give values similar to the simulations [26] [27]. This is especially the case for the work of Comandini et al that give a good agreement with the Jet surf 2.0 mechanism simulations [17].

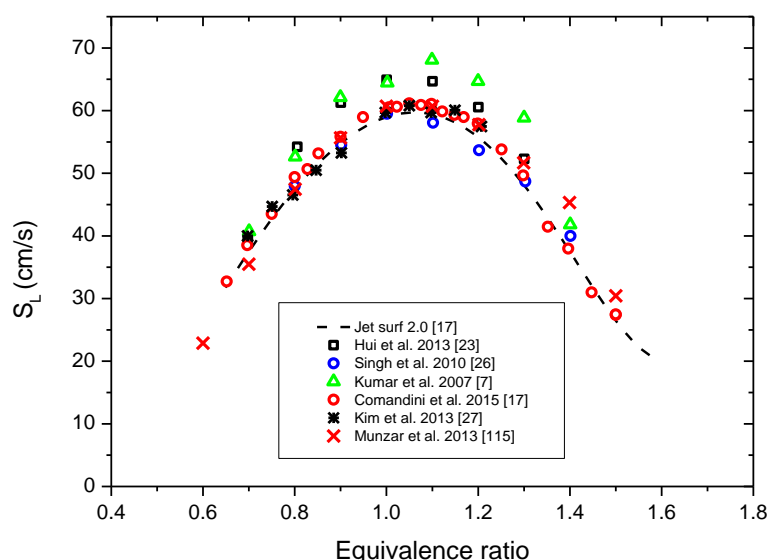


Figure 2.7 : review of laminar flame speeds of n-decane.

- n-propylbenzene

N-Propylbenzène is a heavy aromatic species which enters as a significant species in the kerosene fuel composition. However, information about the understanding of the evolution of the laminar flame speeds with equivalence ratio, inlet temperature and pressure are still rare in the published literature. All the results found in literature are shown in Figure 2.8. The earlier experimental study on the laminar flame speed of n-propylbenzène was carried out by Xin et al [101] using a twin flame counter-flow set-up. Laminar flame speed of several aromatic hydrocarbon fuel components such as 1, 2, 4-trimethylbenzene, 1, 3, 5-trimethylbenzene and toluene were also measured in this study. Much later, Ji et al. [116]

measured the laminar flame speeds of n-propyl-benzene/air mixtures using the counter flow flame method. Experiments were performed at atmospheric pressure, 353 K and over the equivalence ratio ranging from 0.7 and 1.5. However, the measurements in both studies being performed at different inlet temperature prevent any possible comparison between these measurements. More recently, Mehl et al. [117] published results on alkyl aromatic components including n-propylbenzene and n-butylbenzene in conditions similar to the ones investigated by Hui et al. A rapid observation of these results observed in Figure 2.8 reveals noticeable discrepancies.

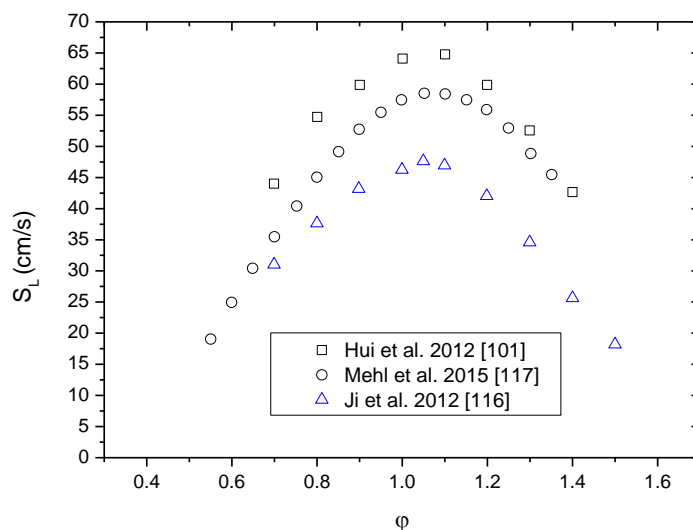


Figure 2.8: review of laminar flame speeds of n-propylbenzene.

- n-propylcyclohexane

This molecule belongs to family of cycloalkanes that are usually found in diesel and aviation fuels. In the past, the combustion characteristics and oxidation kinetic mechanism of n-propylcyclohexane has not been studied extensively compared to others families such as n-alkanes, branched alkanes, or aromatics. Recent interests of the knowledge of laminar flame speed n-propylcyclohexane stem from their relevance to the development of surrogates of these fuels. All the results found in literature are displayed in Figure 2.9.

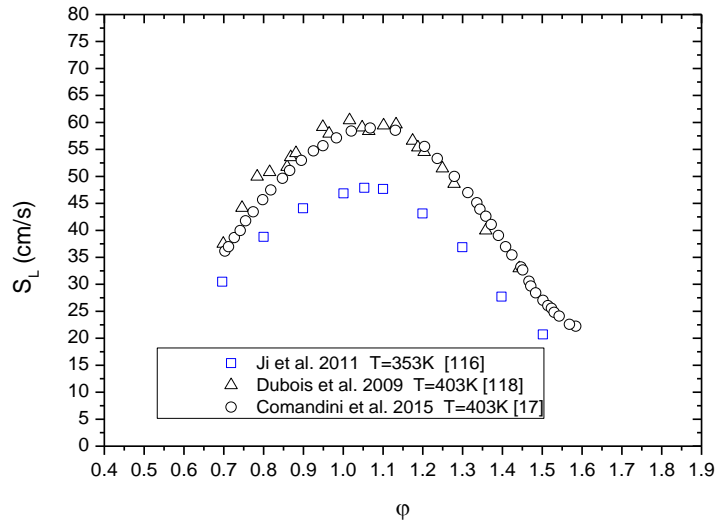


Figure 2.9: Laminar flame speed of *n*-propylcyclohexane comparison between present works with literatures

Among the results listed in the published literature, Dubois et al. [118] have studied the evolution of the laminar flame speed with equivalence ratio with a spherical bomb running at 0.1MPa and 403 K. A linear extrapolation technique was then used to obtain the laminar flame speeds from measurements. Results in the same conditions were also reproduced by A. Comandini et al. [17] using the same spherical bomb method. A non-linear extrapolation technique was then used to obtain the laminar flame speeds. It is then observed a good agreement between both measurements as shown in Figure 2.9. The last information available in literature comes from the data reported by Ji et al. [116] that measured the laminar flame speeds with a stagnation flame at a temperature of 353 K.

#### 2.2.4 Oxygenated fuels

With the progressive introduction of increasingly stringent world-wide gas emissions regulations and the need for fuel diversification, it is expected that the use of renewable no fossil fuels in aeronautic and automotive transportations will increase in the future. In recent years, biomass-derived fuels (biofuels) have gained much attention as potential alternatives to petroleum-based fuels. Apart from the advantage of renewability, biofuels have shown to be sustainable and less harmful to the environment; especially those derived from 2<sup>nd</sup> generation biofuels where lignocellulosic are used as feedstock. Compared with the 1<sup>st</sup> generation biofuels in which mainly linear and branched members of the alcohol family (from methanol to hexanols) were added to gasoline, the 2<sup>nd</sup> generation biofuels derived from biomass can be produced sustainably as it solved the problem of low productivity of today's crops-based biofuels, as well as the potential competition with the global food supply.

Although vast quantities of sustainable biomass exist for conversion into advanced biofuels, a major imperative for the transportation sector is that these advanced biofuels can be classified as ‘drop-in’ fuels; i.e., they are directly compatible with existing refinery and distribution infrastructure as well as existing engine technology. However, biofuels derived via base catalyzed depolymerization of lignin [119] or fast pyrolysis [120] [121], contain numerous oxygenated compounds. The biofuel derived from biomass which has high oxygen content from 40 % to 60 % in weight and molar O/C ratio could up to 0.6. The oxygenated compounds that is difficult to remove but potentially impact the ability of these fuels to be used drop-in replacement of existing petroleum-based fuels [122]. Accordingly, biofuels derived via these processes must go through upgrading processes to remove these oxygenated compounds and produce a fuel that contains only hydrocarbons [123]. Upgrading processes are expensive, and their costs increase as the levels of oxygenated compounds in the final fuel product decrease [124]. As a result, these upgrading processes will result in exceedingly high prices for renewable hydrocarbon fuel compared to petroleum derived fuel. To reduce upgrading costs and produce drop-in biofuels at a market-competitive price, it is therefore economically desirable to leave a small fraction of oxygenated compounds in the final upgraded fuels. However, for this approach to be technically viable, it must be shown that the presence of these oxygenated compounds in the final fuel blends does not adversely affect the operation of existing engines. The investigation of small percentages of oxygenated compounds presents in upgraded advanced biofuels on fuel properties, performance, emissions, and durability of diesel and spark ignited engines therefore becomes important. One of the open issues related to biofuels is to study the oxygenated additive effects to laminar flame speed of commercial gasoline and diesel fuels.

Up to now, increasing attention has been paid on the use of alcohols (predominantly ethanol) with up to five or even more carbon atoms as replacements of fossil gasoline fuels or as fuel additives. These fuels and their combustion properties, including their ignition, flame propagation, and extinction characteristics, their pyrolysis and oxidation reactions and their potential to produce pollutants have been intensively investigated in dedicated experiments. A compilation of the results of these studies can be found in excellent reviews [125] [126]. In parallel to these studies, Additional works were also focused on the role of alcohol blending with conventional petroleum hydrocarbon fuels [127] [128] [33] [34] [35] [29] [28]. These studies are mainly focused on the addition of oxygenated fuels to commercial or surrogate gasolines of alcohols such as ethanol or butanol. These investigations are especially dedicated to conventional biofuels (i.e. 1<sup>st</sup> generation) issues using low molecule weight oxygenated molecules as additives. For instance, Dirrenberger recently reported information on the relationship between the laminar burning velocities of gasoline with addition of ethanol. In this study, the measurements were first conducted for a gasoline model fuel of n-heptane, iso-octane and toluene mixtures at 0.1 MPa and 358 K using the heat flux method. Another experiment on the laminar flame speed of these blends was also performed in the same direction. This is especially the case in the work reported by Varea et al [29] in

which alcohol additive effects to laminar flame speed in high-pressure conditions using a spherical flame were addressed.

In parallel to this exhaustive work on alcohols, the shift from petroleum fossil fuels to 2<sup>nd</sup> generation biofuels also involves a specific role of oxygenated compounds other than alcohols on the reduction of soot formation in diesel engines, but also on the promotion of the formation of some toxic pollutants, such as aldehydes. These features have recently promoted fundamental studies on oxygenated molecules such as esters, acyclic ethers and cyclic ethers and carbonyl compounds on the combustion characteristics of biofuels. In particular, several comprehensive reviews were reported on the evolution of the laminar flame speeds of various oxygenated hydrocarbons of general formula  $C_xH_yO_z$  [129] [126]. While numerous oxygenated compounds were investigated and summarized the work carried out since the 1950s, recent evidence on the existence of other oxygenated compounds in lignocellulosic biomass fuel still needs to be taken into account in future environments assessments [130]. In the present work, efforts have been undertaken in this direction. The oxygenated components, anisole, 4-methylanisole and ethyl-valerate (ethyl pentanoate) components were selected in our study because they are considered as relevant oxygenated molecules in lignocellulosic fuels [130]. Unfortunately, information about the laminar burning velocity of these chemical compounds is still rare in the open literature. Only Dayma et al. [131] have reported measurements of laminar burning velocities of ethyl valerate at 0.1, 0.3, 0.5 and 1 MPa conditions.

## **2.3 Numerical tools for one-dimensional flames**

Apart from the aforementioned experimental experiments, numerical tools have also been used to complete our knowledge on the theoretical evolution of the laminar flame speeds with all the operating conditions explored. One-dimensional free propagating, unstretched, adiabatic, laminar, premixed flame simulations were systematically performed using the COSILAB code to deduce the laminar flame speeds and to calculate the theoretical distributions of temperature and species concentrations of the different flames. Depending of the fuels investigated, several detailed kinetic mechanisms were tested in the current study. Finally, numerical predictions were compared to experimental results for evaluating the capacity of these kinetic mechanisms to predict the flame speed of the fuels under investigation.

### **2.3.1 Laminar, one-dimensional, premixed, and freely propagating flames**

Solving the conservation equations for 1D freely propagating flame configuration is a numerical task for which various mathematical tools have been developed in the two last decades. For laminar one-dimensional premixed flames, the conservation equations derived from the classical 3D conservation equations (mass, species, energy conservation and equation of state) can be simplified as described in the reference books of K. Kuo [80] and T. Poinso [39]. The simplified equations describe the wave

propagating from the burnt to the fresh gas at a velocity which reaches a constant value when transients are ignored. Usually, the resolution of these equations involves the use of detailed kinetic mechanisms involving two to hundreds of chemical species and one to thousands of chemical reactions. When boundary conditions are well-defined and the problem is discretized on a finite difference grid, the resulting system is strongly nonlinear value problem which can be written:

$$L(U_i) = 0 \quad (2.11)$$

where  $U_i = (T, Y_1, Y_2, \dots, Y_N, U)_i$  is the vector of unknown at location  $x_i$ . This system is usually solved with Newton-typed methods. In the current work, the user friendly commercial software COSILAB code was used to resolve the conservation equations for calculating the laminar flame speeds of various hydrocarbon fuel/air mixtures. In addition to the detailed kinetic mechanism, the simulation of 1D freely propagating flames requires specific databases of thermodynamic properties and transport models (diffusion coefficients, viscosity and heat diffusion coefficient).

### 2.3.2 Chemical kinetic mechanisms

Different kinetic mechanisms are tested in the current study: the GRI-Mech 3.0 mechanism for methane/air flames, a mechanism developed by Chong et al.'s [31] for acetone/air flames and the LUCHE skeletal kerosene mechanism for kerosene/air flames. All of these kinetic mechanisms are now briefly described in the remaining part of this section.

#### (a) Methane kinetic mechanism: GRI-Mech 3.0

Numerous experimental and numerical studies have been conducted in the last decades for studying the methane/air combustion. From these studies, several detailed chemical mechanisms were developed for resolving the full chemistry of methane/air flames. These include the GRI-Mech 3.0 mechanism [132] and those proposed by Konnov [133] and Hughes [134]. In these kinetic mechanisms, the number of chemical species varies between 2 to 120 and the chemical reactions are ranging from 2 to 1200. The kinetic mechanism selected in the current work is the GRI-Mech 3.0 (53 species and 325 elementary reactions). It is the mechanism commonly used for modeling the combustion of methane and this one has been validated by numerous experimental results for a wide range of temperature, pressure and equivalence ratio operating conditions.

#### (b) Acetone kinetic mechanism

Acetone oxidation in the gas phase has been studied extensively and several kinetic mechanisms have been developed and published in literature. For instance, Sato and Hidaka [135] conducted a study on acetone pyrolysis and oxidation. From the experimental results, they propose a detailed kinetic



mechanism involving 51 species and 164 reactions. Chao et al. [136] developed a chemical kinetic mechanism involving in 46 species and 248 reversible reactions. In the current work, acetone/air flames are modeled using a sub-mechanism added to the GRI-Mech 3.0 mechanism which has been initially developed by Pichon et al. [99] and recently modified by Chong and Hochgreb [31]. This modified kinetic mechanism involving 81 species and 419 reversible reactions, was extended to simulate the acetone oxidation and pyrolysis processes. This kinetic mechanism was selected because of its pertinence to already validate experimental laminar flame speeds obtained with the stagnation flame method.

(c) *Kerosene: LUCHE skeletal mechanism*

Detailed kinetic mechanisms for kerosene (and the associated surrogates) have been developed by several research teams in the past. These included, the DAGAUT detailed kinetic mechanism [16] and the EL-BAKALI\_RISTORI chemical mechanism [32]. These mechanisms include up to 300 species and 500 elementary irreversible reactions. Details relating to these mechanisms can be found in a detailed review proposed by DAGAUT [16]. Since the detailed reaction mechanisms involved consists of hundreds of species and thousands of reactions, it cannot be used for industrial simulation purposes due to the very excessive computational time requirements. Thus, reduced reaction mechanisms, which simulate properly some characteristics of the detailed one (auto ignition delay, combustion temperature, laminar flame speeds ...), are used instead. In the current work, the reduced kinetic mechanism selected to simulate the kerosene combustion is the LUCHE surrogate kerosene mechanism [137] that is derived from the EL-BKALI\_RISRTORI mechanism. This surrogate fuel is composed of three molecular components already present in the kerosene composition: 76.7 % n-decane, 13.2 % n-propylbenzene and 10.1 % propylcyclohexane. It includes 91 chemical species and 991 reactions and has been validated in the range of temperature  $T = 300 - 1800$  K,  $P = 0.05 - 1.0$  MPa and equivalence ratio  $\phi = 0.5 - 2.0$ . As this skeletal mechanism seems to give good similarities with the kerosene kinetic mechanism, it is widely used for industrial applications. However, the LUCHE kinetic mechanism has not yet been compared with experimental laminar flame speeds in the full range of the operating conditions encountered in real combustion engines. Moreover, the performances of LUCHE surrogate kerosene compared to the commercial Jet-A1 fuel has not been referred previously especially in high-temperature and high-pressure conditions. In the current work, the measured laminar flame speeds of the LUCHE surrogate fuel mixed with air are compared with simulation results derived from the use of the LUCHE kinetic mechanism. The further discussion and comparison between LUCHE surrogate fuel and commercial jet fuels are performed to validate the LUCHE surrogate fuels.

## 2.4 Conclusions

In this chapter, the propagation mechanism of a combustion wave in a fuel/air mixture was presented. Based on simple one-dimensional concept of one-dimensional free propagating flames, the structure of laminar flames was described and discussed. The main characteristics of laminar flames were then introduced, among which the laminar burning velocity and the flame thickness. The effect of the flame stretch on the laminar flame speed was also discussed.

The experimental methodologies for generating the laminar flames are reviewed and the advantages and limitations attributed to each method were discussed in detail. From these methods, the Bunsen flame method was chosen to be used in the current study. This methodology produces conical flames stabilized on converging nozzles. Reasons that explain this choice were then discussed.

To introduce the numerical tools and the detailed kinetic mechanisms selected in this study, a review of the main results on the laminar flame speeds of the fuels investigated in the current study are reviewed. These include various gaseous and pre-vaporized fuels, namely methane, acetone, kerosene and its associated LUCHE surrogate and oxygenated fuels. Literature data on the laminar flames speeds shows that the data are relatively numerous but they are sometimes scarce, often out-of-date and lack consistency. Flame speeds of the fuels under investigation are not extremely different from one fuel to another. This is why it is necessary to get an important point about the value of the measured laminar flame speeds in order to look at the fuels studied to each other appropriately. The effects of temperature and pressure on the laminar flame velocities notions are necessary to study in regards of the real thermodynamic conditions encountered of a combustion engine but also for the validation of detailed kinetic mechanisms. These effects are still detailed on only few molecules in the literature. That is why the study performed in the framework of this thesis aims to complement these data along with providing additional accuracy on flame speed measurements.

Finally, the numerical tools and the detailed kinetic mechanisms employed in this study were described. The capacity of these mechanisms to calculate the laminar flame speeds of  $\text{CH}_4/\text{air}$ , acetone/air and multi-component fuels such as kerosene/air and associated LUCHE surrogate/air mixtures in a wide range of operating conditions will be presented.

## Chapter 3 Experimental Setup

---

This section is dedicated to the description of the high-pressure laminar burner and the associated optical diagnostics that will be used to measure the laminar burning velocity. The architecture of the high-pressure burner and its characteristics are described. As a reminder, this burner is able to be feed with gaseous or liquid fuels in a large range of preheated temperature pressure and equivalence ratios. A discussion about the monitoring of the high-pressure burner follows. An analysis of the accuracy of reliability of this experimental setup completes this presentation. Finally, the optical diagnostics used in the current work to measure the laminar flame speed are presented. These techniques are the OH\* chemiluminescence optical imaging and the OH-PLIF, acetone-PLIF and aromatics-PLIF laser diagnostics respectively.

### 3.1 High-pressure burner

The burner assembly and pressure vessel used to produce a laminar flame at elevated pressure are illustrated in Figure 3.1. The chamber is designed to burn up a premixed fuel/air mixture at 3.0 MPa at a maximum wall temperature of 600 K.

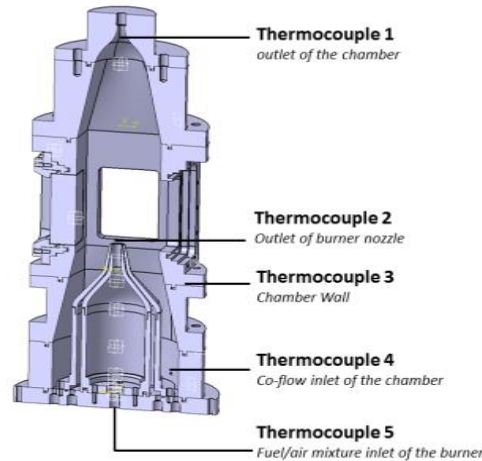


Figure 3.1: Schematic of the high-pressure experimental facility.

An axisymmetric premixed burner is designed and developed to generate a steady conical laminar premixed flame stabilized on the outlet of a contoured nozzle in a high-pressure chamber. The shape of the axisymmetric central contracting nozzle is designed with a fifth-order polynomial to reduce the boundary layer thicknesses by accelerating the flow and providing a flat velocity profile at the nozzle outlet. The contoured nozzle has an outlet diameter of  $d_1$  (10 mm for  $\text{CH}_4/\text{air}$  and acetone/ $\text{N}_2/\text{O}_2$  mixtures and 7 mm for kerosene/ $\text{N}_2/\text{O}_2$ , biofuel/ $\text{N}_2/\text{O}_2$  and pure hydrocarbon fuels/ $\text{N}_2/\text{O}_2$  mixtures) and a contraction ratio of  $\delta = (D/d_1)^2 = 49$  ( $d_1=10$  mm) or 100 ( $d_1=7$  mm). A second concentric contoured nozzle of outlet diameter of  $d_2 = 10.6$  mm (or 7.6 mm) surrounding the central nozzle is used to produce a flat, fuel/air pilot flame to anchor the conical laminar premixed flame in high-pressure operating conditions. Both nozzles are mounted on the bottom flange of the pressure chamber as well as a guard-flow housing located between the walls of the second nozzle and the pressure chamber.

The high-pressure chamber, constructed in stainless steel has an inner surface of  $100 \times 100 \text{ mm}^2$  and a height of 511 mm. It is equipped with four large UV quartz optical windows tailored to probe the flame with optical imaging diagnostics. The top of the pressure chamber is designed as a convergent nozzle adopting a contraction ratio of 100 along a length of 160 mm and a honeycomb plate is placed on the top of the vessel as a flow straightener to suppress the presence of large circulation zones inside the pressure chamber. For more details, all the dimensions of the burner are reported in Appendix 1.

### 3.2 Liquid fuel vaporization and gas feeding

The burner can operate with gaseous or liquid fuels. Liquid fuel was pressurized in a 1.0 L tank while nitrogen, oxygen and gaseous fuels were supplied by pressurized tanks. The gas flowrates are regulated by an electronics unit connected to different mass flow controllers, previously calibrated with the related gases. For liquid fuels, the 1.0 L tank is connected to liquid flowmeter associated with a Controlled Evaporator and Mixer (CEM, Bronkhorst) which heats and mixes fuel vapor with N<sub>2</sub> carrier gas at controlled mass flowrate and temperature. The exit of the CEM is connected to a stainless steel mixing cell preheated at temperature ranging from 373 to 600 K and controlled with a type K thermocouple to prevent any condensation of the fuel vapor in the pipes. Additional nitrogen and oxygen initially mixed and preheated by a circulation heater before the entrance of the mixing cell are used to reproduce the synthetic species composition of air and to modify the equivalence ratio of the heated vapor fuel/air mixture (see Figure 3.2). In the current study, for liquid fuel flame speed measurements air is assumed to be a gaseous O<sub>2</sub>/N<sub>2</sub> mixture with a volume ratio of 20/80.

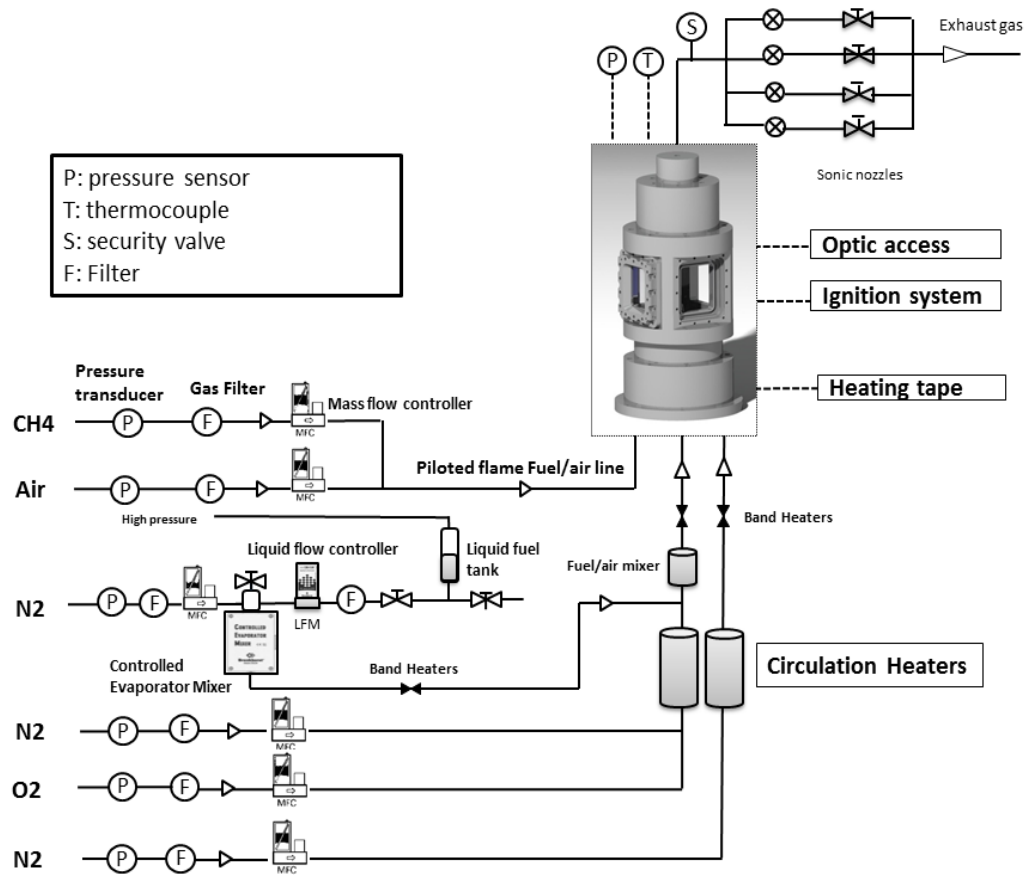


Figure 3.2: Schematic of the experimental facility process flow diagram

The vapor fuel/air mixture is injected into the central nozzle that is filled with high-temperature resistant glass beads (1 to 3 mm diameter) to prevent any flow inhomogeneity at the nozzle exit. The same strategy is also applied for the fuel/air mixture required for the pilot flame as well as for the nitrogen guard-flow.

The annular nitrogen guard-flow is used to adjust the pressure in the vessel and to dilute the exhaust gases. It is first preheated by a circulation heater and then delivered to the pressure vessel by a combination of four rigid stainless steel pipes (4 mm i.d.) connected to the bottom flange of the high-pressure vessel. The combustion reactants (gaseous methane and air) used to feed the pilot flame, are delivered to the burner by two rigid stainless steel tubes. A T-connection of both pipes is then achieved to mix methane with air before their injection inside the burner via a set of four rigid stainless steel pipes connected to the bottom flange of the vessel. To minimize the effect of the pilot flame on possible disturbances on the laminar flame, the methane/air mixture flowrate for the pilot flame is kept as low as reasonably achievable. For CH<sub>4</sub>/air laminar flames, the equivalence ratio of the piloted flame is kept the same as that of the central flame while for acetone/air flames, the equivalence ratio of the piloted flame is fixed to 1.2 for all the operating conditions investigated.

Combustion products are finally evacuated and cooled through a rigid stainless steel tube connected to the top of the high-pressure vessel. This exhaust pipe is then split into four channels, including, respectively, sonic throats of 0.5, 0.7, 1.0 and 1.1 mm internal diameters assuring a control of pressure inside the combustion chamber.

### **3.3 Monitoring of the high-pressure burner**

#### **3.3.1 Temperature monitoring**

As discussed before, the measurements of laminar flame speeds have to be processed for various preheating temperatures of the fresh gases that are injected into the central nozzle. To this end, a monitoring of temperatures of the different mechanical parts of the experimental facility must be provided to control with accuracy the preheating of the fuel/air mixture downstream from the nozzle exit. It is then required to heat:

- The walls of the mechanical parts of the lower part of the burner with flexible electrical wire heaters positioned around its external surfaces (Hillesheim HBS/020).
- The rigid stainless steel tubes used to transport gases between the heat exchangers and CEM to the entrance of the burner with flexible electrical wire heaters.
- The nitrogen and oxygen flows injected into and outside the central nozzle with heat exchangers (CAST X2000).

- The vapor fuel/nitrogen mixture at the exit of the CEM via the internal electrical wire heater inserted into the CEM.

Several type K thermocouples are placed on the heated mechanical parts of the combustion facility to monitor and ensure temperature uniformity throughout the combustion chamber. All these thermocouples are connected to a time-dependent control system assuring the control of the different heaters. Depending of the desired level of the preheating temperature of the gaseous mixture at the nozzle exit, the warm-up period to preheat the mixture can take several hours. Control of this temperature is finally achieved by a type K thermocouple positioned at the nozzle exit before and after the experiment.

For liquid organic fuels, the maximum temperature which can be reached downstream from the nozzle with this heating system is fixed to 500 K. This value is chosen to avoid the thermal cracking of the vapor fuel along the gas feeding tubing. Indeed, it is well known that organic fuels can undergo pyrolysis and oxidation processes leading to the thermochemical decomposition of the fuel. This maximum temperature is well within the auto-ignition temperature of the organic molecules studied ( $> 700$  K) for which a breaking of some chemical bonds can occur. Likewise, a minimal temperature was also fixed to avoid the condensation of the vapor fuel in the tubing during the laminar burning velocity measurements. Depending of the boiling point of each organic fuel, this value is ranging between 370 and 400 K.

### **3.3.2 Pressure monitoring**

As aforementioned, the pressure inside the combustion chamber is monitored with the sonic nozzles located at the exit of the combustion chamber. The increase in pressure inside the combustion chamber was achieved in several steps by successively closing each of the sonic throats. High-pressure laminar flames are obtained by adopting the following procedures: (1) the flame is first ignited at 0.1 MPa using an igniter, (2) the flow rates of fuel/air mixtures are then adjusted to achieve a stable laminar flame at a fixed equivalence ratio; (3) the flowrate of nitrogen guard-flow is adjusted to achieve a flow velocity ratio with the fuel/air mixture of about 1/10; (4) the nitrogen guard-flow and fuel/air mixture flowrates are finally increased proportionally to increase the pressure slowly and to prevent any flashback or extinction of the flame. This procedure thus enables to control pressure with accuracy and to avoid any thermal-acoustic instabilities and flashback. To avoid a disturbance of the laminar flame structure from the pilot flame, the equivalence ratio of the piloted flame is also adapted according to the pressure range under study.

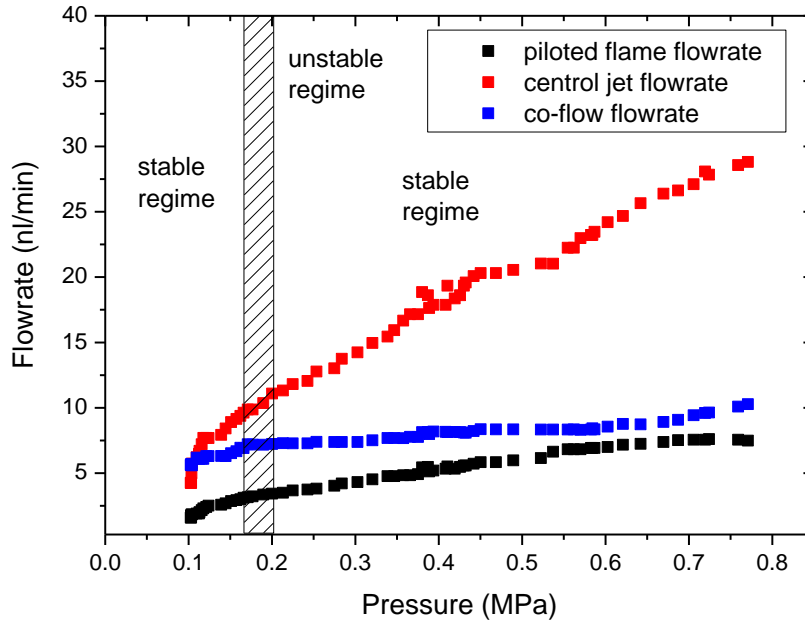


Figure 3.3: Evolution of the flowrates of the different gases with pressure. Operating conditions: Jet A-1 fuel,  $T = 400\text{ K}$ ,  $\phi = 0.8$ .

An example of the application of this procedure is illustrated in Figure 3.3. The evolution of the flowrates of the piloted flow, nitrogen guard-flow and Jet A1/N<sub>2</sub>/O<sub>2</sub> mixture flow with pressure are reported. It can be observed from the results that the variation of the flowrate for each fluid must be finely tuned to constantly keep a regime of laminar flame. For most of the fuels under study, this methodology used to control the pressure allows to obtain laminar flames for pressure up to 1.0 MPa. However, for some limited fuels like kerosene, it has been observed small disturbances on the laminar flame structure for a limited pressure range (between 0.16 to 0.2 MPa for kerosene). One possible reason explaining these disturbances could arise from the presence of recirculation zones of hot gases inside the combustion chamber that induce small fluctuations of pressure and then producing a flickering of the laminar flame.



### 3.4 Reliability and accuracy of physical parameter control

The error sources on the measurement of the laminar burning velocity lie in the control of the physical parameters leading to the generation of the laminar flame. Before the data processing of the measurements will be reviewed more precisely for defining the uncertainty of laminar flame speed in chapter 4, all parameters having influence on the establishment of the laminar flame will be discussed. Evidently, the control of the temperature and pressure reliability for constant set points has to be rated, as well as the fluid control of gas and liquid flow rate.

#### 3.4.1 Reliability and accuracy of temperature and pressure control

The reliability of temperature and pressure parameters for given setpoints are controlled for a time series corresponding to several minutes. For the relative temperature error, a maximum error bound of  $\sim 3$  K is found. The relative pressure error can be described as 2.2% FS/RD in which FS is the full-scale of the pressure transducer (3.0 MPa) and RD is the actual readout.

#### 3.4.2 Reliability and accuracy of fluid flow control

The equivalence ratio of a given set point of a premixed laminar flame is defined mainly by the flow rates of the different fluids, which are the primarily controlled parameters of the premixed inlet gaseous mixture. Two cases must be considered depending on whether the fuel is initially gaseous or liquid.

- In case of gaseous fuel applications (i.e. methane), the equivalence ratio  $\phi$  is expressed by

$$\phi = \frac{\dot{m}_{CH_4}/\dot{m}_{air}}{(\dot{m}_{CH_4}/\dot{m}_{air})_{st}} \quad (3.1)$$

where  $\dot{m}_{CH_4}$  and  $\dot{m}_{air}$  are respectively the volumetric flowrates of methane and air and  $(\dot{m}_{CH_4}/\dot{m}_{air})_{st}$  is the ratio between methane and air volumetric flowrates for the stoichiometric condition.

Generally, if a function  $q$  consist of number  $i$  of independent quantities  $x_i$  measured each with a small uncertainty  $\Delta x_i$ , the relative uncertainty of  $q$  is given as

$$\Delta q = \sqrt{\sum_i \left( \frac{\Delta q_{x,i}}{x_i} \right)^2} = \sqrt{\sum_i \left( \frac{\partial q}{\partial x_i} \frac{\Delta x_i}{x_i} \right)^2} \quad (3.2)$$

See e.g. [138]. Further, the error is limited to an upper bound of uncertainty to

$$\Delta q \leq \sum_i \left| \frac{\partial q}{\partial x_i} \cdot \frac{\Delta x_i}{x_i} \right| \quad (3.3)$$

which is always true and which has moreover to be chosen if quantities are independent. Since the measurement parameters in Eq. 3.1 are all independent, the relative error or the uncertainty of the equivalence ratio is derived as follows

$$\Delta \varphi = A \sqrt{\left( \frac{1}{\dot{m}_{air}} \right)^2 (\Delta \dot{m}_{CH_4})^2 + \left( \frac{\dot{m}_{CH_4}}{\dot{m}_{air}^2} \right)^2 (\Delta \dot{m}_{air})^2} \quad (3.4)$$

$$A = 1 / \left( \frac{\dot{m}_{CH_4}}{\dot{m}_{air}} \right)_{st} \quad (3.5)$$

With known values of the volumetric flowrates of methane and air, the relative error of the equivalence ratio can be derived for each individual condition. The uncertainties on the different volumetric flowrates are derived from the reliability of the Bronkhorst controllers (model EL-FLOW series L-201C) defined by the manufacturer ( $\Delta \dot{m} = 0.5\%$  Readout +  $0.1\%$  Full Scale). In our conditions, the respective flow controls range from 0.3 to 5 nl/min for atmospheric pressure condition measurements ( $\dot{m}_{CH_4} = 0.3 - 0.6 \text{ nl/min}$  and  $\dot{m}_{air} = 4.5 - 5 \text{ nl/min}$ ), leading to maximum uncertainties of  $\Delta \dot{m}_{CH_4} / \dot{m}_{CH_4} \cong 1.8\%$  and  $\Delta \dot{m}_{air} / \dot{m}_{air} \cong 1.0\%$  respectively. Detailed values of the evolution of the relative uncertainty  $\Delta \varphi / \varphi$  with equivalence ratio are listed in Table 3.1. The resulting uncertainty  $\Delta \varphi / \varphi$  calculated from 3.4, ranges then from 3.60 % in a lean running mode to 2.20 % in a rich running regime.

$\varphi$	0.7	0.8	0.9	1	1.2	1.3
$\dot{m}_{CH_4}$ (nl/min)	0.33	0.38	0.43	0.47	0.55	0.60
$\dot{m}_{air}$ (nl/min)	4.84	4.79	4.75	4.71	4.62	4.58
$\Delta \varphi / \varphi$ (%)	3.60	3.12	2.85	2.63	2.31	2.20

Table 3.1: Exemple of error calculation for the equivalence ratio of  $CH_4$ /air mixtures with equation 3.4.

- For liquid fuel applications, the control of the equivalence ratio for the gaseous fuel/ $O_2/N_2$  mixtures injected into the combustion chamber needs additional fluid flow controllers. As aforementioned, the liquid flow control is split up to a Bronkhorst sensor model mini- CORI- FLOW M12 and the 3-way mixing valve of the CEM unit (model series W-202). The gas flow is controlled by Bronkhorst controller (model EL-FLOW series L-201C). The respective flow controller range from 0.2 to 200 g/h for the liquid flow and from 0.2 to 10 nl/min for the  $N_2$  carrier gas flow. Additional Bronkhorst

controllers control the volumetric flowrates of N<sub>2</sub> and O<sub>2</sub> used for reproducing the gaseous fuel/O<sub>2</sub>/N<sub>2</sub> mixtures under study. In such cases, the equivalence ratio is now derived as follows:

$$\varphi = \frac{\dot{m}_{\text{fuel}} / (\dot{m}_{\text{N2c}} + \dot{m}_{\text{N2}} + \dot{m}_{\text{O2}})}{(\dot{m}_{\text{fuel}} / (\dot{m}_{\text{N2c}} + \dot{m}_{\text{N2}} + \dot{m}_{\text{O2}}))_{st}} \quad (3.6)$$

In this expression, N2C is the nitrogen flowrate circulating into the CEM while N2 is the nitrogen flow rate used to reproduce the synthetic composition of air.

Applying Eq. 3.6, the relative uncertainty  $\frac{\Delta\varphi}{\varphi}$  can be expressed like:

$$\Delta\varphi = AB \sqrt{(\Delta\dot{m}_{\text{fuel}})^2 + (B\dot{m}_{\text{fuel}})^2(\Delta\dot{m}_{\text{N2c}})^2 + (B\dot{m}_{\text{fuel}})^2(\Delta\dot{m}_{\text{N2}})^2 + (B\dot{m}_{\text{fuel}})^2(\Delta\dot{m}_{\text{O2}})^2} \quad (3.7)$$

with  $A = 1 / \left( \frac{\dot{m}_{\text{fuel}}}{\dot{m}_{\text{N2c}} + \dot{m}_{\text{N2}} + \dot{m}_{\text{O2}}} \right)_{st}$ ,  $B = 1 / (\dot{m}_{\text{N2c}} + \dot{m}_{\text{N2}} + \dot{m}_{\text{O2}})$

$\varphi$	0.7	0.8	0.9	1	1.2	1.3
$\dot{m}_{\text{N2c}}$ (nl/min)	1	1	1	1	1	1
$\dot{m}_{\text{N2}}$ (nl/min)	3.42	3.38	3.34	3.30	3.22	3.18
$\dot{m}_{\text{O2}}$ (nl/min)	1.11	1.09	1.08	1.07	1.06	1.05
$\dot{m}_{\text{fuel}}$ (g/h)	30.06	34.03	37.93	41.76	49.21	52.84
$\Delta\varphi/\varphi$	2.33	2.32	2.32	2.32	2.33	2.34

Table 3.2: Exemple of error calculation for the equivalence ratio of liquid fuel/air mixtures calculated with 3.7.

Using the manufacturer's specifications, the maximum uncertainties on the volumetric flowrates of each fluid are  $\frac{\Delta\dot{m}_{\text{N2c}}}{\dot{m}_{\text{N2c}}} \cong 1.5\%$ ,  $\frac{\Delta\dot{m}_{\text{N2}}}{\dot{m}_{\text{N2}}} \cong 3.5\%$ ,  $\frac{\Delta\dot{m}_{\text{O2}}}{\dot{m}_{\text{O2}}} \cong 2.7\%$  and  $\frac{\Delta\dot{m}_{\text{fuel}}}{\dot{m}_{\text{fuel}}} = 0.2\%$ . The final uncertainty on the equivalence ratio calculated with Eq. 3.7 is presented in Table 3.2. The resulting uncertainty  $\frac{\Delta\varphi}{\varphi}$  calculated from equation 3.7, ranges then from 2.32% to 2.34% for equivalence ratio range 0.7 – 1.3.

The above uncertainties are calculated for the atmospheric pressure conditions. For measurements at elevated pressure, the flowrate being increasing with pressure, most of the flow meters will be used on their full scales that will make the measurements more accurate than at atmospheric pressure conditions.

### 3.4.3 Reliability and accuracy of the velocity profile at the burner outlet

To estimate the effect of the flow parameter on the velocity profile at the nozzle exit, the velocity profiles downstream from the nozzle were measured using a hot wire anemometry system. As illustrated in Figure 3.4, the velocity profiles recorded for two height positions (1 and 10 mm) downstream from the nozzle of diameter 7 mm are presented. The Reynolds number was fixed to 1000, value comparable for our experiments in reactive flows. The experiments were performed at room temperature and atmospheric pressure. The resulting velocity distributions show top-hat profiles with a limited boundary layer thickness.

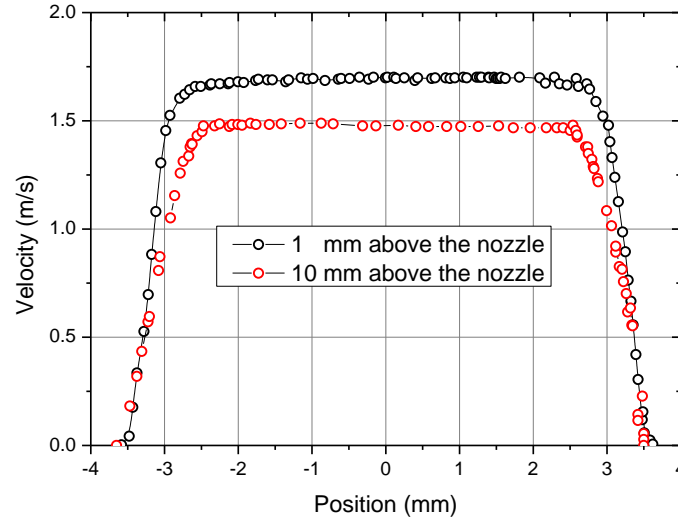


Figure 3.4: Velocity profiles measured above the nozzle outlet  $z=1$  mm and 10 mm

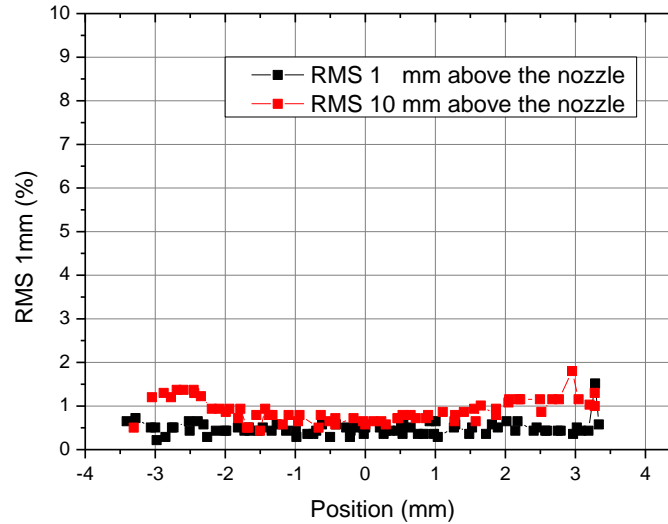


Figure 3.5: Velocity RMS fluctuation above the nozzle outlet  $z=1$  mm and 10 mm

The RMS fluctuations also plotted in Figure 3.5 shows very weak fluctuations of velocity less than 1%, demonstrating that the burner apparatus and especially the proposed nozzle with a five-order polynomial

profile is able to produce well-controlled laminar flow fields required for establishing straight sided conical flames.

### 3.5 Optical diagnostics

Various optical diagnostics were used to detect the flame contour. The choice of the optical techniques was directed by the suitability for the measurement environment and the desired type of information: quantitative or qualitative, spatial extent, time resolution. As the purpose of this work was the measurement of laminar flame speeds, two-dimensional measurements would be the most appropriate, thus OH\*-chemiluminescence and planar laser-induced fluorescence (PLIF) were used. The last laser diagnostic was declined into several versions including a selective excitation of different tracer molecules. Only the instrumentation will be described in this section. The theory and the methodology developed to measure the laminar flame speeds from the information delivered from the different optical techniques will be detailed in the next chapter.

#### 3.5.1 OH\* chemiluminescence

The first optical technique used in the current study is based on the detection of the flame contour with the OH\* chemiluminescence optical imaging technique. The camera used to record the OH\* radical emission is a thermoelectrically cooled, 16-bit intensified CCD camera (Roper Scientific) with a 1024 x 1024 array. The camera is equipped with an f/2.8, f = 100 mm, achromatic UV lens (CERCO) combined with a short pass optical filter centered at 310 nm and having a bandwidth of 10 nm. The exposure time selected to record the OH\* emission image is defined by opening the intensifier gate at 1  $\mu$ s. A 40  $\times$  40 mm<sup>2</sup> area of the flame is imaged by the ICCD camera, so that the spatial resolution is about 40  $\mu$ m per pixel. The acquisition repetition rate of the camera is kept at 10 Hz.

#### 3.5.2 OH-PLIF

The OH planar laser-induced fluorescence laser diagnostic (OH-PLIF) depicted in Figure 3.6 consists of a cluster system regrouping a Nd:YAG laser, a dye laser, a calibration system and a high-resolution ICCD camera.

A frequency-doubled, Q-switched Nd:YAG laser was used to pump a dye laser, which was then frequency doubled to obtain wavelengths in the 280 – 290 nm spectral range. The UV laser beam was tuned to 282.75 nm to excite the Q<sub>1</sub>(5) line of the (1, 0) vibrational band of the OH (X<sup>2</sup>II - A<sup>2</sup> $\Sigma^+$ ) system. The laser energy was fixed at 5 mJ to maintain the fluorescence of OH radical within the linear regime in order to keep the proportionality between the OH fluorescence signal and the OH concentration.

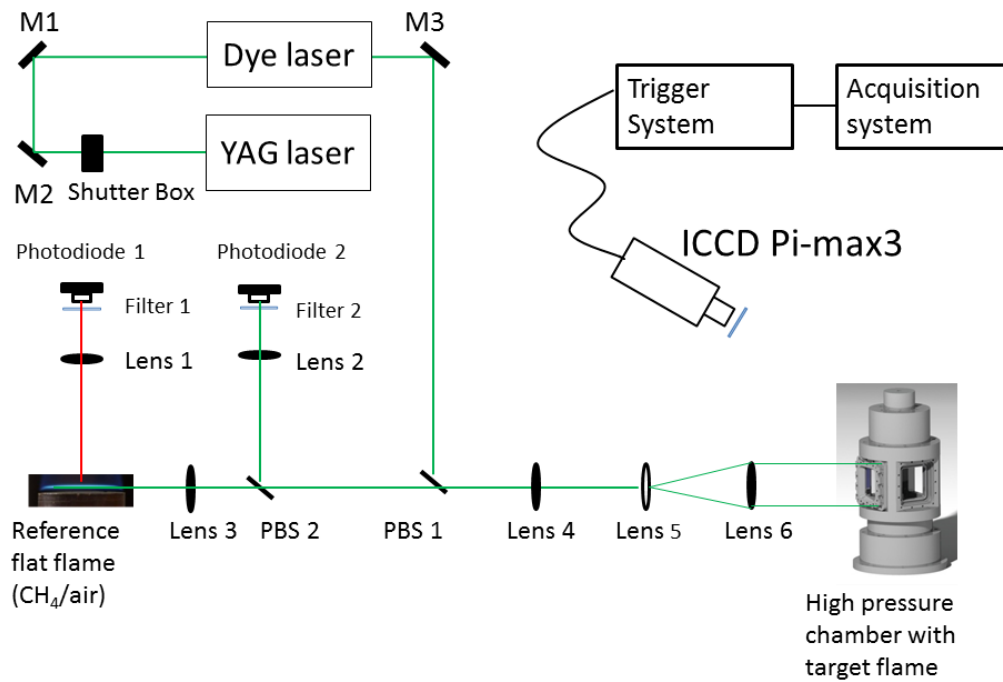


Figure 3.6: Schematic of Planar laser induced fluorescence.  $M_1$ ,  $M_2$ ,  $M_3$ : mirrors, PBS: UV plane windows.

As illustrated in Figure 3.6, the UV beam is initially split in two parts at the exit of the laser source with a plane UV window (PBS 1).

- The function of the 4% reflected laser beam is to tune the laser wavelength to the line-center of the OH transition. To do this, a second plane UV window (PBS-2) enables to take out again 4% of the reflected UV beam to control in time the laser energy with a fast UV photodiode. The resulting transmitted UV beam is then enabled the excitation of the OH radical produced in a reference flame. The premixed flame is generated via a porous burner fed with a methane/air mixture. Fluorescence of OH is collected at right angle with a UV photomultiplier (PMT). For each detection channel, optical filters are inserted to 1) limit the spectral bandwidth of the detection to the collection of the OH-fluorescence and 2) adapt the signal-to-noise ratio of the reference and measurement signals within the dynamic range of both detectors. The signal collected from the PMT is then amplified by a high-current amplifier to deliver a 0 - 10 V DC signal.
- The remaining UV laser beam after the first plane UV window is formed into a collimated laser sheet using two cylindrical and one spherical lens. The cylindrical lenses, 50 mm and 300 mm focal length, form a cylindrical telescope which spreads the beam into a collimated, 5 cm tall

sheet. The spherical lens, 1 m focal length, focuses the sheet to a 150  $\mu\text{m}$  waist. The laser sheet is then oriented inside the combustion chamber to excite the OH radical.

The spatial distribution of the OH fluorescence into the flame is recorded on the ICCD camera used for the OH\* chemiluminescence technique. The intensifier gate width is set to 1  $\mu\text{s}$  and the framing rate of the acquisition of fluorescence images is 10 Hz. The camera is equipped with the same optical lens and optical filters as for the OH\* chemiluminescence diagnostic.

Finally, the sensing instrumentation (ICCD camera, PMT and fast UV photodiodes) is interfaced to a PC computer which is used to control the camera and acquire the experimental signals via a LABVIEW program.

### 3.5.3 Ketone-PLIF

In case of premixed acetone/air laminar flames, the acetone planar induced fluorescence imaging technique offers the advantage to easily image the frontiers of the consumption of the fuel inside the flame. Generally, acetone is selected as an efficient fluorescent tracer owing to the following attractive properties: (i) this fluorescing hydrocarbon molecule has a broadband absorption feature extending from 220 to 320 nm (ii) the same pulsed UV laser source required for the OH-excitation can be used for acetone excitation, (ii) its high fluorescence yield ( $\sim 0.21\%$ ) allows the detection of small amount of acetone (typically  $\sim 100$  ppm), (iii) the blue broadband fluorescence between 350 - 550 nm, can be used as a good indicator of fuel concentration below the molecule decomposition temperature of 1000 K; (iv) the fluorescence signal is insensitive to the effects of collisional quenching; (v) the photophysics of acetone fluorescence is well characterized, allowing temperature and concentration measurements.

In the current work, laser excitation of acetone is provided by the laser source used for the OH-PLIF diagnostic. As acetone displays a broadband absorption spectrum extending from 230 to 320 nm, the excitation wavelength of acetone can be fixed to any convenient wavelength located in this domain. However, for a flame, the excitation wavelength of acetone must be selected to ensure that this wavelength is far from resonance of an OH transition. Thanks to this procedure, only the acetone fluorescence can be collected onto the optical detector. For instance, Figure 3.7 displays a portion of the OH fluorescence spectrum recorded in the 282.65 – 282.90 nm spectral domain. As observed in this fluorescence spectrum, the OH transitions, i.e. the  $Q_1(5)$  and  $Q_1(6)$  rotational lines, are well separated, giving the opportunity to tune the excitation wavelength of acetone at 282.85 nm in a spectral region in which only the collection of acetone fluorescence will be permitted.

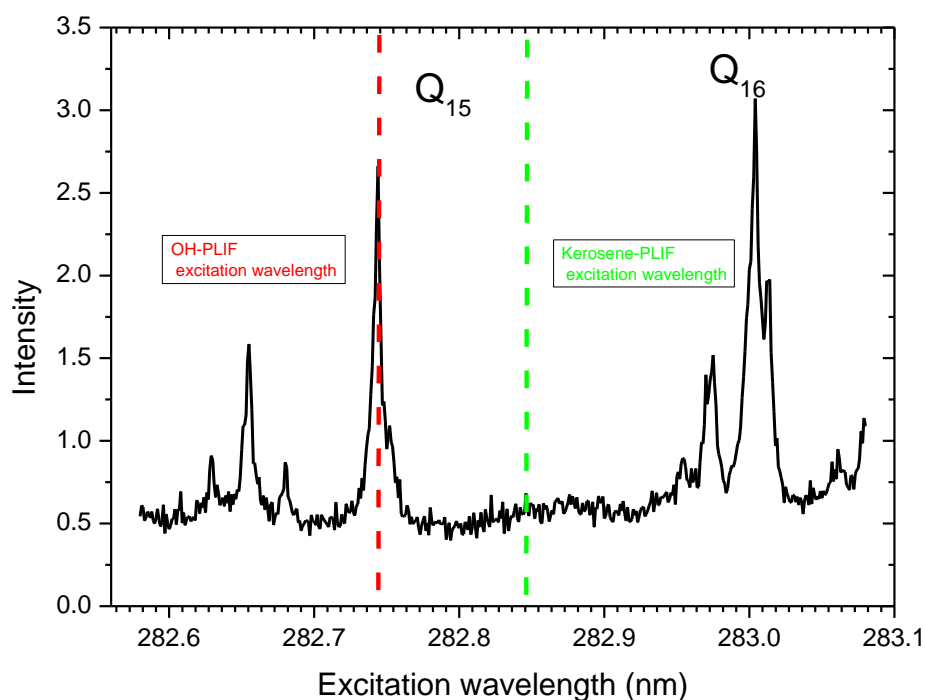


Figure 3.7: Excitation fluorescence spectrum of the OH radical recorded into the reference flame.

Fluorescence images of acetone were acquired by illuminating the acetone/air flame with the same optical arrangement than the one used for OH-PLIF. Only the spectral optical filters placed in front of the ICCD camera were changed for collecting the whole broadband fluorescence spectrum of acetone (i.e. between 300 to 550 nm).

### 3.5.4 Aromatics-PLIF

By analogy with the previous optical diagnostic, kerosene or assimilated surrogate fuels (LUCHE surrogate for instance) present the advantage to also issue a broadband fluorescence emission covering the 260 – 420 nm spectral domain. This fluorescence emission arises from the excitation of aromatics (i.e. mono- and di-aromatics) naturally present in the chemical composition of these multi-component fuels. Aromatics may be excited at the same wavelength as that used for acetone, and, as it is consumed with the fuel at the flame front, it can be used to image the un-burnt regions of the combustion volume. In the current work, fluorescence images of aromatics were acquired by illuminating the kerosene/air flames with the same optical arrangement than the one used for acetone-PLIF.



## Chapter 4 Laminar flame speed determination

---

Various approaches of laminar flame speed measurement methodologies will be detailed in this chapter: the flame cone angle and the flame area methods. Advantages and limitations of these measurement strategies are then discussed. The description of the optical imaging techniques selected to apply these methods follows. These are OH\*-chemiluminescence, OH-PLIF, acetone-PLIF and aromatics-PLIF. Finally, the data processing methods used to measure the laminar flame speed from images recorded with each method are subsequently described.

## 4.1 Laminar flame speed measurement approaches

The Bunsen flame method selected for the current work generates a two-dimensional axisymmetric conical premixed flame stabilized on the lip of a contoured nozzle. As mentioned in chapter 2, the laminar flame speed is the velocity that a planar flame front travels relative to the unburned gas in a direction normal to the flame surface. Though this definition is straightforward, in practice, it is difficult to measure this scalar parameter because a real laminar flame is usually influenced either by flow non-uniformity hydrodynamic strain (i.e. tangential velocity gradient along the flame surface) or by flame motion (curvature at the flame tip and azimuthal curvature for 3D conical flame) or by both (stretch). In the last case, their combined influence on local laminar flame speed depends also on the Markstein length (or stretch sensitivity) of the reactant mixture [55]. Since it is nearly impossible to get experimentally a planar, adiabatic flame in a uniform velocity field, it is extremely challenging to make a direct measurement of the one-dimensional, unstretched, laminar flame speed. To overcome this difficulty, various approaches were proposed to measure the laminar flame speed from the shape of a conical premixed flame. Two are very popular in the literature, the flame angle method and the flame area.

### 4.1.1 Flame angle method

In a premixed Bunsen burner, if the velocity of the issuing flow is larger than the laminar burning velocity to be defined below, a Bunsen flame cone is establishing at the top of the contoured nozzle or a straight tube. Incoming flow velocity  $U_0$  of the unburnt mixture can be split into a component  $U_{t,0}$  tangential to the flame and a component  $U_{n,0}$  normal to the flame front (Figure 4.1). Due to thermal expansion within the flame front, the normal velocity component is increased, since the mass flow density  $\rho U_n$  through the flame must be the same in the unburnt mixture and in the burnt gas

$$(\rho U_n)_0 = (\rho U_n)_b \rightarrow U_{n,b} = U_{n,0} \frac{\rho_0}{\rho_b} \quad (4.1)$$

while the tangential velocity  $U_t$  is not affected by gas expansion.  $\rho_0$  and  $\rho_b$  are the unburned and burned density respectively. The vector addition of the velocity components in the burnt gas leads to  $\mathbf{U}_b$ , which points into a direction which is deflected from the flow direction of the unburnt mixture. Since flame front is stationary, the burning velocity  $S_L$  with respect to the unburnt mixture must be then equal to the flow velocity of the unburnt mixture normal to the front. This condition is then respected by

$$\cos\left(\frac{\pi}{2} - \alpha\right) = \frac{S_L}{U_0} \rightarrow S_L = U_0 \sin\alpha \quad (4.2)$$

with  $\alpha$  is the half Bunsen flame cone angle.

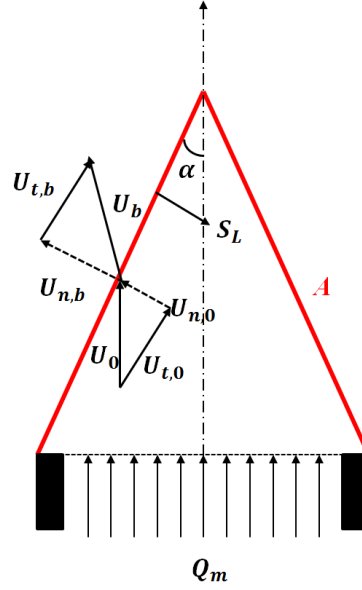


Figure 4.1: Illustration of the surface area and flame angle method.

This allows determining an estimate of the burning velocity by measuring the half cone angle  $\alpha$  under the condition that the flow velocity  $U_0$  is uniform across the contoured nozzle, which is the case when a contoured nozzle is used. Furthermore, the nearly uniform exit velocity profile gives a fairly straight edge along the shoulder of the flame to determine the half cone angle more accurately. However, the main drawback of this method, apart from the measurements not corrected for stretch, is the huge uncertainty even if there is a small divergence in the streamline approaching the flame. For that reason, this method will be not be investigated in the current work.

#### 4.1.2 Flame area method

The flame area method is introduced here to determine the average laminar flame speed  $S_L$  over the entire flame front surface. Assuming that the laminar burning velocity is the same all over the flame surface, the laminar flame speed can be expressed by applying the overall mass balance as

$$\rho_0 S_L A = Q_m \rightarrow S_L = \frac{Q_m}{\rho_0 A} \quad (4.3)$$

This relation expresses the average flame speed as the ratio between the total volume flow rate of the injected fuel/air mixture ( $Q_m/\rho_0$ ), and  $A$  is the flame area at appropriately chosen location.

Many of the difficulties associated with this approach lie on the following question: which part of the flame should be detected for measurements of laminar flame speed. Evidently, from Eq. (4.3), any surface within the flame front at which the corresponding values of density and mass flow rate can be accurately and reproducibly determined would be suitable. Undoubtedly, the best surface is that at which the

temperature just starts to deviate from the unburnt gas value (see chapter 2, Eq. 2.5). Unfortunately, this position is not easily measureable due to the asymptotic nature of the temperature profile. Traditionally, various methods of locating the position of the flame front have been proposed and used in the past. These mainly include the Shadowgraph, Schlieren and flame emission imaging techniques. Unfortunately, as shown in Figure 4.2: Bunsen flame with the popular optical accessible flame edges. The evolution of the signals delivered from each technique give widely different locations of the flame making a precise measurement of the laminar flame speed more challenging.

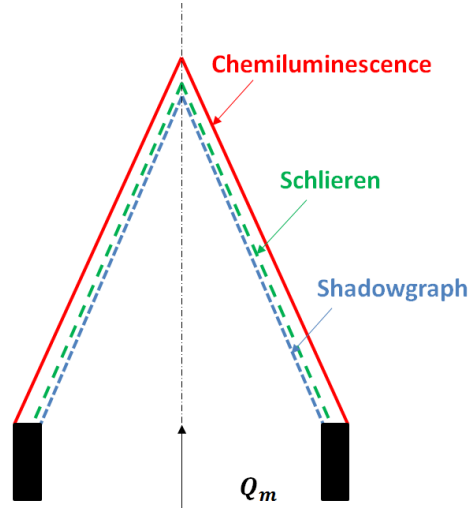


Figure 4.2: Bunsen flame with the popular optical accessible flame edges.

Schlieren imaging yields a focused image of the flame, enabling the position of maximum intensity, given approximately by the first derivative of density ( $d\rho/dx$ ) or the first derivative of temperature  $(1/T)(dT/dx)$ . In a flame front, this means that the surface marked by the Schlieren image is not the point of maximum temperature gradient, as has been stated by the literature, but is actually at a location much lower in temperature. In a plane flame front, Weinberg [139] has shown that the image occurs at  $3/2$  times the initial temperature. In curved flame front, the deviation from this value is insignificant. It has also been pointed out that the refractive index gradient is inversely proportional to the radius of curvature of the light beam being deflected in the flame. As a consequence, this means that correction of concentration and edge on the Schlieren signals is necessary that complicates the measurement of laminar flame speeds in axisymmetric premixed flames.

The image produced by a shadowgraph is complex and measures the second derivative of density ( $d^2\rho/d^2x$ ) or both the first and second derivatives of temperature  $(1/T)^2(dT/dx)^2 + 1/T(d^2T/d^2x)$ . Experiments performed in the past revealed that the sharp inner shadowgraph edge is dependent of the distance between the flame and the optical detector. This edge is located ahead of the preheat region and approaches the start of this region as the distance between the flame and optical detector is decreased.

This well-defined edge may therefore only be used if suitable corrections can be made. On the other hand, the outer shadowgraph edge, which is coincident with the Schlieren edge and is not dependent of distance, is not well defined and is hence difficult to measure.

Since the emission signal of a luminous zone is generally sufficiently high, particularly for hydrocarbon/air mixtures, a record of the spatial distribution of the flame front emission is possible and has frequently been used in combustion sensing and diagnostic applications and flame front visualization. However, as was discussed in chapter 2, this zone, representing the zone of the reactive species present into the flame front is located some distance behind the initial temperature rise and hence do not directly represent the outer position of the preheat gases. This surface would therefore appear to be unsuitable for directly determining burning velocities unless the corresponding unburnt gas density can also be measured or an estimation of the flame thickness can be estimated.

Of course, these are not the only techniques that exist, they represent just the popular optical techniques that were proposed and used in the past to locate the position of the flame front. For instance, some of the other techniques include: interferometry, particle track measurements, ionization gaps and temperature measurements. These techniques present also limitations which complicates their use for precisely determining the edge of the reactive zone. Several corrections have then to be applied to obtain with accuracy the location of the outer edge of the preheating zone that is required to measure the laminar flame speed [140]. Wherever possible, therefore, alternative methods of observing the flame front would appear to be desirable. Laser-based diagnostics techniques such as planar laser-induced fluorescence (PLIF), which has been widely used in combustion diagnostics, may provide a good solution to these limitations. This technique, which has been recently introduced for measuring the laminar flame speed [141] [142] [143] has been specifically developed in the current study and will be detailed in the next section.

## **4.2 Optical diagnostics**

In the present study, the popular OH<sup>\*</sup>-chemiluminescence technique was revisited. The fact that this technique is once again be addressed lies in the progresses of numerical tools which promote new attractiveness in the data processing of OH<sup>\*</sup> chemiluminescence images. Furthermore, a better knowledge of the evolution of the theoretical flame thicknesses deduced from simulations performed with detailed kinetic mechanisms authorize possibilities to bring a better correction on the raw signals for determining with accuracy the flame area. This work will be discussed in section 4.4 dedicated on the description of the data processing of flame images. In parallel to this work, the planar laser-induced fluorescence (PLIF) diagnostic was also developed for measuring the laminar flame speed. The technique has been declined in various forms. First of all, the OH radical was selected to locate with accuracy the flame front and

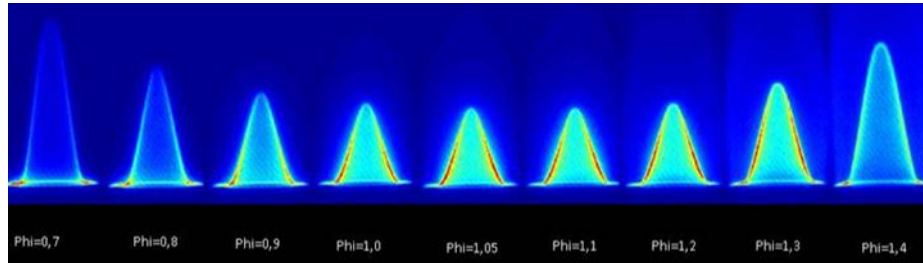
especially its inner edge representing the outer edge of the first rise of temperature in the flame. All the methodology developed to process OH-PLIF images will be detailed hereafter. Then, another approach, rare in practice was developed as an alternative for measuring the laminar flame speed. This approach consists in determining the location of the consumption of fuel when organic fluorescence fuel/air premixed flames were studied. To do this, specific fluorescence tracers entering into the species composition the fuels under study were selected in regards to their attractive properties combining fluorescence signals and temperature. The first fluorescence tracer was a ketone molecule, i.e. acetone. This one was used to measure the laminar flame speed for acetone/air mixtures. A second set of fluorescent molecules were also used to probe kerosene/air flames. These are aromatics that are naturally present into both fuel compositions.

#### 4.2.1 OH\* Chemiluminescence

The light naturally emitted by flames is termed luminescence, and includes both chemiluminescence and gray and blackbody radiation from soot and other particulates [144]. Chemiluminescence is the electromagnetic radiation emitted through the de-excitation of electronically excited species (atoms and molecules) formed by chemical reactions in the reaction zone. It occurs in flames due to the high temperatures in the reaction zone, which leads to the spontaneous emission of light. In hydrocarbon-air flames, much of the visible and ultraviolet light is emitted by e.g. the CH\*, OH\*, and C<sub>2</sub>\* radicals as well as CO\* and CO<sub>2</sub>\* [145]. An excellent detailed analysis of basic aspects of OH\*, CH\* and C\* chemiluminescence in the reaction zone of laminar premixed flames is also reported in Kojima and al.'s work [146]. The flame luminosity can provide information useful in combustion sensing (by optical sensors) and in diagnostic applications (through spatially resolved signals) and can also be a source of interference in PLIF and PIV measurements [147].

The recording of flame chemiluminescence is one of the simplest methods of visualizing flames. This natural (passive) radiation can be observed by the naked eye or can be recorded with a camera. The equipment required for this imaging is simply a sufficiently light-sensitive camera, together with filters, when desired, for selecting a part of the emission spectra, the ultraviolet radiation of the OH radicals, for example (see more details in chapter 3). A drawback of this technique is its line-of-sight nature, which needs to be taken into account when interpreting images of chemiluminescence. Since the signal is averaged over the volume of the flame as a whole, the local two-dimensional (2D) structure of it is not fully revealed. Due to its simplicity, this diagnostic is employed routinely to detect the global position and shape of the combustion region in industrial combustors. In premixed flames, it is also possible to interpret the radiation intensity of free radicals in terms of fluctuations in the heat release. This approach is used in studies of combustion dynamics in which the imaging of fluctuations in heat release can be carried out spatially and temporally resolved (high-speed imaging), keeping in mind the integration over the line-of-sight. In the present experiment, chemiluminescence imaging was used to record the emission

from the  $\text{OH}^*$  excited species to determine the reaction-zone location. As the dimensions of the flame thickness are relatively small, the  $\text{OH}^*$  chemiluminescence images provided a clear picture of the flame structure taking place.



*Figure 4.3: Instantaneous images of  $\text{OH}^*$  chemiluminescence for various equivalence ratios. Operating conditions:  $\text{CH}_4/\text{air}$  mixture,  $T = 300 \text{ K}$ ,  $P = 0.1 \text{ MPa}$ , fresh gas velocity  $1.1 \text{ m/s}$ ,  $\Phi = 0.7 - 1.4$ . The color scale represents the intensity variation of the 16-bit chemiluminescence images.*

For instance, Figure 4.3 shows typical images of the flame emission of laminar premixed  $\text{CH}_4/\text{air}$  flames recorded for various equivalence ratios. The majority of the flame emission comes from the flame edges, i.e. the  $\text{OH}^*$  chemiluminescence from the reaction zone. The less intense region in the central portion of each image is due primarily to  $\text{OH}^*$  chemiluminescence from the front and the back edges of the flame. Finally, the global intensity of the flame edges representative of the  $\text{OH}^*$  production rate and thus the heat release is greatly enhanced at high temperatures, i.e. at equivalence ratio approaching the stoichiometry.

#### 4.2.2 Planar Laser-induced fluorescence

Fluorescence is the spontaneous emission of radiation by which the molecule or atom relaxes from an upper energy level to the ground level [148]. In laser-induced fluorescence (LIF), the optical excitation is by means of a laser pulse, carefully tuned to a transition from a lower to an upper state of the fluorescent species.

If the tracer molecule is resonantly excited by the laser radiation, a photon of energy  $h\nu$  is absorbed, bringing the molecule from a ground state to a given vibrational and rotational level in a higher electronic state. Here,  $h$  is Plank's constant and  $\nu$  is the tuned frequency. The population in the new state is unstable, due to collisions between molecules. Rapid energy redistribution occurs immediately after excitation, resulting in a population of closely-lying rotational levels. Shortly thereafter, the molecule spontaneously emits another photon (fluorescence) of energy  $h\nu$  or lower, before it decays to the rotational and vibrational sub-levels in the ground electronic state [148]. Due to the energy redistribution in the excited state, fluorescence occurs not only at the excitation wavelength (resonant fluorescence), but also at other wavelengths, mainly shifted towards longer wavelengths. This property is an advantage in the detection

of the fluorescence, generally done at non-resonant wavelengths to minimize interference by seeding particles (Mie) or spurious laser scattering. The fluorescence signal can be collected by an intensified CCD camera (2D measurements) or by a PMT (point measurements).

Since each species has unique absorption and fluorescence patterns, this technique enables species-selective measurements. To do this in practice, a tunable laser source is required such as a dye laser. The success of LIF is clearly linked to the high sensitivity that can be achieved through the relatively large cross-sections of the resonant absorption process involved. In the combustion area, LIF can be used to detect flame radicals, reaction intermediates and pollutants at ppm (parts per million) and even at sub-ppm levels. The high sensitivity also enables planar (2D) laser-induced fluorescence (PLIF) imaging to be carried out [149]. Fluorescence tracers in the combustion environment may be naturally occurring or seeded into the combustion system. Fluorescence measurements may be used to indicate the location of flame structures, e.g., the flame front, burnt and un-burnt fraction; or, when quantitative measurements are made, can indicate chemical production rates or local temperature. Examples of naturally occurring species are the hydroxyl radical (OH), nitric oxide (NO), carbon monoxide (CO), the methyl radical (CH<sub>3</sub>) and formaldehyde (CH<sub>2</sub>O) but also fuels components such as aromatics. Commonly seeded fluorescence targets are acetone, toluene, nitric oxide, indium, thallium lead; etc. [5]. As discussed in the previous chapter, several fluorescent tracers were used in the current work for measuring the laminar flame speed. These are OH for detecting the reaction zone as well the burned regions, acetone for visualizing the location of the zone of the fresh acetone/air mixtures and aromatics for the detection of the position of the fresh region of kerosene/air flames.

#### *(a) OH - PLIF*

The OH radical is an oft-used fluorescence tracer for LIF diagnostics in combustion. OH signal appears just after the highly reactive flame front and extends into the post combustion regions of the flame. Fluorescence originates from an electron excited from the  $v'' = 0$  vibrational level of the ground electronic state to the  $v' = 1$  first vibrational level of the first excited state. The transition is shown in Figure 4.4. Fluorescence signal is filtered to remove the scatter from the excitation beam. The measured signal is primarily from the numerous rotational transitions of the lowest vibrational level upper electronic state to the lowest vibrational level of the ground electronic state a wavelength region around 308 nm.



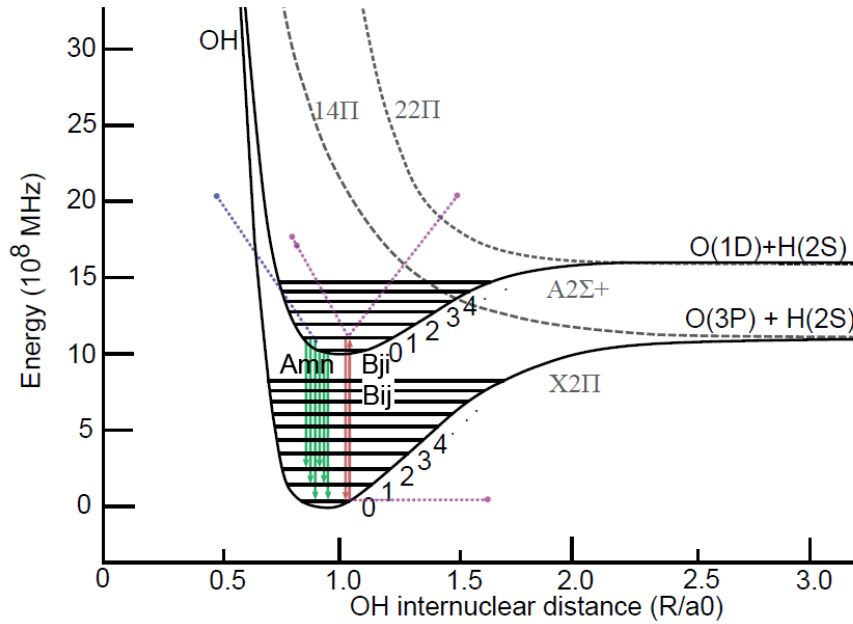


Figure 4.4: Selected potential energy curves for the OH molecule showing electronic and vibrational energy levels. Stable electronic levels are solid black lines, pre-dissociative levels in dashed gray. Transition pathways in red show stimulated pathways while green are spontaneous pathways.

In case of laminar premixed flames, the flame front, or reaction zone, is the thin region where most of the chemical reactions which convert fuel and oxidizer to combustion products take place. This flame front also separates burned and unburned gases. Usually, OH is considered as a good flame front indicator. Indeed, OH is formed by fast two-body reactions, such as the attack of H radicals on O<sub>2</sub> molecules, and appears as an intermediate species in many reaction pathways of both hydrogen and hydrocarbon combustion. The OH radical is then consumed by slower three-body recombination reactions, these one being located in the flame front zone [15]. Its detection using planar laser-induced fluorescence (PLIF) can be then an attractive method to detect with accuracy the reaction zone with high-spatial resolution and high signal to noise ratio. The production of this radical is indeed well correlated with the increase of temperature inside this zone. Furthermore, as the OH fluorescence varies linearly with the OH number density, it is then possible to measure the gradient of OH number density into the flame front. However, one limitation of this technique also appears when probing OH because this radical stays into the post reaction zone and burned gas zone. The existence of high temperature level into these regions provides still chemical reactivity that promotes the existence of OH.

For instance, Figure 4.5 shows typical images of the OH-fluorescence images of laminar premixed CH<sub>4</sub>/air flames recorded for various equivalence ratios. As compared with OH\* chemiluminescence images displayed in Figure 4.3, the main part of the OH fluorescence signal comes from the flame edges, i.e. the reaction zone. Furthermore, the OH fluorescence signal is not part of the central portion, simplifying the location of the start of the reaction zone. Finally, as noted previously, the global intensity

of OH signal in the burned gas region is a function of the equivalence ratio, i.e. of the temperature level of burned gases. More the gas temperature will be elevated and more the OH fluorescence signal will be high.

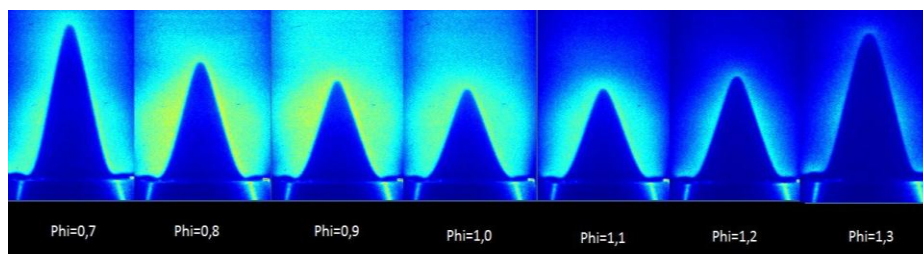


Figure 4.5: Instantaneous images of OH fluorescence for various equivalence ratios. Operating conditions:  $\text{CH}_4/\text{air}$  mixture,  $T = 373 \text{ K}$ ,  $P = 0.1 \text{ MPa}$ , fresh gas velocity  $1.1 \text{ m/s}$ ,  $\Phi = 0.7 - 1.3$ . The color scale represents the intensity variation of the 16 bit fluorescence images.

#### (b) Acetone - PLIF

Acetone ( $\text{CH}_3\text{COCH}_3$ ) is a fluorescing hydrocarbon molecule which can be added to the fuel or air for laser-induced fluorescence imaging of the pre-combustion region. It is often used to determine the degree of mixing and equivalence ratios of the combustion mixture [149] [143]. Acetone fluorescence may be excited by the same wavelength as the OH molecule, and, as it is consumed with the fuel at the flame front, it can be used when measured simultaneously with OH to image the burnt and un-burnt regions of the combustion volume [150].

This fluorescent tracer has transitions which can be easily excited with commercial lasers and the fluorescence, which is shifted to the red, is spectrally well-separated from the absorption spectrum. The absorption feature of acetone is accessible by fixed-frequency pulsed lasers in the wavelength interval between 225 and 320 nm, with a maximum absorbance around 280 nm. Their fluorescence spectrum is broadband, extending in the visible from 330 nm to 600 nm, with a peak around 430 nm, permitting imaging with unintensified CCD cameras. Acetone has been applied to PLIF imaging of jet mole fraction in turbulent-free jets and in jets in crossflow and as a marker of unburned fuel in reacting environments: methane and hydrogen jet diffusion flames, supersonic reacting mixing layers [151] and also used to trace iso-octane in SI engines [152] or in practical combustors as a tracer of unburned fuel. Nonetheless, at temperatures above 1000 K, acetone starts to pyrolyze and reacts with radicals such as H, O and OH [153] [154]. Therefore, differences of chemical behavior between acetone when seeding in a fuel must then be considered. Indeed, the pyrolysis rate of acetone is found to be higher than that of hydrogen and methane, but comparable with that of heavier hydrocarbons, e.g. ethane and propane. This limitation prevents the use of acetone in elevated temperature, long residence time hydrogen or methane flows, but presents no drawbacks with heavier hydrocarbon fuels. When combustion takes place, the overall rate of destruction

of acetone, hydrogen and hydrocarbons by radical attacks are similar. Differential diffusion also represents a limitation when light fuels such as hydrogen or methane are used, but for heavier hydrocarbon fuels, with molar weights closer to acetone, the effects are not significant. Of interest here is then the attractiveness to use acetone-PLIF for marking the zone of consumption of fuel in laminar premixed acetone/air flames. Due to the small gas velocities conditions, the destruction of acetone by chemical reactions will allow the determination of the outer edge of the first temperature rise (maximal temperature of 800 K) and so will give the opportunity to measure the laminar flame speed. To illustrate this potentials of acetone-PLIF, the spatial distribution of acetone fluorescence inside various laminar acetone/air flames are displayed in Figure 4.6. Unlike the previous case, acetone fluorescence is only located in the central part of the flow field representing the region of the injection of the fresh fuel/air mixture. A well-defined sharp outer edge delimiting the location of the fast complete chemical removal of the fuel can be then observed for all the operations conditions investigated.

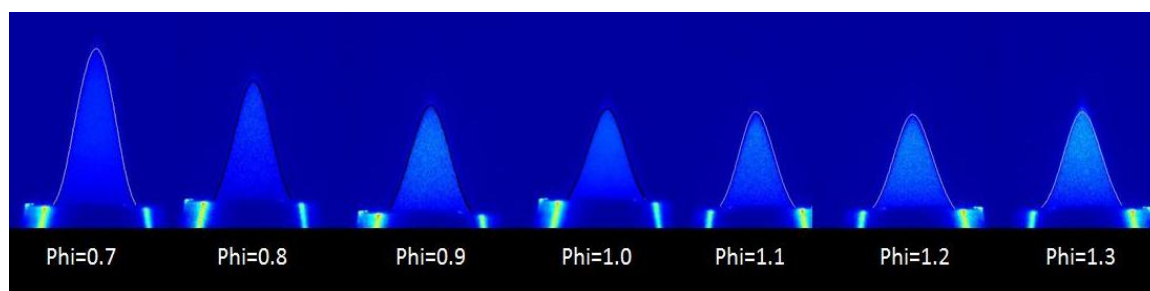


Figure 4.6: Instantaneous images of acetone fluorescence for various equivalence ratios. Operating conditions: acetone/air mixture,  $T = 473$  K,  $P = 0.1$  MPa, fresh gas velocity 1.1 m/s,  $\Phi = 0.7 - 1.3$ . The color scale represents the intensity variation of the 16 bit fluorescence images.

### (c) Aromatics - PLIF

These species exhibit interesting features such as a strong absorption in the UV and thus large fluorescence emission. For instance, single-ring aromatics like 1,2,4-trimethylbenzene and two-ring aromatics like naphthalene and its derivatives can be used to trace multi-component fuel such as gasoline, Diesel as well as typical aviation fuels containing a variety of fluorescing aromatic compounds. They typically have high fluorescence quantum yields and their absorption and emission spectra shift towards the red with increasing size of the aromatic structure [155]. Shown in Figure 4.7 are the spectra of fluorescence of kerosene vapor after excitation at 282 nm and 266 nm respectively [156]. This fluorescence displays two peaks, one arising from the fluorescence of mono-aromatics (i.e. 1, 2, 4 trimethylbenzene) and the second from di-aromatics (naphthalene family).

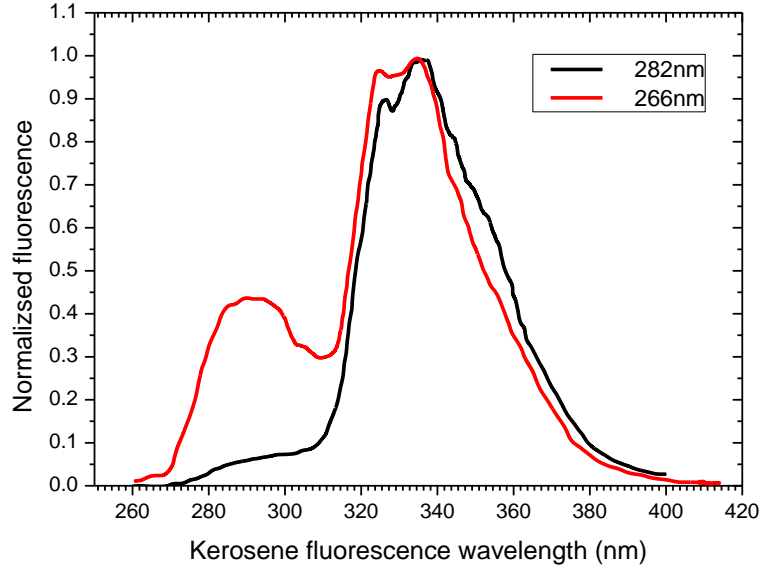


Figure 4.7: Kerosene fluorescence spectra for laser excitation wavelengths 282 nm and 266 nm  $T = 450$  K,  $P = 0.1$  MPa, kerosene diluted in  $N_2$  [156]

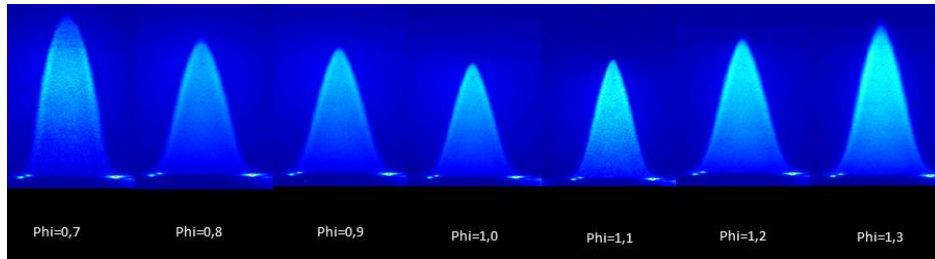


Figure 4.8: Instantaneous images of aromatics fluorescence for various equivalence ratios. Operating conditions: Jet A-1/air flame  $T = 405$  K,  $P = 0.1$  MPa,  $\Phi = 0.7 - 1.3$ . The color scale represents the intensity variation of the 16 bit fluorescence images.

The wide variety of molecular sizes and, therefore, boiling points, makes this class of molecules attractive as tracers that can be adjusted to the evaporation behavior of the fuel or that are representative for vaporization classes in multi-component fuels. Another feature of these aromatics is the strong quenching of fluorescence with oxygen. The fluorescence signal intensities do not only depend on the tracer concentration but also on the oxygen molar fraction. As a result, fluorescence from aromatics is found to be proportional to the fuel/air ratio, which is a parameter of major interest to industrials [157] [158] [159] [160] [156]. In the current work, aromatics-PLIF was used to measure the laminar flame speed of multicomponent fuels/air mixtures. These fuels are the commercial Jet-A1 fuel and one of its surrogates, the LUCHE surrogate. As in the previous ketone molecule, the fluorescence of aromatics will be indicative of the location of the fresh multicomponent fuel/air mixtures and the outer edge of this region will delimit the chemical consumption of the fuel. Examples of images of aromatics images in

kerosene/air flames are presented in Figure 4.8. Similar features than the ones observed on acetone-PLIF images are noted. Aromatics fluorescence is located in the fresh region and a sharp edge delimiting the removal of fluorescence signals is well-defined.

To summarize, therefore, it would appear that the measurements techniques which have been selected for the present study give large potentialities to measure accurately the laminar flame speed of conical premixed flames. These methods however are not fully ideal. They usually require edge corrections in regards of possible effects interfering on the laminar flame structure. These interferences can be of several kinds: heat losses at the rim of the nozzle, stretch and curvature effects on the flame tip, and flame-front thickness and potential flame-front irregularities due to effects of buoyancy. We will now deal with each of these in turn.

### 4.3 Sources of interferences on laminar premixed flame structure

To get an accurate laminar flame speed from the flame methods detailed in section 4.1, the parameters adopted to control the Bunsen flame and the measurement techniques as well as the data processing of the experimental data should be optimized. According to the literature, numerous experimental investigations on measurements of laminar flame speeds on Bunsen flames were reported in the last decade (Table 4.1). During these studies, considerable attention was devoted to evaluate the impact of these interferences on laminar flame speed measurements.

Year	Author	Optic technique	P (MPa)	T (K)	Fuel
2007	Natarajan et al. [161]	Chemiluminescence	0.1	300 K	H <sub>2</sub> /CO
2009	Dong et al. [162]	Chemiluminescence	0.1	300 K	H <sub>2</sub> /CO
2010	Mazas et al. [92]	Schlieren	0.1	373 K	CH <sub>4</sub> /H <sub>2</sub> O
2011	Selle et al. [40]	Chemiluminescence	0.1	300 K	CH <sub>4</sub> /H <sub>2</sub> O
2011	Burbano et al. [15]	Schlieren	<0.1	300 K	H <sub>2</sub> /CO
2011	Bouvet et al. [76]	Chemiluminescence	0.1	300 K	H <sub>2</sub> /CO
2012	He et al. [163]	OH-LIF	0.1	300 K	H <sub>2</sub>
2013	Jin et al [164]	OH-LIF	0.1	300 K	H <sub>2</sub> /CO
2013	Denis et al [165]	Chemiluminescence	0.1	295-450 K	H <sub>2</sub> /CO
2014	Xianzhong et al. [166]	Chemiluminescence	0.1	300 K	CH <sub>4</sub> /O <sub>2</sub> /CO <sub>2</sub>
2013	Dagaut et al. [16]	Chemiluminescence	0.1	480 K	Kerosene
2015	Wang et al. [167]	OH-PLIF	0.1	300K	H <sub>2</sub> /CO
2015	Gao et al. [141]	Chemiluminescence	0.25	300K	O <sub>3</sub> /CH <sub>4</sub>
2016	Sun et al. [142]	Chemiluminescence	0.1	300K	CO/H <sub>2</sub>

Table 4.1: Overview of laminar flame speed measurements with the Bunsen flame.

#### 4.3.1 Heat losses

Conical flames stabilized on the lips of nozzle are commonly affected by heat losses. This effect is however difficult to estimate and few detailed studies have been published on this topic. Among the rare studies, the work reported by L. Selle et al. [40] on experiments performed with a slot burner found that the optimized design of the burner nozzle (shape and thickness of the lips) can significantly reduce heat exchanges between the flame and the nozzle. These tendencies were confirmed with DNS simulations of heat transfer. The percentage of heat losses calculated in their experiments was less than 0.7% and then negligible compared to the total heat release. According to these results and considering the small thickness of the lips of our burner (0.5 mm), the heat transfer between the flame and the burner can be neglected in our experiment compared to the total heat released by the flame.

#### 4.3.2 Buoyancy effects

Because of the large density ratio between the burnt gases and the diluent gases, the flame stabilized on the lips of the nozzle could be subject to buoyancy effects [168] [169]. To quantify this effect, the magnitude of the ratio between buoyant and advective forces can be estimated by the Richardson number  $Ri = gl/u^2$ , where  $g$  is the acceleration due to gravity,  $l$  a characteristic length scale and  $u$  the velocity. For atmospheric condition,  $Ri \sim 10^{-2}$  in our experiment so that it is a priori unlikely to be buoyancy driven. At higher pressure, it was sometimes noted for organic fuel/air mixtures such as kerosene/air flames, limited buoyancy effects (see chapter 3) due to the presence of recirculation zones inside the combustion chamber. Performing experiments outside these reduced ranges of pressure was the solution adopted to circumvent this limitation.

#### 4.3.3 Stretch effects

Conical premixed flames are also affected by stretch effects arising mainly from aerodynamic straining and flame curvature [55]. Various studies were focused on estimate the impact of stretch to laminar flame speeds. Thus, stretch effects on a slot burner flame were reported into the work of L. Selle et al. [40]. The authors showed from DNS simulations that stretch effects occurs preferentially at the flame base and at the tip while these effects were very small everywhere along the flame. Effects of strain or curvature were found very limited along the main part of the flame front excepted at the flame tip (i.e. on a very limited region) in which stretch becomes very negative leading to Karlovitz numbers of the order of  $\sim 10$ . Choi et al. [170] also supported these conclusions for the case of a slot burner. The authors also studied in the same work these effects on axisymmetric premixed  $\text{CH}_4/\text{air}$  flames. They revealed not only that the results in the slot burner and axisymmetric burner were qualitatively similar indicating a similar response of the flames to curvature effects but they also were highlighted quantitative difference on such effect. The magnitude of the strain rate measured at the reaction zone in the shoulder region of the conical flame was much less compared to that at the tip, and its effect on the reaction zone speed was minimal. Studies

on conical laminar  $\text{CH}_4/\text{air}$  and  $\text{CH}_4/\text{O}_2$  flames reported by Mazas et al. reinforced these conclusions [92]. Using the expression of the ratio between the measured laminar flame speed and the unstretched laminar flame speed defined by Law et al. [55], they found that the relative difference between the measured flame speed and the unstretched laminar flame speed was 15 % for  $\text{CH}_4/\text{air}$  and 10 % for  $\text{CH}_4/\text{O}_2$ .

In the current study, as the design of the nozzle was optimized to minimize the boundary layer thicknesses, the velocity profile downstream from the nozzle presents a flat response demonstrating that the aerodynamic strain is thus limited. Moreover, it is found that the curvature effects are decreased when pressure increases (discussion in chapter 5). From these considerations, effects of flame stretch were disregarded.

#### 4.3.4 Flame thickness effects

The magnitude of the flame thickness plays also an important role in the determination of the laminar flame speed. As mentioned in Chapter 2, the laminar flame speed is defined by the velocity of gases located at the outer edge of the preheated zone. However, none of the imaging techniques used to visualize the flame allows a direct measurement of this location and details of how to select the flame edge remains unclear. For instance, various references describing the use of  $\text{OH}^*$  chemiluminescence [161] [162] [165] [166] [76] [56] reveal that the location of the maximum gradient of  $\text{OH}^*$  is used to delimit the reactive zone. Instead of using the edge of consumption of fresh gases, the use of the maximum  $\text{OH}^*$  contour could yield to significant differences in the laminar flame speed. These differences can be illustrated from Figure 4.9 showing the comparison between the temperature and  $\text{OH}$  concentration profiles issued from a one-dimensional n-decane/air flame simulation and the location of the flame edges measured with different diagnostic techniques.

The numerical simulation was performed in a one-dimensional configuration with COSILAB and the full LUCHE skeletal mechanism. The calculation was performed at  $T = 400 \text{ K}$ ,  $P = 0.1 \text{ MPa}$  and for an equivalence ratio  $\phi = 1.0$ . The flame sheet of Figure 4.9 is expanded to reveal a preheat zone in which initiation reactions take place and a reaction zone in which intermediates are chemically produced and consumed (in particular the  $\text{OH}$  radical). However, the distinction between both zones is difficult to establish experimentally. As shown in Figure 4.9, the chemiluminescence imaging technique give a peak of  $\text{OH}^*$  characteristic of the zone of the maximum temperature and also therefore of the outer edge of the reaction zone. The gap between this location and the position of the outer edge of the preheat zone, i.e. the thermal flame thickness is then quite significant. Possibility to get a substantial bias for the laminar flame speed will then be inevitable if the outer edge of the reaction zone is employed. Regarding now the  $\text{OH}$ -PLIF diagnostic performances, this technique allows the detection of the inner edge of the reaction zone when  $\text{OH}$  fluorescence becomes to be detected (i.e. at temperature around 800 K). In such cases, the error on the laminar flame speed will be now greatly reduced because of the shorter gap between this new

location and the outer edge of the preheat zone. With the organic tracer-PLIF, the visualization of the outer edge of the fresh gases will be obtained. As the organic tracers fluorescence is going to disappear at temperature around 800 K (see section 4.2.2), the outer edge delimiting the contour of the fluorescence signal of the organic tracer will correspond to a position quite similar to that for the apparition of the OH fluorescence.

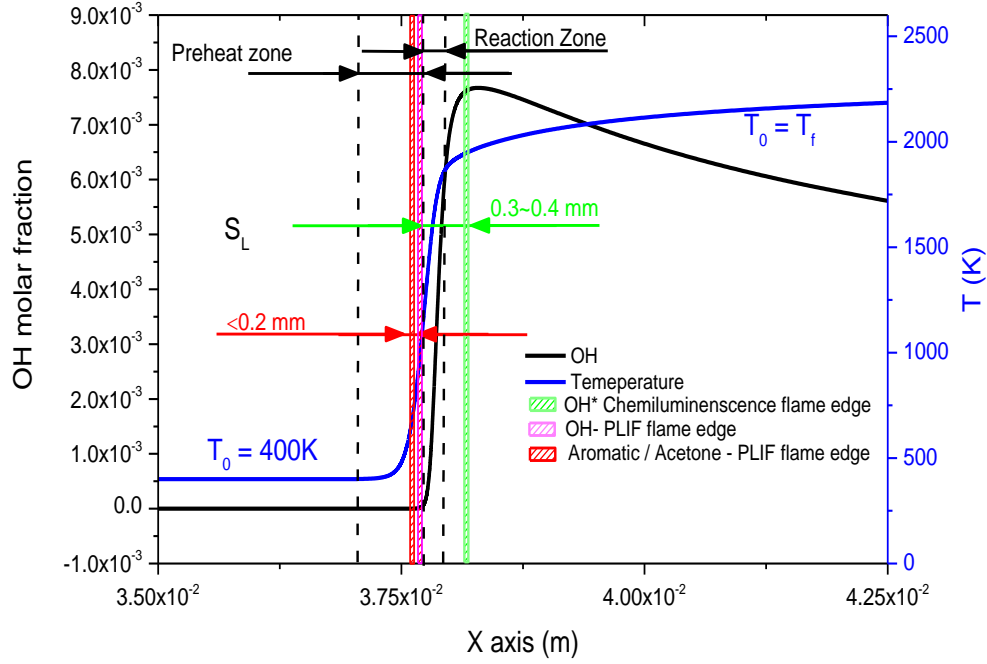


Figure 4.9: Numerical simulation of one-dimensional laminar premixed flame. Profiles of temperature (blue curve) and OH (black curve) for an *n*-decane/air mixture ( $T = 400$  K,  $P = 0.1$  MPa,  $\phi = 1.0$ ). The locations of the flame edges measured with various measurement techniques are also displayed.

To summarize, it appears that the OH\* chemiluminescence imaging technique cannot derive directly the location of the outer edge of the preheat gases. To be in accordance with the laminar flame speed definition, it is then necessary to make a correction on the position of the OH\* peak. For this purpose, it is proposed for finding the position of the outer edge to subtract the thermal flame thickness from the position measured with chemiluminescence imaging. As the measurement of this thermal flame thickness is challenging, these ones were deduced from numerical calculations performed using a detailed kinetic mechanism. Of course, this method is only valid when the detailed kinetic mechanism of the fuel under study is available. On the contrary, the position measured from PLIF images were directly used for measuring the laminar flame speeds.



## 4.4 Data processing of OH\*-chemiluminescence and PLIF images

As aforementioned, laminar flame speed determination based on a Bunsen flame is mainly defined by the location of the flame front for both flame angle and flame surface area methods. Precise and accurate image processing solver for determining the flame area therefore is key condition for obtaining accurately the laminar flame speed. In this section, the image processing procedures of OH\* chemiluminescence and PLIF signals are now detailed.

### 4.4.1 OH\* chemiluminescence

As mentioned previously, the Bunsen burner produces axisymmetric premixed flames. Recording the emission signals with the OH\* chemiluminescence technique provides then line-of-sight projections of the flame field. Figure 4.10 illustrates the relation between the projection and the spatial distribution of a flame property in a plane normal to the stream wise axis of the axisymmetric flame. The projection function  $S(y)$  is related to the line-of-sight integration of the flame property  $I(r)$  by the following equation:

$$S(y) = \int_{-\infty}^{+\infty} I(r) dz \quad (4.4)$$

With a large number of simultaneous projection lines, an entire flame image can be recorded instantaneously. For instance, see the flame emission images shown in Figure 4.3.

It is a crucial step in experimental data reduction to reconstruct the spatial distribution of the flame property, based on the measured line-of-sight projections. This requires the inversion of Eq. 4.4. Many methods for the reconstruction of axisymmetric distributions have been reported in the literature. Among them, the Abel transformation method, reported in the year of 1826 [171] gives a concise, exact solution for the reconstruction. A complete description of the method can be found in the following references [172] [173]. Only the key elements of this method will be now detailed.

Let us consider the light emitted by a given region of the flame and recorded by a detector in the  $(x, y)$  plane (Figure 4.10). When self-absorption and scattering of the emitted light are neglected, the signal  $S(x, y)$  detected by the pixel  $(x, y)$  of the ICCD camera is a sum over the line-of-sight of the local intensity, and one may write

$$S(x, y) = \eta_{opt} \int_0^z I(x, y, z) dz \quad (4.5)$$

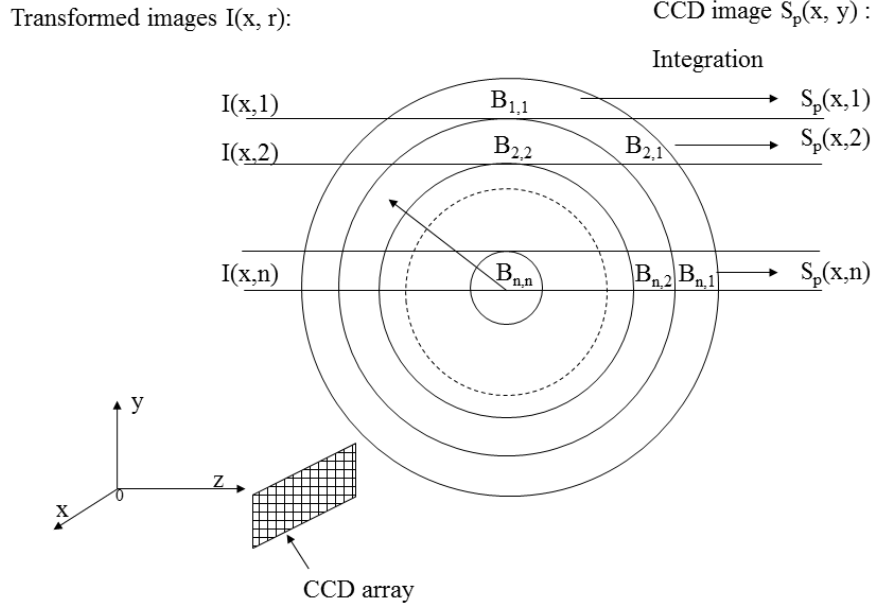


Figure 4.10: Schematic view of the algorithm used for inversion of Abel's integral of the detected emission signal.

where  $z$  is the distance from the ICCD camera,  $Z$  designates the maximum distance from which light may be emitted, and  $I(x, y, z)$  is the volumetric light emission intensity. The parameter  $\eta_{opt}$  describes the solid angle of light collection and the transmission efficiency of optical components. In the present experiments,  $\eta_{opt}$  is assumed to be constant over the range of frequencies of interest.

Assuming that the mean  $I(x, y, z)$  has a rotational symmetry with respect to the nozzle axis, and that this axis is perpendicular to the line-of-sight of the ICCD camera, then by changing the variable of integration into  $r = (x^2 + y^2)^{1/2}$

$$S(x, y) = \eta_{opt} \int_0^R I(x, r) \frac{r}{(r^2 - y^2)^{1/2}} dr \quad (4.6)$$

where  $r$  is the radial distance from the symmetric axis and  $R$  designates the maximum radial distance at which light is emitted. Eq. 4.6 provides an analytical expression for the projection function  $I(x, r)$ . A well-known analytical inverse of Eq. 4.6 is the Abel transform [172],

$$I(x, r) = \frac{1}{\eta_{opt}} \frac{-1}{\pi} \int_r^R \frac{\partial S(x, y)}{\partial y} \frac{dy}{(y^2 - r^2)^{1/2}} \quad (4.7)$$

The interest of the Abel transform lies in the exactness and conciseness. Since the Abel transform is an exact solution to Eq. 4.6, it can in principle be calculated as accurately as desired. Because Eq. 4.7 involves the derivative of the detected experimental signal, the inversion method is sensitive to noise. This sensitivity increases towards the center due the decreased volume contributing to the experimental

signal. The accuracy of the results is also limited by the numerical integration. Finally, the Abel transform is also unique. This can be deduced from the fact that  $I(x, r) = 0$  if  $S(x, y) = 0$ .

While expression Eq. 4.7 is well adapted to theoretical studies of a given problem, practical inversion of the experimental signal detected by the ICCD camera will be best accomplished with applying the onion-peeling method on Eq. 4.6. In the onion-peeling method, the entire domain of the spatial distribution is divided into a series of concentric rings, as shown in Figure 4.10. Within each ring the value of the spatial function  $S(x, y)$  is assumed to be constant, Thus, Eq. 4.6 is approximated by the following summation

$$S(x, y) = \sum_{r'=y}^R I(s, r') B(y, r') \quad (4.8)$$

where  $B$  is a matrix of geometrical factors and  $B(y, r')\Delta x$  represents the volume in which the emission  $I(x, r')$  contributes to the emission signal  $S(x, y)$ . Once the  $B(x, r')$  elements are obtained, Eq. 4.8 can be solved by multiply the inverse of the matrix  $B$  with the signal vector  $S$  in each section  $x$  to yield the matrix of volumetric light emission  $I(x, r)$ . For instance, if the image is composed by a  $6 \times 6$  matrix of pixels, Eq. 4.8 becomes:

$$\begin{bmatrix} B(1,1) & B(1,2) & B(1,3) & B(1,4) & B(1,5) & B(1,6) \\ 0 & B(2,2) & B(2,3) & B(2,4) & B(2,5) & B(2,6) \\ 0 & 0 & B(3,3) & B(3,4) & B(3,5) & B(3,6) \\ 0 & 0 & 0 & B(4,4) & B(4,5) & B(4,6) \\ 0 & 0 & 0 & 0 & B(5,5) & B(5,6) \\ 0 & 0 & 0 & 0 & 0 & B(6,6) \end{bmatrix} \cdot \begin{bmatrix} I(1,1) & \dots & I(1,6) \\ I(2,1) & \dots & I(2,6) \\ I(3,1) & \ddots & I(3,6) \\ I(4,1) & \ddots & I(4,6) \\ I(5,1) & \dots & I(5,6) \\ I(6,1) & \dots & I(6,6) \end{bmatrix} = \begin{bmatrix} S(1,1) & \dots & S(1,6) \\ S(2,1) & \dots & S(2,6) \\ S(3,1) & \ddots & S(3,6) \\ S(4,1) & \ddots & S(4,6) \\ S(5,1) & \dots & S(5,6) \\ S(6,1) & \dots & S(6,6) \end{bmatrix}$$

Once this numerical procedure is done, the flame front becomes easier to detect. This one is obtained by measuring the maximum intensity contours on the Abel transform image. This procedure enables to measure the spatial location of the flame front on the emission image.

For clarity, Figure 4.11 resumes the entire procedure used to determine the location of the flame front from the  $\text{OH}^*$  chemiluminescence images. First of all, the  $\text{OH}^*$  emission image detected by the ICCD camera (Figure 4.11a) (single-shot or averaged image on a given delay) is firstly split in half along the burner axis (Figure 4.11b) to be treated separately. Then the Abel transform is applied on each half of the flame images (Figure 4.11c). The distribution of the maximum  $\text{OH}^*$  intensity on each half image is then

used by applying a threshold selection method to get the spatial position of the flame front contour. The same procedure is repeated for the other half of the flame image.

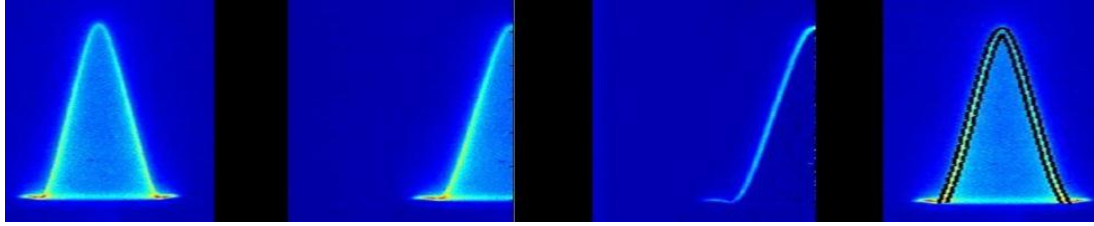


Figure 4.11:  $OH^*$  chemiluminescence image processing: (a)  $OH^*$  chemiluminescence raw image (b) image split in half along the burner axis (c) Abel-transform image (d) unburned gas contours detection with flame thickness consideration.

Effects of the flame thickness and stretch are then taken into account for determining the “true” position of the outer edge of the preheat zone. As mentioned in section 4.1.2, any surface within the flame front, at which corresponding values of area and density are measured, can in principle be used as a reference to specify the laminar burning velocity. In our case, the flame thickness cannot be estimated to be thin, excepted may be when experiments will be performed under elevated pressures. As the experimental measurement of the flame front thickness is challenging, the methodology retained in the current work consisted of the calculation of the flame thickness from simulation performed with the COSILAB code. For the fuel and the operating conditions under study, the one-dimensional laminar flame of the fuel/air mixture was calculated with a detailed reaction mechanism. A simulated flame thickness is obtained. The location of the outer edge of the preheat zone is then calculated by shifting towards the burner axis direction the outer position of the flame front measured with chemiluminescence images of the theoretical flame thickness. From this new location, the flame area  $A$  is calculated by pivoting the outer preheat edge profile  $f(x)$  along the burner axis using the following expression:

$$A = 2\pi \int_a^b f(x) \sqrt{1 + [f'(x)]^2} dx \quad (4.9)$$

$a$  and  $b$  are the boundary limits of integration. The laminar flame speed is then deduced from Eq. 4.3. The laminar flame speed is then calculated from the surface area calculated from each half of the flame image. This procedure is the one which has been tested and validated for fuels in which detailed kinetic mechanisms are available. To illustrate in detail this procedure, the application of this procedure on different fuels will be presented in chapter 5 that deals with the laminar flame speed measurements of methane/air mixtures and acetone/air mixtures.

#### 4.4.2 PLIF diagnostic

Compared to the methodology presented in section 4.3, the data processing of OH-PLIF images is largely simplified. The inner contour delimiting the region of OH-fluorescence on the fresh gases side is determined by considering the first pixel in which OH fluorescence appears (See Figure 4.12 a). Typically, this value corresponds to the detectivity of our experimental setup which allows a detection of several dozen of ppm (see section 5.1.2). Furthermore, the beginning of detection of OH signals on fluorescence images corresponds roughly to a temperature of about 800 K that coincides with the location of the outer frontier of the fresh gases zone.

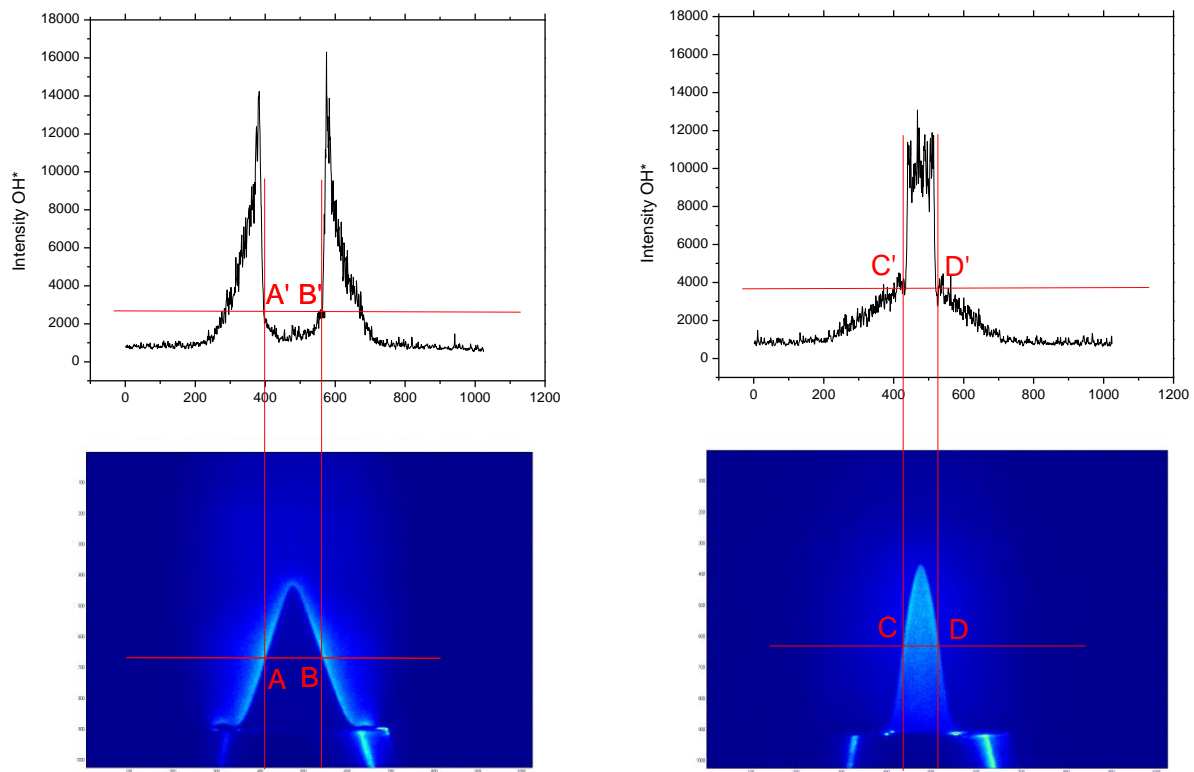


Figure 4.12: Illustration of the (a) OH-PLIF and (b) acetone/aromatics-PLIF image processing.

For organic tracers such as acetone and aromatics, the data processing of image is similar to the preceding one. The outer edge of the fresh gases is defined as the position in which the fluorescence of the organic tracer disappears (see Figure 4.12b). As for OH, this location corresponds to the frontier delimiting a chemical transformation of these organic molecules through the action of chemical reactions. Typically, these organic molecules disappear when OH starts to be optically detected. A detailed illustration of this methodology will be presented in chapters 5 and 6 that deal with the laminar flame speed measurements of methane/air, acetone/air and Jet-A1 mixtures.

## 4.5 Measurement Uncertainties

For all the measurements, 30 instantaneous images were systematically recorded and the resulting laminar flame speed was determined by data processing of averaged images deduced from the set of the instantaneous images. This measurement was repeated five times and the final results of laminar flame speed presented in this thesis are the averaged values of these five set of measurements.

The uncertainty of the measured flame speed takes into account the two main following sources: the uncertainty on the total flow rate of unburned gas ( $U_{Qm}$ ) and the uncertainty on the calculated flame area ( $U_A$ ) from experimental images of the flame shape.

- $U_{Qm}$  comes from the massflow controller uncertainty which was estimated to be  $\sim 2-3\%$ . For more details, see the section 3.4.
- $U_A$  derives from the spatial resolution used to record our experimental images of the flame shape. Typically, this one after calibration was estimated to  $40\text{ }\mu\text{m}$  corresponding to the size of an element of volume of the flame imaged by one pixel of the ICCD camera. This uncertainty  $U_A$  supposed then that the location of the experimental flame contour extracted from the data processing of flame images is known with an accuracy of  $40\text{ }\mu\text{m}$ . An integration of this error in our image data process then yielded an error on the laminar flame speed of about  $3\%$ .

The overall uncertainty was calculated from the relation  $\sqrt{U_{Qm}^2 + U_A^2}$ . According to the preceding values  $U_{Qm}$  and  $U_A$ , a net value equal to  $\sim 4\%$  was estimated for all the laminar flame speeds that were recorded at a preheating temperature ranging between 300 and 523 K, an equivalence ratio range of 0.6 – 1.3 and at ambient pressure conditions. For instance, for these experimental conditions, the overall uncertainty on the laminar flame speed varied from  $\pm 1\text{ cm/s}$  (300 K, 0.1 MPa) up to  $\pm 4\text{ cm/s}$  (523 K, 0.1 MPa).

It can be noted that this order of magnitude was also valid in the case of lean laminar flame speeds recorded at elevated pressure (up to 1 MPa). However this uncertainty could increase in case of rich flames. Indeed, another major source of uncertainty was related to the stability of the flame that may deteriorate when experiments were performed in conditions of rich flames. The fluctuation of the position of the flame during time displays an artificial thickening of the flame front during the time integration of the signal on the camera. This effect modifies the position of the flame contours giving an overall uncertainty of  $\sim 7\%$  in the worst situation. In the most unfavorable case of our study, i.e. for an acetone/air mixture at 0.35 MPa, 473 K and  $\phi = 1.2$ , the uncertainty of  $S_L$  was then estimated to be about  $\pm 4.5\text{ cm/s}$ .

## Chapter 5 Measurements on CH<sub>4</sub>/air and Acetone/N<sub>2</sub>/O<sub>2</sub> mixtures

---

This chapter is dedicated to the validation of the measurement methodologies detailed in chapters 3 and 4.

CH<sub>4</sub>/air mixtures were firstly investigated over a wide range of operating conditions including preheating temperature 300 – 523 K, pressure 0.1 – 1.0 MPa and equivalence ratio 0.6 – 1.3. All these experiments were devoted to quantify the performances of the newly high-pressure burner when gaseous fuels are used. Both OH\* chemiluminescence and OH-PLIF optical diagnostics were applied for measuring the laminar flame speeds. Comparisons were then performed between experimental data recorded with both optical techniques for evaluating the limitations and the potentialities of the different methodologies used to extract the laminar flame speeds. These experimental data were further compared with simulations performed with the detailed kinetic mechanism GRI-Mech 3.0 and with experimental results issued from literature.

A similar work was performed on acetone/O<sub>2</sub>/N<sub>2</sub> mixtures. The objective consisted in the validation of the experimental setup and more precisely, in the evaluation of the benefits of the evaporation system used to evaporate liquid fuels. To this purpose, measurements of laminar flame speeds were also measured over a wide range of operating conditions including preheating temperature 373 – 523 K, pressure 0.1 - 1 MPa and equivalence ratio 0.6 - 1.3. The optical diagnostics are the OH\* chemiluminescence and the OH- and acetone-PLIF techniques. Experimental data were then compared with numerical simulations conducted with published detailed kinetic mechanisms of acetone and with measurements reported in the literature. Comparing to the CH<sub>4</sub>/air mixtures tested to validate the experimental setup, the experimental results of acetone have thus made it possible to establish new empirical correlations of laminar flame speeds with pressure, temperature and equivalence ratio, the predictions being suitably compared with the newly obtained experimental data.

## 5.1 Validation of the measurement methodologies

Preliminary measurements of laminar flame speeds were first conducted on  $\text{CH}_4/\text{air}$  mixtures in order to validate the high-pressure Bunsen burner, the optical measurement techniques and their associated post-processing routines over a wide range of equivalence ratio, temperature and pressure.  $\text{CH}_4$  fuel was selected to validate the measurement methodology because it is one of the gaseous fuels whose laminar flame speed has been extensively studied in the past. Results of numerous experimental and numerical results already available in literature allowed a detailed comparison with our data in conjunction with a characterization of the benefits of our measuring instrument.

### 5.1.1 $\text{OH}^*$ chemiluminescence imaging

As discussed previously and according to the laminar flame speed definition, the “true” flame front area for laminar flame speed determination using the flame area method should be located at the upstream boundary of the preheating zone of fresh gases. In the event that the  $\text{OH}^*$  chemiluminescence technique is used, the location of the maximum  $\text{OH}^*$  signals issued from the data processing of the emission signals differs from the upstream boundary of the preheating zone of fresh gases.

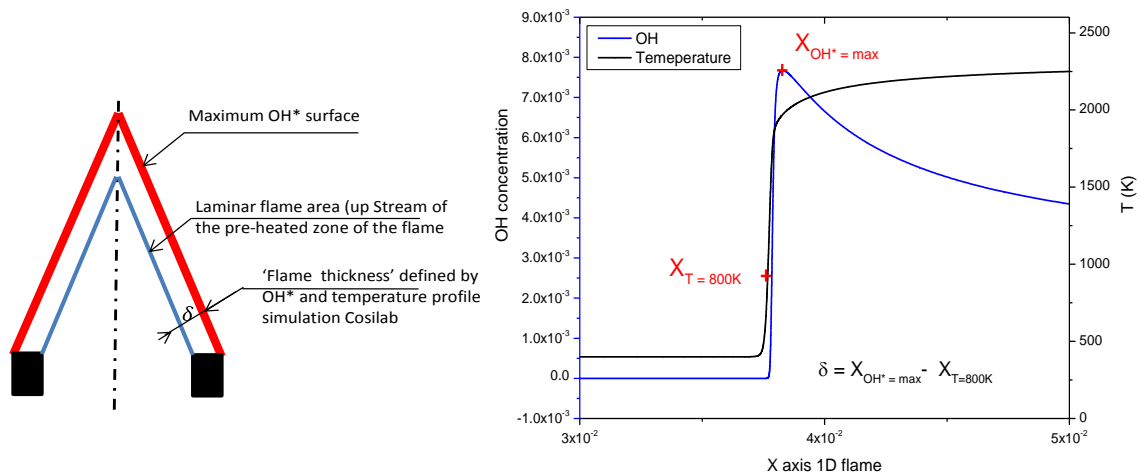


Figure 5.1: Illustration of the flame area method and flame thickness simulation

As illustrated in Figure 5.1, the  $\text{OH}^*$  chemiluminescence edge is indeed located on the right side of the fresh gas edge. According to the expression given by Eq. 4.3, the  $\text{OH}^*$  chemiluminescence edge when used, could yield a broader underestimation of laminar flame speeds. A precise knowledge of the flame thickness is then required to correct the measurements for determining the “true” fresh gas boundary. In cases of “simple” fuels such as  $\text{CH}_4$  and acetone, the availability of detailed kinetic mechanisms in literature offers potentialities to simulate their resultant flame thicknesses in the operating conditions tested during the experiments. To this purpose, 1D adiabatic premixed flame simulations with the Cosilab



solver were performed and simulated “*flame thicknesses  $\delta$* ” were deduced. Once the theoretical flame thicknesses have been obtained, the location of the flame front area  $A$  initially deduced from the chemiluminescence images has been corrected by defining a new position of the contour. This new location is defined as the position of the contour of the maximum OH\* signals minored by  $\delta$ . A discussion on the validation of this correction procedure is now presented for CH<sub>4</sub>/air mixtures.

#### 5.1.1.1. Flame thickness simulation

The Cosilab commercial software package including full transport properties is used to simulate one-dimensional laminar flames of CH<sub>4</sub>/air for various equivalence ratios, preheating temperatures and pressures. The transport properties are calculated by using the mixture averaged diffusion model. The Newton unsteady adaptive mesh algorithm has been used and allows an adaptive mesh refinement during the computation (“grad” and “curve” values are fixed to  $1e^{-5}$ ). The number of the grid points is fixed to 200 for simulating a physical domain of 0.1 m and to ensure a chemical equilibrium state in the burned gases. This grid point number has been chosen to guarantee the numerical grid-independent results. As mentioned in chapter 2, CH<sub>4</sub>/air flames are modelled using the establish GRI-Mech 3.0 kinetic mechanism [132]. The 1D adiabatic premixed flame simulations with the Cosilab software allowed the determination of the temperature and the OH radical profiles. The theoretical “flame thickness  $\delta$ ” is calculated as the distance separating the isotherm  $T = 800$  K in which OH\* emission signal begin to be detected on a camera and the zone in which the OH\* signal is maximum as illustrated in Figure 5.1 (right). Here is now presented the simulation of the flame thicknesses of CH<sub>4</sub>/air flames in function of equivalence ratio, temperature and pressure conditions.

##### (a) *Equivalence ratio*

Firstly, flame thicknesses of CH<sub>4</sub>/air flame at  $T = 373$  K,  $P = 0.1$  MPa are plotted in function of the equivalence ratio  $\phi = 0.6 - 1.3$  (see Figure 5.2). It can be observed that the flame thickness decreases with equivalence ratio on the lean side and has a minimum value when approaching stoichiometric conditions. Meanwhile, it increases on the rich side of the curve. The domain of the flame thickness extends from 0.38 to 0.60 mm. Even at  $\phi = 1.1$  for which the flame thickness is minimal, the order of its magnitude remains significant and a correction of the effect of the flame thickness on the position of the preheating fresh gases is always necessary whatever the range of equivalence ratio investigated.

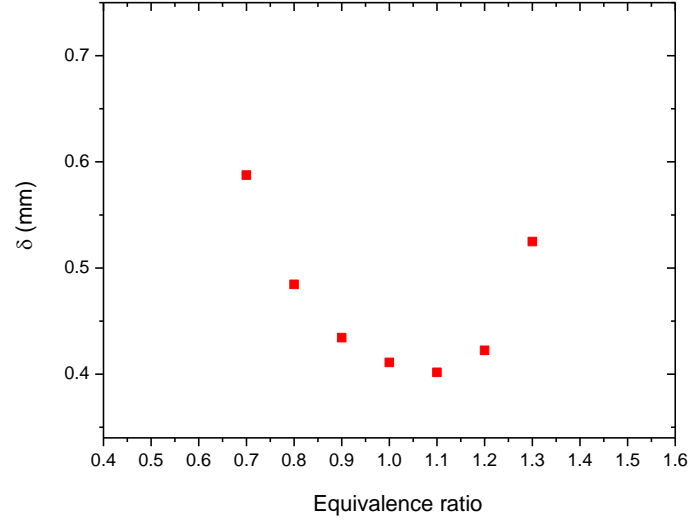


Figure 5.2: Evolution of the calculated flame thickness with equivalence ratio ( $\text{CH}_4/\text{air}$  mixture,  $T = 373$  K,  $P = 0.1$  MPa,  $\phi = 0.7 - 1.3$ )

(b) Preheating temperature

To investigate the temperature effect on the flame thickness, the flame thickness of  $\text{CH}_4/\text{air}$  flames for equivalence ratio  $\phi = 1.0$  is plotted in Figure 5.3 as a function of the preheating temperature (290 – 473 K). Whatever the preheating temperature, the flame thickness decreases almost linearly when the preheating temperature increases. As for the pressure effect, the order of the magnitude of the flame thickness (between 0.45 and 0.37) specifies that a correction of flame thickness on the determination of the location of the position of the preheating fresh gases remains necessary even at elevated temperatures.

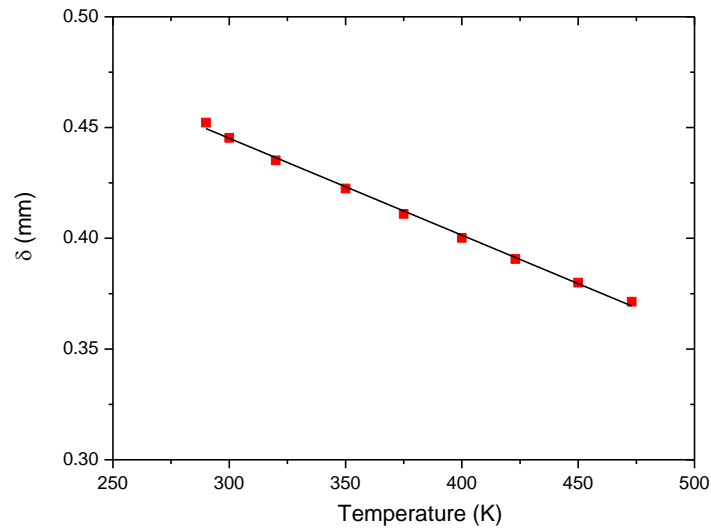


Figure 5.3: Evolution of numerical flame thickness with temperature ( $\text{CH}_4/\text{air}$  mixture,  $P = 0.1$  MPa,  $\phi = 1.0$ ,  $T = 290 - 473$  K)

### (c) Pressure

An investigation of the effect of pressure on flame thickness was finally performed by calculating the flame thickness of  $\text{CH}_4/\text{air}$  mixtures for  $\phi = 1.0$ ,  $T = 473$  K and for pressures ranging between 0.1 and 1.0 MPa. Figure 5.4 displays the evolution of the resulting flame thickness as a function of pressure. An observation of this figure reveals a decline of the flame thickness with increasing pressure. A large value of the flame thickness is observed at pressure close to the atmospheric pressure ( $\delta = 0.38$  mm) while this one is significantly reducing for elevated pressures. For pressure above 0.7 MPa, the reduction of the flame thickness becomes limited and a minimum limit of 0.08 mm is attained. These results indicate that a flame thickness correction for the location of the preheating fresh gases should be carried out especially for pressure not exceeding 0.7 MPa. Note that beyond this pressure, the contour of the maximum  $\text{OH}^*$  signals could be representative of the preheating zone boundary in regards to our experimental spatial resolution adopted in the current work.

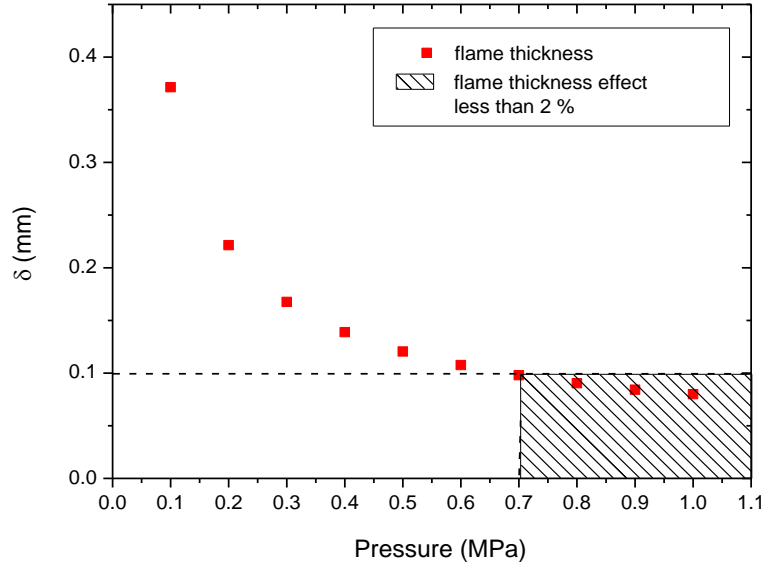


Figure 5.4: Evolution of the numerical flame thickness with pressure ( $\text{CH}_4/\text{air}$  mixture,  $T = 473$  K,  $P = 0.1 - 1.0$  MPa,  $\phi = 1.0$ ).

#### 5.1.1.2. Validation of the flame thickness correction

To evaluate the impact of the flame thickness on the laminar flame speed measurements, the variations of the laminar flame speed with pressure with and without the flame thickness correction are plotted in Figure 5.5. Measurements are performed for a preheating temperature of 473 K and an equivalence ratio of  $\phi = 1.2$ . Also shown on the same figure are the data measured with the OH-PLIF images and those of the GRI-Mech 3.0 prediction.

In a general way, the experimental results obtained with the OH-PLIF technique give particularly good agreement when compared to the GRI-Mech 3.0 simulations. For each set of measurements, the laminar flame speeds decrease nearly logarithmically with pressure. It can be also shown in Figure 5.5 that the OH\* chemiluminescence measurements corrected from the flame thickness are also in well accordance with the OH-PLIF measurements but also with the GRI-Mech 3.0 predictions. On the contrary, the uncorrected OH\* chemiluminescence signals underestimate the laminar flame speeds especially for pressure less than few bars. For elevated pressures, the difference between corrected and uncorrected values vanishes in regards to the large decline of the flame thickness with pressure (see Figure 5.5).

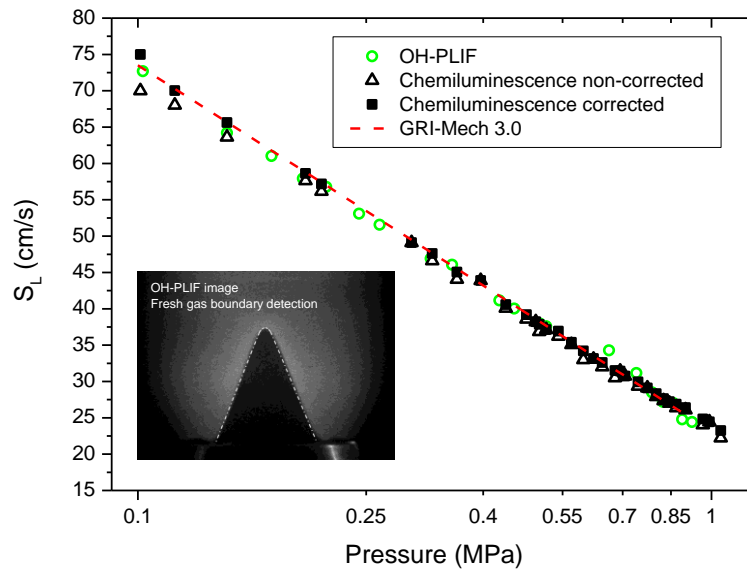


Figure 5.5: Relationship between the laminar flame speed and pressure ( $\text{CH}_4/\text{air}$  mixture  $\phi = 1.2$ ,  $T = 473 \text{ K}$ ,  $P = 0.1 - 1.0 \text{ MPa}$ ). Comparison of data obtained with OH\* chemiluminescence and OH-PLIF methodologies.

### 5.1.1.3. Flame stretch

As the flame is conical in shape and not one-dimensional (1D), the importance of the flame stretch effect on behalf of the aerodynamic strain and flame curvature on the laminar flame speed measurements has to be evaluated with pressure variation [55]. As mentioned in chapter 4, the geometry of the nozzle was designed to minimize the boundary layer thicknesses, the velocity profile at the nozzle exit is enough flat that the aerodynamic strain is thus limited. Concerning the flame curvature effect, the condition involving a constant burning velocity on the surface area of the flame front is evidently not respected. For instance, Figure 5.6 shows the evolution of the  $\text{CH}_4/\text{air}$  flame structure recorded at various levels of pressure. Temperature and equivalence ratio are fixed to 473 K and 0.8 respectively. As observed on the OH\* images, the region in which a flame curvature is observed is only visible at the tip of the flame. To estimate the importance of the flame curvature on the surface area of the flame front, the evolution of the

curvature rate with the radius of the flame is plotted for various pressures (Figure 5.7). It is found that the flame curvature becomes smaller and sharper when the pressure increases. For conditions of elevated pressure, the flame structure becomes similar as a straight edge triangle flame: a curvature gradient appears at the tip of the flame in a thin region that significantly reduces the magnitude of the flame curvature on the measurement of the laminar flame speed. From the  $\text{OH}^*$  chemiluminescence images recorded in the range of pressure 0.1 – 1.0 MPa, the maximal magnitude of the surface of the flame curvature represents only  $\sim 2\%$  of the whole surface area of the flame front. In considering this value comparable to the accuracy of our laminar flame speed measurements, the flame stretch effect could be then disregarded [92].

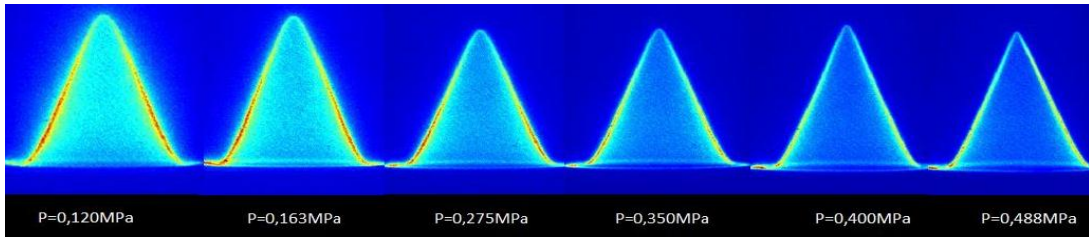


Figure 5.6:  $\text{OH}^*$  chemiluminescence images of laminar flame structure of  $\text{CH}_4/\text{air}$  mixture versus pressure ( $\phi = 0.8$ ,  $T = 473\text{ K}$ ).

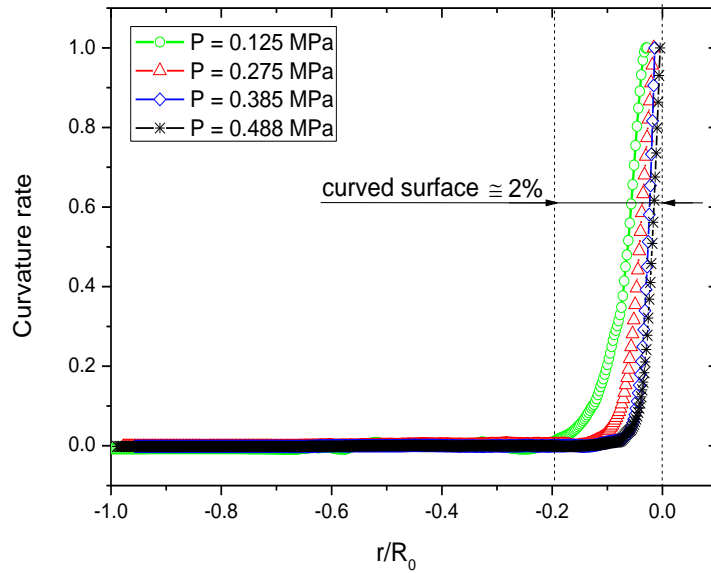


Figure 5.7: Normalized flame curvature rate along radius axis for various pressures ( $\text{CH}_4/\text{air}$  flame,  $T = 473\text{ K}$ ,  $\phi = 0.8$ ,  $P = 0.1 - 0.5\text{ MPa}$ ). Burner rim starts at  $r / R_0 = -1$  and burner center position is at  $r / R_0 = 0$  with a burner radius  $R_0 = 5\text{ mm}$ .

#### 5.1.1.4. Piloted flame

Another source of perturbation relating to the piloted flame can also affect the laminar flame speed when using the flame area method. The magnitude of this effect was estimated by comparing measurements of laminar flame speeds of  $\text{CH}_4/\text{air}$  flames at atmospheric pressure assisted with and without the piloted flame. For instance, Figure 5.8 depicts a comparison of the variation of laminar flame speeds with the equivalence ratio. Measurements were performed with a preheating temperature of 375 K. An observation of the results plotted in Figure 5.8 reveals tiny differences between both sets of laminar flame speeds, i.e. typically 0.5 ~ 1 cm/s at  $\phi = 1$ . Although this deviation represents ~ 2 % variation of the laminar flame speed, both values remain within the experimental uncertainty delivered from the image processing of the  $\text{OH}^*$  chemiluminescence and OH-PLIF images. Moreover, this deviation tends to come down for higher preheating temperatures because of the increase of the laminar flame speed. Similar tendencies also observed on the laminar flame speed measurements of acetone/  $\text{N}_2/\text{O}_2$  mixtures (section 5.3) enable us to disregard the influence of the piloted flame in the current study.

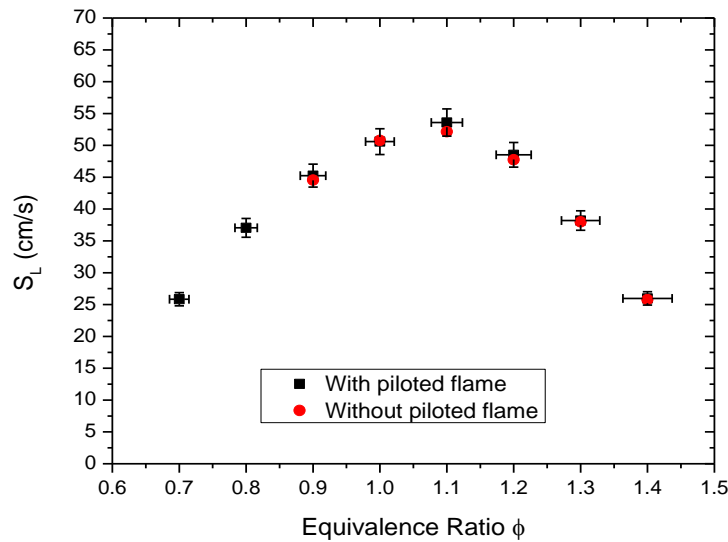


Figure 5.8: Effect of the piloted flame on the laminar flame speed measurements ( $\text{CH}_4/\text{air}$  mixture,  $T = 375 \text{ K}$ ,  $P = 0.1 \text{ MPa}$ ).

#### 5.1.2 OH-PLIF and acetone-PLIF imaging

In this section, experimental results obtained by OH-PLIF, acetone-PLIF and  $\text{OH}^*$  chemiluminescence are now discussed. Showing in Figure 5.9 are the laminar flame speeds of acetone/air mixtures derived from the three measurements techniques. The experimental conditions are the followings:  $T=453 \text{ K}$ ,  $P=0.1 \text{ MPa}$  and  $\phi = 0.7 - 1.3$ . For each condition of equivalence ratio, differences (up to 2~ 4 cm/s) between the resulting laminar flame speeds are observed. The laminar flame speeds deduced from acetone-PLIF are in good accordance with those deduced from the  $\text{OH}^*$  chemiluminescence images that are corrected of the flame thickness. Depending of the equivalence ratio, slight differences are however

noted but these ones are comparable to the uncertainty of our measurements. By contrast, significant differences between OH-PLIF and acetone-PLIF measurements are observed especially for equivalence approaching the stoichiometry.

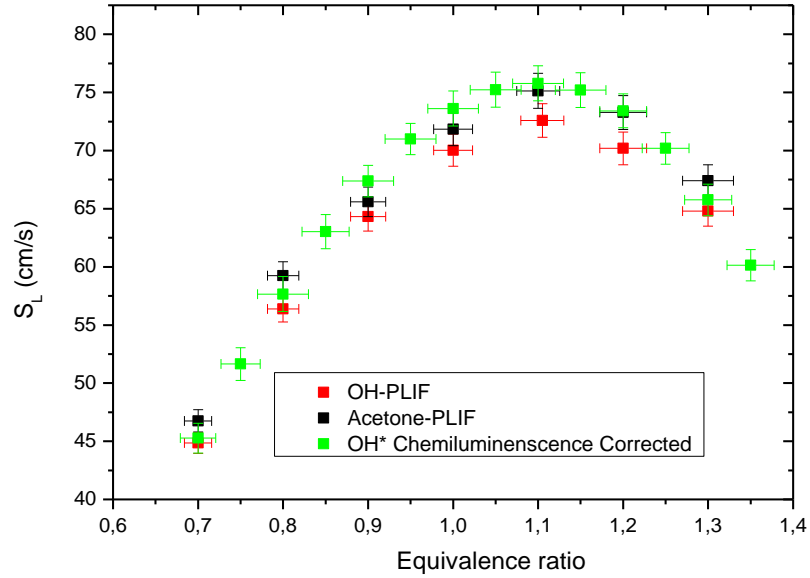


Figure 5.9: Laminar flame speed of acetone/air mixtures measured by OH-PLIF, acetone-PLIF and OH\* chemiluminescence with correction of the flame thickness.  $T = 453$  K,  $P = 0.1$  MPa,  $\phi = 0.7 - 1.3$ .

This result is in opposition with the following basis which states that the location of the beginning of the flame front must coincide with the frontier of consumption of fresh gases. Experimentally, OH is usually detectable by PLIF at a temperature equivalent or larger than to 800 K, temperature corresponding in our case to the beginning of the flame front. Acetone-PLIF allows the detection of the location of the consumption of the fresh gases at typically the same temperature. To explain the differences between laminar flame speeds, Figure 5.10 shows a typical example of OH and acetone PLIF images acquired simultaneously. An examination of this fluorescence image reveals that the frontier of consumption of acetone does not coincide with the frontier of detection of OH. We observe between both frontiers a thin opaque zone in which fluorescence signals are not detected (see enlarged view of zone C in Figure 5.10). One probable reason that may explain such behavior relates to the dynamics of the ICCD camera used to record our fluorescence signals. In a flame front with high gradients of concentration and temperature, the OH concentration can vary on a distance of several hundred  $\mu\text{m}$  from 0 to about 1 %. With a “classical” dynamics of 16 bit which is the full dynamic available for an ICCD camera and assuming a peak concentration of OH of about 1% after the flame front, the minimal OH concentration detectable by the ICCD camera will be then close to a few dozen of ppm. Unfortunately, this level of concentration is well above the expected OH concentration produced (few ppm) at the inner frontier of the flame front, significantly hindering early detection of this frontier and leading then to a possible bias of the laminar flame speed measurements. The same type of analysis can be also applied to the acetone-PLIF technique.

However, in that case, a reduction of the acetone fluorescence signal due to chemical reactivity is easier to detect on the fluorescence image because the acetone fluorescence signal inside the fresh gases cone is now elevated. As the consumption of acetone occurs on a distance of few pixels of the camera, the position of the net reduction of fluorescence on the image can be precisely determined and laminar flame speeds can be accurately assess.

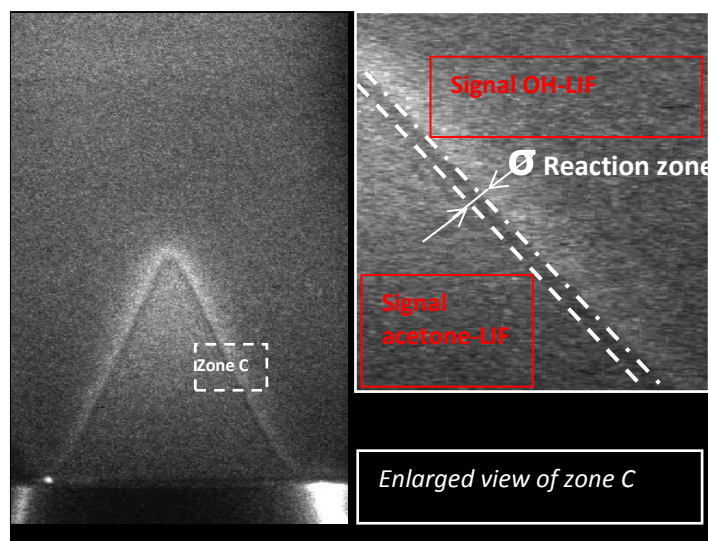


Figure 5.10: Simultaneous visualization of OH-PLIF and acetone-PLIF flame contours

## 5.2 Laminar flame speeds of CH<sub>4</sub>/Air mixtures

### 5.2.1 Comparison with literature data

To evaluate the accuracy of our measurements of laminar flame speeds, Figure 5.11 shows a comparison of the laminar flame speeds measured with our Bunsen burner and data collected in literature. These data have been measured with various measurement methodologies. Laminar flame speeds of CH<sub>4</sub>/air mixtures recorded at 300 K and 0.1 MPa are compared to laminar flame speeds recorded with the spherical expanding flame methods [9] [11] [174] [12] [10] [175], counter-flow and jet-wall stagnation method [176] [89], heat flux method [69] [68] and conical flame method [92]. In addition, Figure 5.11 also includes simulation data obtained with GRI-Mech 3.0 predictions.

Except in the case of the results reported by Huang et al. [89] and those issued from the work of Mazas et al. [92] which depict large deviations from the other measurements, the overall agreement among the data of literature and our laminar flame speeds obtained after flame thickness correction is generally good, with a better agreement between our data and the GRI-Mech 3.0 predictions. For equivalence ratios between 0.55 and 0.7, almost all measurements collected in literature give underestimated values



compared to the results of the simulation. Fortunately, the experimental results present a better accordance with simulations for  $\phi > 0.7$ . Interestingly, it is observed that the laminar flame speeds obtained with the spherical expanding flame and the heat flux methods tend to underestimate the simulations in the lean side and overestimate in the rich side. With regards to the counter-flow flame and stagnation flame methods, they generally overestimate the laminar flame speeds whatever the range of equivalence ratio investigated. Furthermore, the scattering data collected from different studies performed with the heat flux method becomes tighter than for the other methods. In our study, laminar flame speeds measured after flame thickness corrections are contained inside this scattering data when the equivalence ratio is located to the rich side. By contrast, our measurements performed to the lean side are systematically above these scattering data but closer to the simulations results.

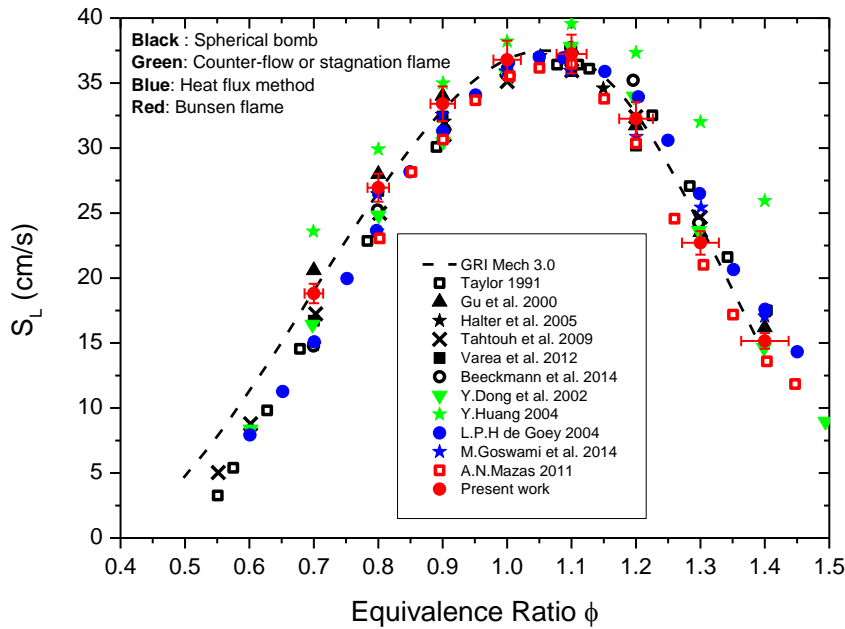


Figure 5.11: Comparison of laminar flame speeds ( $S_u$ ) obtained in our current study and previous data collected in the literature. The simulation data of GRI-Mech 3.0 predictions are also plotted in the same figure ( $\text{CH}_4/\text{air}$ ,  $T_{\text{air}} = 300 \text{ K}$ ,  $P = 0.1 \text{ MPa}$ ).

### 5.2.2 Preheating temperature

To analyze the relationship between the laminar flame speeds of  $\text{CH}_4/\text{air}$  mixtures with the preheating of the fresh gases, a comparison between our experimental data and predictions performed with the GRI-Mech 3.0 mechanism is presented in Figure 5.12. The pressure has been fixed to 0.1 MPa and the preheating temperatures investigated are 300 K, 375 K, 418 K and 477 K respectively. For low preheating temperatures, i.e. between 300 and 400 K, the GRI-Mech 3.0 simulation presents a fairly accurate approximation of our measurements. For higher preheating temperatures, i.e.  $T > 400 \text{ K}$ , the GRI-Mech 3.0 predictions provide a less reliable comparison, especially for  $\phi > 1$ , but qualitatively the profiles of the evolution of the laminar flame speeds remains similar to the experimental ones. As expected, simulations

also reveal an increase of  $S_L$  with the preheating temperature. If the latter rises from room temperature to 477 K, then the laminar flame speed increases by a factor of about 2-2.5 in the range of the equivalence ratios investigated.

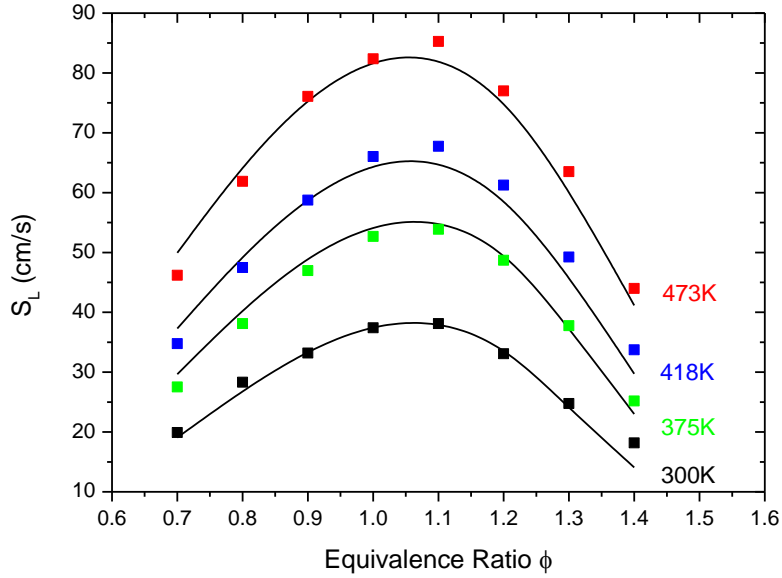


Figure 5.12: Laminar flame speeds of  $\text{CH}_4/\text{air}$  mixtures at atmospheric pressure and various preheating temperatures (the symbols represent our experimental data; the lines are the results of the predictions of GRI-Mech 3.0)

### 5.2.3 Pressure

Laminar flame speeds of  $\text{CH}_4/\text{air}$  mixtures are also measured for a pressure range between 0.1 and 1.0 MPa. The preheating temperature is fixed to 473 K and the equivalence ratio is maintained to 1.2. The influence of pressure on the laminar flame speed is depicted in logarithmic coordinates in Figure 5.13. As there are no experimental results available in literature for these operating conditions, the current experimental data are compared with numerical simulations performed with the formalisms proposed by Takizawa et al. [88] and Stone et al. [177] and with the GRI-Mech 3.0 mechanism. Generally speaking, our current experimental data fit well the numerical data of the GRI-Mech 3.0 mechanism unlike the others mechanisms listed above which show very different variations with pressure. It is however observed a slight overestimation of our experimental laminar flame speeds when pressure is close to the atmospheric pressure and when pressure exceeds 0.8 MPa. Between both pressures, a satisfied accordance is noted.

From the data displayed in Figure 5.13, the pressure dependence of flame speed was evaluated. The most-frequently used power-law expression pressure dependence as developed from the thermal approaches was used and this expression is given by:

$$S_L = S_{L0}(P/P_0)^\beta \quad (5.1)$$

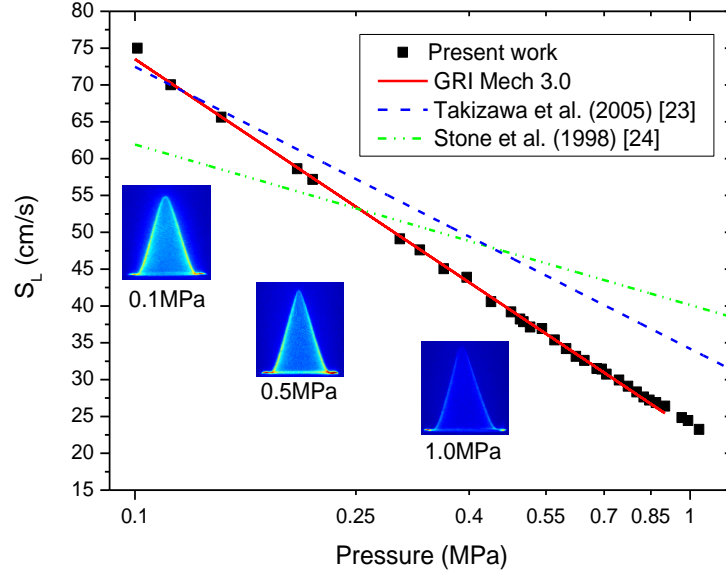


Figure 5.13: Variation of the laminar flame speed with pressure ( $CH_4/air$  mixture,  $T = 473$  K,  $\phi = 1.2$ ). The symbols represent the experiments; the solid line displays the numerical predictions of the GRI-Mech 3.0 mechanism and the dashed lines represent the results of [88] and [177].

in which  $S_{L0}$  is the laminar flame speed at reference conditions ( $P_0 = 0.1$  MPa,  $T_0 = 473$  K,  $\phi = 1.2$ ), and  $P_0$  is the reference pressure.  $\beta$  is a power exponent defined as  $\beta = n/2 - 1$  and  $n$  is the overall order of reaction.  $\beta$  is therefore equal to 0 for bimolecular reactions and -0.5 for first-order reactions. This consideration is still often used for interpreting changes of the overall reaction order with pressure. In observing experimental measurements of laminar flame speed as a function of pressure, the laminar flame speed follows a straight line decline with a  $\beta$  dependence of  $-0.4557$  (see Figure 5.13). The power exponent derived from the present experiments is then compared with the selected literature data [12] [178]. Excepted for the value reported by F. Halter et al. of  $\beta = -0.60$  [10], our power exponent is in qualitative agreement with the values reported by Goswami et al. [178] ( $\beta = -0.417$  at  $\phi = 1.2$  and 298 K) and Gu et al. ( $\beta = -0.438$  at  $\phi = 1.2$  and 300 K) [12]. Furthermore, the power exponent obtained experimentally fits well the theoretical value delivered from the GRI-Mech 3.0 simulation. As the parameter  $\beta$  is a function of the overall order of reaction  $n$  that is generally lower than 1.5 for hydrocarbons [179], our power exponent brings confidence in the validity of our measurement methodology to determine the laminar flame speed at elevated pressure.

To conclude, all the data measured in various operating conditions of equivalence ratio, pressure and preheating temperature have revealed good potentialities of the experimental device and of the images post-processing for measuring the laminar flame speed with accuracy. This measurement methodology

has been then used for testing other types of fuels such as pure liquid fuel (acetone) and multi-component fuels representing practical fuels.

### 5.3 Laminar flame speeds of acetone/N<sub>2</sub>/O<sub>2</sub> mixtures

After developing the measurement methodology of laminar flame speeds on CH<sub>4</sub>/air mixture in various operating conditions, this method was applied to acetone/N<sub>2</sub>/O<sub>2</sub> mixtures in similar preheating temperature and pressure conditions. Acetone was selected in the present experiment as a useful molecule for testing the high-pressure burner when liquid fuels are tested. Indeed, this molecule is a small molecule weight liquid fuel which can be easily vaporized with the Controller Evaporator Mixer (CEM) installed on our experimental facility. As acetone is stocked as a liquid, the use of this molecule has permitted a validation of our evaporation system when used in high-pressure conditions. This step was an initial key condition before to perform measurements of laminar flame speeds of complex liquid multi-component fuels (kerosene, biofuel). Furthermore, this molecule represents a good candidate to build a first combustion mechanism block required for the development of more accurate kinetic models for larger oxygenated hydrocarbons that concerns to renewable biofuels issues. The investigation of laminar flame speed of acetone/air mixture constitutes then an important step towards improving our understanding on combustion. In particular, it is therefore important to quantify the effect of pressure and temperature on the adiabatic laminar flame speed of many practical fuels. One of the motivations of this work is then to provide a general expression able to propose an empirical correlation describing the variation of the laminar flame speed of acetone/ N<sub>2</sub>/O<sub>2</sub> mixture with preheating temperature and pressure. Indeed, it seems to the authors' knowledge that for acetone/ N<sub>2</sub>/O<sub>2</sub> flames, the pressure dependence on the laminar flame speed has received limited attention.

#### 5.3.1 Correlation formulation

As already known, laminar burning velocity is a strongly dependent parameter of mixture features, e.g. preheating temperature, pressure and mixture equivalence ratio. Generally, this fundamental parameter is determined at standard temperature and pressure conditions or at relatively low preheating temperature and pressure, primarily owing to difficulties in the operating of the experimental setups and measurements. However, in practical applications, initial conditions of pressure and temperature of fuel/air mixtures are often larger than the standard values. Therefore, it is very important to quantify the effects of pressure and temperature on this fundamental parameter [180]. The most-frequently temperature and pressure dependence correlation published in the literature is a power law initially proposed by Metghalchi and Keck [181]:

$$S_L = S_{L0}(T/T_0)^\alpha(P/P_0)^\beta \quad (5.2)$$

In this formula, the laminar flame speed,  $S_{L0}$  is expressed at reference conditions of temperature ( $T_0$ ) and atmospheric pressure ( $P_0$ ) and is multiplied by correction factors displaying the temperature and pressure dependencies. This relation was deduced by Metghalchi and Keck from flame speed measurements of isooctane/air mixtures in the temperature range 298 – 700 K and the pressure range 0.04 – 0.5 MPa. In this study, Metghalchi determined laminar burning velocities from the pressure rise of explosions in a spherical bomb. Then, Gülder [182] validated this empirical formula by measuring the propagation of ethanol/air spherical flames over a preheating temperature ranging from 300 to 500 K and at pressure up to 0.8 MPa. Several empirical correlation expressions were also suggested to refine the pressure and temperature dependences. For instance, Agnew and Graiff [2] proposed from results recorded in stoichiometric methane/air flame produced in a spherical bomb the following expression:

$$S_L = S_{L0}[1 + \beta_2 \log(P/P_0)] \quad (5.3)$$

Smith and Agnew [183] proposed another pressure dependency expression

$$S_L = S_{L0} \exp[(b(1 - (P/P_0)^x)] \quad (5.4)$$

This expression was tested and validated by Konnov et al. [14] on sub-atmospheric  $\text{CH}_4/\text{H}_2/\text{air}$  laminar flames with the heat flux method. In the study reported by Varea et al. [9], the pressure dependency of the empirical correlation was improved by introducing the effect of the fuel blending when multi-component fuels were studied. The empirical correlation expression used in the current work is by far the one most widely suggested in the literature (see Eq. 5.2). This is a generalized correlation that gives the laminar flame speed in terms of pressure, preheat temperature and equivalence ratio,

$$S_L = S_{L0}(\varphi) \left(\frac{T}{T_0}\right)^\alpha \left(\frac{P}{P_0}\right)^\beta \quad (5.5)$$

Hereby the effect of the equivalence ratio is taken into account in Eq. (5.6) to (5.8) by using extended formulations proposed by Metghalchi and Keck [181].

$$S_{L0}(\varphi) = S_{L0,\varphi=1} + S_{L,1}(\varphi - 1) + S_{L,2}(\varphi - 1)^2 + S_{L,3}(\varphi - 1)^3 + S_{L,4}(\varphi - 1)^4 \quad (5.6)$$

$$\alpha(\varphi) = \alpha_0 + \alpha_1(\varphi - 1) + \alpha_2(\varphi - 1)^2 + \alpha_3(\varphi - 1)^3 \quad (5.7)$$

$$\beta(\varphi) = \beta_1 + \beta_2(\varphi - 1) + \beta_3(\varphi - 1)^2 \quad (5.8)$$

$S_{L0, \phi=1}$  is the laminar flame speed at  $\phi = 1$  and  $S_{L0,i}$  are the parameters determined for the standard conditions  $T_0 = 373$  K and  $P_0 = 0.1$  MPa. The power exponent coefficients  $\alpha$  and  $\beta$  are dependent of the equivalence ratio [181] [9]. The parameters  $S_{L0}(\phi)$ ,  $\alpha$ , and  $\beta$  were determined from laminar flame speed measurements of acetone/ $N_2/O_2$  mixtures for the following range of operating conditions:  $0.6 \leq \phi \leq 1.3$ ,  $373 \leq T \leq 523$  K,  $0.1 \leq P \leq 1$  MPa. Their values and the thermodynamic effects on the acetone/ $N_2/O_2$  laminar flame speed are presented in the next section.

### 5.3.2 Preheating temperature dependence

In order to illustrate the effect of the preheating temperature on the acetone/  $N_2/O_2$  laminar flame speed, experimental measurements are performed at the following temperatures: 373 K, 403 K, 443 K, 468 K and 523 K. Experimental and numerical results obtained with the detailed reaction mechanism of Chong [31], are compared and the results are presented in Figure 5.14. As agreed, the laminar flame speed increases with the preheating temperature of the fuel/air mixture. As observed in Figure 5.14, both the experimental and numerical predictions are in qualitative agreement excepted in the rich side for which small deviations are noted at  $T = 443$  K and  $T = 523$  K. However the discrepancies, about  $\sim 5$  cm/s remain reasonable in regards to the accuracy of our measurements.

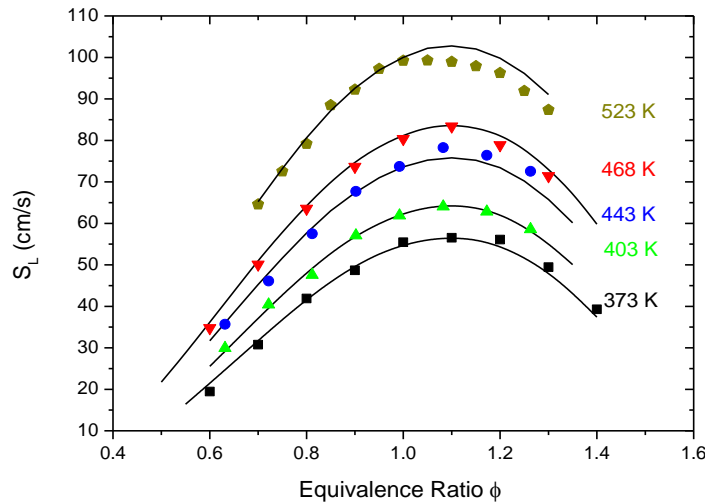


Figure 5.14: Evolution of the laminar flame speed versus equivalence ratio for various preheating temperatures (acetone/ $N_2/O_2$  mixture,  $P = 0.1$  MPa). The symbols represent experimental data; the lines are numerical predictions of the Chong detailed kinetic mechanism.

From the laminar flame speeds in Figure 5.14, the flame speed  $S_{L0}(\phi)$  is deduced at reference conditions (373 K, 0.1 MPa). The polynomial expression introduced above (Eq. 5.4) allows a well description of the variation of the flame speed with the equivalence ratio and the resulting parameters  $S_{L0,i}$  are summarized in Table 5.1.

$\alpha_0$	1.73	$\beta_1$	-0.3177	$S_{L_0,\varphi=1}$	54.8
$\alpha_1$	-0.44	$\beta_2$	0.2154	$S_{L_0,1}$	39.4
$\alpha_2$	2.01	$\beta_3$	-0.3286	$S_{L_0,2}$	-161.9
$\alpha_3$	-0.50			$S_{L_0,3}$	-91.4
				$S_{L_0,4}$	14.4

	Experimental data	Chong's mechanism		Experimental data	Chong's mechanism
$\alpha_{\varphi=0.7}$	$2.259 \pm 0.294$	2.098	$\beta_{\varphi=0.7}$	$-0.403 \pm 0.080$	-0.4027
$\alpha_{\varphi=0.8}$	$2.056 \pm 0.393$	1.925	$\beta_{\varphi=0.8}$	$-0.384 \pm 0.053$	-0.3621
$\alpha_{\varphi=0.9}$	$1.902 \pm 0.116$	1.804	$\beta_{\varphi=0.9}$	$-0.356 \pm 0.047$	-0.3384
$\alpha_{\varphi=1.0}$	$1.794 \pm 0.113$	1.743	$\beta_{\varphi=1.0}$	$-0.305 \pm 0.040$	-0.3289
$\alpha_{\varphi=1.1}$	$1.730 \pm 0.235$	1.728	$\beta_{\varphi=1.1}$	$-0.288 \pm 0.058$	-0.3317
$\alpha_{\varphi=1.2}$	$1.767 \pm 0.300$	1.758	$\beta_{\varphi=1.2}$	$-0.297 \pm 0.090$	-0.3537

Table 5.1: Correlation parameters  $\alpha_i$ ,  $\beta_i$  and  $S_{u_{0,i}}$  used in Eqs. 5.5 to 5.8 (acetone/N<sub>2</sub>/O<sub>2</sub> mixtures) and Values of the power exponents  $\alpha(\varphi)$  and  $\beta(\varphi)$ : comparison between experiments and numerical simulation.

To further illustrate the temperature dependence on the laminar flame speed, the evolution of the laminar flame speed recorded at atmospheric pressure when presented in a log-log graph should become a straight line. This was indeed observed for all equivalence ratios (Figure 5.15). The power exponent  $\alpha(\varphi)$  is then determined from the data processing of these data and their values are listed in Table 5.1. To illustrate these results, the variation of  $\alpha$  parameter is plotted in function of the equivalence ratio in Figure 5.16. As shown in this graph, the evolution of  $\alpha$  follows an inverted bell-shaped curvature with a minimum value around  $\varphi = 1.05$ . The simulations carried out with the detailed kinetic mechanism of Chong [31] agree remarkably with the experiments over the whole range of equivalence ratio, excepted for the case of rich mixtures ( $\varphi = 1.4$ ). A similar shape is also observed with the kinetic model developed by Nilsson et al. [98]. However, this model underestimates clearly the current experimental data by  $\sim 10\%$ . Finally, the single data delivered by Nokov [4] leads to an overestimation by 20% of our data. This discrepancy with literature could be due to the different air composition. The air used in the current work is composed by 20% O<sub>2</sub>+80% N<sub>2</sub>, however the air in literature results by default is composed by 21%O<sub>2</sub>+79N<sub>2</sub> which could potentially yield to difference in flame speeds. By fitting the experimental data  $\alpha(\varphi)$  with the third-order polynomial expression (Eq. 5.7), the equivalence ratio dependence coefficients  $\alpha_i$  can now be calculated and results are summarized in Table 5.1.

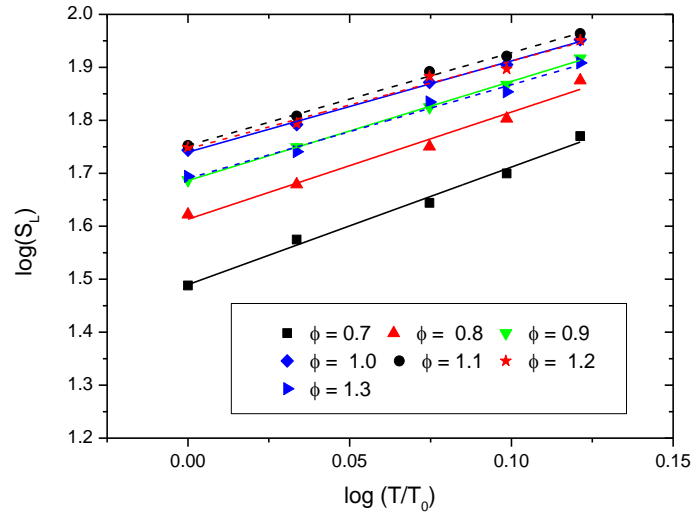


Figure 5.15: Evolution of the laminar flame speed versus  $\log(T/T_0)$  for various equivalence ratios (acetone/ $N_2/O_2$  mixture,  $P = 0.1$  MPa). The lines represent the results of the empirical correlation expression proposed in the current experiment.

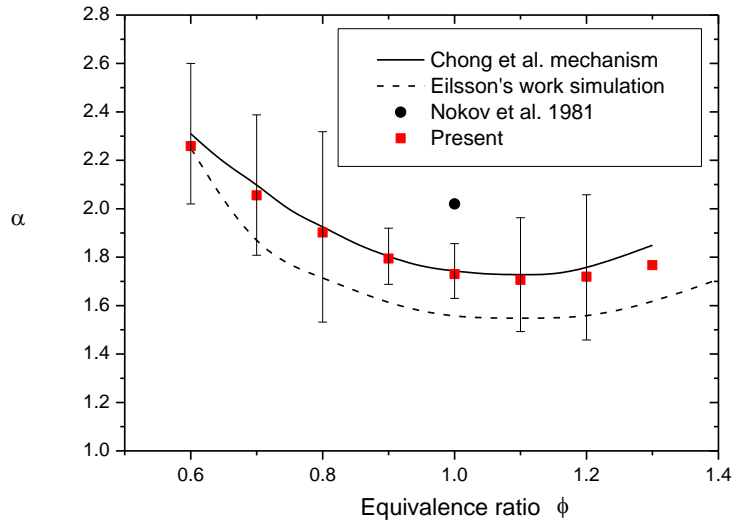


Figure 5.16: Evolution of the power exponent  $\alpha$  versus equivalence ratio (acetone/  $N_2/O_2$  mixture,  $P = 0.1$  MPa).

### 5.3.3 Pressure dependence

Laminar flame speed measurements of acetone/ $N_2/O_2$  mixture are performed for various pressures ranging between 0.1 and 1.0 MPa. The equivalence ratios investigated are in the range 0.7-1.2. The preheating temperature is fixed at  $T = 473$  K. Table 5.2 resumes the operating conditions investigated in this study.



Equivalence ratio $\phi$	Pressure (MPa)
0.7	0.1- 0.75
0.8	0.1 - 1.0
0.9	0.1 - 0.65
1.0	0.1 - 0.45
1.1	0.1 - 0.45
1.2	0.1- 0.35

*Table 5.2: Experimental conditions of pressure and equivalence ratio for measurements of laminar flame speed of acetone/N<sub>2</sub>/O<sub>2</sub> mixture at  $T = 473$  K.*

To analyze the apparent pressure dependence, measured laminar flame speed of acetone/air mixture at different equivalence ratios were first plotted in Figure 5.18. For comparison, the COSILAB prediction with the detailed reaction mechanism of Chong has also been plotted. As opposed to the temperature evolution, the laminar flame speed decreases with pressure whatever the equivalence ratio. For each equivalence ratio, the evolution of the laminar flame speed is slightly curved in shape. This result is in agreement with literature [11] where the effect of pressure on laminar flame speed is numerically investigated for higher pressure, whilst the flame speed becoming almost constant for pressure higher than 0.8 MPa. Numerical predictions globally match the experimental data for each equivalence ratio even though the concavity of the experimental curves is not perfectly reproduced.

According to the procedure used for the determination of the temperature dependence coefficients, the pressure dependence coefficients are then deduced from the evolution of the laminar flame speeds with pressure plotted in Figure 5.18 on logarithmic scale. The resulting pressure dependence coefficients  $\beta(\phi_i)$  are listed in Table 5.3. As anticipated, the evolution of the laminar flame speed for each equivalence ratio follows power-law pressure dependence as the one expressed in Eq. 5.5. The power exponents obtained with fitting experimental data to Eq. (5.5) are presented in Figure 5.19 together with the corresponding power exponents derived using the kinetic model of Chong. As observed in Figure 5.19, both the pressure power exponents show parabola-like variation with equivalence ratio from lean to moderately rich mixtures. The differences between the current experimental data and calculations are minor in the lean side, increasing significantly towards moderately rich flames. From the results of Figure 5.19, the equivalence ratio effect on the power exponent  $\beta(\phi)$  is observed by fitting with a second-order polynomial law (Eq. 5.8) the experimental data at different equivalence ratios. Then the equivalence ratio dependence coefficients  $\beta_i$  have been deduced and are summarized in Table 5.1.

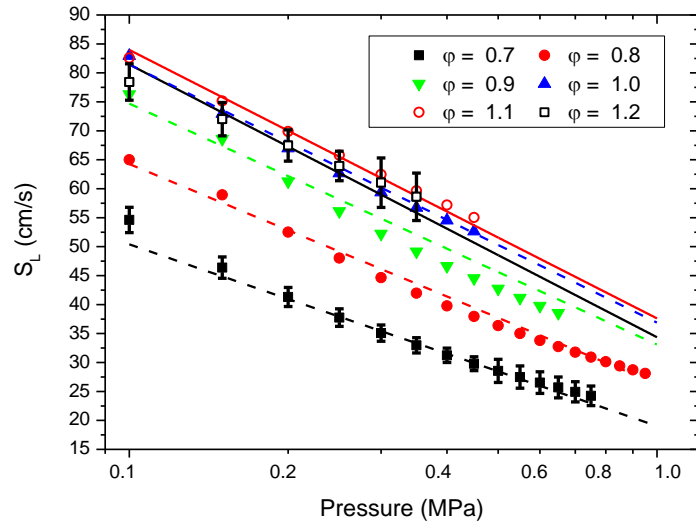


Figure 5.17: Variation of the laminar flame speed with pressure (acetone/  $N_2/O_2$  mixture,  $T = 473$  K,  $\phi = 0.7 - 1.2$ ). The dash and solid lines are the numerical simulation data using the kinetic mechanism of Chong; the symbols are the experimental results.

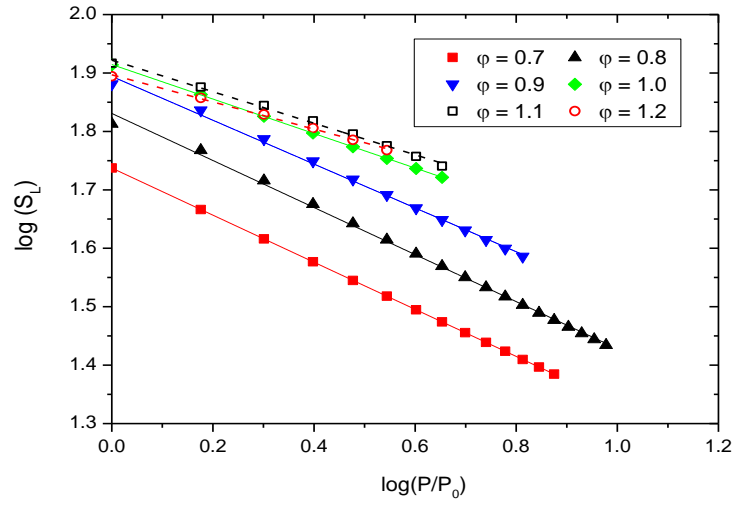


Figure 5.18: Evolution of the laminar flame speed versus  $\log P/P_0$  for different equivalence ratios (acetone/ $N_2/O_2$  mixture,  $T = 473$  K). The lines represent the results of the correlation proposed in this study.

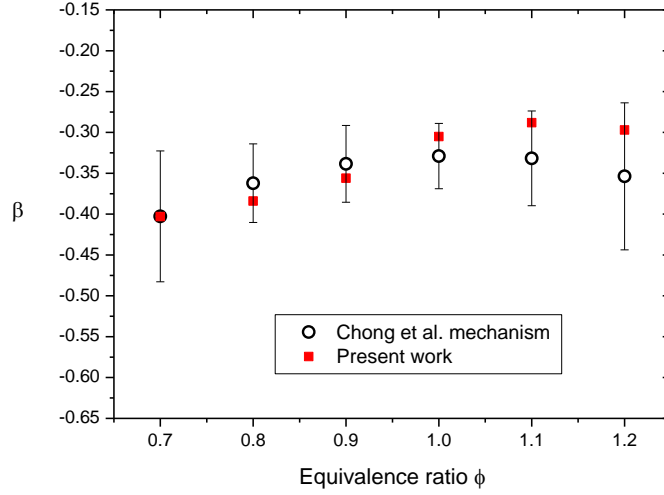


Figure 5.19: Evolution of the power exponent  $\beta$  versus equivalence ratio (acetone/  $N_2/O_2$  mixture,  $T = 473$  K).

#### 5.3.4 Validation of the empirical correlation expression

The overall accuracy of the empirical correlation expression is shown in Figure 5.20. The calculated flame speed  $S_{L,corr}$  is reported with the experimental flame speed  $S_{L,exp}$ . The uncertainties of the correlation based from the  $2\sigma$  intervals ( $2 \times 1.65 = 3.3$  cm/s) of the residue  $\Delta S_L = S_{L,exp} - S_{L,corr}$  are reported in Figure 5.20 (dashed lines:  $\pm \sigma$ ). This can be compared to the experimental uncertainties evaluated in section 3.2 of this study, varying from  $\pm 1$  cm/s (at 300 K and 0.1 MPa) and close to  $\pm 4.5$  cm/s (at 473 K, 0.35 MPa and  $\phi = 1.2$ ). These experimental uncertainties are consistent with the  $2\sigma$  intervals of the correlation that demonstrates the reliability of the empirical correlation function.

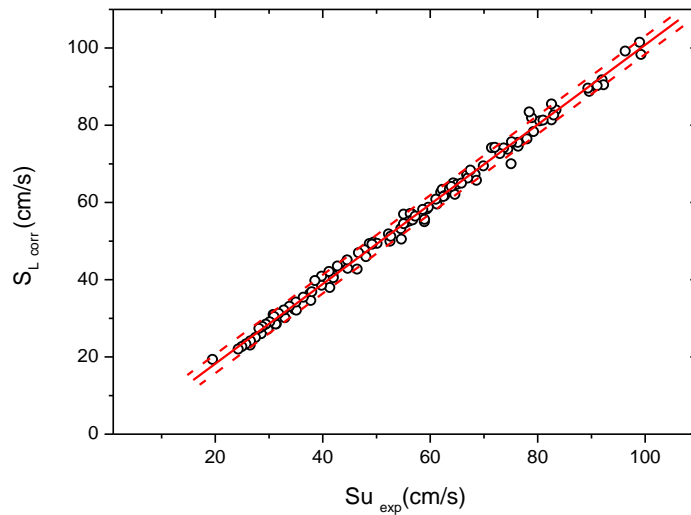


Figure 5.20: Laminar flame speed obtained with the empirical correlation expression compared to the experimental data. The dash lines indicate  $2\sigma$  ( $\sigma = \pm 1.65$  cm/s) uncertainties interval obtained from the residual  $\Delta S_L$  distribution. The solid line corresponds to  $S_{L,exp} = S_{L,corr}$ .

## 5.4 Conclusions

Experimental measurements of laminar flame speeds of  $\text{CH}_4/\text{air}$  and acetone/ $\text{N}_2/\text{O}_2$  mixtures were performed using the Bunsen flame methodology. From this work, it is found that for elevated pressures and preheating temperatures, the method used in the current work to measure the laminar flame speed gives reliable information with a good accuracy. Prior to the mostly used spherical expanding flame method, the conical Bunsen flame experimental methodology developed in the current experiment would therefore be an appropriate alternative solution for high-pressure laminar flame speed measurements. It is also verified by the  $\text{OH}^*$  chemiluminescence with flame thickness correction and PLIF techniques could be used to measure the flame area required to deduce the laminar flame speed. In particular, an analysis of the effect of flame thickness on the data processing of the  $\text{OH}^*$  chemiluminescence images require a good knowledge of the variation of this parameter with pressure. Thus, more the pressure will be elevated and less the effect of the flame thickness on the location of the contour of the preheated gases will be negligible for laminar flame speed measurement with  $\text{OH}^*$  chemiluminescence.

The laminar flame speeds measured on  $\text{CH}_4/\text{air}$  mixture show good agreement with data published in literature, proving then that the high-pressure Bunsen burner developed in the present work could be used to obtain precise and reliable laminar flame speeds in a wide range of preheating temperature, pressure and equivalence ratios.

Results obtained on acetone/ $\text{N}_2/\text{O}_2$  laminar flames in a large range of operating conditions including pressure 0.1 - 1.0 MPa, preheating temperature 373 K - 523 K and equivalence ratio 0.6 - 1.3 have allowed the establishment of a unique empirical correlation expression  $S_L = S_{L0}(\varphi)(T/T_0)^\alpha(P/P_0)^\beta$  able to reproduce the dependence of pressure and temperature on the laminar flame speed. This empirical correlation function also displayed fair agreement with numerical simulation results and with experimental results published in literature. Particular attention has been paid to include the effect of equivalence ratio on the power exponents  $\alpha$  and  $\beta$ .

## Chapter 6 Laminar flame speed of kerosene fuel

---

This chapter is devoted to present the evolutions of the laminar flame speeds of kerosene, specific pure hydrocarbons of kerosene and mixture of pure compounds in function of the preheating temperature, pressure and equivalence ratio. The methodology adopted to measure the laminar flame speed of heavy hydrocarbons compounds with the optical techniques previously described (OH\* chemiluminescence, OH-PLIF and aromatics-PLIF) will be first detailed. The phenomenon of the flame tip opening is then introduced and its influence on measurements of laminar flame speeds of heavy hydrocarbon fuels is discussed. Finally, the laminar flame speeds of pure compounds of kerosene (n-decane, n-propylbenzene, and n-propylcyclohexane), surrogate for kerosene (LUCHE surrogate) and commercial jet fuel (Jet A-1) are detailed.

## 6.1 Introduction and objectives

The understanding of combustion characteristics of practical jet fuels is a key point to the development of affordable and efficient aero-combustors. To achieve this objective, improvement of performances of aeronautical propulsion systems therefore needs a better understanding of the chemical kinetic mechanisms of multi-component fuels such as the Jet A-1 fossil fuel. In this case, the detailed chemical mechanisms include several hundreds of different species and around a thousand elementary reactions. To achieve mechanical Computational Fluid Dynamics calculation using detailed kinetic mechanisms, it is necessary to solve a transport equation for each species present into the fuel and calculate all the sources terms for each species involved in the chemical mechanism. At present, even in the near future, this kind of simulations for an industrial complex geometry remains elusive. It is therefore necessary to simplify calculations induced by the detailed chemistry for performing such simulations. Using pure hydrocarbons or simplified surrogate fuels to emulate the physicochemical properties of a commercial jet fuel is usually an alternative solution. One of the criteria of this approach will be then to obtain combustion properties similar to those of multi-component fuels. One of these parameters to characterize is obviously the laminar flame speed.

Laminar flame speed measurements of heavy hydrocarbon fuels under high pressure and elevated preheating temperature conditions are not easily achieved. A review of the literature reveals that few experimental measurements of laminar flame speed of kerosene are available in the literature. Accurate laminar flame speed measurement of kerosene under these complex conditions is still one of the open issues. In this chapter, before analyzing the laminar flame speed measurements of a commercial jet fuel, the limitations and the benefits of the optical techniques (OH\* chemiluminescence, OH-PLIF and aromatics-PLIF) used to (1) visualize the Bunsen flame structure and (2) accurately determine the flame speed in case of heavy hydrocarbon fuels are firstly discussed. Furthermore, the specific effect of flame tip opening phenomenon occurring on such heavy hydrocarbon flames and that could perturb the data processing of measurements is detailed. Then, laminar flame speeds of the LUCHE surrogate fuel and of the associated pure compounds (n-decane, n-propylbenzene, and n-propylcyclohexane) are also subsequently measured over a wide range of temperature, pressure and equivalence ratio conditions. After this part, laminar flame speed measurements of commercial Jet-A1 fuel are performed at the same operating conditions. Finally, a further comparison between numerical and experimental results of laminar flame speeds recorded for these types of complex fuels is addressed.

## 6.2 Operating conditions

The first part of this work concerns pure fuels which represent three major hydrocarbon classes of kerosene: n-decane (paraffins), n-propylbenzene (aromatics) and propylcyclohexane (naphthenics).

Measurements were performed at different preheating temperatures, 400 K, 423 K and 473 K, atmospheric pressure and equivalence ratio ranging from 0.6 to 1.3.

The second part concerns the LUCHE surrogate fuel, which is a mixture of three pure compounds: n-decane (76.7%), n-propylbenzene (13.2%) and n-propylcyclohexane (10.1%). Their physical properties are listed in Table 6.1. The LUCHE surrogate fuel was firstly reported in the work of J. Luche [32] that was dedicated to the development of a skeletal kerosene mechanism for the Jet A-1 fuel. In the present work, laminar flame speeds of LUCHE surrogate fuel were measured at  $T = 400$  K, 423 K and 473 K,  $P = 0.1 - 1.0$  MPa and  $\phi = 0.6 - 1.3$  using OH-PLIF and OH\* chemiluminescence techniques.


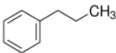
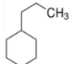
Component	Formula	Mass (%)	Boiling point (°C)	Molar (%)	Molecule structure
n-decane	$C_{10}H_{20}$	0.767	174	0.7396	
n-Propylbenzene	$C_9H_{12}$	0.132	159	0.1507	
Propylcyclohexane	$C_9H_{18}$	0.101	155	0.1097	

Table 6.1: Composition of the LUCHE surrogate fuel.

In order to evaluate potential deviations between the combustion performances of the surrogate fuel and those of the commercial Jet-A1 fuel, measurements of the laminar flame speeds of Jet A-1 was then investigated. In this case, the flame speed measurements are conducted over a wide range of conditions ( $T = 400$  K, 423K, 453 K and 473 K,  $P = 0.1 - 1.0$  MPa and  $\phi = 0.6 - 1.3$ ) using OH-PLIF, aromatics-PLIF and OH\* chemiluminescence diagnostics. It should be noted that measurements under elevated pressure are limited to lean equivalence ratios due to the apparition of flame instabilities for rich mixtures. The operating conditions investigated in the present section are resumed in Table 6.2.

Fuels tested in this work are provided by VWR supplier with the following specifications: n-decane purity 99 % (CAS No.: 124-18-5), n-propylbenzene purity 99 % (CAS No.: 103-65-1) and the n-propylcyclohexane purity 99 % (CAS No.: 1678-92-8). The LUCHE surrogate is a blend of these three molecules (mixed at laboratory with the proportions indicated in Table 6.1).

Fuels	Temperature (K)	$\phi$	Pressure (MPa)	Optical diagnostic
n-decane	400, 423, 473	0.6 – 1.3	0.1	OH* Chemiluminescence OH - PLIF
n-propyl-benzene	400, 423, 473	0.6 – 1.3	0.1	OH* Chemiluminescence
n-propylcyclohexane	400, 423, 473	0.6 – 1.3	0.1	OH* Chemiluminescence
Jet A-1	400, 423, 473	0.6 – 1.3	0.1	OH* - Chemiluminescence OH – PLIF Aromatics-PLIF
Jet A-1	423, 473	0.7, 0.8	0.1 - 1.0	OH* Chemiluminescence
LUCHE surrogate	400, 423, 473	0.6 – 1.3	0.1	OH* - Chemiluminescence OH - PLIF
LUCHE surrogate	423, 473	0.7, 0.8	0.1 - 1.0	OH* Chemiluminescence

Table 6.2 : Experimental conditions.

### 6.3 Limitations of the optical techniques for laminar flame speeds determination

As previously mentioned, the accuracy of the laminar flame speed measurement depends on how the reference surface delimiting the consumption of the fresh gases is defined. For fuels with small molecular weights such as methane and acetone for which detailed kinetic mechanisms are available, the knowledge of the temperature profiles predicted with the detailed kinetic mechanisms can be used to evaluate the flame thicknesses required to correct the OH\* chemiluminescence signals. In the case of heavy hydrocarbon fuels such as kerosene, this information is now more difficult to obtain due to the lack of knowledge of detailed kinetic mechanisms. It is then necessary to define experimental methodologies useful to directly measure with accuracy the location of the contour delimiting the consumption of the fresh gases.

#### 6.3.1 OH\* Chemiluminescence versus OH-PLIF

To develop experimental methodologies able to measure accurate measurements of laminar flame speeds with heavy hydrocarbon fuels, a pure compound of kerosene, n-decane, was firstly studied at the following operating conditions :  $T = 400$  K,  $P = 0.1$  MPa and  $\phi = 0.65 - 1.3$ . This molecule is one of the main straight chain paraffin compounds of kerosene and it has been frequently used as one of proposed surrogate fuels used for replacing kerosene [17] [7] [23] [115] [27]. As this fuel is optically transparent, only the detection of the shape of n-decane/air flames were undertaken with the OH\* chemiluminescence and OH-PLIF diagnostics. For instance, Figure 6.1 presents a comparison of images of the flame shape of n-decane recorded with both techniques. Depending of the diagnostic, a detection of different “flame” contours occurs. Therefore, an “outside” contour of the flame can be easily visualized by OH\*



chemiluminescence while an “inside” contour is observed with OH-PLIF. Unfortunately, as depicted on Figure 6.1, the contours are not located at the same position and the distance separating both contours can reach 0.1 ~ 0.3 mm. So one question arises: What is the best contour to use for measuring accurate laminar flame speed in such flames? One element of answer is then to compare the laminar flame speeds obtained with these contours with measurements reported in the literature (see section 6.4.1).

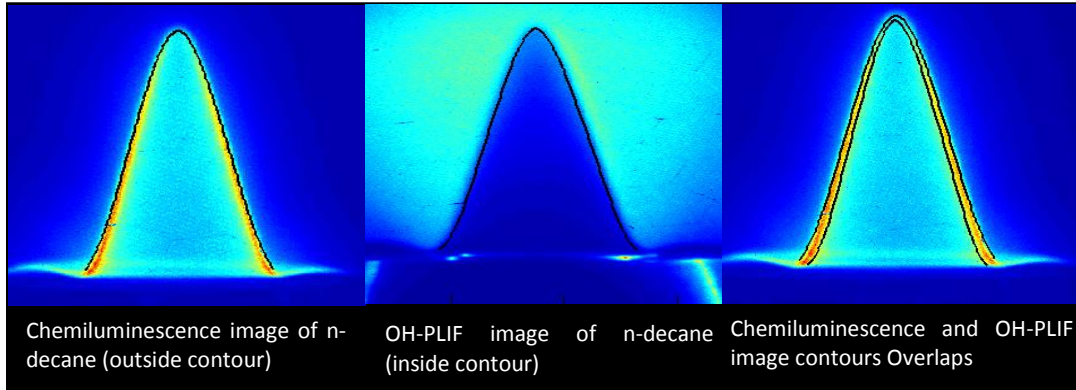


Figure 6.1: Flame contours measured with OH\* chemiluminescence and OH-PLIF. Case of a n-decane/air mixture,  $T = 400\text{ K}$ ,  $P = 0.1\text{ MPa}$ ,  $\phi = 0.8$ .

Determination of the laminar flame speed was firstly determined from the analysis of OH\* chemiluminescence images (Figure 6.2). Two flames contours were detected on the OH\* images. The first one consisted of the “classical” detection of the contour for which OH\* signals are maximal. As discussed in chapter 4, this location leads to an underestimation of the laminar flame speeds if no correction of the flame thickness was undertaken. Typically, a deviation of up to 10 cm/s on peak values was observed after comparison of the laminar flame speeds with measurements reported by Comandini et al. [17] and calculations performed with the Jet Surf 2.0 mechanism. As shown in section 6.4.1, these results were taken as a reference case for n-decane. A second approach which was also suggested in the literature [76] was to isolate on the fresh gases side, one “inside” contour delimiting the beginning of the gradient of the OH\* chemiluminescence signals. This position corresponds to the inner frontier detected on the Abel transform images (see section 4.4.1). The area defined from this “inside” contour offered a new set of laminar flame speeds which was in much better agreement with the literature data (see Figure 6.2). One evident constraint of this methodology was that the position of this contour could be defined with a less precision. The resulting accuracy will depend of the Abel transform method and the SNR of the experimental signals. Indeed, the Abel transform when used correctly is sensitive to the noise existing in the center of the axisymmetric flame image. In case of elevated SNR, this noise could be significantly reduced while at low SNR, this one can greatly influence the resolution of Eq. 4.7 and then changes the location of the zone of signals after Abel transform. As the flames investigated in our study are laminar, the record of OH\* chemiluminescence signals was performed by optimizing the integration time of the detector in order to get elevated SNR, increasing then the reproducibility of this methodology.

As observed in Figure 6.1, the OH-PLIF technique enabled us to detect precisely the beginning of the zone in which OH fluorescence can be optically detected. As this molecule is usually detectable with PLIF at a temperature roughly equal to 800 K, the position in which OH starts to be detected offers a good opportunity to visualize the location of the consumption of the fresh gases. An analysis of the data issued from OH-PLIF images and reported in Figure 6.2 revealed that OH-PLIF measured laminar flame speeds in closer agreement with the flame speeds deduced from the “inner” OH\* chemiluminescence contour. However, the laminar flame speeds were slightly underestimated compared to the literature data. One reason that may explain such deviation (see chapter 5) probably arises from the dynamics of our fluorescence detector (16 bit) which is not sufficiently large to detect with accuracy on the same fluorescence image, the variation of signals representative of an OH concentration variation from few ppm (start of the kinetic mechanism) to about 1% (peak value in the flame front). However, this observation should be put into perspective in regards to the measurements accuracy which is about  $\pm 2.5$  m/s in the current study.

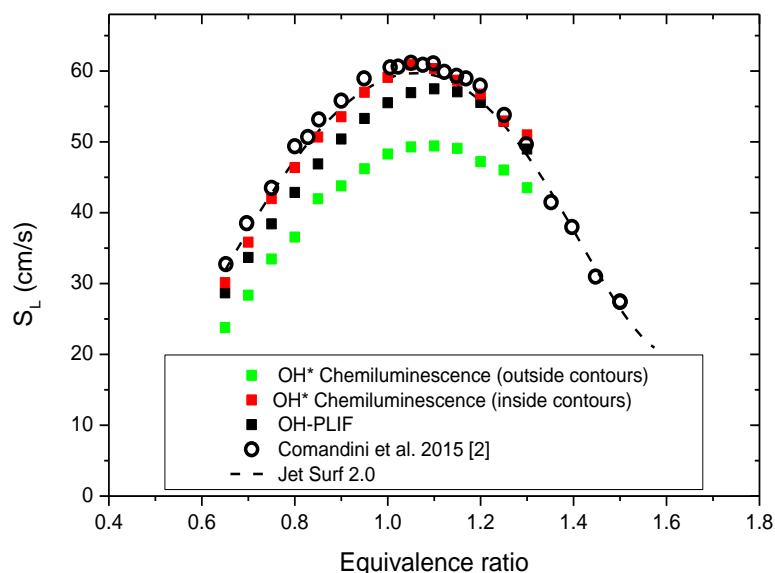


Figure 6.2: Laminar flame speed comparison between results obtained in the present work (OH\* chemiluminescence and OH-PLIF) and literature results of Comandini et al. for n-decane/N<sub>2</sub>/O<sub>2</sub>  $T = 400$  K,  $P = 0.1$  MPa,  $\phi = 0.65 - 1.3$ .

### 6.3.2 Comparison between OH-PLIF, chemiluminescence and aromatics-PLIF

To further complete the comparison of performances of the optical diagnostics, an application of OH\* chemiluminescence, OH-PLIF but also aromatics-PLIF diagnostics was carried out on Jet A-1/N<sub>2</sub>/O<sub>2</sub> mixtures. Measurements of laminar flame speeds were performed at  $T = 400$  K,  $P = 0.1$  MPa and  $\phi = 0.65 - 1.3$ . Unlike the previous case, the aromatics-PLIF technique can now visualize the zone of fresh gases and locate precisely the frontier of fuel consumption. Furthermore, this technique will also ensure

measurements in fuel rich conditions, conditions in which flame tip opening can disturb the data processing of signals recorded with OH\* chemiluminescence and OH-PLIF (see the next section).

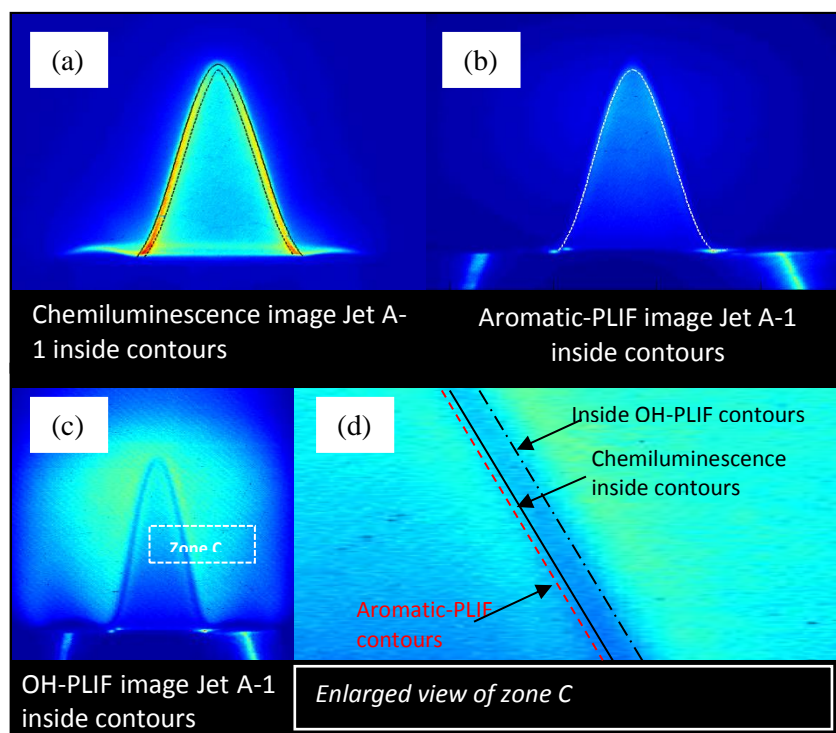


Figure 6.3: Comparison between OH\* chemiluminescence, aromatics-PLIF and OH-PLIF results: Jet A-1/ $N_2/O_2$  mixture,  $T = 400\text{ K}$ ,  $P = 0.1\text{ MPa}$ ,  $\phi = 0.8$ .

Figure 6.3 shows examples of kerosene/air flame images recorded with OH-PLIF, OH\* chemiluminescence and aromatics-PLIF. From these figures, the location of different contours were determined and plotted on Figure 6.3d. It is observed that the different contours deduced from OH-PLIF, OH\* chemiluminescence and aromatics-PLIF signals are not located at the same position. Typically, the location of the “inner” contour deduced from OH\* chemiluminescence are in adequacy with results obtained with aromatics-PLIF, demonstrating that this last technique is able to detect the frontier of the fuel consumption. What is more surprising is the deviation existing between the contour deduced from OH-PLIF and the one obtained by aromatics-PLIF. By analogy with similar results detailed in section 5.1.2, one explanation at the origin of this deviation could come from the dynamics of our detector (16 bit) which is not able to detect on the same fluorescence image the variation of signals representative of an OH concentration change of few ppm (start of the kinetic mechanism) to about 1% (peak value in the flame front).

Results of laminar flame speed measurements with aromatics-PLIF, OH\* chemiluminescence and OH-PLIF are resumed in Figure 6.4. As in the case of n-decane/ $N_2/O_2$  mixtures, the same trends were observed: the laminar flame speed deduced from the inside contour of OH\* chemiluminescence is slightly

larger than the one acquired with OH-PLIF. On the other hand, aromatics-PLIF gives laminar flame speeds similar to those obtained with OH\* chemiluminescence. Note also that the deviations between laminar flame speeds are minima in the lean and rich sides and maximal when the equivalence ratio approaches the stoichiometry. Furthermore, the maximum deviation at  $\phi = 1.0$ , about 5 cm/s, exceeds slightly the uncertainty of our measurements.

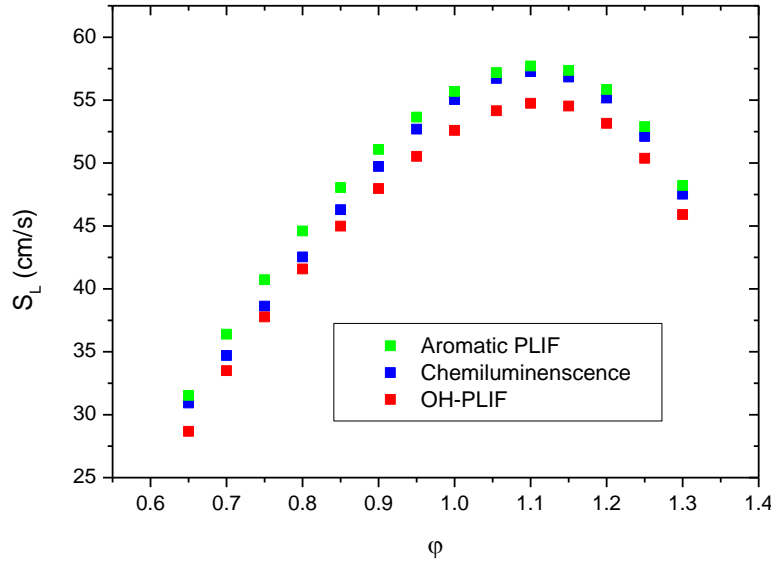


Figure 6.4: Laminar flame speeds determined from OH\* chemiluminescence, aromatics-PLIF and OH-PLIF images. Case of a Jet A-1/air mixture,  $T = 400$  K,  $P = 0.1$  MPa,  $\phi = 0.65 - 1.3$ .

In conclusion, aromatics-PLIF compared to OH\* chemiluminescence can directly determine the fresh gas edge and there is no need to correct the flame area by the flame thickness. However, one limitation of this diagnostic is its applicability limited to the case of fluorescence fuels. In case of optically transparent fuels, the use of a tracer fuel seeded into the fuel could be an alternative to visualize the zone of fresh gases but this will inevitably lead to a systematic bias on the resulting laminar flame speed (modification of the fuel composition).

### 6.3.3 Flame tip opening phenomenon

Tip opening of the laminar Bunsen flame is the local combustion extinction which is located at the cusp of the flame where strong negative flame stretch exists [72] [184]. Tip opening will locally change the flame speed which will subsequently influence the average flame speed over the whole flame surface. When the OH\* chemiluminescence technique is applied, the local quenching increases the difficulty to accurately define the flame contours and a better understanding of the flame tip opening is necessary to assess the level of perturbations of this phenomenon on the laminar flame speeds.

With the recent investigation published in literature [185] [186], it is found that this local extinction is closely related with some fundamental and critical factors such as stretch rate and preferential diffusion. From the work of Vu et al. [185], it is mentioned that the opening phenomenon could be controlled by local Karlovitz number defined by  $K_{aL} = \frac{\alpha}{\bar{U}R}$ , where  $\alpha$  is the thermal diffusivity,  $\bar{U}$  is the centerline velocity and  $R$  is the radii of the flame curvature. When the local Karlovitz number approaches to unity, a flame opening phenomenon occurs.

In the case of heavy hydrocarbons fuels such as kerosene, this phenomenon can occur for rich mixtures exceeding  $\phi = 1.15$  meanwhile for light fuels such as methane/air, this phenomenon typically occurs for equivalence ratio larger than  $\phi = 1.4$ . In the present work, the tip opening phenomenon occurs at a constant equivalence ratio around  $\phi = 1.15$  for n-decane, LUCHE surrogate and Jet A-1 fuels. However, for n-propylbenzene, it occurs at  $\phi = 1.20$  and for n-propylcyclohexane, this one appears at  $\phi = 1.25$ . Moreover, it is found that the opening phenomenon is likely independent of the jet velocity and preheating temperature (i.e.  $T = 400 - 523$  K in the current work).

Laminar flame speed measurement methodology used in present work is the flame area method which needs the fresh gas edge detection. However, when OH\* chemiluminescence technique is applied, flame tip opening phenomenon could yield to local extinction which makes it difficult to localize precisely the entire fresh gas edge. In order to guarantee the accuracy of our measurements, it is necessary to define the “true” flame contours. In the current work, OH-PLIF and aromatics-PLIF were applied to highlight the boundary edge of the flame tip opening part. Figure 6.5 and Figure 6.6 show typical Jet A-1/N<sub>2</sub>/O<sub>2</sub> flame images acquired simultaneously with OH\* chemiluminescence and aromatics-PLIF at the following conditions:  $T = 400$  K,  $P = 0.1$  MPa and  $\phi = 1.3$ . In Figure 6.5, the OH\* emission image and the intensity variation along the nozzle centerline are plotted. It is observed that the OH\* intensity decreases along the flame axis at the top part of the flame (**Region A**). The tip flame opening phenomenon appears at equivalence ratio  $\phi = 1.15$  and the tip flame opening enlarges when the mixture equivalence ratio increases.

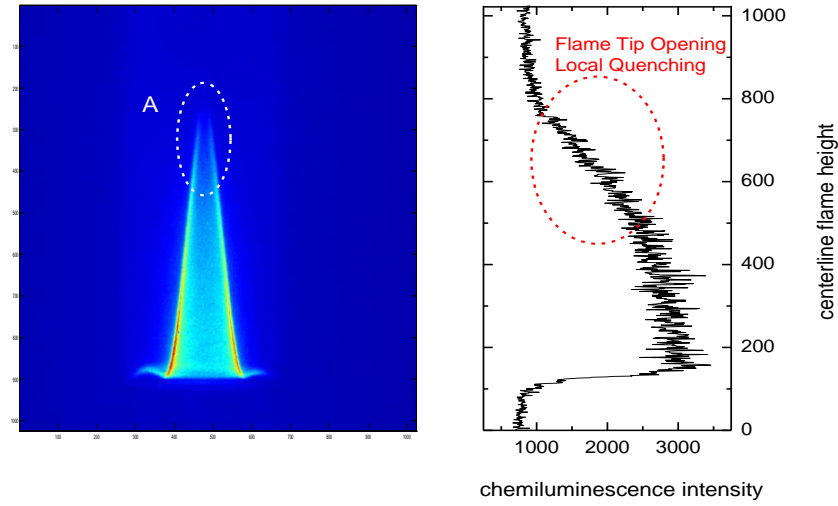


Figure 6.5: Flame tip opening visualizing with  $\text{OH}^*$  chemiluminescence and variation of the emission signal along the nozzle centerline. Jet A-1/ $\text{N}_2/\text{O}_2$  flame,  $T = 400 \text{ K}$ ,  $P = 0.1 \text{ MPa}$  and  $\phi = 1.3$ .

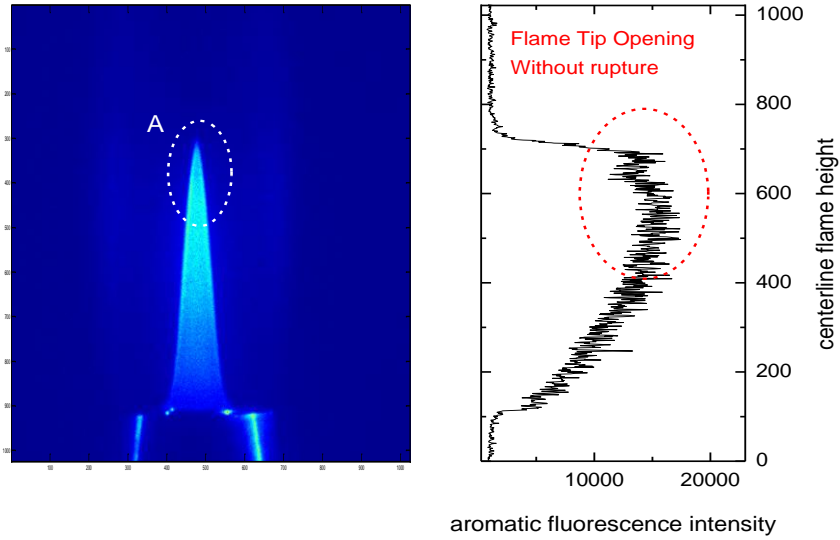


Figure 6.6: Flame tip opening of Aromatic-PLIF image and aromatic fluorescence intensity variation along nozzle centerline (Jet A-1/ $\text{N}_2/\text{O}_2$  flame,  $T = 400 \text{ K}$ ,  $P = 0.1 \text{ MPa}$  and  $\phi = 1.3$ ).

Complementary experiments were also performed with aromatics-PLIF to visualize the zone of the fresh gas. In Figure 6.6, the zone of the fresh gases and the variation of the fluorescence intensity along the nozzle centerline are plotted. By contrast with  $\text{OH}^*$  images, the full zone of the fresh gases is now observed and no attenuation of fluorescence signals at the tip of this zone is discernable. This clearly indicates that the fresh gases are still present at the top part of the conical zone while a combustion quenching occurred because of strong negative flame stretch. It indicates subsequently that the flame consumption speed over the flame surface is not homogeneous: flame speed at the top of the conical flame will be quite different from the linear peripheral contour of the flame. When  $\text{OH}^*$  chemiluminescence technique is used, the flame area useful for flame speed determination is obtained by extending the linear peripheral contour to the tip of the flame using a high-order interpolation method.

Nevertheless, due to the intensity rupture at the flame tip, the contour obtained by the interpolation method tends to underestimate the flame surface and consequently overestimate the laminar flame speed value.

#### **6.3.4 Concluding remarks**

The benefits and limitations of the different optical techniques for measuring the laminar flame speed are summarized below:

- When OH\* chemiluminescence technique is applied, two possible flame contours can be used: An “outside” and “inside” frontier. The “inside” frontier assesses the laminar flame speed with a good accuracy comparing to the one obtained with the “outside” frontier. One benefit of this method is that OH\* chemiluminescence allows high SNR and requires a simple experimental set-up. However, limitations of this method come from the fact that OH\* chemiluminescence is based on the integration of signals over the line-in-sight making it difficult the visualization of the frontier of consumption of the fresh gases.
- Aromatics-PLIF technique offers the benefit to obtain accurate laminar flame speeds from a direct observation of the fresh gas cone. Moreover, this technique has the advantage to prevent any flame tip opening phenomenon on measurements which can significantly influence the detection of the fresh gases edges for rich mixtures. The main limitation of this method lies into its application on only fuels containing fluorescence markers.
- OH-PLIF technique allows the detection of the beginning of the reaction zone. Unfortunately, the existence of high gradients of OH into the flame makes it difficult the localization of the frontier delimiting the appearance of the production zone of OH within the dynamics of the ICCD camera. Therefore, information detected on the OH PLIF images slightly underestimate flame speed values. For instance, the maximal difference between laminar flame speeds derived from OH-PLIF and aromatics-PLIF can be up to 5cm/s for kerosene fuels.

### **6.4 Laminar Flame Speeds of neat kerosene compound**

To obtain a good representativeness of the respective effects of compounds entering into the LUCHE surrogate composition, the laminar flame speeds of n-decane, n-propylbenzene and n-propylcyclohexane were examined at three preheating temperatures  $T = 400, 423$  and  $473$  K,  $\phi = 0.6 - 1.3$  and atmospheric pressure conditions. All the experimental set parameters including jet velocity, CEM heating temperature and parameters for piloted flame (flowrate and equivalence ratio) are kept constants.

### 6.4.1 n-Decane

Figure 6.7 shows a comparison between our experimental results, a numerical prediction with the JetSurF 2.0 chemical mechanism and the experimental data collected in the literature.

Except the data reported by Hui et al. [23] and those obtained by Kumar et al. [7] which depict large deviations from the other measurements, the overall agreement among the data of the literature and our laminar flame speeds is generally excellent, with a better agreement between our data and the Jet Surf 2.0 predictions. In particular, the position of the peak value of the laminar flame speeds at  $\phi = 1.05$  is well reproduced by the chemical kinetic mechanism. Our current data are also close to laminar flame speeds obtained using spherical flames [17] [115] [27]. For  $\phi = 1.3$ , a deviation of our data with the numerical predictions is however observed. This could be caused by the flame opening phenomenon mentioned previously that prevents an accurate description of the flame contours. Note however that the experimental results reported in the literature are comparable to our measurements.

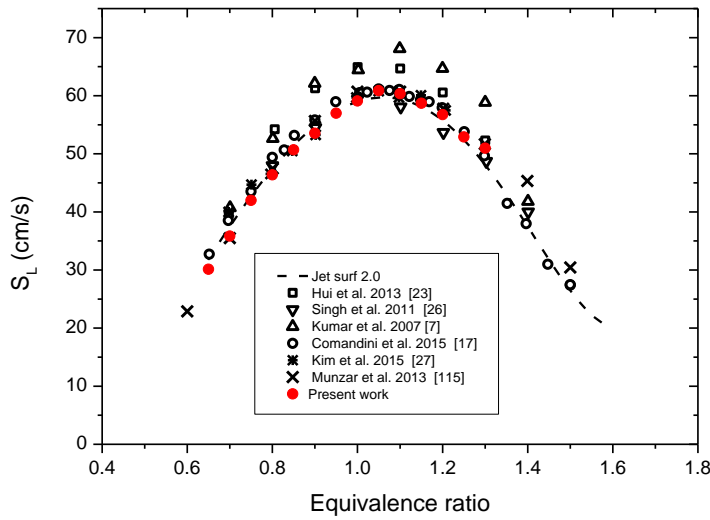


Figure 6.7: Comparison between our experimental results and data from literature:  $T = 400\text{K}$ ,  $P = 0.1\text{ MPa}$  and  $\phi = 0.6 - 1.5$ .

Measurements were then performed at 423 and 473 K as shown in Figure 6.8. As expected, the laminar flame speed increases with the preheating temperature of the mixture.



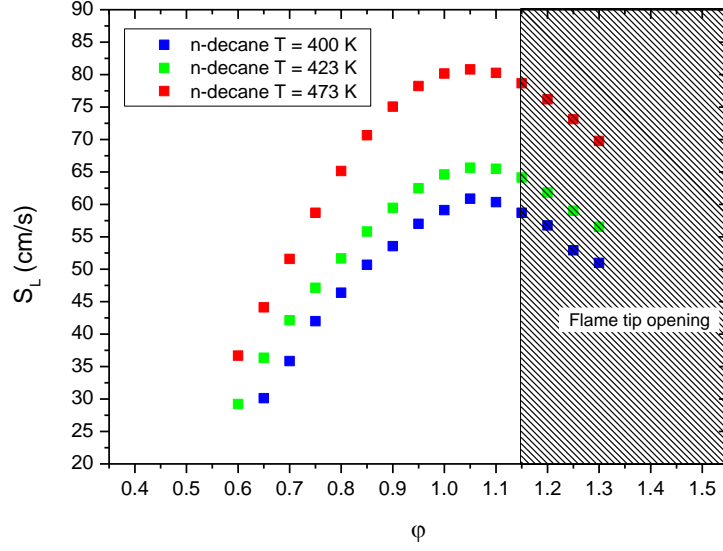


Figure 6.8: Effect of the temperature on the laminar flame speed of *n*-decane/ $N_2/O_2$  mixture at  $P = 0.1$  MPa and  $\phi = 0.6 - 1.3$ .

#### 6.4.2 n-Propylbenzene

N-propylbenzene is a heavy aromatic species present in large amounts in kerosene and diesel fuels. Its laminar flame speed has rarely been studied in the past and only measurements performed with the stagnation flame [101] [116] and the heat flux method [117] were until now reported.

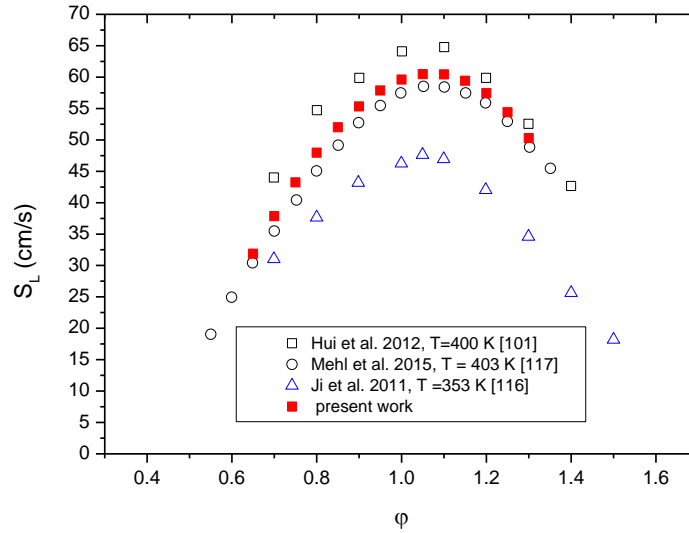


Figure 6.9: Comparison between present work and literature. Laminar flame speeds of *n*-propylbenzene. ( $T = 400$  K,  $P = 0.1$  MPa and  $\phi = 0.6 - 1.3$ ) [101] [116] [117]

Figure 6.9 shows a comparison between our current results and those reported in [101] [116] [117]. First of all, the results of our current work are in close agreement with those obtained from Mehl et al. [117]

whatever the investigated equivalence ratio. The maximal deviation observed from this comparison is about 5 cm/s, value which remains largely comparable with our measurement uncertainty. It is also observed that the data issued from the study of Hui et al. [101] give overestimated values. As reported in [17], the deviation of these laminar flame speeds is not evident to explain since the authors used the non-linear technique to determine the flame speed.

Effects of the preheating temperature on laminar flame speeds are now presented in Figure 6.10. Measurements were performed at preheating temperatures of 423K and 473K respectively. The general evolution of the laminar flame speeds with temperature observed on this graph agrees well with the theory prediction: the laminar flame speed of n-propylbenzene increases when the preheating temperature increases. This result is confirmed by the data of Ji et al. [116] which measured the evolution of the laminar flame speed at a lower preheating temperature ( $T=353$  K). A comparison of these evolutions with those observed on n-decane also reveals that these laminar flame speeds have similar values with those of n-decane whatever the preheating temperature.

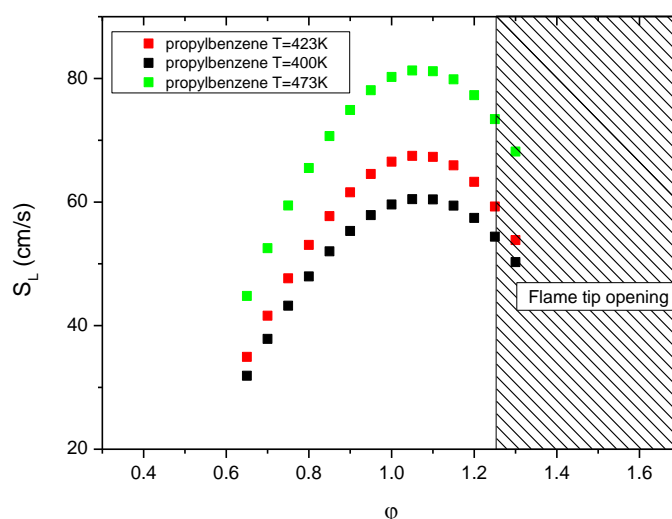


Figure 6.10: Effect of the temperature on the laminar flame speed of n-propylbenzene,  $P = 0.1$  MPa,  $\phi = 0.6 - 1.3$ .

### 6.4.3 Propylcyclohexane

N-propylcyclohexane is one of the main cycloalkanes that are usually found in the diesel and kerosene fuels. Contrary to n-alkanes, branched alkanes or aromatics, studies of the behavior of laminar flame speeds with preheating temperature and equivalence ratios are rarely been previously investigated. In the current work, measurements were performed firstly at  $T = 400$  K,  $P = 0.1$  MPa and  $\phi = 0.65 - 1.3$  and compared with the literature results (see Figure 6.11). Our experimental results for lean mixtures are in good agreement with data of Comandini et al. [17] (non-linear extrapolation at zero stretch rate) and of

Dubois et al. [118] (linear extrapolation at zero stretch rate). A significant deviation is also observed for rich mixtures for which our measurements give faster laminar flame speeds. This deviation could be caused by perturbations occurring from the tip opening phenomenon which is active or these operating conditions.

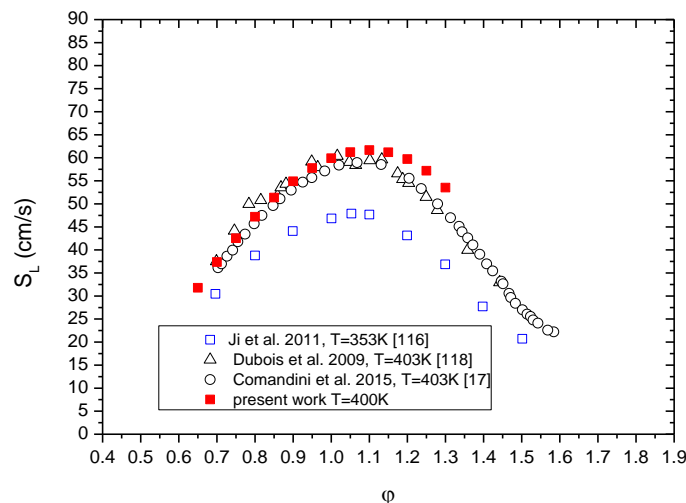


Figure 6.11: Laminar flame speed of *n*-propylcyclohexane, comparison between present work and literature. ( $T = 400 \text{ K}$ ,  $P = 0.1 \text{ MPa}$ ,  $\phi = 0.65 - 1.3$ ) [17] [116] [118]

Measurements are complemented in higher temperature conditions  $T = 423 \text{ K}$ ,  $473 \text{ K}$  as shown in Figure 6.12. General agreement with theory prediction is observed: the flame speed increases with higher preheating temperature. To give a better description of the effect of the preheating temperature over a wide range of preheating temperature, the data of Ji et al [116] acquired at preheating temperature of  $353 \text{ K}$  are also reported in the same figure.

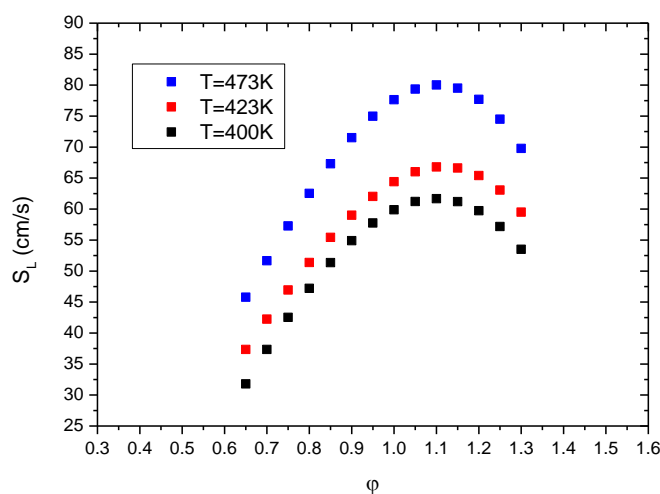


Figure 6.12: Effect of the temperature on the laminar flame speed of *n*-propylcyclohexane. ( $P = 0.1 \text{ MPa}$ ,  $\phi = 0.65 - 1.3$ )

#### 6.4.4 Comparison between the pure compounds

Figure 6.13 presents the evolutions of the laminar flame speeds of the three pure compounds at  $T = 400$  K,  $P = 0.1$  MPa and  $\phi = 0.6 - 1.3$ .

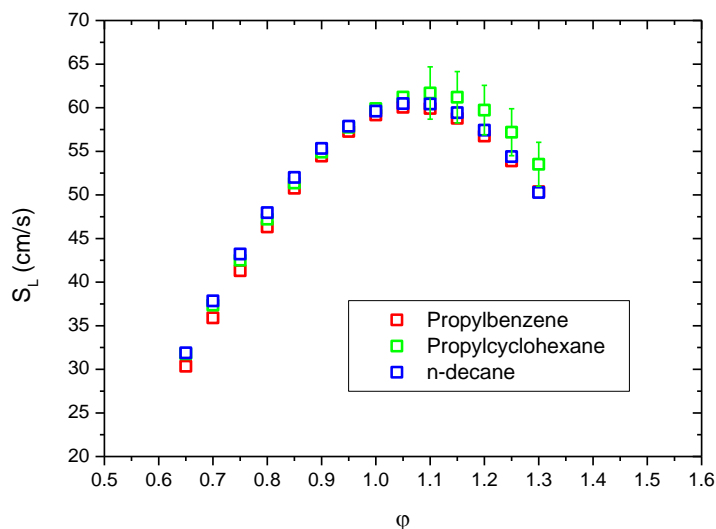


Figure 6.13: Comparison of the laminar flame speeds of *n*-decane, *n*-propylbenzene, *n*-propylcyclohexane:  $T=400$  K,  $P=0.1$  MPa.

First of all, an observation of results presented in this figure shows that the laminar flame speeds of the three pure compounds are quite similar whatever the equivalence ratio. However, a detailed examination of these evolutions shows that *n*-decane has slightly faster flame speeds (around 2.5 cm/s at maximum at lean equivalence ratio) compared to the values of *n*-propylbenzene. This difference is somewhat limited compared to the experimental uncertainties which are in the same order of magnitude.

As discussed in [17], *n*-propylbenzene is an aromatic molecule and compared to *n*-alkanes, the existence of a ring chemical structure plays a particular role in the combustion reactions. Indeed, although the overall flame speed is controlled by the chemistry of small radicals, the burning velocities of aromatics were found to be influenced by fuel specific intermediates. In the study reported in [17], a sensitivity analysis of their results confirmed that the flame speed is influenced by the ring structure, in particular by the reactions involving the radical intermediates such as phenoxy, benzyl and the phenyl radicals. For instance, Mehl et al. [117] found that the high concentration of benzyl radicals in the pre-flame zone inhibits the flame propagation and can reduce the burning velocity. On the other hand, the alkane components, *n*-decane and *n*-propylcyclohexane have similar behaviors and thus can be directly compared. Results of studies reported by Ji et al. [116] and Wu et al. [187] observed that the flame speeds of mono-alkylated cyclohexane compounds (from methylcyclohexane to *n*-butylcyclohexane) should be almost identical but uniformly lower than those of *n*-alkanes (such as *n*-hexane and *n*-decane probably).

This can be explained by kinetic effects: while the flame speed of n-decane is only affected by chemistry involving small intermediates, the ring structure of mono-alkylated cyclohexane compounds decomposes slower compared to the linear structure of the n-alkane, thus the primary steps in the fuel decomposition and the chemistry of the small intermediates are not completely decoupled as for the case of n-decane [17].

In the fuel lean side, this trend is observed in Figure 6.13: n-decane > n-propylcyclohexane > n-propylbenzene. However, differences between these data are so small (around 2-3 cm/s) that it is difficult to determine with certainty on this tendency. In view of our measurements, these three compounds have globally similar flame speeds when working in lean mixtures. For rich mixtures, the n-propylcyclohexane gives obviously larger values of laminar flame speed compared to those observed for n-decane, which is in contradiction with results reported in the literature. These contrary observations could be due to the phenomenon of flame tip opening that make the data processing of flame shape images more difficult. Therefore, the level of measurements uncertainties are increasing making the reading of the evolutions of the different laminar flame speeds more complex. For a better clarity, error bars for the n-propylcyclohexane measurements in fuel rich conditions were added in the Figure 6.13, these ones representing now a global uncertainty of about 4.5%.

## **6.5 Laminar flame speeds of fuel surrogate and Jet A-1 kerosene**

### **6.5.1 LUCHE surrogate**

After taken the pure compounds of kerosene and LUCHE surrogate in consideration, the laminar flame speed of the LUCHE surrogate has been studied over a wide range of operating conditions including temperature (400 - 473 K), pressure (0.1 – 1.0 MPa) and equivalence ratio (0.65 – 1.3). Experimental results were then compared with predictions with the LUCHE detailed kinetic mechanism. The ability of this chemical mechanism to deliver “true” information on chemistry was then evaluated by taking account pressure and preheating temperature effects.

#### *(a) Comparison with the pure compounds.*

The purpose of this work presented in this section was to estimate the relative importance of the different compounds entering in the composition of the LUCHE surrogate on the LUCHE surrogate combustion properties. Figure 6.14 shows a comparison of the laminar flame speeds of the LUCHE surrogate with those of the three pure compounds studied. The values obtained for the LUCHE surrogate at T= 400 K are close to those measured for the three compounds for equivalence ratios between 0.6 and 1.3. A closer examination of Figure 6.14 shows that the laminar flame speeds of the LUCHE surrogate mimic very well the laminar flame speed values of n-decane. This was expected as n-decane represents the main

compound in the species composition of the LUCHE surrogate (78%). While n-propylbenzene is marginally slower according to Figure 6.14, the contribution of this species on the global laminar flame species of the LUCHE surrogate can be considered effectively comparable to the n-decane. For n-propylcyclohexane, the faster laminar flame speeds observed could have an impact on flame velocities of the LUCHE surrogate for rich mixtures. Given the fact that the concentration of this compound into the LUCHE surrogate is very weak (10 %), this impact on the laminar flame speed of the surrogate fuel becomes however marginal.

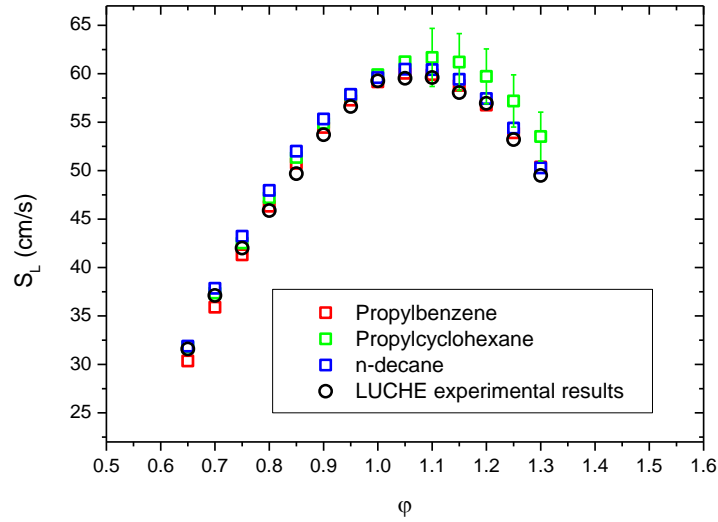


Figure 6.14: Comparison of the laminar flame speeds of n-decane, n-propylbenzene, n-propylcyclohexane and the LUCHE surrogate.  $T=400$  K,  $P=0.1$  MPa.

(b) Preheating temperature dependence

Experimental data and numerical predictions at  $T=400$  K,  $P=0.1$  MPa and  $\phi=0.6-1.3$  are compared and plotted in Figure 6.15. The model developed by LUCHE predicts quite well the laminar burning velocities. Only a slight underestimate of the flame speed of about 2~3 cm/s is observed whatever the equivalence ratios. Note that this deviation is comparable to our measurement uncertainties.

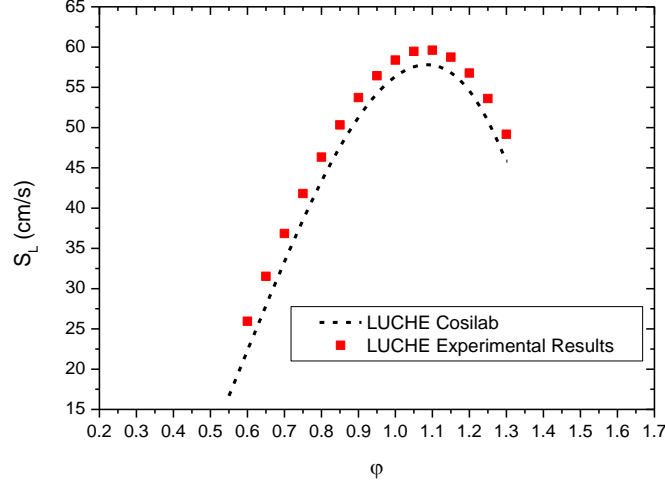


Figure 6.15: Comparison between experimental measurements and simulation results using the LUCHE model ( $T = 400$  K,  $P = 0.1$  MPa).

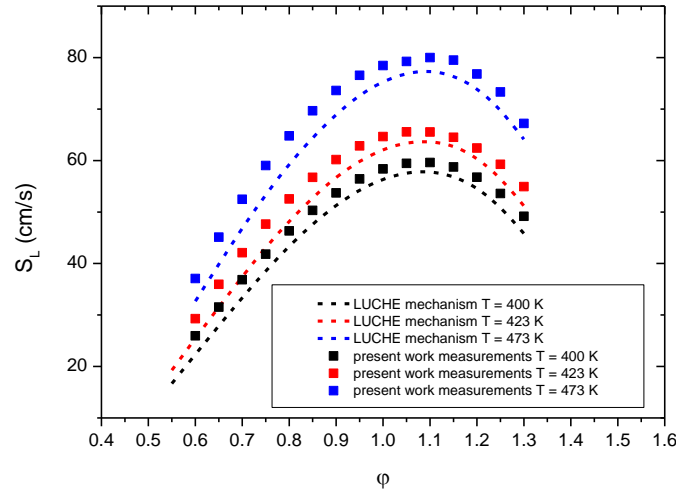


Figure 6.16: Laminar flame speed of LUCHE surrogate fuel with temperature variation. (Lines are the simulation results and points are the measured values)

As observed in Figure 6.16, the experimental results measured at  $T = 423$  K and  $473$  K also shows that the LUCHE kinetic mechanism predicts well the qualitative evolution of the laminar flame speed with preheating temperature. However, the model systematically underpredicts our measurements whatever the preheating temperature and the equivalence ratio with a maximal deviation of about 3-4 m/s.

### (c) Pressure dependence

To verify the potential of the LUCHE kinetic mechanism in elevated pressure conditions, laminar flame speed measurements are conducted at  $T = 423$  K,  $\phi = 0.7$  and  $0.8$  and pressure ranging from  $0.1$  to  $0.8$  MPa. This temperature condition was selected in order to assure a stabilization of the flame at the nozzle

outlet during the experiments and to prevent fuel pyrolysis especially at elevated pressure. This is essential to guarantee the measurement accuracy and to make sure that no chemical reaction modifies the fuel composition during the transport of the fuel/air mixture inside the combustion chamber.

In Figure 6.17, a comparison in a logarithmic graph is made between the present measurements and the predictions of the LUCHE mechanism. As observed previously, the LUCHE model underpredicts our measurements for both equivalence ratios. In contrast, the qualitative dependence of pressure seems to be quite covered at  $\phi = 0.8$  while a deviation of the dependence of pressure is noted at  $\phi = 0.7$ . The larger the pressure, the larger the deviation between simulation and measurements is. Note however that this behavior has to put in perspective because the maximum deviation between simulation and our measurements does not exceed 5 cm/s, value corresponding to the uncertainty of our measurements in elevated pressure conditions (see chapter 4).

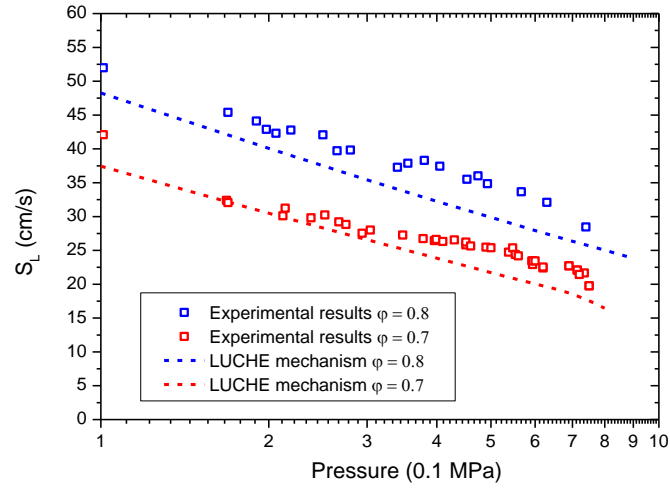


Figure 6.17: Evolution of the laminar flame speed of LUCHE surrogate as a function of pressure.  $T = 423$  K,  $\phi = 0.7$  and  $0.8$ . Points are our measurements and dash lines are the LUCHE predictions.

### 6.5.2 Jet A-1

In this section, measurements of the laminar flame speed of the Jet A-1 commercial fuel are presented over a large range of operating conditions. The effects of preheating temperature and pressure on the laminar flame speeds are studied and temperature and pressure dependence correlations are proposed. The Jet A-1 fuel is a multi-component mixture containing several hundreds of hydrocarbons; the average molecular formulation is:  $C_{11.16}H_{20.82}$  with a molar mass of 154 g/mol [22].



(a) Preheating temperature dependence

Laminar flame speeds have been measured for the Jet-A1 at two preheating temperatures: 400 and 473 K. In Figure 6.18 and Figure 6.19, there is a comparison between the present measurements and data from literature.

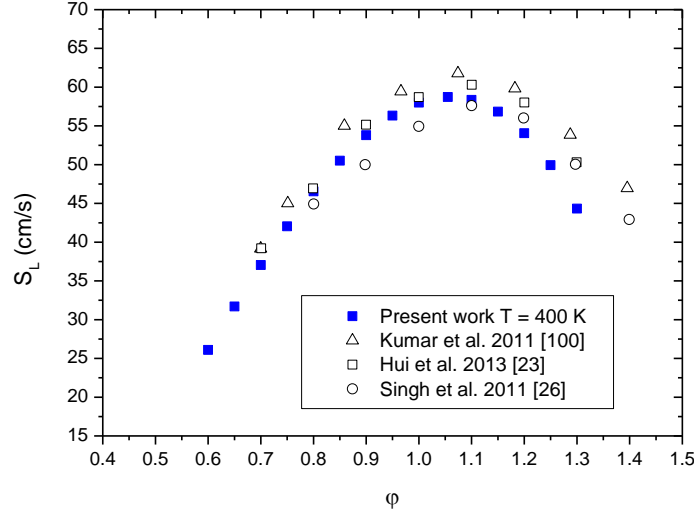


Figure 6.18: Comparison of the present measurements and data reported in the literature. Jet A-1,  $T = 400$  K,  $P = 0.1$  MPa. [23] [26] [100]

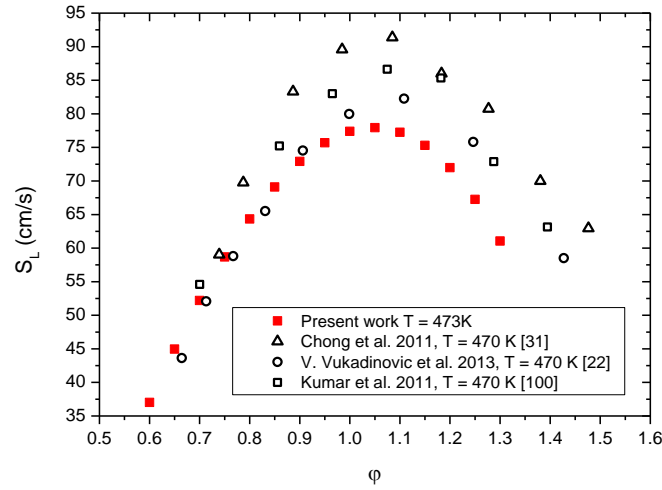


Figure 6.19: Comparison of the present measurements and data reported in the literature. Jet A-1,  $T = 473$  K,  $P = 0.1$  MPa. [22] [100] [31]

For Jet-A1 at  $T = 400$  K, there is a good agreement with the measurements reported by Hui et al. [23], Singh et al. [26] and Kumar et al. [100] and our measurements for lean conditions, i.e. between 0.7 and 0.8. For  $0.8 < \phi < 1.1$ , good agreement is still observed with the data of Hui et al. In contrast, significant deviations are noted with data of Kumar et al. who used counterflow flames and Singh et al. [26] who

used spherically expanding flames. Typically, the data of Kumar et al. overpredict our measurements while those of Singh et al. underpredict our laminar flame speeds. For  $\phi > 1.2$ , all the data referenced in literature are systematically higher.

At  $T = 473$  K, measurements performed in lean conditions ( $0.65 < \phi < 0.75$ ) are in well agreement with measurements from literature. Apart from the data of Vukadinovic et al. [22] that present comparable values with our measurements until  $\phi=1.0$ , the difference between our measurements and those reported in literature are more marked for equivalence ratio larger than 0.75 (Figure 6.19) than at  $T=400$  K. Furthermore, our measurements are systematically lower than data from literature [100] [31]. It is also observed a large scattering of measurements reported in literature. Explanation of this scattering can probably arise from a mutual interaction of several phenomena. The first one can be attributed to the probable use of different Jet-A1 compositions, which exist even for the same kerosene fuel supplied by different producers. The second one is partly ascribed to the variety of experimental facilities and of extrapolation methods used to determine the laminar flame speed (linear correlation for Kumar, non-linear extrapolation for Vukadinovic) that inevitably multiply the chances to get large deviations of measurements.

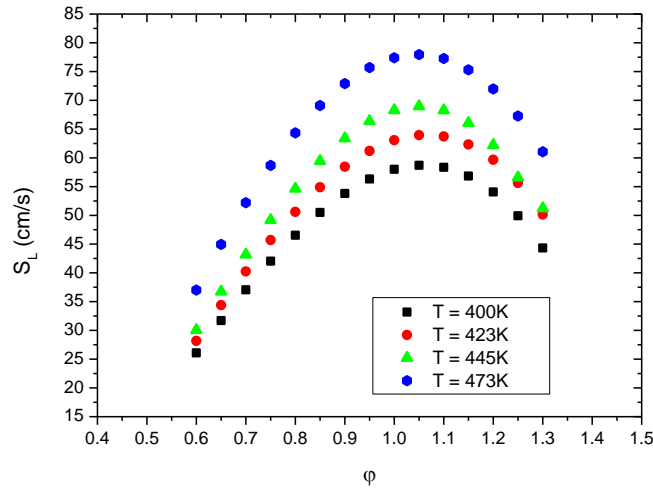


Figure 6.20: Laminar flame speed of Jet A-1/N<sub>2</sub>/O<sub>2</sub> with temperature variation,  $T = 400$  K, 423 K, 445 K and 473 K with  $\phi = 0.6 - 1.3$ ,  $P = 0.1$  MPa.

Influence of the preheating temperature on the flame speed of Jet A-1/N<sub>2</sub>/O<sub>2</sub> mixtures was also investigated. Measurements were performed for the temperature range 400 - 473 K at atmospheric pressure. Results are plotted in Figure 6.20. The general tendency of the effect of preheating temperature on the laminar flame speed is in accordance with theoretical predictions, i.e. the laminar flame speed increases in function of the preheating temperature. The temperature dependence can be then expressed by plotting the laminar flame speed as a function of the preheating temperature using log-log scales. As

shown in Figure 6.21, this temperature dependence is depicted by a straight line for all the equivalence ratios tested.

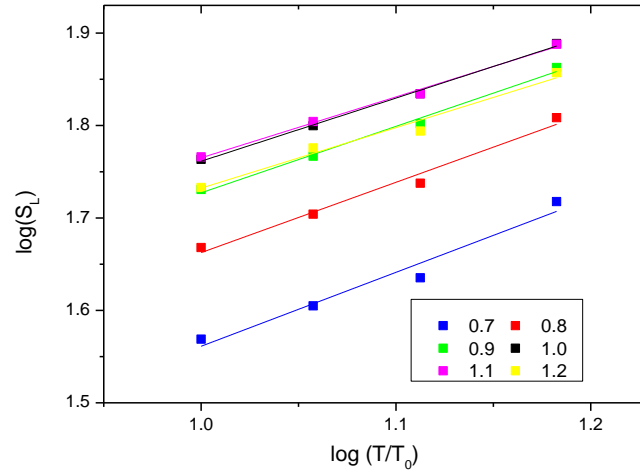


Figure 6.21: Log-Log plot of laminar flame speed of Jet A-1/N<sub>2</sub>/O<sub>2</sub> at atmospheric pressure and different preheating temperatures. Symbols are the experiments; lines are linear fits.

A temperature dependence of the laminar flame speed is then proposed for the equivalence ratios tested by using the aforementioned equations (5.5) and (5.6), where  $S_{L0}(\varphi)$  is defined as the laminar flame speed at  $T = 400$  K and  $P = 0.1$  MPa. The resulting parameters for  $S_{L0,i}$  and  $\alpha_i$  are listed in Table 6.3.

$S_{L0,\varphi=1}$	58.001	$\alpha_0$	1.654
$S_{L0,1}$	24.075	$\alpha_1$	-0.5547
$S_{L,2}$	-192.32	$\alpha_2$	-1.08
$S_{L,3}$	-132.8	$\alpha_3$	2.9718

Table 6.3: Correlation parameters  $S_{L0,i}$  and  $\alpha_i$  in equation 5.5 and 5.6.

#### (b) Pressure dependence

The pressure dependence of the laminar flame speed was investigated at  $T = 423$  K and  $\varphi = 0.7 - 0.8$ . Measured laminar flame speed for pressure ranging from 0.1 to 0.8 MPa are shown in Figure 6.22 using a logarithmic scale. Apart from the experimental data represented by symbols, lines are included to show the best fits to Eq. 5.5. The derived power exponents  $\beta$  are:  $\beta_{\varphi=0.7} = -0.235$  and  $\beta_{\varphi=0.8} = -0.198$  demonstrating that for lean conditions, the larger the pressure, the lowest the exponent power is.

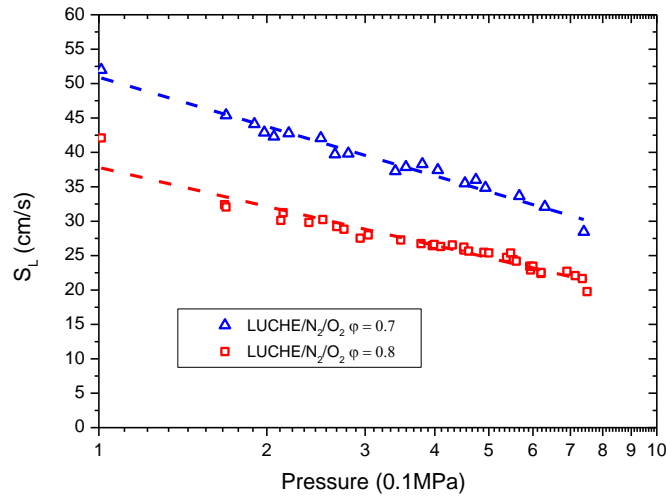


Figure 6.22: Evolution of the laminar flame speed of Jet A-1/ $N_2/O_2$  mixture versus pressure.  $T = 423$  K,  $\phi = 0.7$  and  $0.8$ . Points are our measurements and dash lines are the linear fits.

### 6.5.3 Comparison between LUCHE surrogate and Jet A-1 fuels

Comparison between the laminar flame speeds of Jet A-1 and the LUCHE surrogate for various conditions of preheating temperature and pressure are presented in Figure 6.23. Measurements reported on this graph were performed at  $T = 400$  K,  $P = 0.1$  MPa and  $\phi = 0.6 - 1.3$ . The evolution of the laminar flame speed of the LUCHE surrogate is in excellent agreement with the flame speeds of Jet-A1 for lean conditions. For rich mixtures, i.e.  $\phi > 1.1$ , the surrogate LUCHE gives faster laminar flame speed values compared to the commercial jet fuel. This difference may reach a maximum of 5 cm/s at  $\phi = 1.3$ . This result is in accordance with previous investigations [16] explaining that the surrogate fuel normally gives higher values compared with real commercial jet fuels. The LUCHE is also in good accordance with our measurements. Minor deviations are however observed for lean mixtures while a good prediction of measurements is noted for rich mixtures.

Figure 6.24 presents the effect of pressure on the laminar flame speeds of both fuels. Measurements reported on this graph were performed at  $T = 423$  K and for two equivalence ratios,  $\phi = 0.7$  and  $0.8$ . Results show that the LUCHE surrogate and Jet-A1 fuels present certain stunning pressure dependence similarities whatever the investigated equivalence ratios. By contrast, the model underpredicts the measurements but the qualitative dependence of pressure is properly covered.

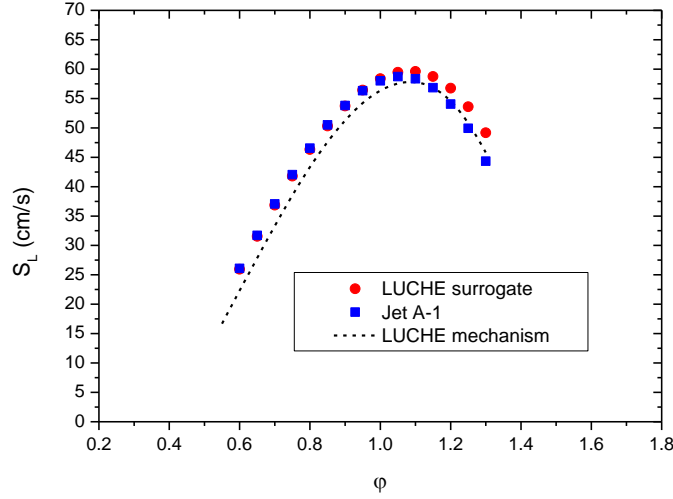


Figure 6.23: Comparison between laminar flame speed of LUCHE surrogate fuel and Jet A-1. Symbols are the measurements; dashed line is the prediction of the LUCHE model.

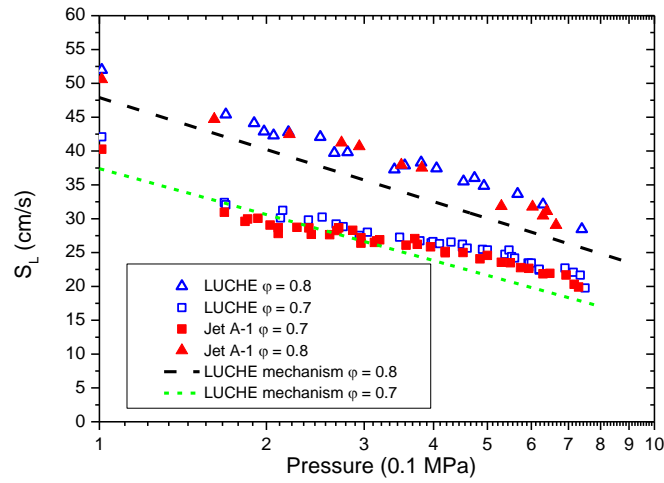


Figure 6.24: Comparison between laminar flame speeds of LUCHE surrogate and Jet A-1 in function of pressure. Symbols are our measurements; line is the prediction of the LUCHE model.

## 6.7 Conclusions

Laminar flame speeds of Jet-A1 and LUCHE surrogate have been studied in this chapter. Firstly, the benefits and limitations of the different optical techniques able to measure the laminar flame speeds of heavy hydrocarbons fuels have been quantitatively investigated. It has been confirmed that the use of the frontier delimiting the maximum OH\* chemiluminescence intensity leads to a significant underestimation of the laminar flame speeds (up to 25%). By contrast, the frontier delimiting the consumption of fresh gases with aromatics-PLIF and the “inner” frontier visualized from the Abel transform of OH\*

chemiluminescence images offer good experimental potentialities to accurately determine the laminar flame speeds.

Laminar flame speed measurements are then conducted for various pure compounds entering in the kerosene composition. It includes n-decane, n-propylbenzene and n-propylcyclohexane. Then, measurements on a specific mixture of these molecules (referenced as the LUCHE surrogate) were performed. Finally, this study was focused on the determination of laminar flame speeds of the commercial Jet A-1. All the measurements were performed over a wide range of preheating temperature, pressure and equivalence ratio conditions.

Concerning the pure compounds, n-decane presents slightly higher laminar flame speeds compared to those measured with n-propylbenzene and n-propylcyclohexane. Nevertheless, the deviations of laminar flame speeds observed between these compounds are so small that a mixture of these molecules with adequate concentrations is able to well reproduce the evolution of the laminar flame speeds of the commercial Jet A-1 fuel. Therefore, the mixture composition of the LUCHE surrogate that was initially proposed to develop a detailed chemical mechanism of kerosene gives remarkable similarities with the measured laminar flame speeds of Jet-A1. These results indicate that the LUCHE surrogate is off to a very good start to reproduce experimentally the combustion properties of the commercial Jet-A1 fuel. By contrast, the LUCHE detailed kinetic mechanism slightly underpredicts the laminar flame speeds of the LUCHE surrogate and practical Jet-A1 fuels whatever the range of pressure studied. A refinement of this model should be recommended in the future.

## **Chapter 7 Laminar flame speed of biofuels containing oxygenated compounds**

---

Laminar flame speeds of various commercial gasoline and bio-gasoline fuels are investigated in the Bunsen flame configuration using the methodology developed and validated in the precedent chapters. Specific efforts were oriented towards the effect of oxygenated molecules in biofuels derived via based-catalyzed depolymerization of lignin or fast pyrolysis. Predictions of the impacts of these oxygenated molecules for biofuel combustion are compared and discussed in the light of available experimental results.

## 7.1 Introduction and objectives

Despite the recent crises in the world economy and the uncertainties in the future perspective, the world global energy demand is expected to increase by almost 30% in 2040 as compared to 2010. Combustion processes account for more than 90% of the energy conversion on earth. Fossil fuels are still carrying over 80% of the energy involved in these combustion systems. The International Energy Agency (IEA) foresees that the share of fossil fuels in the global primary energy consumption tends to slightly decrease (except for natural gas) while renewable energy technologies will increase significantly. In this scenario and despite the large uncertainties about effective fossil resources, the GHG emissions associated with fossil fuel combustion motivate intense research on alternative fuels and on clean (low emissions of NO<sub>x</sub>, soot, unburnt HC and CO) and efficient (low fuel consumption) combustion processes.

Among the candidates for partial replacement of fossil fuels are the biofuels, and particularly the biofuels of second generation based on lignocellulosic biomass that do not compete with the food industry. Among the production routes currently proposed to transform solid biomass into liquid fuels, the base-catalyzed depolymerization of lignin [119] [188] or thermochemical pyrolysis [121] [189] [190] processes become mature technologies. However, the produced “bio-oils” contain large amounts of oxygen in their molecular constitution [up to 45 wt %]. To ensure their stability and allow their blending and co-processing with fossil oil, a pre-treatment is required to remove a large fraction of oxygen while starting their conditioning for refining operations. One of the promising co-processing routes explored till now in conventional refineries is to treat bio-oils together with crude oil distillates by FCC (Fluid Catalytic Cracking) to obtain a gasoline containing a fraction of bio-carbon meeting the international objectives fixed to about 10-20% at horizon 2020. This “hybrid” gasoline has different specifications than “fossil” gasoline, since it contains oxygen molecules (few percent, depending on process conditions) mainly from phenolic or similar types as well as larger amount of aromatics and olefinics. The presence of these impurities might have important consequences for the combustion step. From preliminary studies it appears that oxygenated compounds decrease the soot formation of diesel engine but enhance the CO and NO production whereas the effect on combustion efficiency depends on the oxygen content. For gasoline engine, it can be foreseen that increasing the aromaticity of these hybrid fuels will impact the combustion efficiency as compared to standard gasoline. However, no rationalization of these effects with the nature and amount of impurities is presented in the literature as well as information for gasoline engine. In addition, no data is given about the formation of new potentially toxic molecules, whereas oxygenated pollutant like formaldehyde (cancerigenic) are regulated in California and will be probably soon regulated in Europe. Similarly, GHG emissions effect is much more harmful for aldehydes than for methane (acetaldehyde and formaldehyde are 320 and 457 times more harmful than methane for ozone destruction, respectively).



To understand the associated combustion mechanism and to identify recurring reaction patterns, it is important to study prototypical variants of potential biofuels. In this regard, examining the kinetic mechanisms including fuel decomposition and oxidations mechanisms of different types of pure oxygenated molecules found in true biofuels or blend of biofuels in which various concentrations of oxygenated molecules are included is a valuable step towards understanding the reacting pathways guiding their consumption. In the public discussion, the term biofuels is often referred to the association of few molecular oxygenated molecules such as ethanol for bio-gasoline and large methyl esters for bio-diesel fuels (biofuels of first generation). Therefore, numerous experiments were addressed in the past to study the effects of blends of gasoline with ethanol or butanol and blends of diesel with esters to the laminar flame speeds [28] [127] [128] [33] [34] [35] [29]. However, others biofuels issued from biomass, especially those derived from biofuels of second generation where large quantities of sustainable lignocellulosic biomass are used as feedstocks, are rarely discussed. Compared with biofuels of first generation, biofuels of second generation derived from biomass show attractive advantages as it solved the problem of low productivity of today's crops-based biofuels, as well as the potential competition with the global food supply. These oxygenated compounds found in upgraded biomass pyrolysis oils are typically high molecular weight fuels with carbon number varying from  $C_5$  to  $C_{11}$  which have higher boiling points compared to alcohol molecules.

This chapter is intended to investigate the laminar flame speed of oxygenated compounds contained in upgraded biomass pyrolysis oil and the role of the addition of these oxygenates on the laminar flame speeds. Of course, it is outside of the scope of this chapter to describe all the respective effects of oxygenated molecules on combustion. Only some selected oxygenated molecules contained in "true" biomass fuels will be studied in the present study. The main objectives of this chapter are the followings:

- A surrogate bio-gasoline fuel referenced to a commercial gasoline fuel without any oxygenates is firstly proposed. Laminar flame speed of this surrogate gasoline fuel was measured over a large range of conditions including temperature, pressure and equivalence ratio. Comparison between laminar flame speeds of both fuels were further carried out to validate that the proposed composition of the surrogate fuel can successfully reproduce the flame speed properties of a commercial gasoline fuel.
- A study of the laminar flame speeds of several single oxygenated molecules was then undertaken. Anisole, 4-methyl-anisole and ethyl valerate were selected to understand the effect of their chemical structure on possible modifications of laminar flame speed.

- Finally, laminar flame speed of the proposed surrogate gasoline with addition of different percentages of the selected oxygenate were then measured over a large range of operating conditions including equivalence ratio, temperature and pressure.

## 7.2 Commercial and surrogate gasoline fuels

As the commercial gasoline fuel consists of hundreds or thousands chemical components and its composition varies among the different sites of production, a quantitative understanding of the role of the species composition on the laminar flame speed properties is still complex to perform for the wide range of operating conditions generally investigated. To reduce these constraints, the definition of a surrogate gasoline fuel can be then carried out to successfully reproduce the properties of commercial gasoline fuel with a limited number of molecules such as the distillation curves, research octane number (RON), laminar flame speed ...


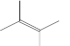
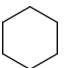

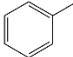
	Volume (%)	Formula	Boiling point (°C)	Density (kg/m <sup>3</sup> )	
Hexane	24.31	C <sub>6</sub> H <sub>14</sub>	69	660.4	
2,3 dimethyl-2-butene	8.15	C <sub>6</sub> H <sub>14</sub>	72	669.4	
Cyclohexane	14.21	C <sub>6</sub> H <sub>12</sub>	80	771.1	
Isooctane	17.75	C <sub>8</sub> H <sub>18</sub>	99	687.2	
Toluene	35.58	C <sub>7</sub> H <sub>8</sub>	110	861.9	

Table 7.1: Composition of surrogate gasoline proposed in the present work

Generally, the chemical compounds of typical European gasoline fuels can be separated in six molecular families, each having a carbon number ranging mainly from 4 to 10. They are linear alkanes (n-paraffins), branched alkanes (iso-paraffins), ethers, cyclic alkanes (naphthenics), alkenes (olefins) and aromatic compounds [8]. However, a surrogate fuel must be composed by a limited number of components if accurate detailed kinetic models have to be developed and validated. Moreover, a surrogate fuel with many compounds could yield to misleading or inaccurate predicted simulations. According to the literature, various surrogate gasoline fuels and primary commercial gasoline reference fuels are proposed and studied concerning to laminar flame speed measurements over a large set of conditions such as temperature, pressure and equivalence ratios [128] [191] [89] [13] [192] [193] [194]. However, published data of the laminar flame speed are not always consistent with one another and the spread of the measured values often exceeds the reported experimental uncertainty, even for the primary reference pure

component fuel which is investigated thoroughly like iso-octane and n-heptane. Laminar flame speed measurements must still be improved and the effect of temperature, pressure and equivalence ratio on flame speed has to be investigated in further details.

Hereby, we proposed a surrogate bio-gasoline to match the commercial gasoline. This work was carried out with the help of researchers of the LCS (Laboratory de Catalyse et de Spectrochimie) of Caen (France). The methodology used to define the surrogate fuel was the following. First, a reference commercial gasoline retained for the present study was analysed. Results of these analyses have shown that this gasoline fuel is composed of 57% of alkanes, 8% of olefins and 35% of aromatics compounds. From this chemical composition, a determination of the proportions of compounds was then performed in order to match experimental data such as distillation curve of the commercial fuel; this kind of data is a classical lab analysis and is generally available without any difficulty. The best agreement has consisted of using only five pure compounds: hexane, 2, 3 dimethyl-2-butene, cyclohexane, iso-octane and toluene with an averaged formula of  $C_{6.6672}H_{11.6045}$ . Fractions of alkanes and aromatics compounds (i.e. toluene in the current study) were closed to those mainly present in the commercial gasoline fuel. The resultant RON calculated from the works of N. Morgan et al. [195] and P. Ghosh et al. [196] was estimated to 94.2. Physical properties and species composition of the studied compounds are listed in Table 7.1.

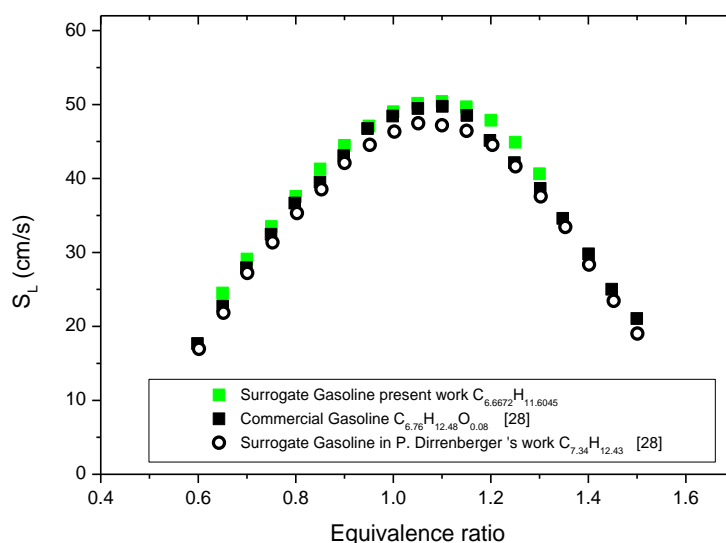


Figure 7.1: variation of the laminar flame speeds of our surrogate gasoline, commercial gasoline and surrogate gasoline referenced in [28] in function of the equivalence ratio.  $P=0.1$  MPa.

Measurements of laminar flame speeds were initially recorded at 358 K and  $P=0.1$  MPa and then compared with data measured on the commercial gasoline and surrogate gasoline fuels studied in the following reference [28]. For information, the commercial gasoline fuel studied in the reference work was provided by TOTAL (Ref. IFPen: TAE7000) with an estimated RON of 95.6 which is close with that of our surrogate fuel. Chemical analysis of this gasoline fuel gives a composition of 10.5 % of n-alkanes,

40.7% of iso-alkanes and 32.5% of aromatic compounds. The average molecular formula is then  $C_{6.76}H_{12.46}O_{0.08}$ . The composition of the surrogate fuel defined in the same work to match the properties of the TAE7000 was the followings: 13.7% n-heptane, 42.9% iso-octane and 43.4% of toluene and the average chemical formulae was  $C_{7.34}H_{12.43}O_{0.00}$ . A RON of 98.1 was then estimated.

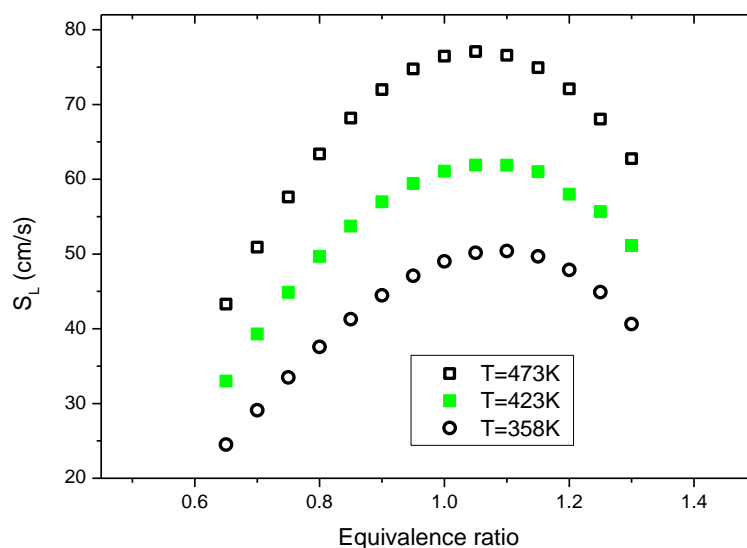


Figure 7.2: Evolution of the laminar flame speed of our surrogate fuel in function of the equivalence ratio for three preheating temperatures: 358 K, 423 K and 473 K.  $P = 0.1$  MPa.

Figure 7.1 displays the measurements recorded for the three fuels. Very close agreement between laminar flame speeds are observed for the complete range of the investigated equivalence ratio. Despite the similarity between the average chemical formula of the commercial gasoline and our surrogate fuel, a slight overestimation of our measurements was observed for equivalence ratio between 1.1 and 1.3. This difference could be attributable to the air composition used in our work which is 20%  $O_2$  and 80 %  $N_2$ . This air mixture is indeed slightly different from the air mixture, 21 %  $O_2$  and 79 %  $N_2$  used in the referenced work [28]. This decrease of  $O_2$  into the fuel/air mixture probably leads to a deviation of the peak of laminar burning velocity with equivalence ratio. Moreover, a systematic underestimate of laminar flame speeds between the surrogate fuel referenced in [28] and our surrogate fuel was also observed whatever the equivalence ratio. Considering that the discrepancies between laminar flame speeds are tiny ( $\sim 3$  cm/s at  $\phi=1.2$ ) but comparable to the measurement accuracy (see chapter 4), the proposed surrogate gasoline fuel in the present work is a good support to reproduce the laminar flame speeds of commercial gasoline fuels.

The effect of the preheating temperature on the laminar flame speed of our surrogate fuel was then complimented by performing additional measurements at two higher temperature conditions: 423 and 473

K. Results presented in Figure 7.2 resumes the variation of the preheating temperature on the laminar flame velocity of such surrogate fuel.

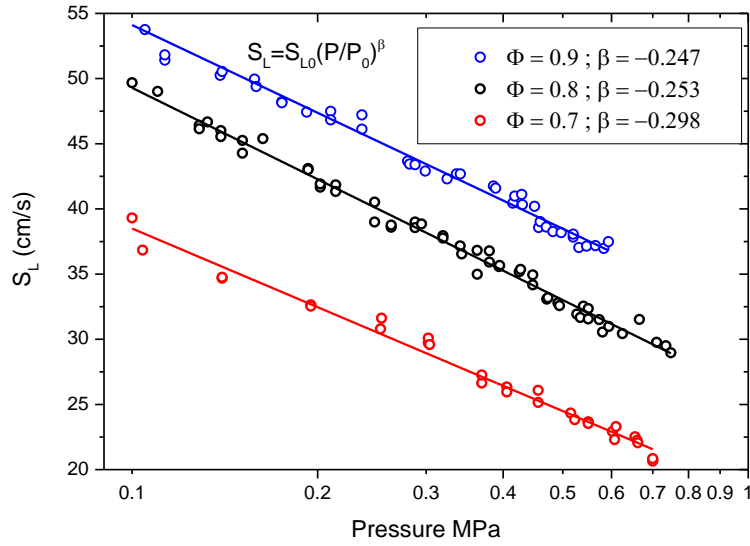


Figure 7.3: Variation of the laminar flame speeds of our surrogate gasoline in function of pressure.  $P = 0.1 - 0.8$  MPa  $\phi = 0.7, 0.8$  and  $0.9$  and  $T = 423$  K

Finally, laminar flame speed measurements were performed for various pressures ranging between 0.1 and 1.0 MPa. The equivalence ratios investigated are in the range 0.7-0.9. The preheating temperature is fixed at  $T = 423$  K. The measured flame speeds are plotted in Figure 7.3. As originally intended, the flame speed decreases linearly with logarithmic pressure. From these results, the flame speed pressure dependence using power law was calculated and the  $\beta$  coefficient values of - 0.247, - 0.253 and - 0.298 corresponding to equivalence ratio of 0.9, 0.8 and 0.7 were found. The higher the equivalence ratio, the larger the sensitivity with the pressure is.

### 7.3 Oxygenated fuels

This section is dedicated to investigate the effect of the addition of oxygenates on the laminar flame speeds of biofuels derived via catalytic or pyrolysis conversion process of lignin or cellulose. However, these biofuels contain numerous oxygenated compounds that are difficult to remove but potentially impact the ability of these fuels to be used as drop-in replacements for existing petroleum-based fuels. Accordingly, biofuels derived from these conversion processes must go to sophisticated processes to remove parts of these oxygenated compounds and produce ideally fuels that contain only hydrocarbons molecules. Unfortunately, these processes lead to an upgrading of costs and to a limitation of producing market-competitive fuels. To obtain economically desirable fuels, the solution consists of the production of biofuels with a limited fraction of oxygenated compounds in the final fuel composition. Of course, to

be technically viable, this approach requires that the presence of these oxygenated compounds does not affect the combustion properties of fuels and so the operation of existing engines. To this end, the present work was to select some of the oxygenated compounds present naturally in biofuels and to study separately their combustion performances. The oxygenated molecules retained are the followings: anisole, 4-methy-anisole and ethyl-valerate. Laminar flame speeds of these compounds were then compared and discussed in this section.

### 7.3.1 Selection of oxygenates

According to the work reported by Talmadge et al. [121] residuals that remain after hydro-processing of a bio-crude are presented in Figure 7.4. They contain a significant amount of reactive, oxygenated species including organic acids, esters, aldehydes, alcohols, ketones, furans, sugars, phenolics and oxygenated aromatics. These oxygenated species present significant challenges that will undoubtedly require pre-processing of a pyrolysis-derived stream before the pyrolysis oil can be integrated into the existing refinery infrastructure. In case of gasoline fuels issued from biomass pyrolysis, the oxygenated molecules contained in the fuel are distributed on the gasoline distillation curve in function of their boiling points.

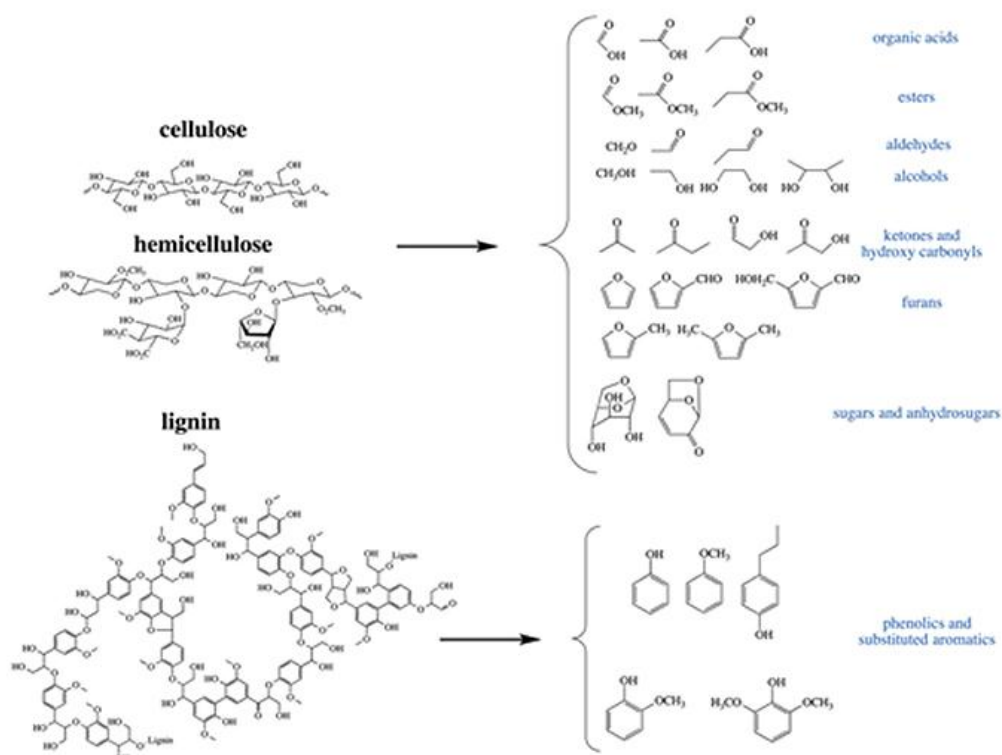


Figure 7.4: Residuals remaining after hydro-processing of a bio-crude

Figure 7.5 shows the main oxygenated molecules able to cover the gasoline boiling-point range. Furan molecules (2, 5-dimethylfuran, methyltetrahydrofuran and 2-methylfuran) are located in the light fuel fraction. These compounds have been extensively studied in the past and numerous studies reported in the

literature can be found [197] [198] [199]. For instance, the work reported by Ma [199] shows measurements of laminar flame speed of 2-methylfuran and isooctane blends fuels at various preheating temperatures and equivalence ratios. Wu and al. [198] measured the laminar flame speed of a 2, 5-dimethylfuran/air mixture at elevated pressures over a wide range of equivalence ratio. Oxygenated compounds such as anisole, 2-hexanone, phenols or ethyl valerate are covering the 120-180°C temperature range characteristic of the medium fuel fraction. Oxygenated molecules having boiling points larger than 180°C including 2, 4-xyleneol, 1, 2-dimethoxybenzene, guaiacol, p-cresol or 4-propylanisole covers the heavy fuel fraction.

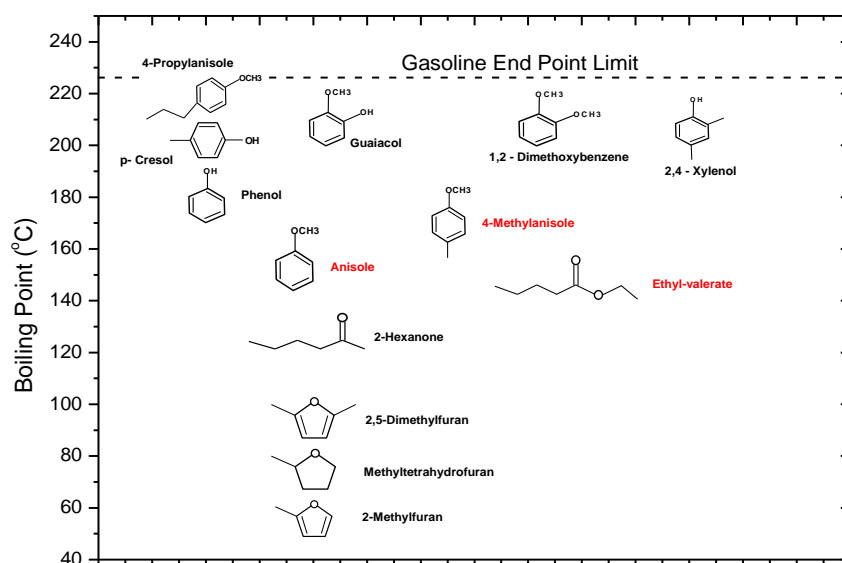


Figure 7.5: Oxygenates distribution in function of the boiling point in a gasoline composition

As furan molecules were the subject of numerous well documented studies about laminar flame speeds, these molecules were not investigated in the current work [197] [198] [199]. Molecules belonging to the heavy fuel fraction were also not investigated in regards to their high boiling points that complicate their evaporation in our combustion facility. So, efforts were focused in the current study on molecules contained in the medium fuel fraction. In particular, the oxygenated residual components from upgraded pyrolysis oil selected here are the molecules plotted in red in Figure 7.5: anisole, 4-methy-anisole and ethyl valerate. The others molecules contained in the medium fuel fraction were not studied because of their molecular properties and their toxicity requiring extreme conditions of safety during their manipulations. Details of their physical properties of these oxygenates are listed in Table 7.2. Anisole and 4-methylanisole (i.e. methyl aryl ethers) have been chosen because they appear to be the best drop-in fuel components for gasoline because they significantly increase research octane number (RON) and slightly reduce vapor pressure without significant negative fuel property effects [123]. Therefore, mixing of gasoline with these methyl aryl ethers will provide a fuel with a higher octane rating which will be less prone to auto-ignition and will be able to support a greater rise in temperature during the compression

stroke of an internal combustion engine without auto-igniting, thus allowing more power to be extracted from the Otto-Cycle. The interest of ethyl valerate comes from the progresses in biomass processing which have made lignocellulose more attractive for the production of liquid biofuels. Indeed, levulinic acid obtained from lignocellulose can be converted into esters by hydrogenation and esterification. As for anisole and 4-methylanisole, this molecule has an elevated RON ( $\sim 100$ ). The use of blends of ethyl valerate with gasoline shows a favorable increase in octane number (RON) without deterioration of properties such as corrosion and gum formation. Ethyl valerate blending also increases the gasoline density and oxygen-content, reduces its volatility and lowers its content of aromatics, olefins and sulfur [200]. As a prime benefit of the use of ethyl valerate blends, modern cars will be able to use valerate biofuels without any modification to their motor engines.

Fuel	Formula	Boiling point (°C)	Density (kg/m <sup>3</sup> )	RON
Anisole	CH <sub>3</sub> OC <sub>6</sub> H <sub>5</sub>	155	660	119
4-methylanisole	C <sub>8</sub> H <sub>10</sub> O	174	669	> 130
Ethyl valerate	C <sub>7</sub> H <sub>14</sub> O <sub>2</sub>	145	875	$\sim 100$

*Table 7.2: Oxygenates properties*

### 7.3.2 Laminar flame speeds of pure oxygenates

Measurements of laminar flame speed of pure oxygenated fuels were performed to obtain a good understanding of the effects of the molecular structure and oxygen content on the resultant laminar flame speeds. As presented in Figure 7.6, laminar flame speed of anisole/N<sub>2</sub>/O<sub>2</sub>, 4-methyl-anisole/N<sub>2</sub>/O<sub>2</sub> and ethyl-valerate/N<sub>2</sub>/O<sub>2</sub> mixtures at T=423 K are presented. Whatever the equivalence ratio, it can be observed that 4-methylanisole and ethyl-valerate fuels have similar laminar flame speeds values while the laminar flame speed of anisole is always higher compared to that of 4-methylanisole and ethyl-valerate. However, the maximum deviation between the different laminar speeds values is up to 5 cm/s when approaching stoichiometric conditions.



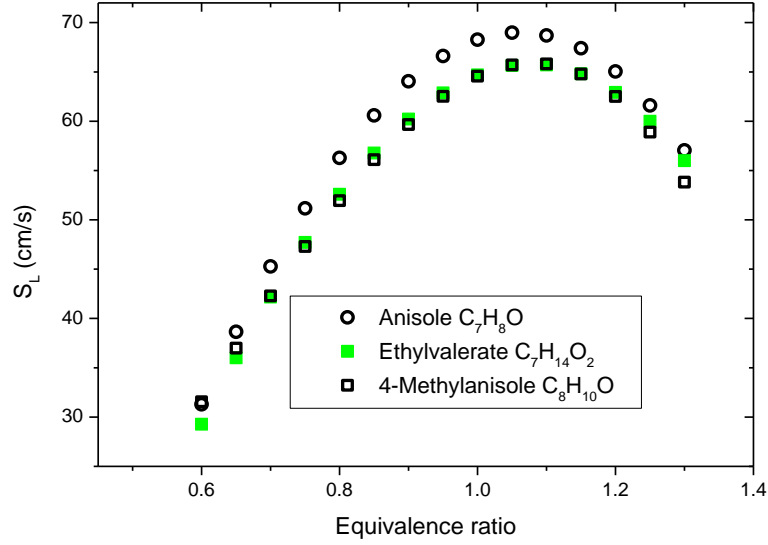


Figure 7.6: Laminar flame speeds of anisole/ $N_2/O_2$ , 4-methylanisole/ $N_2/O_2$  and ethyl valerate/ $N_2/O_2$  mixtures at  $T = 423\text{ K}$ ,  $P = 0.1\text{ MPa}$  and  $\phi = 0.6 - 1.3$

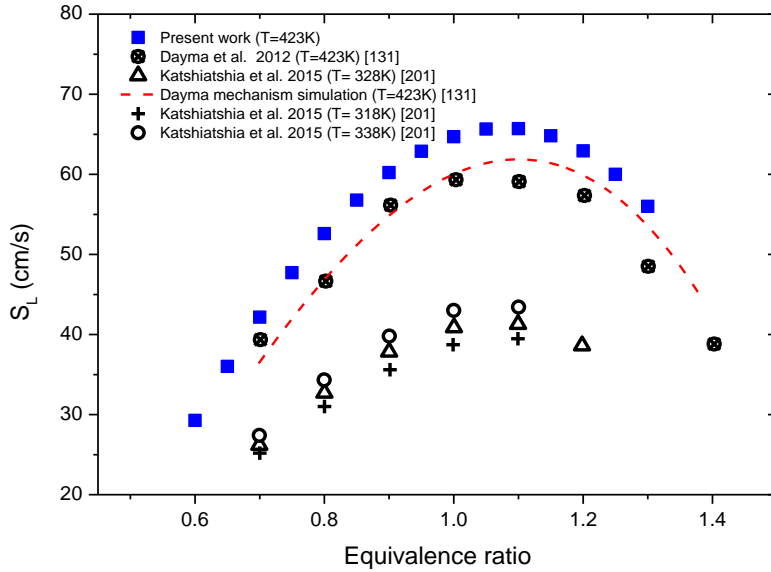


Figure 7.7: Comparison of laminar flame speeds of ethyl valerate/ $N_2/O_2$  mixtures between our measurements and literature results [131] [201].

Figure 7.7 displays the obtained results for ethyl valerate with the few data found in literature. Our measurements are first compared with the results reported by Dayma et al. [131] who performed measurements of laminar flame speeds at the same operating conditions. The present work gives general faster flame speeds for all the investigated equivalence ratio conditions with a maximal difference of 7 cm/s when approaching the stoichiometry condition. Meanwhile compared to the literature experimental results, our experimental results are more approaching to the simulation results proposed by Dayma et al. [131] especially at lean and rich sides. Also plotted in Figure 7.7 are the recent data recorded by

Katshiatshia et al. [201]. Although these measurements were performed at lower preheating temperatures, the representation of the variation of the laminar flame speeds of ethyl valerate with equivalence ratio for various preheating temperatures highlights the sensitivity of temperature on laminar flame speeds in the temperature range 318 – 423 K.

#### 7.4 Effect of the addition of oxygenates on the laminar flame speeds of surrogate gasoline

It has been shown in section 7.2 that our surrogate reference fuel is appropriate to have similar combustion characteristics to gasoline in practical conditions. For a better clarity, this surrogate will be referenced in the following as SA0. In a first step, mixtures of SA0 with different amounts of oxygenates were prepared in two groups. The first group consists of the mixture of constant percentages of the five compounds (isooctane, hexane, cyclohexane, 2,3 dimethyl-2-butene, toluene) used to represent SA0, while the volume fraction of oxygenates are varied. Using this approach, the RON value of the resultant mixtures ranges from 94.2 to 119. The second group allows for a substitution of the percentage of toluene by the same percentage of anisole with a RON varying from 94.2 to 94.3. Details of the mixture compositions investigated are given in Table 7.2. To simplify the experiments, only anisole has been added in SA0 in regards to the strong similarities observed on laminar flame speeds for the different oxygenated already investigated.

Mixture	Hexane (%)	2,3 dimethyl-2- butene (%)	Cyclohexane (%)	Isooctane (%)	Toluene (%)	Anisole (%)	Estimated RON
SA0	24.31	8.15	14.21	17.75	35.53	0	94.2
SA10	21.88	7.35	12.8	15.98	31.98	10	97.8
SA20	19.45	6.52	11.37	14.2	28.42	20	100.1
SA30	17.02	5.71	9.95	12.43	24.87	30	102.8
SA50	12.16	4.08	7.11	8.88	17.77	50	107.7
SA75	6.08	2.04	3.55	4.44	8.88	75	113.2
SA100	0	0	0	0	0	100	119
ST0	24.31	8.15	14.21	17.75	0	35.53	94.3

Table 7.2: Compositions of fuel mixtures by liquid volume

In order to study the influence of the addition of oxygenates on the laminar burning velocities of SA0, measurements have been made for mixtures of SA0 containing various fraction of anisole varying from 0 to 100 %. The use of a large range of anisole concentration was dictated on the basis to get a wide variation of the laminar flame speeds but also that the RON value can vary over a large domain

(estimation between 94.2 and 119). The comparison of the laminar flame speeds in function of the equivalence ratio is shown in Figure 7.8. In these experiments, measurements were conducted at atmospheric pressure and a preheating temperature of 423 K. In general, the laminar flame speed increases with the percentage of anisole contained into the mixtures whatever the equivalence ratio. The peak value of laminar flame speeds for each mixture is located at  $\phi=1.1 - 1.2$  with a variation of the peak value of about 15%. In order to get a better understanding, the aforementioned results were reported in function of the percentage of anisole as shown in Figure 7.9. A linear variation of the laminar flame speed with the percentage of oxygenates is then observed and the slope of this variation is similar for each equivalence ratio. Note however that the slope at  $\phi=1.1-1.2$  appears to be slightly higher than for the other equivalence ratios.

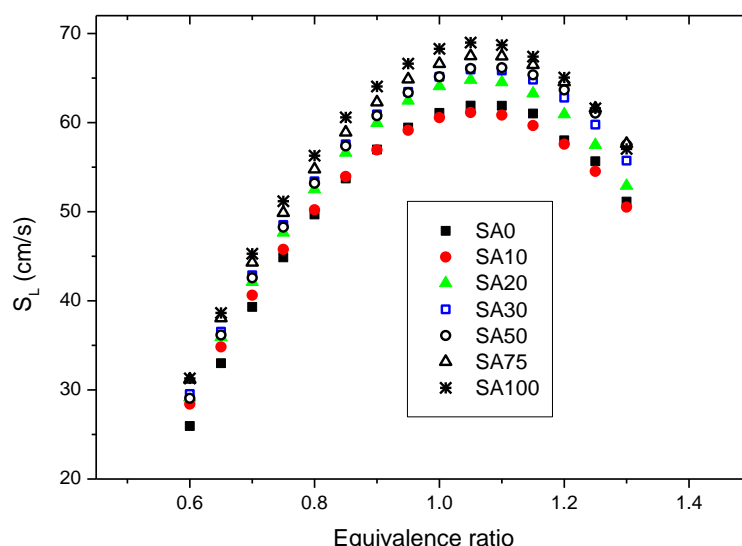


Figure 7.8: Laminar flame speed of the SA0, SA10, SA20, SA30, SA50, SA75 and SA100 surrogates.  $T = 423\text{ K}$ ,  $P = 0.1\text{ MPa}$  and  $\phi = 0.6 - 1.3$

For a practical view of combustion in engines, and considering that the content of oxygenates in a biofuel of second generation can reach a maximum level of 40%, the resultant laminar flame speeds can potentially increase of a maximum value of  $\sim 2-3\text{ cm/s}$ . Note also that the laminar flame speed of bio-gasolines with a maximum percentage of 10% of oxygenates will be relatively insensitive to the quantity of oxygenates and so, will not modify the combustion efficiency of an internal combustion engine. As the RON value increases in function of the amount of oxygenates, the increase of the laminar flame speed could be also used to promote combustion with higher flame speeds while not sacrificing the octane rating as shown in Figure 7.8.

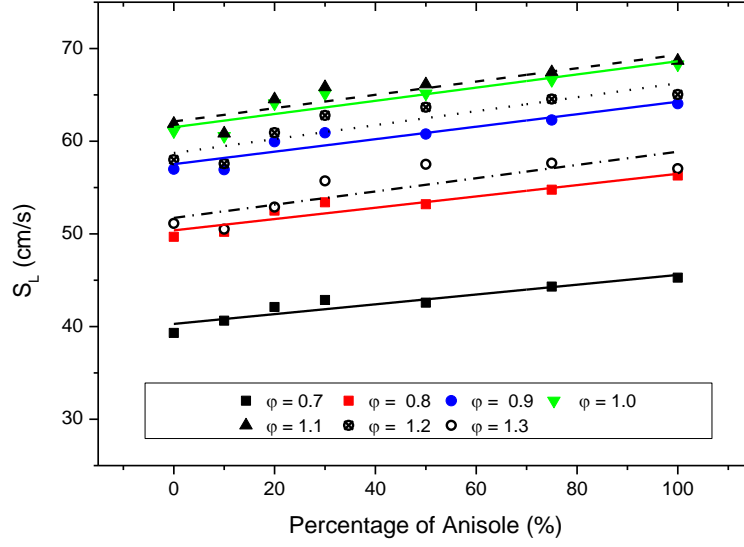


Figure 7.9: Variation of the laminar flame speed of the mixture in function of the anisole fraction:  $T = 423 \text{ K}$ ,  $P = 0.1 \text{ MPa}$  and  $\phi = 0.6 - 1.3$  (slope value with linear fittings,  $\phi = 0.7 - 1.3$ , 0.053, 0.061, 0.067, 0.071, 0.072, 0.075, 0.071);

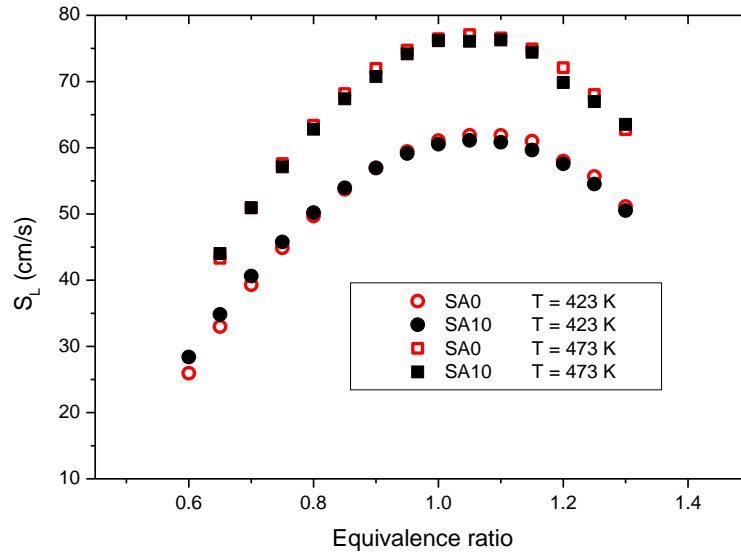


Figure 7.10: variation of the laminar flame speed of the SA0 and SA10 surrogates at two preheating temperatures, 423 and 473 K.  $P = 0.1 \text{ MPa}$ ,  $\phi = 0.6 - 1.3$

Laminar flame speeds of the SA0 and SA10 mixtures, at two preheating temperatures (i.e. 423 and 473 K) are shown in Figure 7.10. Whatever the equivalence ratio, both mixtures exhibit comparable flame speeds for the two preheating temperatures investigated. These results indicate that the effect of the addition of few contents of oxygenates into the reference surrogate gasoline remains similar whatever the preheating temperature.

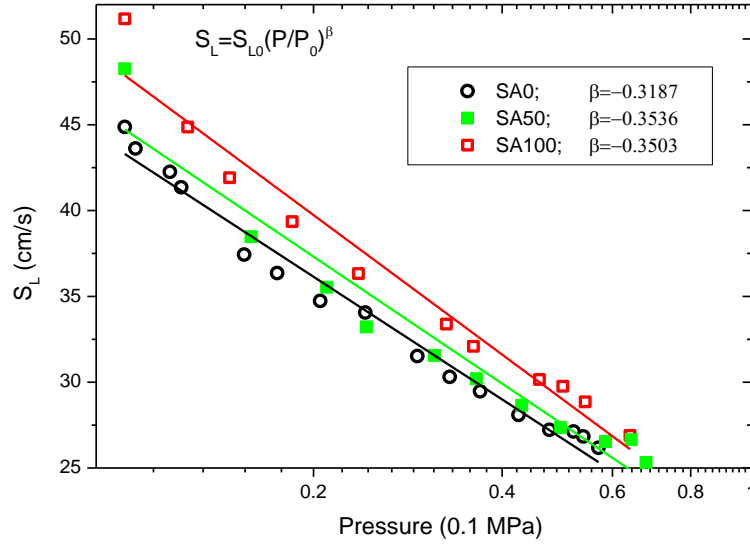


Figure 7.11: Laminar flame speeds versus pressure of reference surrogate gasoline, pure anisole and blend of 50 % surrogate gasoline and 50 % anisole:  $T = 423 \text{ K}$ ,  $P = 0.1 - 0.75 \text{ MPa}$  and  $\phi = 0.75$ .

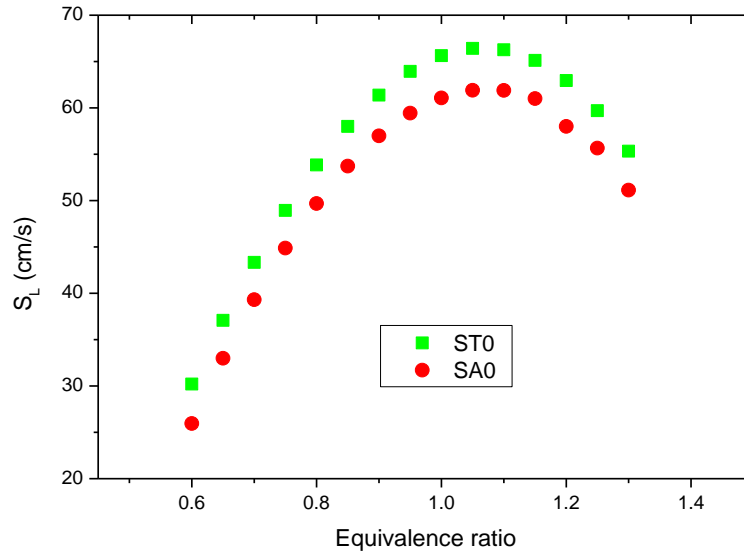


Figure 7.12: Comparison of the laminar flame speeds of the SA0/air and ST0/air mixtures at 423 K and atmospheric pressure.

Finally, the pressure behavior of the laminar flame speeds of the SA0, SA50 and SA100 mixtures were measured and compared in Figure 7.11. As scheduled, the laminar flame speeds for the three surrogates follow power-law pressure dependence as the one expressed in Eq. 5.5. The power exponents obtained with fitting experimental data to Eq. (5.5) are the followings: -0.3187 for the SA0, -0.3503 for SA100 and -0.3536 for SA50 surrogates. Comparison of these exponent parameters shows that even though the existence of a dependence of the pressure parameter with the amount of oxygenates, the effects is meanwhile limited. The larger the concentration of anisole, the larger the pressure dependence on laminar

flame speed will be. Therefore, SA100 surrogate will present a larger sensitivity to the pressure than the observed for the SA0 surrogate.

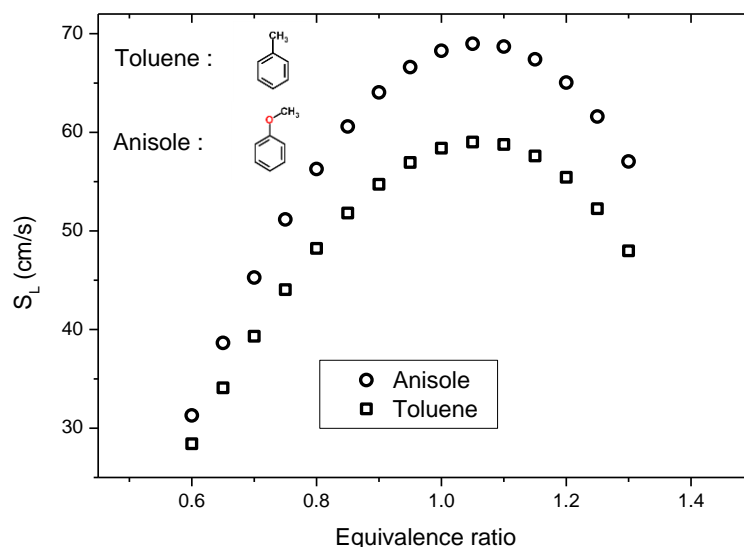


Figure 7.13: Comparison of the laminar flame speeds of anisole and toluene at 423 K and atmospheric pressure.

A final experiment was to study the respective influence of toluene and anisole when added to the SA0 surrogate. To achieve this, the laminar flame speeds of SA0, along with ST0, at 423 K are shown in Figure 7.12. In general, the substitution of toluene by anisole into the same mixture (isooctane, hexane, cyclohexane, 2, 3 dimethyl-2-butene) systematically exhibits faster laminar flame speeds. It is however observed that for lean mixtures, both surrogates tend to the same laminar flame speed while the deviation between both laminar flame speeds is increasing for rich mixtures. The laminar flame speed of SA0 is found to have a peak value of approximately 67 cm/s at  $\phi = 1.1$ , significantly higher than that of toluene, around 60 cm/s. Although these two molecules have typically the same RON value (118 for toluene and 119 for anisole), the increase of the laminar flame speed with addition of anisole (or similar oxygenates) in significant contents would lead to an increase in fuel efficiency and engine performance. This result reflects the combustion properties of anisole which alone displays larger values of the laminar flame speeds compared to the toluene. As proof, Figure 7.13 shows the comparison of the laminar flame speeds of anisole with those of toluene. From these results, it is clear that the evolution of the laminar flame speeds of each compound follows the same tendency than the ones observed when these molecules are included into the SA0 and ST0 surrogates. As the other oxygenates investigated in the present study show similar behaviors to anisole (high RON and laminar flame speeds), It can be concluded that these oxygenates that belong to the methyl aryl ethers or ethyl ester chemical families offers good potentialities to improve the combustion efficiency of modern cars while reducing auto-ignition and knocking effects.

## 7.5 Conclusions

Laminar flame speed measurements of oxygenated compound present in pyrolysis oil dedicated to gasoline were addressed. A five-component surrogate gasoline was firstly proposed and its laminar flame speed was compared with those of surrogate and commercial gasoline referenced in literature. It is found that the surrogate gasoline proposed in the current study has the ability to reproduce the laminar flame speed of commercial gasoline. Then, anisole, 4-methylanisole and ethyl valerate were chosen as oxygenated compounds to study the effect of the addition of oxygenates to gasoline. Laminar flame speed of pure oxygenate fuels were measured in a wide range of operating conditions and results were discussed.

Finally, the aforementioned oxygenates are added to the surrogate gasoline to study the effects of oxygenates on laminar flame speed. It is found that the laminar flame speed generally increases with the addition of oxygenates. However, when the percentage of oxygenates is less than 10%, the laminar flame speed is relatively insensitive. It is also observed that the use of oxygenates at higher concentration could improve the combustion efficiency of modern cars in regards to their capacities to increase laminar flame speeds and to have an elevated RON.

## Chapter 8 Conclusions and future work

---

Nowadays, the major objectives in modern design of technical combustion systems where heat release and species transfer, play a key role are optimization of combustion efficiency and reduction of pollutants. In modern engines, either in the field of power generations systems or in aircraft jet engines, efforts to meet these requirements need to be supported by a profound understanding and an accurate prediction of the complex flow phenomena and interaction mechanisms occurring in the system. Since the combustion behavior of liquid fuels has a strong influence on the engines performances, a detailed knowledge of the associated combustion mechanisms and an identification of the recurring reaction patterns is necessary to obtain. This is true for practical fossil fuels such as gasoline, diesel, and kerosene but also for new renewable fuels issued from biomass. The combustion of these fuels is further complicated by their variables and complex chemical formulation. To study the associated combustion characteristics for such fuels, the development of detailed chemical mechanisms becomes indispensable. However, the validation of such chemical models is a complex task due to the large classes of molecules (e.g. between  $C_1$  to  $C_{12}$ ) playing different roles on their formation and consumption in flames. A useful approach is to use surrogate mixtures of a limited number of molecules able to replicate the physical and chemical characteristics as well as the global characteristics of the practical fuels. The corresponding chemical models and those associated to the pure molecules of mixtures need then to be validated in a wide range of conditions of pressure, preheating temperature and equivalence. One physical parameter required to validate these kinetic mechanisms is the laminar flame speed. The objective of this thesis falls within the framework of these studies and consists of the measurements of laminar flame speeds for pure heavy hydrocarbon molecules, blends of these hydrocarbons and practical multi-component fuels in conditions relevant of those encountered in combustion engines.

The following sections summarize the major accomplishments and results acquired during this thesis.

### 8.1 Summary and conclusions

The present work was oriented towards the following objectives: 1/ develop and validate a specific experimental facility to investigate laminar flame speed measurements using a high-pressure Bunsen flame burner, 2/ Apply various optical measurements to measure laminar flame speeds of fuels including pure hydrocarbons and oxygenates compounds, surrogate kerosene, practical Jet-A1, bio-gasoline and blends of bio-gasoline containing oxygenates. The major achievements of this work are:

- A literature review related to the methodologies of laminar flame speed measurements and their use on various gaseous and liquid fuels was realized. The fuels referenced in this thesis are gaseous  $CH_4$ , liquid acetone, pure compounds of Jet-A1 (n-decane, n-propylbenzene,



propylcyclohexane), LUCHE surrogate, commercial Jet-A1, bio-gasoline, pure oxygenated molecules (anisole, methyl-anisole ethyl valerate) and mixtures of bio-gasoline with oxygenated molecules. This study revealed that there is serious lack of available data for the understanding of the relationship between the laminar flame speeds of these compounds with pressure, preheating temperature and equivalence ratio. Moreover, the published data of the laminar flame speed, when existing, are not always consistent with one another and the spread of the measured values often exceeds the reported experimental uncertainties, even for the primary referenced pure hydrocarbons and oxygenated compounds which are investigated thoroughly.

- A new experimental facility has been specifically developed and applied to investigate laminar flame speeds of gaseous or liquid fuels in high-pressure and elevated preheat temperatures. An axisymmetric premixed burner was designed and developed to generate a steady conical laminar premixed flame stabilized on the outlet of a contoured nozzle in a high-pressure chamber. This facility includes: 1/ a contracting nozzle designed with a fifth-order polynomial to reduce the boundary layer thicknesses by accelerating the flow and providing a flat velocity profile at the nozzle outlet 1/ a high-pressure vessel built with standard stainless-steel materials allowing experiments up to 3.0 MPa; 3/ a heating system allowing the heat of gaseous fuel/air mixtures up to 600 K; 4/ optical accesses with 10 cm clear aperture on three sides. The experimental burner and associated flow controls were designed to operate with gaseous fuel/O<sub>2</sub>/N<sub>2</sub> flows. The gaseous mixture flowing into the burner was produced by a “controller evaporator and mixer” system which guarantees well-defined equivalence ratio of the reactive mixtures studied. The whole system allows generate a stable and a quasi-straight triangle shaped conical flame over a large working condition including equivalence ratio, temperature and pressure. The operating flow conditions inside the high-pressure high-temperature combustion chamber were regulated by mass flowmeters for both phases. Measurements of laminar flame speeds were undertaken by the OH\* chemiluminescence, OH-PLIF, acetone-PLIF and aromatics-PLIF imaging techniques.
- Preliminary measurements of laminar flame speeds of CH<sub>4</sub>/air and acetone/air mixtures were firstly performed over a large range of operating conditions  $T = 300 - 523 \text{ K}$ ,  $P = 0.1 - 1.0 \text{ MPa}$  and  $\phi = 0.6 - 1.3$  to validate the experimental system. The methodologies developed to measure the laminar flame speed from the experimental images recorded with the different optical diagnostics were subsequently analyzed. Therefore, a method to correct the chemiluminescence images of the effect of the flame thickness was specifically elaborated. It was found that the flame thickness, if not known, could have a strong impact on the accuracy of the measurement of laminar flame speed from the data processing of the OH\*chemiluminescence images. It has also been demonstrated that the measurements

recorded with OH-PLIF are slight underestimated compared to those obtained with the previous technique. Furthermore, acetone-PLIF is able to detect an accurate localization of the fresh gases leading to a precise measurement of laminar flame speeds. Measurements of laminar flame speeds on various CH<sub>4</sub>/air mixtures revealed good agreement with data published in the literature; demonstrating the reliability of the new experimental setup in conditions relative to those encountered in combustion engines. Results obtained on acetone/N<sub>2</sub>/O<sub>2</sub> laminar flames also served to the establishment of a new empirical dependence correlation formulation  $S_L = S_{L0}(\varphi)(T/T_0)^\alpha(P/P_0)^\beta$  able to reproduce with accuracy the dependences of pressure, temperature and equivalence ratio on laminar flame speeds. This correlation function also displayed fair agreement with numerical simulations conducted with the Cosilab software using detailed kinetic mechanisms and with experimental results reported in literature.

- Laminar flame speeds of Jet-A1 and LUCHE surrogate have been studied. Firstly, the benefits and limitations of the optical techniques able to measure the laminar flame speeds of heavy hydrocarbons fuels have been quantitatively investigated. It has been confirmed that the frontier delimiting the maximum OH\* chemiluminescence intensity leads to a significant underestimation of the laminar flame speeds (up to 25%). By contrast, the frontier delimiting the consumption of fresh gases with aromatics-PLIF and the “inner” frontier visualized from the Abel transform of OH\* chemiluminescence images offer potentialities to accurately determine the laminar flame speeds. Laminar flame speed measurements are then conducted for various pure hydrocarbon compounds present in the kerosene composition. (n-decane, n-propylbenzene and n-propylcyclohexane). Then, measurements on a specific mixture of these molecules (referenced as the LUCHE surrogate) were performed. Finally, this study was dedicated on the determination of laminar flame speeds of the commercial Jet A-1. All the measurements were performed over a wide range of preheating temperature, pressure and equivalence ratio conditions. About the pure hydrocarbon compounds, n-decane presents slightly higher laminar flame speeds compared to those measured with n-propylbenzene and n-propylcyclohexane. Nevertheless, the deviations of laminar flame speeds observed between these compounds are so small that a mixture of these molecules with adequate concentrations is able to well reproduce the evolution of the laminar flame speeds of the commercial Jet A-1 fuel. Therefore, the LUCHE surrogate composition initially proposed to develop a detailed chemical mechanism of kerosene gives remarkable similarities with the measured laminar flame speeds of Jet-A1. These results indicate that the LUCHE surrogate is off to a very good start to reproduce the experimental combustion properties of the commercial Jet-A1 fuel. By contrast, the LUCHE detailed kinetic mechanism slightly underpredicts the laminar flame speeds of the LUCHE surrogate and the commercial Jet-A1 fuels

whatever the range of pressure studied. A refinement of this model should be recommended in the future.

- Effects of oxygenates addition on the flame speeds of bio-gasoline/air mixtures were addressed. A five-compound surrogate gasoline was firstly proposed and its laminar flame speed was compared with those of surrogate and commercial gasoline referenced in the literature. It is found that the surrogate gasoline proposed in the current study has the ability to reproduce the laminar flame speed of commercial gasoline. Then, anisole, 4-methylanisole and ethyl valerate were selected as oxygenated compounds to study the effect of the addition of oxygenates to gasoline. Laminar flame speed of pure oxygenate fuels were measured in a wide range of operating conditions and results were discussed. Finally, the aforementioned oxygenates were added to the surrogate gasoline to study the effects of oxygenates on the laminar flame speed. It is found that the flame speed generally increased with the addition of oxygenates. However, when the percentage of oxygenates is less than 10%, the laminar flame speeds is relatively insensitive. It is also observed that the use of oxygenates at higher concentration could improve the combustion efficiency of modern cars in regards to their capacity to increase the laminar flame speeds and their elevated RON.

## 8.2 Recommendations for further study

The current study suggests numerous fruitful avenues for further exploration, both in characterizing the laminar flame speed using a high-pressure Bunsen burner and associated optical diagnostics and in extending and applied the optical diagnostics to pure heavy hydrocarbon molecules and practical fuels in conditions representative of those encountered in real combustors (e.g. high pressure, elevated preheating temperature and wide equivalence ratio range).

- Comparison of performances between the optical diagnostics applied in the current study revealed that the measurement of laminar flame speeds remains a critical task. Regarding the laminar flame speeds data, a scatter in results from measurements performed in the same conditions is then observed that raises the question of how the values measured are precise. One of the reasons explaining this scatter arises from the fact that the frontier delimiting the zone of the fresh gases is based on the detection of signals related to species concentration and not directly the temperature. Having an optical diagnostic that measures directly the distribution of temperature inside the fresh gases region would guarantee a better accurate location of this frontier. An opportunity to access this ambitious goal could be to use a laser-induced fluorescence diagnostic based on a temperature-dependent fluorescent tracer. For instance, the seeding of the fresh gases with atomic species such as indium known as an

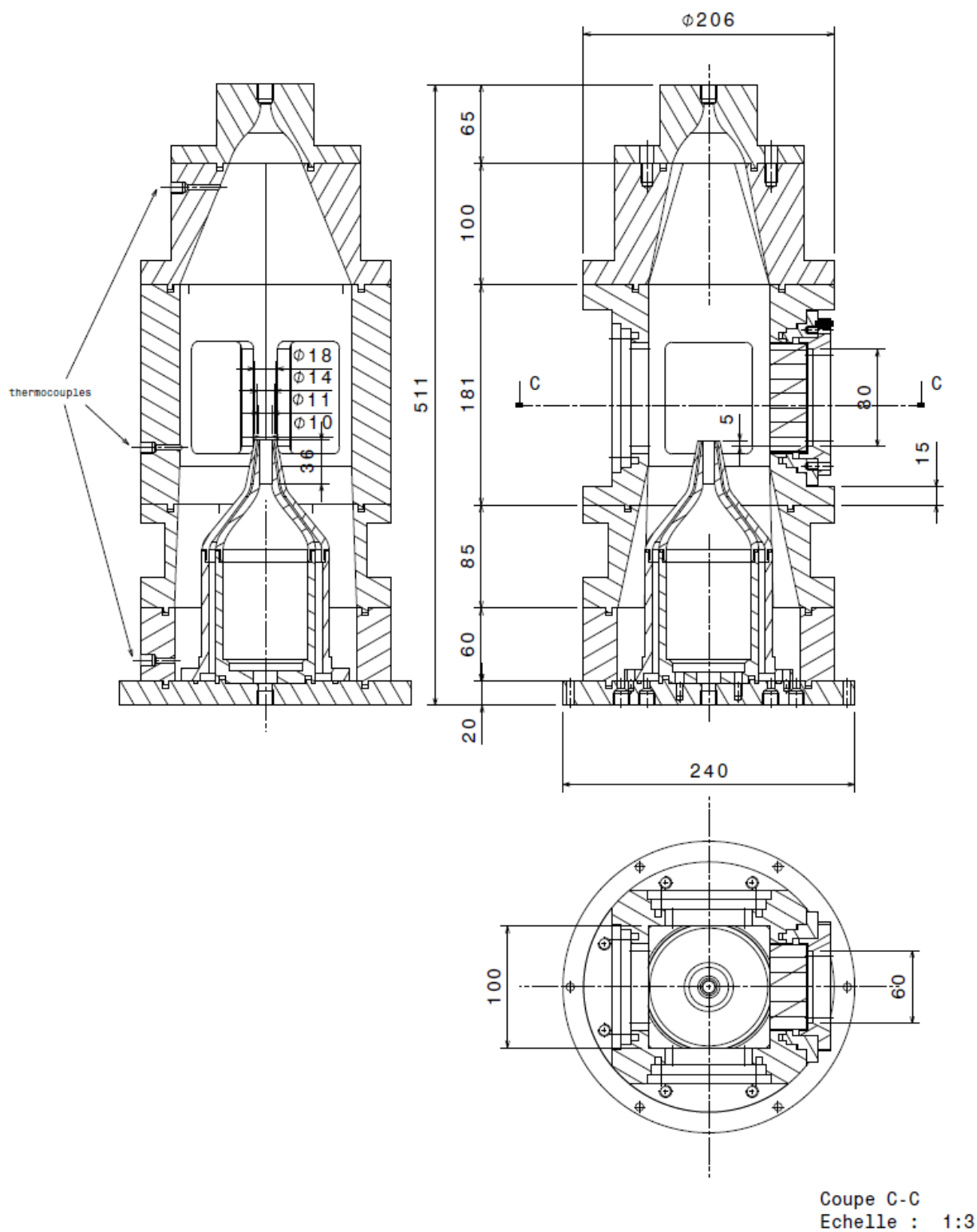
efficient temperature-dependent fluorescence tracer could be driven a real interest to measure the temperature distribution in the fresh gases via a two-line atomic fluorescence imaging diagnostic.

- Measurements of laminar flame speeds of heavy hydrocarbons molecules in a wide range of operating conditions (especially at elevated pressure and preheating temperatures) should be extended. Results will be used to build elementary combustion mechanism blocks required for the development of more accurate reaction models for practical multi-component fuels. Apart from laminar flame speeds, combustion data such as the extinction stretch rate and ignition delay are also desirable from the point of view of refining the kinetic models.
- Concerning the role of oxygenates on the combustion properties of biofuels, the oxygenated molecules present in the different fuel fractions of “classical” biofuels of second generation (2, 5-dimethylfuran, methyltetrahydrofuran and 2-methylfuran 2, phenol, 4-xylenol, 1, 2-dimethoxybenzene, guaiacol, p-cresol, 4-propylanisole...) should be also investigated to elaborate and complete actual databases on laminar flame speeds in a wide range of representative conditions. An exploration of these databases could be fruitful to evaluate the influence of the addition of oxygenates when present in biofuels or fossil fuels. Furthermore, this database could be used to improve detailed kinetic mechanism associated to these fuels.
- Complementary measurements must be carried out on surrogate blends dedicated to replicate the physical and chemical characteristics of practical fuels. From these data, the elucidation of the preheating temperature and pressure dependences on laminar flame speeds will give valuable insights for many practical points of view such as the definition of empirical power law equations to implement in engineering codes, the validation of detailed kinetic mechanisms and the possibility to compare performances between various kind of fuels.
- Finally, it appears from results reported in literature that oxygenated compounds decrease the soot formation of diesel engine but enhance the CO and NO production whereas the effect on combustion efficiency depends on the oxygen content. For gasoline engine, it can be foreseen that increasing the aromaticity of these hybrid fuels will impact the combustion efficiency as compared to standard gasoline. However, no rationalization of these effects with the nature and amount of impurities is presented in literature as well as information for gasoline engine. In addition, no data is given about the formation of new potentially toxic molecules, whereas oxygenated pollutant like formaldehyde (cancerigenic) are regulated in California and will be probably soon regulated in Europe. Therefore, advanced laser diagnostics could be used on this burner to characterize the formation of gaseous pollutant emissions like NO and CO by a combination of Laser-induced fluorescence and Coherent anti-Stokes Raman scattering and

soot particles via Laser-Induced Incandescence. These measurements could in this manner be a useful supplement of the present database for the validation of numerical models of pollutant emission derived from the combustion of biofuels.

# Appendix I: Schematic drawing of the high-pressure burner

---



# List of Tables

---

<b>Table 2.1:</b> Literature review of laminar flame speed methane/air mixtures. ....	24
<b>Table 2.2:</b> Summary of laminar flame speeds of commercial kerosene fuel. ....	27
<b>Table 2.3:</b> Summary of the studies on the laminar flame speed of surrogate kerosene fuels in the last decade. ....	28
<b>Table 3.1:</b> Exemple of error calculation for the equivalence ratio of $\text{CH}_4$ /air mixtures with equation 3.4. ....	45
<b>Table 3.2:</b> Exemple of error calculation for the equivalence ratio of liquid fuel/air mixtures calculated with 3.7. ....	46
<b>Table 4.1:</b> Overview of laminar flame speed measurements with the Bunsen flame. ....	64
<b>Table 5.1:</b> Correlation parameters $\alpha_i$ , $\beta_i$ and $Su_{0,i}$ used in Eqs. 5.5 to 5.8 (acetone/ $\text{N}_2/\text{O}_2$ mixtures) and Values of the power exponents $\alpha$ ( $\varphi$ ) and $\beta$ ( $\varphi$ ): comparison between experiments and numerical simulation. ....	90
<b>Table 5.2:</b> Experimental conditions of pressure and equivalence ratio for measurements of laminar flame speed of acetone/ $\text{N}_2/\text{O}_2$ mixture at $T = 473 \text{ K}$ . ....	92
<b>Table 6.1:</b> Composition of the LUCHE surrogate fuel. ....	98
<b>Table 6.2 :</b> Experimental conditions. ....	99
<b>Table 6.3:</b> Correlation parameters $SL_{0,i}$ and $\alpha_i$ in equation 5.5 and 5.6. ....	118
<b>Table 7.1:</b> Composition of surrogate gasoline proposed in the present work. ....	125
<b>Table 7.2:</b> Compositions of fuel mixtures by liquid volume ....	133

# List of Figures

---

<b>Figure 2.1:</b> Schematic structure of a one-dimensional, planar, steady flame. Simplest model	10
<b>Figure 2.2:</b> schematic structure of a one dimensional, planar, steady flame. Transport dominated model. .....	10
<b>Figure 2.3:</b> Schematic structure of a one dimensional, planar, steady flame. Full description model.	11
<b>Figure 2.4:</b> Illustration of the displacement speed determination with $n$ , normal to the flame front oriented towards fresh gases, $S_f$ , local flame velocity vector evaluated on the flame temperature isolevel, $u$ , local flow velocity vector evaluated at a chosen fresh gas temperature isolevel, $S_d$ , resulting displacement speed.....	14
<b>Figure 2.5:</b> Evolution of the laminar flame speed of CH <sub>4</sub> /air mixtures at 298 K, atmospheric pressure and $\phi = 1.0$ as a function of the years [78]......	23
<b>Figure 2.6:</b> Laminar flame speed acetone/air mixture; literature data at atmospheric pressure and room temperature.....	25
<b>Figure 2.7 :</b> review of laminar flame speeds of n-decane.....	30
<b>Figure 2.8:</b> review of laminar flame speeds of n-propylbenzene. ....	31
<b>Figure 2.9:</b> Laminar flame speed of n-propylcyclohexane comparison between present works with literatures.....	32
<b>Figure 3.1:</b> Schematic of the high-pressure experimental facility.	39
<b>Figure 3.2:</b> Schematic of the experimental facility process flow diagram .....	40
<b>Figure 3.3:</b> Evolution of the flowrates of the different gases with pressure. Operating conditions: Jet A-1 fuel, $T = 400$ K, $\phi = 0.8$ .....	43
<b>Figure 3.4:</b> Velocity profiles measured above the nozzle outlet $z=1$ mm and 10 mm .....	47
<b>Figure 3.5:</b> Velocity RMS fluctuation above the nozzle outlet $z=1$ mm and 10 mm .....	47
<b>Figure 3.6:</b> Schematic of Planar laser induced fluorescence. $M_1$ , $M_2$ , $M_3$ : mirrors, PBS: UV plane windows. ....	49
<b>Figure 3.7:</b> Excitation fluorescence spectrum of OH recorded into the reference flame .....	51
<b>Figure 4.1:</b> Illustration of the surface area and flame angle method.	54
<b>Figure 4.2:</b> Bunsen flame with the popular optical accessible flame edges. ....	55
<b>Figure 4.3:</b> Instantaneous images of OH* chemiluminescence for various equivalence ratios. Operating conditions: CH <sub>4</sub> /air mixture, $T = 300$ K, $P = 0.1$ MPa, fresh gas velocity 1.1 m/s, $\Phi = 0.7 - 1.4$ . The color scale represents the intensity variation of the 16-bit chemiluminescence images.....	58
<b>Figure 4.4:</b> Selected potential energy curves for the OH molecule showing electronic and vibrational energy levels. Stable electronic levels are solid black lines, pre-dissociative levels in dashed gray. Transition pathways in red show stimulated pathways while green are spontaneous pathways.....	60



<b>Figure 4.5:</b> Instantaneous images of OH fluorescence for various equivalence ratios. Operating conditions: CH <sub>4</sub> /air mixture, T = 373 K, P = 0.1 MPa, fresh gas velocity 1.1 m/s, $\Phi$ = 0.7 - 1.3. The color scale represents the intensity variation of the 16 bit fluorescence images. ....	61
<b>Figure 4.6:</b> Instantaneous images of acetone fluorescence for various equivalence ratios. Operating conditions: acetone/air mixture, T = 473 K, P = 0.1 MPa, fresh gas velocity 1.1 m/s, $\Phi$ = 0.7 - 1.3. The color scale represents the intensity variation of the 16 bit fluorescence images. ....	62
<b>Figure 4.7:</b> Kerosene fluorescence spectra for laser excitation wavelengths 282 nm and 266 nm T= 450 K, P=0.1 MPa, kerosene diluted in N <sub>2</sub> [155].....	63
<b>Figure 4.8:</b> Instantaneous images of aromatics fluorescence for various equivalence ratios. Operating conditions: Jet A-1/air flame T = 405 K, P = 0.1 MPa, $\Phi$ = 0.7 - 1.3. The color scale represents the intensity variation of the 16 bit fluorescence images. ....	63
<b>Figure 4.9:</b> Numerical simulation of one-dimensional laminar premixed flame. Profiles of temperature (blue curve) and OH (black curve) for an n-decane/air mixture (T = 400 K, P = 0.1 MPa, $\phi$ = 1.0). The locations of the flame edges measured with various measurement techniques are also displayed. ....	67
<b>Figure 4.10:</b> Schematic view of the algorithm used for inversion of Abel's integral of the detected emission signal. ....	69
<b>Figure 4.11:</b> OH* chemiluminescence image processing: (a) OH* chemiluminescence raw image (b) image split in half along the burner axis (c) Abel-transform image (d) unburned gas contours detection with flame thickness consideration. ....	71
<b>Figure 4.12:</b> Illustration of the (a) OH-PLIF and (b) acetone/aromatics-PLIF image processing.....	72
<b>Figure 5.1:</b> Illustration of the flame area method and flame thickness simulation	75
<b>Figure 5.2:</b> Evolution of the calculated flame thickness with equivalence ratio (CH <sub>4</sub> /air mixture, T = 373 K, P = 0.1 MPa, $\phi$ = 0.7 – 1.3) .....	77
<b>Figure 5.3:</b> Evolution of numerical flame thickness with temperature (CH <sub>4</sub> /air mixture, P = 0.1 MPa, $\phi$ = 1.0, T = 290 – 473 K) .....	77
<b>Figure 5.4:</b> Evolution of the numerical flame thickness with pressure (CH <sub>4</sub> /air mixture, T = 473 K, P = 0.1 – 1.0 MPa, $\phi$ = 1.0).....	78
<b>Figure 5.5:</b> Relationship between the laminar flame speed and pressure (CH <sub>4</sub> /air mixture $\phi$ = 1.2, T = 473 K, P = 0.1 - 1.0 MPa). Comparison of data obtained with OH* chemiluminescence and OH-PLIF methodologies. ....	79
<b>Figure 5.6:</b> OH* chemiluminescence images of laminar flame structure of CH <sub>4</sub> /air mixture versus pressure ( $\phi$ = 0.8, T = 473 K).....	80
<b>Figure 5.7:</b> Normalized flame curvature rate along radius axis for various pressures (CH <sub>4</sub> /air flame, T = 473 K, $\phi$ = 0.8, P = 0.1 - 0.5 MPa). Burner rim starts at $r / R_0 = -1$ and burner center position is at $r / R_0 = 0$ with a burner radius $R_0 = 5$ mm.....	80
<b>Figure 5.8:</b> Effect of the piloted flame on the laminar flame speed measurements (CH <sub>4</sub> /air mixture, T = 375 K, P = 0.1 MPa).....	81

<b>Figure 5.9:</b> Laminar flame speed of acetone/air mixtures measured by OH-PLIF, acetone-PLIF and OH* chemiluminescence with correction of the flame thickness. $T = 453\text{ K}$ , $P = 0.1\text{ MPa}$ , $\phi = 0.7 - 1.3$ ....	82
<b>Figure 5.10:</b> Simultaneous visualization of OH-PLIF and acetone-PLIF flame contours.....	83
<b>Figure 5.11:</b> Comparison of laminar flame speeds ( $S_u$ ) obtained in our current study and previous data collected in the literature. The simulation data of GRI-Mech 3.0 predictions are also plotted in the same figure ( $\text{CH}_4/\text{air}$ , $T_{\text{air}} = 300\text{ K}$ , $P = 0.1\text{ MPa}$ ). ....	84
<b>Figure 5.12:</b> Laminar flame speeds of $\text{CH}_4/\text{air}$ mixtures at atmospheric pressure and various preheating temperatures (the symbols represent our experimental data; the lines are the results of the predictions of GRI-Mech 3.0) .....	85
<b>Figure 5.13:</b> Variation of the laminar flame speed with pressure ( $\text{CH}_4/\text{air}$ mixture, $T = 473\text{ K}$ , $\phi = 1.2$ ). The symbols represent the experiments; the solid line displays the numerical predictions of the GRI-Mech 3.0 mechanism and the dashed lines represent the results of [88] and [176]. ....	86
<b>Figure 5.14:</b> Evolution of the laminar flame speed versus equivalence ratio for various preheating temperatures (acetone/ $\text{N}_2/\text{O}_2$ mixture, $P = 0.1\text{ MPa}$ ). The symbols represent experimental data; the lines are numerical predictions of the Chong detailed kinetic mechanism. ....	89
<b>Figure 5.15:</b> Evolution of the laminar flame speed versus $\log(T/T_0)$ for various equivalence ratios (acetone/ $\text{N}_2/\text{O}_2$ mixture, $P = 0.1\text{ MPa}$ ). The lines represent the results of the empirical correlation expression proposed in the current experiment. ....	91
<b>Figure 5.16:</b> Evolution of the power exponent $\alpha$ versus equivalence ratio (acetone/ $\text{N}_2/\text{O}_2$ mixture, $P = 0.1\text{ MPa}$ ). ....	91
<b>Figure 5.17:</b> Variation of the laminar flame speed with pressure (acetone/ $\text{N}_2/\text{O}_2$ mixture, $T = 473\text{ K}$ , $\phi = 0.7 - 1.2$ ). The dash and solid lines are the numerical simulation data using the kinetic mechanism of Chong; the symbols are the experimental results. ....	93
<b>Figure 5.18:</b> Evolution of the laminar flame speed versus $\log P/P_0$ for different equivalence ratios (acetone/ $\text{N}_2/\text{O}_2$ mixture, $T = 473\text{ K}$ ). The lines represent the results of the correlation proposed in this study. ....	93
<b>Figure 5.19:</b> Evolution of the power exponent $\beta$ versus equivalence ratio (acetone/ $\text{N}_2/\text{O}_2$ mixture, $T = 473\text{ K}$ ).....	94
<b>Figure 5.20:</b> Laminar flame speed obtained with the empirical correlation expression compared to the experimental data. The dash lines indicate $2\sigma$ ( $\sigma = \pm 1.65\text{ cm/s}$ ) uncertainties interval obtained from the residual $\Delta S_u$ distribution. The solid line corresponds to $SL_{exp} = SL_{corr}$ .....	94
<b>Figure 6.1:</b> Flame contours measured with OH* chemiluminescence and OH-PLIF. Case of a n-decane/air mixture, $T = 400\text{ K}$ , $P = 0.1\text{ MPa}$ , $\phi = 0.8$ . ....	100
<b>Figure 6.2:</b> Laminar flame speed comparison between results obtained in the present work (OH* chemiluminescence and OH-PLIF) and literature results of Comandini et al. for n-decane/ $\text{N}_2/\text{O}_2$ $T = 400\text{ K}$ , $P = 0.1\text{ MPa}$ , $\phi = 0.65 - 1.3$ . ....	101

<b>Figure 6.3:</b> Comparison between OH* chemiluminescence, aromatics-PLIF and OH-PLIF results: Jet A-1/N <sub>2</sub> /O <sub>2</sub> mixture, T = 400 K, P = 0.1 MPa, $\phi$ = 0.8.....	102
<b>Figure 6.4:</b> Laminar flame speeds determined from OH* chemiluminescence, aromatics-PLIF and OH-PLIF images. Case of a Jet A-1/air mixture, T = 400 K, P = 0.1 MPa, $\phi$ = 0.65 - 1.3.....	103
<b>Figure 6.5:</b> Flame tip opening visualizing with OH* chemiluminescence and variation of the emission signal along the nozzle centerline. Jet A-1/N <sub>2</sub> /O <sub>2</sub> flame, T = 400 K, P = 0.1 MPa and $\phi$ = 1.3.....	105
<b>Figure 6.6:</b> Flame tip opening of Aromatic-PLIF image and aromatic fluorescence intensity variation along nozzle centerline (Jet A-1/N <sub>2</sub> /O <sub>2</sub> flame, T = 400 K, P = 0.1 MPa and $\phi$ = 1.3). ....	105
<b>Figure 6.7:</b> Comparison between our experimental results and data from literature: T = 400K, P = 0.1 MPa and $\phi$ = 0.6 – 1.5. ....	107
<b>Figure 6.8:</b> Effect of the temperature on the laminar flame speed of n-decane/N <sub>2</sub> /O <sub>2</sub> mixture at P = 0.1 MPa and $\phi$ = 0.6 – 1.3. ....	108
<b>Figure 6.9:</b> Comparison between present work and literature. Laminar flame speeds of n-propylbenzene. (T = 400 K, P = 0.1 MPa and $\phi$ = 0.6 – 1.3).....	108
<b>Figure 6.10:</b> Effect of the temperature on the laminar flame speed of n-propylbenzene, P = 0.1 MPa, $\phi$ = 0.6 – 1.3. ....	109
<b>Figure 6.11:</b> Laminar flame speed of n-propylcyclohexane, comparison between present work and literature. (T = 400 K, P = 0.1 MPa, $\phi$ = 0.65 – 1.3).....	110
<b>Figure 6.12:</b> Effect of the temperature on the laminar flame speed of n-propylcyclohexane. (P = 0.1 MPa, $\phi$ = 0.65 – 1.3).....	110
<b>Figure 6.13 :</b> Comparison of the laminar flame speeds of n-decane, n-propylbenzene, n-propylcyclohexane: T=400 K, P=0.1 MPa. ....	111
<b>Figure 6.14:</b> Comparison of the laminar flame speeds of n-decane, n-propylbenzene, n-propylcyclohexane and the LUCHE surrogate. T=400 K, P=0.1 MPa. ....	113
<b>Figure 6.15:</b> Comparison between experimental measurements and simulation results using the LUCHE model (T = 400 K, P = 0.1 MPa).....	114
<b>Figure 6.16:</b> Laminar flame speed of LUCHE surrogate fuel with temperature variation. (Lines are the simulation results and points are the measured values).....	114
<b>Figure 6.17:</b> Evolution of the laminar flame speed of LUCHE surrogate as a function of pressure. T = 423 K, $\phi$ = 0.7 and 0.8. Points are our measurements and dash lines are the LUCHE predictions.....	115
<b>Figure 6.18:</b> Comparison of the present measurements and data reported in the literature. Jet A-1, T = 400 K, P = 0.1 MPa. ....	116
<b>Figure 6.19:</b> Comparison of the present measurements and data reported in the literature. Jet A-1, T = 473 K, P = 0.1 MPa. ....	116
<b>Figure 6.20:</b> Laminar flame speed of Jet A-1/N <sub>2</sub> /O <sub>2</sub> with temperature variation, T = 400 K, 423 K, 445 K and 473 K with $\phi$ = 0.6 - 1.3, P = 0.1 MPa. ....	117

<b>Figure 6.21:</b> Log-Log plot of laminar flame speed of Jet A-1/N <sub>2</sub> /O <sub>2</sub> at atmospheric pressure and different preheating temperatures. Symbols are the experiments; lines are linear fits.....	118
<b>Figure 6.22 :</b> Evolution of the laminar flame speed of Jet A-1/N <sub>2</sub> /O <sub>2</sub> mixture versus pressure. T = 423 K, $\phi$ = 0.7 and 0.8. Points are our measurements and dash lines are the linear fits. ....	119
<b>Figure 6.23:</b> Comparison between laminar flame speed of LUCHE surrogate fuel and Jet A-1. Symbols are the measurements; dashed line is the prediction of the LUCHE model. ....	120
<b>Figure 6.24:</b> Comparison between laminar flame speeds of LUCHE surrogate and Jet A-1 in function of pressure. Symbols are our measurements; line is the prediction of the LUCHE model. ....	120
<b>Figure 7.1:</b> variation of the laminar flame speeds of our surrogate gasoline, commercial gasoline and surrogate gasoline referenced in [28] in function of the equivalence ratio. P=0.1 MPa. ....	126
<b>Figure 7.2:</b> Evolution of the laminar flame speed of our surrogate fuel in function of the equivalence ratio for three preheating temperatures: 358 K, 423 K and 473 K. P = 0.1 MPa.....	127
<b>Figure 7.3:</b> Variation of the laminar flame speeds of our surrogate gasoline in function of pressure. P = 0.1 – 0.8 MPa $\phi$ = 0.7, 0.8 and 0.9 and T = 423 K.....	128
<b>Figure 7.4:</b> Residuals remaining after hydro-processing of a bio-crude.....	129
<b>Figure 7.5:</b> Oxygenates distribution in function of the boiling point in a gasoline composition .....	130
<b>Figure 7.6:</b> Laminar flame speeds of anisole/N <sub>2</sub> /O <sub>2</sub> , 4-methylanisole/N <sub>2</sub> /O <sub>2</sub> and ethyl valerate/N <sub>2</sub> /O <sub>2</sub> mixtures at T = 423 K, P = 0.1 MPa and $\phi$ = 0.6 -1.3 .....	132
<b>Figure 7.7:</b> Comparison of laminar flame speeds of ethyl valerate/N <sub>2</sub> /O <sub>2</sub> mixtures between our measurements and literature results [130] [200]. ....	132
<b>Figure 7.8:</b> Laminar flame speed of the SA0, SA10, SA20, SA30, SA50, SA75 and SA100 surrogates. T = 423 K, P = 0.1 MPa and $\phi$ = 0.6 -1.3 .....	134
<b>Figure 7.9:</b> Variation of the laminar flame speed of the mixture in function of the anisole fraction: T = 423 K, P = 0.1 MPa and $\phi$ = 0.6 - 1.3(slope value with linear fittings, $\phi$ =0.7 - 1.3, 0.053, 0.061, 0.067, 0.071, 0.072, 0.075, 0.071);.....	135
<b>Figure 7.10:</b> variation of the laminar flame speed of the SA0 and SA10 surrogates at two preheating temperatures, 423 and 473 K. P = 0.1 MPa, $\phi$ = 0.6 - 1.3 .....	135
<b>Figure 7.11:</b> Laminar flame speeds versus pressure of reference surrogate gasoline, pure anisole and blend of 50 % surrogate gasoline and 50 % anisole: T = 423 K, P = 0.1 – 0.75 MPa and $\phi$ = 0.75. ...	136
<b>Figure 7.12:</b> Comparison of the laminar flame speeds of the SA0/air and ST0/air mixtures at 423 K and atmospheric pressure. ....	136
<b>Figure 7.13:</b> Comparison of the laminar flame speeds of anisole and toluene at 423 K and atmospheric pressure.....	137

# References

---

- [1] G. Andrews and D. Bradley, "Determination of burning velocities: A critical review," *Combustion and Flame*, vol. 18, no. 1, pp. 133-153, 1972.
- [2] J. Agnew and L. Graiff, "The pressure dependence of laminar burning velocity by the spherical bomb method," *Combustion and Flame*, vol. 5, pp. 209-219, 1961.
- [3] F. Egolfopoulos, N. Hansen, Y. Ju, K. Kohse-Höinghaus, C. Law and F. Qi, "Advances and challenges in laminar flame experiments and implications for combustion chemistry," *Progress in Energy and Combustion Science*, vol. 43, pp. 36-67, 2014.
- [4] V. Mol'kov and V. Nekrasov, "Normal propagation velocity of acetone-air flames versus pressure and temperature," *Combustion, Explosion and Shock Waves*, vol. 17, no. 3, pp. 280-283, 1981.
- [5] G. Yu, C. Law and C. Wu, "Laminar flame speeds of hydrocarbon + air mixtures with hydrogen addition," *Combustion and Flame*, vol. 63, no. 3, pp. 339-347, 1986.
- [6] Z. Chen, "On the accuracy of laminar flame speeds measured from outwardly propagating spherical flames: Methane/air at normal temperature and pressure," *Combustion and Flame*, vol. 162, no. 6, pp. 2442-2453, 2015.
- [7] K. Kumar and C.-J. Sung, "Laminar flame speeds and extinction limits of preheated n-decane/O<sub>2</sub>/N<sub>2</sub> and n-dodecane/O<sub>2</sub>/N<sub>2</sub> mixtures," *Combustion and Flame*, vol. 151, no. 1-2, pp. 209-224, 2007.
- [8] C. Ji, E. Dames, Y. L. Wang, H. Wang and F. N. Egolfopoulos, "Propagation and extinction of premixed C<sub>5</sub>-C<sub>12</sub> n-alkane flames," *Combustion and Flame*, vol. 157, no. 2, pp. 277-287, 2010.
- [9] E. Varea, V. Modica, B. Renou and A. M. Boukhalfa, "Pressure effects on laminar burning velocities and Markstein lengths for Isooctane/Ethanol/Air mixtures," *Proceedings of the Combustion Institute*, vol. 34, no. 1, pp. 735-744, 2013.
- [10] F. Halter, C. Chauveau, N. Djebaili-Chaumeix and I. Gökalp, "Characterization of the effects of pressure and hydrogen concentration on laminar burning velocities of methane-hydrogen-air mixtures," *Proceedings of the Combustion Institute*, vol. 30, no. 1, pp. 201-208, 2005.
- [11] J. Beeckmann, L. Cai and H. Pitsch, "Experimental investigation of the laminar burning velocities of methanol, ethanol, n-propanol, and n-butanol at high pressure," *Fuel*, Vols. 117, Part A, pp. 340-350, 2014.
- [12] X. Gu, M. Haq, M. Lawes and R. Woolley, "Laminar burning velocity and Markstein lengths of methane/air mixtures," *Combustion and Flame*, vol. 121, no. 12, pp. 41-58, 2000.
- [13] S. Jerzembeck, N. Peters, P. Pepiot-Desjardins and H. Pitsch, "Laminar burning velocities at high pressure for primary reference fuels and gasoline: Experimental and numerical investigation,"

- Combustion and Flame* , vol. 156, no. 2, pp. 292-301, 2009.
- [14] A. Konnov, R. Riemeijer and L. de Goey, "Adiabatic laminar burning velocities of CH<sub>4</sub> + H<sub>2</sub> + air flames at low pressures," *Fuel*, vol. 89, no. 7, pp. 1392-1396, 2010.
  - [15] H. J. Burbano, J. Pareja and A. A. Amell, "Laminar burning velocities and flame stability analysis of syngas mixtures at sub-atmospheric pressures," *International Journal of Hydrogen Energy* , vol. 36, no. 4, pp. 3243-3252, 2011.
  - [16] P. Dagaut and M. Cathonnet, "The ignition, oxidation, and combustion of kerosene: A review of experimental and kinetic modeling," *Progress in Energy and Combustion Science* , vol. 32, no. 1, pp. 48-92, 2006.
  - [17] A. Comandini, T. Dubois and N. Chaumeix, "Laminar flame speeds of n-decane, n-butylbenzene, and n-propylcyclohexane mixtures," *Proceedings of the Combustion Institute* , vol. 35, no. 1, pp. 671-678, 2015.
  - [18] D. Darcy, H. Nakamura, C. J. Tobin, M. Mehl, W. K. Metcalfe, W. J. Pitz, C. K. Westbrook and H. J. Curran, "An experimental and modeling study of surrogate mixtures of n-propyl- and n-butylbenzene in n-heptane to simulate n-decylbenzene ignition," *Combustion and Flame* , vol. 161, no. 6, pp. 1460-1473, 2014.
  - [19] B. Galmiche, F. Halter and F. Foucher, "Effects of high pressure, high temperature and dilution on laminar burning velocities and Markstein lengths of iso-octane/air mixtures," *Combustion and Flame* , vol. 159, no. 11, pp. 3286-3299, 2012.
  - [20] X. Hui, C. Zhang, M. Xia and C.-J. Sung, "Effects of hydrogen addition on combustion characteristics of n-decane/air mixtures," *Combustion and Flame* , vol. 161, no. 9, pp. 2252-2262, 2014.
  - [21] M. Zeng, W. Yuan, Y. Wang, W. Zhou, L. Zhang, F. Qi and Y. Li, "Experimental and kinetic modeling study of pyrolysis and oxidation of n-decane," *Combustion and Flame* , vol. 161, no. 7, pp. 1701-1715, 2014.
  - [22] V. Vukadinovic, P. Habisreuther and N. Zarzalis, "Influence of pressure and temperature on laminar burning velocity and Markstein number of kerosene Jet A-1: Experimental and numerical study," *Fuel* , vol. 111, pp. 401-410, 2013.
  - [23] X. Hui and C.-J. Sung, "Laminar flame speeds of transportation-relevant hydrocarbons and jet fuels at elevated temperatures and pressures," *Fuel* , vol. 109, no. 0, pp. 191-200, 2013.
  - [24] A. Holley, Y. Dong, M. Andac, F. Egolfopoulos and T. Edwards, "Ignition and extinction of non-premixed flames of single-component liquid hydrocarbons, jet fuels, and their surrogates," *Proceedings of the Combustion Institute* , vol. 31, no. 1, pp. 1205-1213, 2007.
  - [25] S. Honnet, K. Seshadri, U. Niemann and N. Peters, "A surrogate fuel for kerosene," *Proceedings of*

- the Combustion Institute* , vol. 32, no. 1, pp. 485-492, 2009.
- [26] D. Singh, T. Nishiie and Q. Li, "Experimental and Kinetic Modeling Study of the Combustion of n-Decane, Jet-A, and S-8 in Laminar Premixed Flames," *Combustion Science and Technology*, vol. 183, no. 10, pp. 1002-1026, 2011.
  - [27] D. Kim, J. Martz and A. Violi, "A surrogate for emulating the physical and chemical properties of conventional jet fuel," *Combustion and Flame* , vol. 161, no. 6, pp. 1489-1498, 2014.
  - [28] P. Dirrenberger, P. Glaude, R. Bounaceur, H. L. Gall, A. P. da Cruz, A. Konnov and F. Battin-Leclerc, "Laminar burning velocity of gasolines with addition of ethanol," *Fuel*, vol. 115, pp. 162-169, 2014.
  - [29] E. Varea, V. Modica, A. Vandel and B. Renou, "Measurement of laminar burning velocity and Markstein length relative to fresh gases using a new postprocessing procedure: Application to laminar spherical flames for methane, ethanol and isooctane/air mixtures," *Combustion and Flame*, vol. 159, no. 2, pp. 577-590, 2012.
  - [30] J. Van Lipzig, E. Nilsson, L. de Goey and A. Konnov, "Laminar burning velocities of n-heptane, iso-octane, ethanol and their binary and tertiary mixtures," *Fuel*, vol. 90, no. 8, pp. 2773-2781, 2011.
  - [31] C. T. Chong and S. Hochgreb, "Measurements of laminar flame speeds of acetone/methane/air mixtures," *Combustion and Flame* , vol. 158, no. 3, pp. 490-500, 2011.
  - [32] J. Luche, M. Reuillon, J.-C. Boettner and M. Cathonnet, "Reduction of large detailed kinetic mechanisms: application to kerosene/air combustion," *Combustion Science and Technology*, vol. 176, no. 11, pp. 1935-1963, 2004.
  - [33] K. Eisazadeh-Far, A. Moghaddas, J. Al-Mulki and H. Metghalchi, "Laminar burning speeds of ethanol/air/diluent mixtures," *Proceedings of the Combustion Institute*, vol. 33, no. 1, pp. 1021-1027, 2011.
  - [34] S. Liao, D. Jiang, Z. Huang, K. Zeng and Q. Cheng, "Determination of the laminar burning velocities for mixtures of ethanol and air at elevated temperatures," *Applied Thermal Engineering*, vol. 27, no. 2–3, pp. 374-380, 2007.
  - [35] K. H. Song, P. Nag, T. A. Litzinger and D. C. Haworth, "Effects of oxygenated additives on aromatic species in fuel-rich, premixed ethane combustion: a modeling study," *Combustion and Flame*, vol. 135, no. 3, pp. 341-349, 2003.
  - [36] C. K. Law, *Combustion Physics*, 2006.
  - [37] E. Mallard and H. Le Chatelier, "Sur la vitesse de propagation de l'inflammation dans les melanges explosifs.," *Comptes rendus de l'Academie des Science, Paris*, pp. 93-145, 1881.
  - [38] Y. B. Zeldovich, *Journal Physics Chemistry*, vol. 22, 1949.

- [39] T. Poinso T and D. Veynante, Theoretical and numerical combustion, 2001.
- [40] L. Selle, T. Poinso and B. Ferret, "Experimental and numerical study of the accuracy of flame-speed measurements for methane/air combustion in a slot burner," *Combustion and Flame* , vol. 158, no. 1, pp. 146-154, 2011.
- [41] Y. Dhue, "Etude numérique et expérimentale de l'influence de l'humidité de l'air sur la combustion. Application aux stratégies de réduction d'émissions polluantes et de consommation des moteurs à pistons.," Ph.D thesis, 2009.
- [42] E. Albin, H. Nawroth, S. Göke, Y. D'Angelo and C. O. Paschereit, "Experimental investigation of burning velocities of ultra-wet methane–air–steam mixtures," *Fuel Processing Technology* , vol. 107, pp. 27-35, 2013.
- [43] F. Williams, Combustion theory, Menlo Park, CA: Benjamin Cumming, 1985.
- [44] M. Matalon, "On flame stretch," *Combustion Science and Technology*, vol. 31, pp. 169-181, 1983.
- [45] S. H. Chung and C. K. Law, "An invariant derivation of flame stretch," *Combustion and Flame*, vol. 55, pp. 123-125, 1984.
- [46] S. Candel and T. Poinso, "flame stretch and the balance equation for the flame area," *combustion science and technology*, vol. 70, pp. 1-15, 1990.
- [47] K. Seshadri, N. Peters and F. Williams, "Asymptotic analyses of stoichiometric and lean hydrogen-air flames," *Combustion and Flame* , vol. 96, no. 4, pp. 407-427, 1994.
- [48] P. Clavin, "Dynamic behavior of premixed flame fronts in laminar and turbulent flows," *Progress in Energy and Combustion Science* , vol. 11, no. 1, pp. 1-59, 1985.
- [49] C.K.Law, "Dynamics of stretched flames," *In 22nd Symp (Int.) on Combustion*, pp. 1381-1402, 1988.
- [50] P. Williams and F., "Premixed flames with general rates of strain," *Combustion Science and Technology*, vol. 54, p. 237, 1987.
- [51] G. Markstein, "Experimental and theoretical studies of flame front stability," *Journal of the aeronautical science* , vol. 70, pp. 199-209, 1951.
- [52] A. Kelley and C. Law, "Nonlinear effects in the extraction of laminar flame speeds from expanding spherical flames," *Combustion and Flame* , vol. 156, no. 9, pp. 1844-1851, 2009.
- [53] F. Halter, T. Tahtouh and C. Mounaïm-Rousselle, "Nonlinear effects of stretch on the flame front propagation," *Combustion and Flame* , vol. 157, no. 10, pp. 1825-1832, 2010.
- [54] Z. Chen, "Effects of radiation and compression on propagating spherical flames of methane/air mixtures near the lean flammability limit," *Combustion and Flame* , vol. 157, no. 12, pp. 2267-2276, 2010.
- [55] C.K. Law and C.J.Sung, "Structure, aerodynamics, and geometry of premixed flamelets," *Progress*



- in *Energy and Combustion Science*, vol. 26, pp. 459-505, 2000.
- [56] Y. N.Kochar, "laminar flame speed and stretch sensitivity of hydrocarbon fuels at high preheat pressure and vitiation," 2014.
  - [57] G. Rozenchan, D. Zhu, C. Law and S. Tse, "Outward propagation, Burning Velocities and chemical effects of methane flames up to 60 atm," *Proceeding of the combustion institute*, vol. 29, pp. 1461-1469, 2002.
  - [58] D. Dowdy, D. T. Smith and A. Willians, "the use of expanding spherical flames to determine burning velocities and stretch effects in hydrogen air mixtures," *Proceeding of the combustion institute*, vol. 23, pp. 325-332, 1990.
  - [59] N. Bouvet, C. Chauveau and H. I., "experimental studies of the fundamental flame speeds of syngas (H<sub>2</sub>/CO)/air mixture," *proceedings of the combustion institute*, vol. 33, pp. 913-920, 2011.
  - [60] C. Vagelopoulos and F. Egolfopoulos, "Laminar flame speeds and extinction strain rates of mixtures of carbon monoxide with hydrogen, methane, and air," *Symposium (International) on Combustion*, vol. 25, no. 1, pp. 1317-1323, 1994.
  - [61] C. Vagelopoulos, F. Egolfopoulos and C. Law, "Further considerations on the determination of laminar flame speeds with the counterflow twin-flame technique," *Symposium (International) on Combustion*, vol. 25, no. 1, pp. 1341-1347, 1994.
  - [62] F. Egolfopoulos, H. Zhang and Z. Zhang, "Wall effects on the propagation and extinction of steady, strained, laminar premixed flames," *Combustion and Flame*, vol. 109, no. 1-2, pp. 237-252, 1997.
  - [63] Z. Zhao, A. Kazakov, J. LI and F. L. Dryer, "The initial temperature and N<sub>2</sub> dilution effect on the laminar speed of propane/air," *Combustion Science and Technology*, vol. 176, no. 10, pp. 1705-1723, 2004.
  - [64] F. Egolfopoulos and C. Law, "Chain mechanisms in the overall reaction orders in laminar flame propagation," *Combustion and Flame*, vol. 80, no. 1, pp. 7-16, 1990.
  - [65] A. Mazas, "Etude de flammes premelangees enriches en oxygene: analyse des effets de dilution par la vapeur d'eau et le dioxyde de carbon," 2010.
  - [66] J. P. Botha and D. B. Spalding, "The Laminar Flame Speed of Propane/Air Mixtures with Heat Extraction from the Flame," *Proceedings of the Royal Society of London A: Mathematical, Physical and Engineering Sciences*, vol. 225, no. 1160, pp. 71-96, 1954.
  - [67] A. V. Maaren, D. S. Thung and L. R. H. D. Goey, "Measurement of Flame Temperature and Adiabatic Burning Velocity of Methane/Air Mixtures," *Combustion Science and Technology*, vol. 96, no. 4-6, pp. 327-344, 1994.
  - [68] K. Bosschaart and L. de Goey, "The laminar burning velocity of flames propagating in mixtures of hydrocarbons and air measured with the heat flux method," *Combustion and Flame*, vol. 136, no.

- 3, pp. 261-269, 2004.
- [69] M. Goswami, R. Bastiaans, A. Konnov and L. de Goey, "Laminar burning velocity of lean H<sub>2</sub>-O mixtures at elevated pressure using the heat flux method," *International Journal of Hydrogen Energy*, vol. 39, no. 3, pp. 1485-1498, 2014.
  - [70] V. Alekseev, "laminar burning velocity of hydrogen and flame structure of related fuels for detailed kinetic model validation," 2015.
  - [71] B. Lewis and G. Von Elbe, *Combustion, Flames, and explosions of gases*, Academic Press, 3rd edition, 1987.
  - [72] C. Law, S. Ishizuka and P. Cho, "On the Opening of Premixed Bunsen Flame Tips," *Combustion Science and Technology*, vol. 28, no. 3-4, pp. 89-96, 1982.
  - [73] C. Sun, C. Sung and C. Law, "On adiabatic stabilization and geometry of bunsen flames," *Symposium (International) on Combustion*, vol. 25, no. 1, pp. 1391-1398, 1994.
  - [74] K. Kumar, "Global combustion response of practical hydrocarbon fuels: n-heptane, iso-octane, n-decane and ethylene," 2007.
  - [75] J. Natarajan, "Experimental and numerical investigation of laminar flame speed of H<sub>2</sub>/CO/CO<sub>2</sub>/N<sub>2</sub> mixtures," 2008.
  - [76] N. Bouvet, C. Chauveau, I. Gkalp, S.-Y. Lee and R. Santoro, "Characterization of syngas laminar flames using the Bunsen burner configuration," *International Journal of Hydrogen Energy*, vol. 36, no. 1, pp. 992-1005, 2011.
  - [77] V. E. G. Lewis B., "Determination of the speed of flames and the temperature distribution in a spherical bomb from time pressure explosion records," *The journal of Chemical physics*, vol. 2, pp. 283-290, 1934.
  - [78] F. N. Egolfopoulos, "laminar flame speed: what do we measure, what do we report, what do we learn how do we use," *New perspective for laminar burning velocity*, 2012.
  - [79] A. Van Maaren and L. De Goey, "Stretch and the adiabatic burning velocity of methane and propane-air flames," *Combustion Science and Technology*, vol. 102, pp. 309-314, 1994.
  - [80] K. K. Kenneth, *Principle of combustion*, 2005.
  - [81] O. Guilder, "Burning velocities of ethanol-isoocatane blends," *Combustion and Flame*, vol. 56, pp. 261-268, 1984.
  - [82] C. Wu and C. Law, "on the determination of laminar flame speeds from stretched flames," *Symposium (international) on combustion*, vol. 20, pp. 1941-1949, 1985.
  - [83] F. N. Egolfopoulos, P. Cho and C. K. Law, "Laminar flame speeds of methane-air mixtures under reduced and elevated pressures," *Combustion and Flame*, vol. 76, pp. 375-391, 1989.
  - [84] M. Haniff, A. Melvin, D. Smith and A. Williams, "The burning velocities of methane and SNG

- mixtures with air," *Journal of the Institute of Energy*, vol. 62, pp. 229-236, 1989.
- [85] L. W. Lauer G., "Laminar burning velocity of coal gases and methane at elevated pressures and temperatures: experiments and," *Archivum Combustionis*, vol. 15, no. 7-23, 1995.
- [86] M. Hassan, K. Aung and F. G.M., "Measured and predicted properties of laminar premixed methane/air flames at various pressures.," *Combustion and Flame*, vol. 14, pp. 539-550, 1998.
- [87] E. F. Vagelopoulos C.M., "Direct experimental determination of laminar flame speeds.," *Proceedings of the Combustion*, vol. 27, pp. 513-519, 1998.
- [88] K. Takizawa, A. Takahashi, K. Tokuhashi, S. Kondo and A. Sekiya, "Burning velocity measurement of fluorinated compounds by the spherical-vessel method," *Combustion and Flame*, vol. 141, no. 3, pp. 298-307, 2005.
- [89] Y. Huang, C. Sung and J. Eng, "Laminar flame speeds of primary reference fuels and reformer gas mixtures," *Combustion and Flame*, vol. 139, no. 3, pp. 239-251, 2004.
- [90] E. Hu, Z. Huang, J. He, C. Jin and J. Zheng, "Experimental and numerical study on laminar burning characteristics of premixed methanehydroge," *International Journal of Hydrogen Energy*, vol. 34, pp. 4876-4888, 2009.
- [91] R. Hermanns, A. Konnov, R. Bastiaans, L. d. Goey, K. Lucka and H. Köhne, "Effects of temperature and composition on the laminar," *fuel*, vol. 89, pp. 114-121, 2010.
- [92] A. Mazas, B. Fiorina, D. Lacoste and T. Schuller, "Effects of water vapor addition on the laminar burning velocity of oxygen-enriched methane flames," *Combustion and Flame*, vol. 158, no. 12, pp. 2428-2440, 2011.
- [93] E. Hu, Z. Huang, X. Jiang, Q. Q. Li and X. Zhang, "Kinetic study on laminar burning velocities and ignition delay times of C1-C4 alkanes.," *Journal of Engineering Thermophysics*, vol. 34, pp. 558-562, 2013.
- [94] K. Y. Troshin, A. A. Borisov, A. N. Rakhmetov, V. S. Arutyunov and G. G. Politenkova, "Burning velocity of methane-hydrogen mixtures at elevated," *Combustion, Explosion and Shock Waves*, vol. 32, pp. 76-87, 2013.
- [95] G. Black, S. Pichon, H. Curren, J. Simmie, R. Donohue and D. Chaumeix, "An experimental and modeling study of the combustion of acetone," *Third European Combustion Meeting, Greece*, 2007.
- [96] E. B. Maxim, V. I. Evgenii, E. J. K. Nilsson, V. A. Vinokurov and A. A. Konnov, "Laminar Burning Velocities of Dimethyl Carbonate with Air," *Energy & Fuels*, vol. 27, no. 9, pp. 5513-5517, 2013.
- [97] A. Burluka, M. Harker, H. Osman, C. Sheppard and A. Konnov, "Laminar burning velocities of three C<sub>3</sub>H<sub>6</sub>O isomers at atmospheric pressure," *Fuel*, vol. 89, no. 10, pp. 2864-2872, 2010.

- [98] E. Nilsson, L. de Goey and A. Konnov, "Laminar burning velocities of acetone in air at room and elevated temperatures," *Fuel* , vol. 105, no. 0, pp. 496-502, 2013.
- [99] S. Pichon, G. Black, N. Chaumeix, M. Yahyaoui, J. Simmie, H. Curran and R. Donohue, "The combustion chemistry of a fuel tracer: Measured flame speeds and ignition delays and a detailed chemical kinetic model for the oxidation of acetone," *Combustion and Flame* , vol. 156, no. 2, pp. 494-504, 2009.
- [100] K. Kumar, C.-J. Sung and X. Hui, "Laminar flame speeds and extinction limits of conventional and alternative jet fuels," *Fuel* , vol. 90, no. 3, pp. 1004-1011, 2011.
- [101] X. Hui, A. K. Das, K. Kumar, C.-J. Sung, S. Dooley and F. L. Dryer, "Laminar flame speeds and extinction stretch rates of selected aromatic hydrocarbons," *Fuel* , vol. 97, no. 0, pp. 695-702, 2012.
- [102] K. E. Far, F. Parsinejad and H. Metghalchi, "Flame structure and laminar burning speeds of JP-8/air premixed mixtures at high temperatures and pressures," *Fuel* , vol. 89, no. 5, pp. 1041-1049, 2010.
- [103] T. Kick, J. Herbst, T. Kathrotia, J. Marquetand, M. Braun-Unkhoff, C. Naumann and U. Riedel, "An experimental and modeling study of burning velocities of possible future synthetic jet fuels," *Energy* , vol. 43, no. 1, pp. 111-123, 2012.
- [104] R. H. Natelson, M. S. Kurman, N. P. Cernansky and D. L. Miller, "Experimental investigation of surrogates for jet and diesel fuels," *Fuel* , vol. 87, no. 10–11, pp. 2339-2342, 2008.
- [105] J. A. Cooke, M. Bellucci, M. D. Smooke, A. Gomez, A. Violi, T. Faravelli and E. Ranzi, "Computational and experimental study of JP-8, a surrogate, and its components in counterflow diffusion flames," *Proceedings of the Combustion Institute* , vol. 30, no. 1, pp. 439-446, 2005.
- [106] P. Dagaut, A. E. Bakali and A. Ristori, "The combustion of kerosene: Experimental results and kinetic modelling using 1- to 3-component surrogate model fuels," *Fuel* , vol. 85, no. 7–8, pp. 944-956, 2006.
- [107] C. P. Wood, V. G. McDonnell, R. A. Smith and G. S. Samuelsen, "Development and application of a surrogate distillate fuel," *Journal of propulsion and Power*, vol. 5, no. 4, pp. 399-405, 1989.
- [108] W. D. Schulz, "Oxidation products of a surrogate JP-8 fuel," *ACS Division of Petroleum Chemistry Preprints*, vol. 37, no. 2, pp. 183-392, 1991.
- [109] T. Edwards, "Surrogate mixtures to represent complex aviation and rocket fuels," *Journal of propulsion and power*, vol. 17, pp. 1-10, 2001.
- [110] A. Agosta, N. P. Cernansky, D. L. Miller, T. Faravelli and E. Ranzi, "Reference components of jet fuels: kinetic modeling and experimental results," *Experimental Thermal and Fluid Science*, vol. 28, pp. 701-708, 2004.
- [111] A. Violi, S. Yan, E. G. Eddings, A. F. Sarofim, S. Granata, T. Faravelli and E. Ranzi, "Experimental formulation and kinetic model for JP-8 surrogate mixtures," *Combustion Science*

- and Technology, vol. 174, no. 11-12, pp. 399-417, 2002.
- [112] C. Montgomery, S. Cannon, M. Mawid and B. Sekar, "Reduced chemical kinetic mechanisms for JP-8 combustion," *40th AIAA Aerospace Science Meeting & Exhibit*, p. 0036, 2002.
- [113] S. Humer, A. Frassoldati, S. Granata, T. Faravelli, E. Ranzi, R. Seiser and K. Seshadri, "Experimental and kinetic modeling study of combustion of JP-8, its surrogates and reference components in laminar nonpremixed flows," *Proceedings of the Combustion Institute*, vol. 31, no. 1, pp. 393-400, 2007.
- [114] C. Guéret, M. Cathonnet, J.-C. Boettner and F. Gaillard, "Twenty-Third Symposium (International) on Combustion Experimental study and modeling of kerosene oxidation in a jet-stirred flow reactor," *Symposium (International) on Combustion*, vol. 23, no. 1, pp. 211-216, 1991.
- [115] J. Munzar, B. Akih-Kumgeh, B. Denman, A. Zia and J. Bergthorson, "An experimental and reduced modeling study of the laminar flame speed of jet fuel surrogate components," *Fuel*, vol. 113, no. 0, pp. 586-597, 2013.
- [116] C. Ji, E. Dames, B. Sirjean, H. Wang and F. N. Egolfopoulos, "An experimental and modeling study of the propagation of cyclohexane and mono-alkylated cyclohexane flames," *Proceedings of the Combustion Institute*, vol. 33, no. 1, pp. 971-978, 2011.
- [117] M. Mehl, O. Herbinet, P. Dirrenberger, R. Bounaceur, P.-A. Glaude, F. Battin-Leclerc and W. J. Pitz, "Experimental and modeling study of burning velocities for alkyl aromatic components relevant to diesel fuels," *Proceedings of the Combustion Institute*, vol. 35, no. 1, pp. 341-348, 2015.
- [118] T. Dubois, N. Chaumeix and C.-E. Paillard, "Experimental and Modeling Study of n-Propylcyclohexane Oxidation under Engine-relevant Conditions," *Energy & Fuels*, vol. 23, no. 5, pp. 2453-2466, 2009.
- [119] P. Azadi, O. R. Inderwildi, R. Farnood and D. A. King, "Liquid fuels, hydrogen and chemicals from lignin: A critical review," *Renewable and Sustainable Energy Reviews*, vol. 21, pp. 506-523, 2013.
- [120] C. U. P. J. Dinesh Mohan and P. H. Steele, "Pyrolysis of Wood/Biomass for Bio-oil: A Critical Review," *Energy & Fuels*, vol. 20, no. 3, pp. 848-889, 2006.
- [121] M. S. Talmadge, R. M. Baldwin, M. J. Bidddy, R. L. McCormick, G. T. Beckham, G. A. Ferguson, S. Czernik, K. A. Magrini-Bair, T. D. Foust, P. D. Metelski, C. Hetrick and M. R. Nimlos, "A perspective on oxygenated species in the refinery integration of pyrolysis oil," *Green Chem.*, vol. 16, pp. 407-453, 2014.
- [122] A. Bridgwater, "Review of fast pyrolysis of biomass and product upgrading," *Biomass and Bioenergy*, vol. 38, pp. 68-94, 2012.
- [123] R. L. McCormick, M. A. Ratcliff, E. Christensen, L. Fouts, J. Luecke, G. M. Chupka, J. Yanowitz,

- M. Tian and M. Boot, "Properties of Oxygenates Found in Upgraded Biomass Pyrolysis Oil as Components of Spark and Compression Ignition Engine Fuels," *Energy & Fuels*, vol. 29, no. 4, pp. 2453-2461, 2015.
- [124] S. Arbogast, D. Bellman, J. Paynter and J. Wykowski, "Advanced bio-fuels from pyrolysis oil: The impact of economies of scale and use of existing logistic and processing capabilities," *Fuel Processing Technology*, vol. 104, pp. 121-127, 2012.
- [125] S. M. Sarathy, P. Oswald, N. Hansen and K. Kohse-Höinghaus, "Alcohol combustion chemistry," *Progress in Energy and Combustion Science*, vol. 44, pp. 40-102, 2014.
- [126] K. Kohse-Höinghaus, P. Oswald, T. A. Cool, T. Kasper, N. Hansen, F. Qi, C. K. Westbrook and P. R. Westmoreland, "Biofuel Combustion Chemistry: From Ethanol to Biodiesel," *Angewandte Chemie International Edition*, vol. 49, no. 21, pp. 3572-3597, 2010.
- [127] A. K. Agarwal, "Biofuels (alcohols and biodiesel) applications as fuels for internal combustion engines," *Progress in Energy and Combustion Science*, vol. 33, no. 3, pp. 233-271, 2007.
- [128] D. Bradley, M. Lawes and M. Mansour, "Explosion bomb measurements of ethanol-air laminar gaseous flame characteristics at pressures up to 1.4 MPa," *Combustion and Flame*, vol. 156, no. 7, pp. 1462-1470, 2009.
- [129] E. J. k. Nillson and A. A. Koonnov, *Flame studies of Oxygenates*, Springer Verlage London, 2013.
- [130] M. E. Baumgardner, T. L. Vaughn, A. Lakshminarayanan, D. Olsen, M. A. Ratcliff, R. L. McCormick and A. J. Marchese, "Combustion of Lignocellulosic Biomass Based Oxygenated Components in a Compression Ignition Engine," *Energy & Fuels*, vol. 29, no. 11, pp. 7317-7326, 2015.
- [131] G. Dayma, F. Halter, F. Foucher, C. Togbé, C. Mounaim-Rousselle and P. Dagaut, "Experimental and Detailed Kinetic Modeling Study of Ethyl Pentanoate (Ethyl Valerate) Oxidation in a Jet Stirred Reactor and Laminar Burning Velocities in a Spherical Combustion Chamber," *Energy & Fuels*, vol. 26, no. 8, pp. 4735-4748, 2012.
- [132] G. Smith, D. Golden, M. Frenklach, N. Moriarty, B. Eiteneer, M. Goldenberg, C. Bowman, R. Hanson, S. Song, W. G. Jr., V. Lissianski and Z. Qin, "GRI-Mech Homepage," *Gas Research Institute*, 1999.
- [133] A. Konnov, "detailed reaction mechanism for small hydrocarbons combustion," [Online]. Available: [http://homepages.vub.ac.be/akonnov/..](http://homepages.vub.ac.be/akonnov/)
- [134] K.J.Hughes, T. Turanyi and C. a. PillingM.J., "development and testing of a comprehensive chemical mechanism for the oxidation of methane," *International journal of chemical kinetics*, vol. 33, pp. 513-538, 2001.
- [135] Hidaka, K. Sato and Yoshikai, "Shock ube and modeling study of acetone pyrolysis and oxidation,"

- Combustion and flame*, vol. 122, pp. 291-311, 2000.
- [136] M. Chao, Z. Zhao, A. Kazakov and F. Dryer, "31st institute symposium on combustion Herdelberg work in progress poster," 2006.
- [137] J. Luche, "obtention de modeles cinetiques reduits de combustion applica un mecanisme du kerosene," Ph.D thesis, 2003.
- [138] J. Taylor, An introduction to eror analysis, The study of uncertainties in physical measurements, Sausalito, Calif.: Univ. Science Book, 1997.
- [139] F. J. Weinberg, The optics of flames and methods for the study of refractive index fields in Gases, London: Butterworth & co, 1963.
- [140] C. Rallis and A. Garforth, "The determination of laminar burning velocity," *Progress in Energy and Combustion Science*, vol. 6, no. 4, pp. 303-329, 1980.
- [141] X. Gao, Y. Zhang, S. Adusumilli, J. Seitzman, W. Sun, T. Ombrello and C. Carter, "The effect of ozone addition on laminar flame speed," *Combustion and Flame*, vol. 162, no. 10, pp. 3914-3924, 2015.
- [142] S. Sun, S. Meng, Y. Zhao, H. Xu, Y. Guo and Y. Qin, "Experimental and theoretical studies of laminar flame speed of CO/H<sub>2</sub> in O<sub>2</sub>/H<sub>2</sub>O atmosphere," *International Journal of Hydrogen Energy*, vol. 41, no. 4, pp. 3272-3283, 2016.
- [143] C. Schulz and V. Sick, "Tracer-LIF diagnostics: quantitative measurement of fuel concentration, temperature and fuel/air ratio in practical combustion systems," *Progress in Energy and Combustion Science*, vol. 31, no. 1, pp. 75-121, 2005.
- [144] A. C. Eckbreth, Laser diagnostics for combustion temperature and species. 2nd Ed., Amsterdam: Gordon & Breach, 1996.
- [145] A. G. Gaydon and H. G. Wolfhard, Flames, their structure, radiation and temperature. 4th Ed., Chapman & Hall, 1979.
- [146] J. Kojima, Y. Ikeda and T. Nakajima, "Basic aspects of OH(A), CH(A), and C<sub>2</sub>(d) chemiluminescence in the reaction zone of laminar methane–air premixed flames," *Combustion and Flame*, vol. 140, no. 1–2, pp. 34-45, 2005.
- [147] K. Kohse-Hoinghaus and J. B. jeffries, Applied combustion diagnostics combustion, New York: Taylor & Francis, 2002.
- [148] R. N.Zare, "My life with LIF: A personal account of Developing Laser induced fluoescence," *Annual Review of analytical chemistry*, vol. 5, pp. 1-14, 2012.
- [149] F. Grisch and M. Orain, "Role of plannar laser induced fluoescence in combustion research," *journal aerospace lab*, vol. 1, pp. 1-10, 2009.
- [150] B. Yip, M. F. Miller, A. Lozano and R. K. Hanson, "A combined OH/acetone planar laser-induced

- fluorescence imaging technique for visualizing combusting flows," *Experiments in Fluids*, vol. 17, no. 5, pp. 330-336, 1994.
- [151] A. Bresson, P. Bouchardy, P. Magre and F. Grisch, "OH/acetone PLIF and CARS thermometry in a supersonic reactive layer," *AIAA paper*, p. 1759, 2001.
- [152] D. Wolff, H. Schlüter, V. Beushausen and P. Andresen, "Quantitative Determination of Fuel Air Mixture Distributions in an Internal Combustion Engine using PLIF of Acetone," *Berichte der Bunsengesellschaft für physikalische Chemie*, vol. 97, no. 12, pp. 1738-1740, 1993.
- [153] F. Grisch, M. C. Thurber and R. K. Hanson, "Mesure de temperature par fluorescence induite par laser sur la molecule d'acetone," *Revue Scientifique et Technique de la Defense*, pp. 51-60, 1997.
- [154] M. C. Thurber, F. Grisch and R. K. Hanson, "Temperature imaging with single- and dual-wavelength acetone planar laser-induced fluorescence," *Opt. Lett.*, vol. 22, no. 4, pp. 251-253, Feb 1997.
- [155] J. F. Le Goz, C. Catalano and T. Baritaud, "Application of laser induced fluorescence for measuring the thickness of liquid films on transparent walls," *International symposium on application of laser techniques to fluide mechanics*, vol. 1, pp. 1-8, 1994.
- [156] M. Orain, P. Baranger, C. Ledier, J. Apeloig and F. Grisch, "Fluorescence spectroscopy of kerosene vapour at high temperature and pressures : potential for gas turbines measurements," *Appl. Phys. B*, pp. 116: 729-745, 2014.
- [157] T. D. Fansler, D. T. French and M. C. Drake, "Fuel Distributions in a Firing Direct-Injection Spark-Ignition Engine Using Laser-Induced Fluorescence Imaging," *SAE Technical Paper*, vol. 1, pp. 1-10, 1995.
- [158] J.-F. Le Coz and T. Baritaud, "Application of laser induced fluorescence for measuring the thickness of evaporating gasoline liquid films," *Symposium on advanced non-insrusive instruments for propulsion engine*, 1997.
- [159] W. Hentschel, B. Block, T. Hoyestadt, H. Meyer, G. Ohmesede, V. Richter, B. Stiebel and A. Winkler, "Optical diagnostics and CFD simulation to support the combustion process development of the Volkswagen FSI direct injection gasoline engine," *SAE Technical paper*, 2001.
- [160] M. Orain, H. Verdier and F. Grisch, "Equivalence ratio measurements in kerosene-full LPP injections using planar laser induced fluorescence," *13th symposium on application of laser techniques to fluid mechanics*, 2006.
- [161] J. Natarajan, T. Lieuwen and J. Seitzman, "Laminar flame speeds of H<sub>2</sub>/CO mixtures: Effect of CO<sub>2</sub> dilution, preheat temperature, and pressure," *Combustion and Flame*, vol. 151, no. 1?2, pp. 104-119, 2007.
- [162] C. Dong, Q. Zhou, Q. Zhao, Y. Zhang, T. Xu and S. Hui, "Experimental study on the laminar flame



- speed of hydrogen/carbon monoxide/air mixtures," *Fuel*, vol. 88, no. 10, pp. 1858-1863, 2009.
- [163] Y. He, Z. Wang, L. Yang, R. Whiddon, Z. Li, J. Zhou and K. Cen, "Investigation of laminar flame speeds of typical syngas using laser based Bunsen method and kinetic simulation," *Fuel*, vol. 95, no. 0, pp. 206-213, 2012.
- [164] J. Fu, C. Tang, W. Jin, L. D. Thi, Z. Huang and Y. Zhang, "Study on laminar flame speed and flame structure of syngas with varied compositions using OH-PLIF and spectrograph," *International Journal of Hydrogen Energy*, vol. 38, no. 3, pp. 1636-1643, 2013.
- [165] D. Lapalme and P. Seers, "Influence of CO<sub>2</sub>, CH<sub>4</sub>, and initial temperature on H<sub>2</sub>/CO laminar flame speed," *International Journal of Hydrogen Energy*, vol. 39, no. 7, pp. 3477-3486, 2014.
- [166] X. Hu, Q. Yu, J. Liu and N. Sun, "Investigation of laminar flame speeds of CH<sub>4</sub>/O<sub>2</sub>/CO<sub>2</sub> mixtures at ordinary pressure and kinetic simulation," *Energy*, vol. 70, no. 0, pp. 626-634, 2014.
- [167] Z. Wang, W. Weng, Y. He, Z. Li and K. Cen, "Effect of H<sub>2</sub>/CO ratio and N<sub>2</sub>/CO<sub>2</sub> dilution rate on laminar burning velocity of syngas investigated by direct measurement and simulation," *Fuel*, vol. 141, pp. 285-292, 2015.
- [168] L. Muñoz and M. Mungal, "Effects of heat release and buoyancy on flow structure and entrainment in turbulent nonpremixed flames," *Combustion and Flame*, vol. 126, no. 1-2, pp. 1402-1420, 2001.
- [169] F. Grisch, B. Attal-Tretout, A. Bresson, P. Bouchardy, V. Katta and W. Roquemore, "Investigation of a dynamic diffusion flame of H<sub>2</sub> in air with laser diagnostics and numerical modeling," *Combustion and Flame*, vol. 139, no. 1-2, pp. 28-38, 2004.
- [170] C. W. Choi and I. K. Puri, "Contribution of curvature to flame-stretch effects on premixed flames," *Combustion and Flame*, vol. 126, no. 3, pp. 1640-1654, 2001.
- [171] N. H. Abel, "Auflosungeiner mechanischen aufgabe," *J. fur dir Reine and Ange, Math*, vol. 1, pp. 153-157, 1826.
- [172] Deans and S. R. Radon, "Radon and Abel Transforms.", Boca Raton: CRC Press LLC, 2000.
- [173] J. N. L. Toulouzan, J. J. Locquet, D. Allano, P. Savary and R. Darrigo, "Abel's inversion of a cylindrical helium plasma. Production of a stigmatic spectrograph using a vidicon detector," *Journal of Optics*, vol. 12, no. 6, p. 369, 1981.
- [174] S.C.Taylor, "Burning velocity and the influence of flame stretch," 1991.
- [175] T. Tahtouh, F. Halter and C. Mounaïm-Rousselle, "Measurement of laminar burning speeds and Markstein lengths using a novel methodology," *Combustion and Flame*, vol. 156, no. 9, pp. 1735-1743, 2009.
- [176] Y. Dong, C. M. Vagelopoulos, G. R. Spedding and F. N. Egolfopoulos, "Measurement of laminar flame speeds through digital particle image velocimetry: Mixtures of methane and ethane with hydrogen, oxygen, nitrogen, and helium," *Proceedings of the Combustion Institute*, vol. 29, no. 2,

pp. 1419-1426, 2002.

- [177] R. Stone, A. Clarke and P. Beckwith, "Correlations for the Laminar-Burning Velocity of Methane/Diluent/Air Mixtures Obtained in Free-Fall Experiments," *Combustion and Flame* , vol. 114, no. 3–4, pp. 546-555, 1998.
- [178] M. Goswami, S. C. Derks, W. J. S. Kris Coumans, M. H. A. Oliveira, R. J. Bastiaans, C. C.M.Luijten and A. A. K. L. Philipus H. de Goey, "The effect of elevated pressure on the laminar burning velocity of methane+air mixtures," *Combustion and Flame*, vol. 160, pp. 1627-1635, 2013.
- [179] O. Manna, M. S. Mansour, W. L. Roberts and S. H. Chung, "Laminar burning velocities at elevated pressures for gasoline and gasoline surrogates associated with RON," *Combustion and Flame*, no. 0, pp. -, 2015.
- [180] A. Konnov, R. Meuwissen and L. de Goey, "The temperature dependence of the laminar burning velocity of ethanol flames," *Proceedings of the Combustion Institute* , vol. 33, no. 1, pp. 1011-1019, 2011.
- [181] M. Metghalchi and J. C. Keck, "Burning velocities of mixtures of air with methanol, isooctane, and indolene at high pressure and temperature," *Combustion and Flame* , vol. 48, no. 0, pp. 191-210, 1982.
- [182] Ö. L. Gülder, "Laminar burning velocities of methanol, ethanol and isooctane-air mixtures," *Symposium (International) on Combustion* , vol. 19, no. 1, pp. 275-281, 1982.
- [183] D. Smith and J. T. Agnew, "The effect of pressure on the laminar burning velocity of methane-oxygen-nitrogen mixtures," *Symposium (International) on Combustion* , vol. 6, no. 1, pp. 83-88, 1957.
- [184] M. Mizomoto, Y. Asaka, S. Ikai and C. Law, "Effects of preferential diffusion on the burning intensity of curved flames," *Symposium (International) on Combustion* , vol. 20, no. 1, pp. 1933-1939, 1985.
- [185] T. M. Vu, M. S. Cha, B. J. Lee and S. H. Chung, "Tip opening of premixed bunsen flames: Extinction with negative stretch and local Karlovitz number," *Combustion and Flame*, vol. 162, no. 4, pp. 1614-1621, 2015.
- [186] J. Wang, Z. Wei, S. Yu, W. Jin, Y. Xie, M. Zhang and Z. Huang, "Effects of stretch and preferential diffusion on tip opening of laminar premixed Bunsen flames of syngas/air mixtures," *Fuel* , vol. 148, pp. 1-8, 2015.
- [187] F. WU, P. A. Kelly and C. K. Law, "Laminar flame speed of cyclohexane and mono-alkylated cyclohexanes at elevated pressures," *Combustion and Flame*, vol. 159, no. 4, pp. 1417-1425, 2011.
- [188] Y. Schuurman, G. Fogassy and C. Mirodatos, "Chapter 10 - Tomorrow's Biofuels: Hybrid Biogasoline by Co-processing in FCC Units," in *The Role of Catalysis for the Sustainable*

- Production of Bio-fuels and Bio-chemicals*, K. S. Triantafyllidis, A. A. Lappas and M. Stöcker, Eds., Amsterdam, Elsevier, 2013, pp. 321-349.
- [189] D. Mohan, C. U. Pittman and P. H. Steele, "Pyrolysis of Wood/Biomass for Bio-oil: A Critical Review," *Energy & Fuels*, vol. 20, no. 3, pp. 848-889, 2006.
- [190] A. Popov, E. Kondratieva, J. M. Goupil, L. Mariey, P. Bazin, J.-P. Gilson, A. Travert and F. Maugé, "Bio-oils Hydrodeoxygenation: Adsorption of Phenolic Molecules on Oxidic Catalyst Supports," *The Journal of Physical Chemistry C*, vol. 114, no. 37, pp. 15661-15670, 2010.
- [191] D. Bradley, R. Hicks, M. Lawes, C. Sheppard and R. Woolley, "The Measurement of Laminar Burning Velocities and Markstein Numbers for Iso-octane–Air and Iso-octane–n-Heptane–Air Mixtures at Elevated Temperatures and Pressures in an Explosion Bomb," *Combustion and Flame*, vol. 115, no. 1–2, pp. 126-144, 1998.
- [192] L. Sileghem, V. Alekseev, J. Vancoillie, K. V. Geem, E. Nilsson, S. Verhelst and A. Konnov, "Laminar burning velocity of gasoline and the gasoline surrogate components iso-octane, n-heptane and toluene," *Fuel*, vol. 112, pp. 355-365, 2013.
- [193] S. Marshall, S. Taylor, C. Stone, T. Davies and R. Cracknell, "Laminar burning velocity measurements of liquid fuels at elevated pressures and temperatures with combustion residuals," *Combustion and Flame*, vol. 158, no. 10, pp. 1920-1932, 2011.
- [194] Z. Zhao, J. Conley, A. Kazakov and F. Dryer, "Burning velocities of real gasoline fuel at 353 K and 500 K.," *SAE paper*, vol. 1, p. 1, 2003.
- [195] N. Morgan, A. Smallbone, A. Bhave, M. Kraft, R. Cracknell and G. Kalghatgi, "Mapping surrogate gasoline compositions into RON/MON space," *Combustion and Flame*, vol. 157, no. 6, pp. 1122-1131, 2010.
- [196] P. Ghosh, K. J. Hickey and S. B. Jaffe, "Development of a Detailed Gasoline Composition-Based Octane Model," *Industrial & Engineering Chemistry Research*, vol. 45, no. 1, pp. 337-345, 2006.
- [197] C. Wang, H. Xu, R. Daniel, A. Ghafourian, J. M. Herreros, S. Shuai and X. Ma, "Combustion characteristics and emissions of 2-methylfuran compared to 2,5-dimethylfuran, gasoline and ethanol in a DISI engine," *Fuel*, vol. 103, pp. 200-211, 2013.
- [198] X. Wu, Z. Huang, X. Wang, C. Jin, C. Tang, L. Wei and C. K. Law, "Laminar burning velocities and flame instabilities of 2,5-dimethylfuran–air mixtures at elevated pressures," *Combustion and Flame*, vol. 158, no. 3, pp. 539-546, 2011.
- [199] X. Ma, c. Jiang, H. Xu, h. Ding and S. Shuai, "Laminar burning characteristics of 2-methylfuran and isooctane blend fuels," *Fuel*, vol. 116, pp. 281-291, 2014.
- [200] J.-P. Lange, R. Price, P. M. Ayoub, J. Louis, L. Petrus, L. Clarke and H. Gosselink, "Valeric Biofuels: A Platform of Cellulosic Transportation Fuels," *Angewandte Chemie International*

*Edition*, vol. 49, no. 26, pp. 4479-4483, 2010.

- [201] M. H. Katshiatshia, E. J. Nilsson, V. Dias, H. Jeanmart and A. A. Konnov, "Experimental Studies and Kinetic Modeling of Ethyl Valerate: Flat Flame Structures and Laminar Burning Velocities," *European Combustion Meeting*, 2015.